frontiers | Research Topics

Inflammatory response and immune disorder in rheumatic and musculoskeletal diseases

Edited by
Lei Zhang, Yuehong Chen, Chuan-ju Liu and Yunpeng Zhao

Published in
Frontiers in Immunology

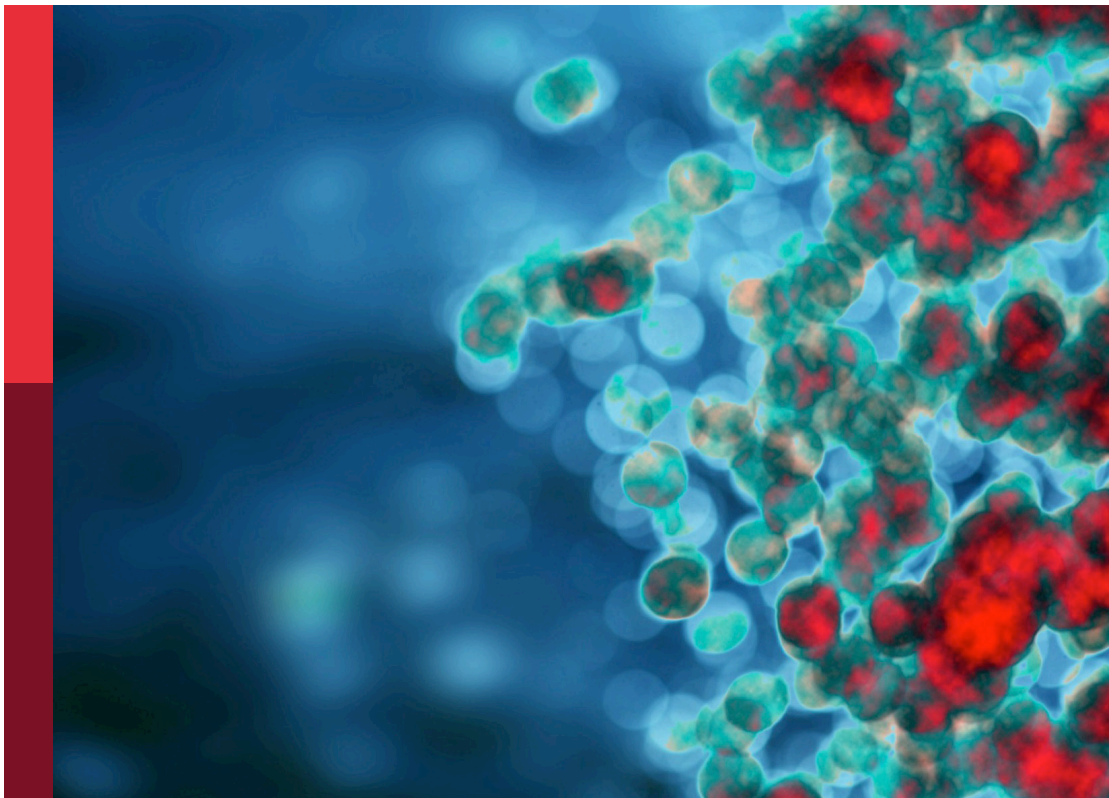

FRONTIERS EBOOK COPYRIGHT STATEMENT

The copyright in the text of individual articles in this ebook is the property of their respective authors or their respective institutions or funders. The copyright in graphics and images within each article may be subject to copyright of other parties. In both cases this is subject to a license granted to Frontiers.

The compilation of articles constituting this ebook is the property of Frontiers.

Each article within this ebook, and the ebook itself, are published under the most recent version of the Creative Commons CC-BY licence. The version current at the date of publication of this ebook is CC-BY 4.0. If the CC-BY licence is updated, the licence granted by Frontiers is automatically updated to the new version.

When exercising any right under the CC-BY licence, Frontiers must be attributed as the original publisher of the article or ebook, as applicable.

Authors have the responsibility of ensuring that any graphics or other materials which are the property of others may be included in the CC-BY licence, but this should be checked before relying on the CC-BY licence to reproduce those materials. Any copyright notices relating to those materials must be complied with.

Copyright and source acknowledgement notices may not be removed and must be displayed in any copy, derivative work or partial copy which includes the elements in question.

All copyright, and all rights therein, are protected by national and international copyright laws. The above represents a summary only. For further information please read Frontiers' Conditions for Website Use and Copyright Statement, and the applicable CC-BY licence.

ISSN 1664-8714
ISBN 978-2-8325-5248-3
DOI 10.3389/978-2-8325-5248-3

About Frontiers

Frontiers is more than just an open access publisher of scholarly articles: it is a pioneering approach to the world of academia, radically improving the way scholarly research is managed. The grand vision of Frontiers is a world where all people have an equal opportunity to seek, share and generate knowledge. Frontiers provides immediate and permanent online open access to all its publications, but this alone is not enough to realize our grand goals.

Frontiers journal series

The Frontiers journal series is a multi-tier and interdisciplinary set of open-access, online journals, promising a paradigm shift from the current review, selection and dissemination processes in academic publishing. All Frontiers journals are driven by researchers for researchers; therefore, they constitute a service to the scholarly community. At the same time, the *Frontiers journal series* operates on a revolutionary invention, the tiered publishing system, initially addressing specific communities of scholars, and gradually climbing up to broader public understanding, thus serving the interests of the lay society, too.

Dedication to quality

Each Frontiers article is a landmark of the highest quality, thanks to genuinely collaborative interactions between authors and review editors, who include some of the world's best academicians. Research must be certified by peers before entering a stream of knowledge that may eventually reach the public - and shape society; therefore, Frontiers only applies the most rigorous and unbiased reviews. Frontiers revolutionizes research publishing by freely delivering the most outstanding research, evaluated with no bias from both the academic and social point of view. By applying the most advanced information technologies, Frontiers is catapulting scholarly publishing into a new generation.

What are Frontiers Research Topics?

Frontiers Research Topics are very popular trademarks of the *Frontiers journals series*: they are collections of at least ten articles, all centered on a particular subject. With their unique mix of varied contributions from Original Research to Review Articles, Frontiers Research Topics unify the most influential researchers, the latest key findings and historical advances in a hot research area.

Find out more on how to host your own Frontiers Research Topic or contribute to one as an author by contacting the Frontiers editorial office: frontiersin.org/about/contact

Inflammatory response and immune disorder in rheumatic and musculoskeletal diseases

Topic editors

Lei Zhang — The First Affiliated Hospital of Shandong First Medical University, China
Yuehong Chen — Sichuan University, China
Chuan-ju Liu — New York University, United States
Yunpeng Zhao — Shandong University, China

Citation

Zhang, L., Chen, Y., Liu, C.-j., Zhao, Y., eds. (2024). *Inflammatory response and immune disorder in rheumatic and musculoskeletal diseases*.
Lausanne: Frontiers Media SA. doi: 10.3389/978-2-8325-5248-3

Table of contents

frontiers | Frontiers in Immunology

TYPE Original Research
PUBLISHED 30 March 2023
DOI 10.3389/fimmu.2023.1156350

Check for updates

OPEN ACCESS

EDITED BY
Chuan-ju Liu,
New York University, United States

REVIEWED BY
Tomonori Kaifu,
Tohoku Medical and Pharmaceutical University, Japan
Guanmin Gao,
First Affiliated Hospital of Zhengzhou University, China

*CORRESPONDENCE
Weidong Xu
xuwdshanghai@126.com

†These authors have contributed equally to this work

SPECIALTY SECTION
This article was submitted to Inflammation, a section of the journal Frontiers in Immunology

RECEIVED 01 February 2023
ACCEPTED 20 March 2023
PUBLISHED 30 March 2023

CITATION
Feng X, Tong W, Li J, Xu Y, Zhu S and Xu W (2023) Diagnostic value of anti-Kaiso autoantibody in axial spondyloarthritis. *Front. Immunol.* 14:1156350. doi: 10.3389/fimmu.2023.1156350

COPYRIGHT
© 2023 Feng, Tong, Li, Xu, Zhu and Xu. This is an open-access article distributed under the terms of the Creative Commons Attribution License (CC BY). The use, distribution or reproduction in other forums is permitted, provided the original author(s) and the copyright owner(s) are credited and that the original publication in this journal is cited, in accordance with accepted academic practice. No use, distribution or reproduction is permitted which does not comply with these terms.

Diagnostic value of anti-Kaiso autoantibody in axial spondyloarthritis

Xinzhe Feng†, Wenwen Tong†, Jia Li†, Yihong Xu, Shanbang Zhu and Weidong Xu*

Department of Joint Bone Disease Surgery, Changhai Hospital, Navy Medical University, Shanghai, China

Objective: Axial spondyloarthritis (axSpA) is a chronic rheumatic disease predominantly characterized by inflammation and progressive structural damage. Patients are often diagnosed very late, which delays the optimal treatment period. Early diagnosis of axSpA, especially non-radiographic axSpA (nr-axSpA), remains a major challenge. This study aimed to investigate the diagnostic value of anti-Kaiso autoantibodies in axSpA and their correlation with clinical disease indicators.

Methods: Two pooled serum samples (seven patients with nr-axSpA and seven healthy controls) were profiled using HuProt arrays to investigate the diagnostic value of autoantibodies in nr-axSpA. Levels of anti-Kaiso autoantibodies in patients with axSpA and controls were determined using the Meso Scale Discovery assay system. Receiver operating characteristic curve analysis was performed to evaluate the diagnostic performance of anti-Kaiso autoantibodies in axSpA. Pearson's correlation was used to assess the correlation between anti-Kaiso autoantibodies and clinical parameters.

Results: Seven candidate autoantibodies were present in the serum of patients with nr-axSpA. The levels of anti-Kaiso autoantibodies were significantly higher in the nr-axSpA group than in the other groups. It can differentiate nr-axSpA from ankylosing spondylitis (AS), healthy controls, and rheumatoid arthritis. The level of early-stage AS among patients with nr-axSpA decreased when they progressed to the late stage. Of all patients with axSpA, serum anti-Kaiso autoantibody levels were positively correlated with the C-reactive protein level and the Bath Ankylosing Spondylitis Disease Activity Index score and negatively correlated with disease duration.

Conclusion: Anti-Kaiso autoantibody may be a valuable diagnostic biomarker for early-stage AS in the nr-axSpA period and may be a potential therapeutic target.

KEYWORDS

axial spondyloarthritis, biomarker, autoantibody, Kaiso, diagnosis

1 Introduction

Axial spondyloarthritis (axSpA) is widely considered a chronic, debilitating, inflammatory disease characterized by clinical signs, such as progressive spinal ankylosis, sacroiliitis, uveitis, and enthesitis (1). Owing to the lack of biomarkers and typical early symptoms, it can take 8–10 years after the onset of the first clinical symptoms to reach a definitive diagnosis (2). Inflammatory back pain and sacroiliitis are the characteristic manifestations of axSpA. As the disease progresses, structural damage becomes more severe, and the spine and peripheral joints become involved. Progressive spinal ankylosis eventually results in significant impairments in physical function, working ability, and quality of life (1). Early diagnosis of axSpA is of the utmost importance for early therapeutic intervention, which is essential for improving the long-term outcome of the disease (3).

AxSpA is commonly viewed as a seronegative disease due to the absence of rheumatoid factors (4). B cells and autoantibodies play important roles in the pathogenesis of axSpA (5). Several studies have revealed the prognostic value of serum autoantibodies, and various antigens have been identified as the sources of these autoantibodies, including microbes, inflammatory targets, and the skeletal/connective tissues (5–7). These antigens play a vital role during axSpA. Microbes and inflammatory targets may be related to the inflammatory process, and autoantibodies against the skeletal/connective tissue can lead to local inflammation, bone destruction, and even new bone formation in axSpA (7).

Structural damage in axSpA incorporates aspects of bone destruction and new bone formation, which are often the result of early inflammation. The current evidence implies that when the structural damage appears to be of a mild extent that often cannot be captured using radiology, clinical intervention could achieve the optimal effect. However, the pathogenesis involved in the structural damage of axSpA is complex and not fully understood (1, 8). Bone morphogenetic proteins (BMPs) and wingless proteins (Wnt) are key pathways driving structural damage in ankylosing spondylitis (AS) (8). Recently, the possible roles of autoantibodies and their corresponding antigens in new bone formation have been explored (9). Thus, the diagnostic value of autoantibodies in non-radiographic axSpA (nr-axSpA) and their possible roles in early inflammation and structural damage require further investigation.

In this study, we extensively profiled autoantibodies in the serum of patients with nr-axSpA and healthy controls using human proteome microarrays. We then validated that anti-Kaiso autoantibodies were higher in patients with nr-axSpA than in other controls (AS, rheumatoid arthritis [RA], and healthy controls). Furthermore, we found no significant difference in the expression of the Kaiso protein in the synovial and ligament tissues of patients with AS and RA. In addition, we investigated the prognostic value of anti-Kaiso autoantibodies in patients with axSpA and nr-axSpA. The relationship between anti-Kaiso autoantibodies and clinical characteristics was also evaluated.

Abbreviations: axSpA, axial spondyloarthritis; nr-axSpA, non-radiographic axSpA; AS, ankylosing spondylitis; BMPs, Bone morphogenetic proteins; Wnt, wingless proteins; RA, rheumatoid arthritis; BASDAI, Bath Ankylosing Spondylitis Disease Activity Index; BASFI, Bath Ankylosing Spondylitis Functional Index; m-SASSS, modified Stoke Ankylosing Spondylitis Spinal Score; HuProt, human proteome arrays; MSD, Meso Scale Discovery; ECL, enhanced chemiluminescence; IHC, Immunohistochemistry; DAB, diaminobenzidine; ROC, Receiver operating characteristic; PPV, Positive predictive value; NPV, negative predictive value; ITGA10, Integrin subunit alpha 10; POZ, poxvirus and zinc finger; KBS, Kaiso binding site; ZBTB16, zinc finger and BTB domain containing 16.

2 Materials and methods

2.1 Biological samples

Serum samples were obtained from patients recruited from the outpatient clinic of Changhai Hospital (Shanghai, China). Synovial and ligament tissues were obtained from patients with AS and RA who underwent surgical treatment (spinal osteotomies or hip replacements) at the late stage of the disease. Puncture biopsy samples were obtained from the sacroiliac joints of the nr-axSpA patients. The study was approved by the Medical Ethics Committee of Changhai Hospital, and informed consent was obtained from all patients. The patients were classified according to the Assessment of SpondyloArthritis International Society criteria (10). Patients with AxSpA were divided into two subgroups (AS and nr-axSpA), and patients with AS were classified according to the modified New York criteria (11). All patients with nr-axSpA were followed up. Patients with RA fulfilled the American College of Rheumatology's revised criteria (12). Healthy controls and patients with RA should not have any disease involving the axial joint. Disease activity and functional capacity were determined based on the Bath Ankylosing Spondylitis Disease Activity Index (BASDAI) and the Bath Ankylosing Spondylitis Functional Index (BASFI), respectively. Syndesmophytes in AS with axial involvement were assessed according to the modified Stoke Ankylosing Spondylitis Spinal Score (m-SASSS) by two experienced radiologists who were blinded to the patients' clinical data (13). The final score is the average score. The erythrocyte sedimentation rate (ESR) (mm/h), C-reactive protein (CRP) (mg/L), and serum alkaline phosphatase (ALP) (U/L) levels were measured at the time of the assessment.

2.2 Serum profiling with human proteome arrays

The HuProt microarrays used in this study were provided by CDI Laboratories Inc. (Mayaguez, USA). The array contains duplicate spots of approximately 20,000 individually purified human proteins with an N-terminal glutathione S-transferase (GST) tag and is widely used to screen autoantibodies in various diseases (14, 15). Autoantibodies in nr-axSpA were profiled using HuProt arrays of two pooled serum samples (seven nr-axSpA *vs.* seven healthy controls) according to the manufacturer's protocol.

2.3 Measurement of anti-Kaiso autoantibody using the meso scale discovery assay system

Levels of anti-Kaiso autoantibody in all included patients with axSpA (nr-axSpA and AS) and controls (RA and healthy controls)

were determined using the MSD assay system, which is based on the detection of the light emitted by an electrochemiluminescent Sulfo-tag label following electrochemical stimulation (16, 17). The concentration of coated recombinant protein, dilution of serum and standard antibody, and amount of Sulfo-tag-labeled IgG used in the experiment were all optimized in a series of preliminary experiments. A mouse monoclonal anti-Kaiso antibody (Abcam, Cambridge, UK) was used as the internal standard positive control in the assay, and a standard curve was generated using serial dilutions (2,500, 625, 156.25, 39.06, 9.77, 2.44, 0.61, and 0 ng/ml) of the Kaiso antibody. The 96-well plates (MSD, Rockville, Maryland, USA) were then coated with 40 µl (5 µg/ml) of recombinant human Kaiso protein (Abcam) and incubated overnight at 4°C. The plates were washed three times with PBST (PBS + 0.05% Tween 20) and blocked with Blocker A (MSD) at room temperature (RT) for 2 h. After washing with PBST, 50 µl plasma (diluted 1:250 in PBS) was added to the coated plates and incubated for 2 h at RT. After washing the plates three times with PBST, 50 µl (1 µg/ml) of Sulfo-tag goat anti-human IgG secondary antibody (MSD) was added to each well and incubated for 2 h at RT on a shaker. After three more washes, 150 µl MSD read buffer (MSD) was added to each well, and the plates were read using an MSD Sector Imager S600. The serum antibody concentrations were determined by referencing the enhanced chemiluminescence (ECL) responses against the standard curve.

2.4 Immunohistochemistry

Synovial and ligament tissues were fixed in 4% paraformaldehyde, embedded in paraffin, and sliced into sections. The sections were then de-waxed, hydrated, and washed. After antigen retrieval using microwaves, endogenous peroxidase activity was blocked in a 3% H2O2 solution. The sections were subsequently incubated overnight with anti-Kaiso antibodies or control IgG (Proteintech, Rosemont, USA). They were then washed and incubated with horseradish peroxidase-conjugated secondary antibodies, followed by treatment with diaminobenzidine (DAB) to visualize the signal. Sections were examined and photographed using an Olympus BX51 microscope (Olympus Corporation, Tokyo, Japan).

2.5 Statistical analysis

Statistical analyses were performed using SPSS Statistics software version 19.0. All data were analyzed using a normal distribution test. A comparison of measurement data with a normal distribution was performed using the Student's t test. A comparison of measurement data with non-normal data was performed using the Mann–Whitney U test. A receiver operating characteristic (ROC) curve analysis was performed to evaluate the diagnostic performance of anti-Kaiso antibodies in AS. The optimal cut-off values in the ROC curves were defined as the points at which sensitivity and specificity were maximized. The positive predictive value (PPV) and negative predictive value (NPV) were calculated. Pearson's correlation was used to assess the correlation between anti-Kaiso autoantibodies and other clinical parameters. Logistic regression was used to analyze the anti-Kaiso antibody level and its associated clinical indicators in patients with axSpA. Differences were considered statistically significant at $^{*}P < 0.05$ and $^{**}P < 0.01$.

3 Results

3.1 Detection of autoantibodies in nr-axSpA serum with human proteome microarrays

We used the HuProt microarray to identify autoantibodies in two pools of samples collected from patients with nr-axSpA (n = 7) and healthy controls (n = 7). Data analysis revealed that 47 autoantibodies were detected in the serum of healthy controls and 42 autoantibodies were found in the serum of patients with nr-axSpA. Further analysis showed that seven candidate autoantibodies were specifically present in the serum of patients with nr-axSpA but not in healthy controls (Figure 1A). Representative images of the autoantibodies detected on HuProt microarrays are shown in Figure 1B. High-magnification images of the seven specific autoantibodies (ASAP, BCL7A, EIF2C1, IGHG1, MYLK, SUGT1, and KAISO) are presented in Figure 1C.

3.2 Validation of novel autoantibodies using the MSD assay system

As inflammation and progressive new bone formation are hallmarks of axSpA, especially in AS, we focused on Kaiso-specific autoantibodies, which have been shown to affect inflammation and Wnt signaling (18, 19). We measured the amount of anti-Kaiso antibodies in serum samples using MSD in a large cohort comprising 50 patients with nr-axSpA, 40 with AS (20), 40 with RA, and 45 healthy controls. The clinical characteristics of patients and healthy controls are shown in Table S1. The results revealed that levels of anti-Kaiso antibodies were significantly higher in the nr-axSpA group than in the other groups (Figure 2A). We then sought to explore the differential expression of Kaiso proteins in tissues. Synovial and ligament tissues were collected from patients with transcervical fracture (healthy control, HC), AS, RA, and nr-axSpA patients who had ever undergone puncture biopsy of the sacroiliac joint and then sent for IHC analysis. IHC analysis revealed higher expression of Kaiso in synovial and ligament tissues from nr-axSpA patients compared with HC, AS, and RA (Figure 2B). Integrin subunit alpha 10 (ITGA10), as a key downstream molecule of Kaiso regulating osteogenic differentiation (21), was found to make no significant difference in the synovial and ligament tissues of patients with AS, RA, nr-axSpA, and HC (Figure S3).

3.3 Validation of the diagnostic value of the serum anti-Kaiso autoantibody level in axSpA and nr-axSpA

The results presented suggest a possible role for anti-Kaiso autoantibodies as diagnostic biomarkers to discriminate nr-axSpA

10.3389/fimmu.2023.1156350

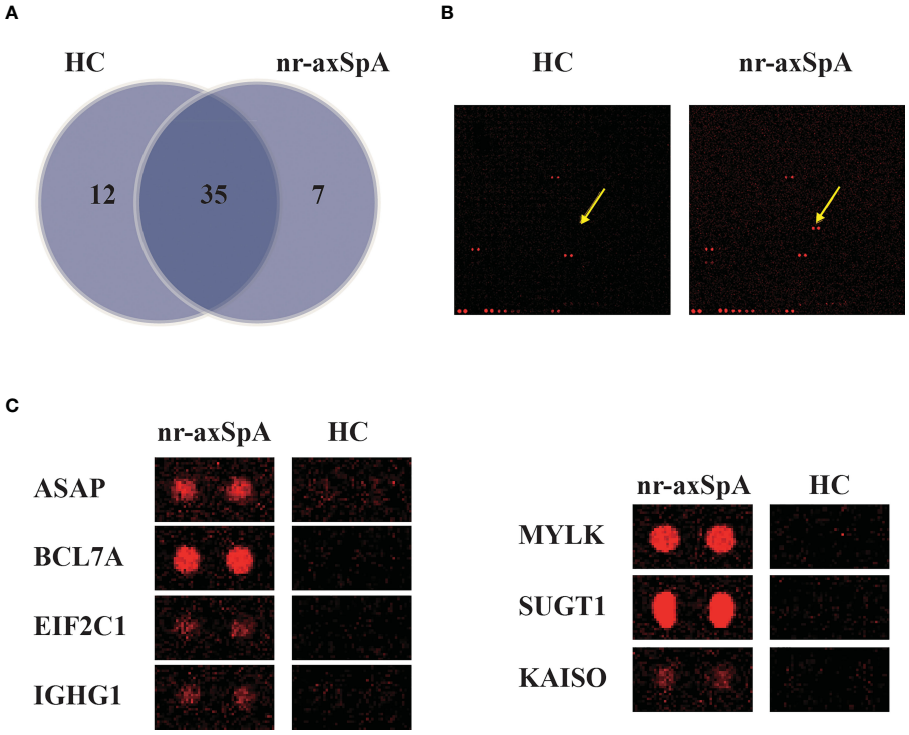

FIGURE 1
Identification of autoantibodies in the serum of patients with nr-axSpA using human proteome (HuProt) microarrays. **(A)** The Venn diagram shows the number of autoantibodies identified in the serum of patients with nr-axSpA and healthy controls. **(B)** Representative images of the autoantibody detected in the HuProt microarrays. The arrows indicate the duplicate spots of the antigen protein. **(C)** High magnification images of the seven specific autoantibodies, including ASAP, BCL7A, EIF2C1, IGHG1, MYLK, SUGT1, and KAISO, identified in patients with nr-axSpA.

from AS and controls. We further analyzed the ROC curve of serum anti-Kaiso autoantibody levels to assess their diagnostic value (Figure 3). We found that serum anti-Kaiso autoantibody levels could differentiate patients with axSpA (nr-axSpA and AS) from healthy controls with an AUC (area under the curve) of 0.74 (cut-off value 4,065.49 ng/ml, sensitivity 61.1%, specificity 84.4%), and differentiate patients with axSpA from those with RA with an AUC of 0.72 (cut-off value 4,426.73 ng/ml, sensitivity 55.6%, specificity 80%). Using 4,574.98 ng/ml as the cut-off value, the AUC of anti-Kaiso autoantibody to discriminate nr-axSpA from AS was 0.86 (95% CI 0.78–0.94, sensitivity 76%, specificity 87.5%). Moreover, the diagnostic performance of serum anti-Kaiso autoantibodies in differentiating nr-axSpA from other groups (RA and healthy controls) was also assessed. The AUC value for differentiating nr-axSpA from healthy controls was 0.88 (with a cut-off value of 4,263.57 ng/ml, and a sensitivity of 80%, and a specificity, of 87%). The AUC value for differentiating nr-axSpA and RA was 0.87 (cut-off value: 4,574.98 ng/ml, sensitivity 74%; specificity 87.5%). The results of the ROC analysis are shown in Table S2.

3.4 Association between anti-Kaiso autoantibody and clinical characteristics

Next, we sought to analyze the associations between anti-Kaiso autoantibodies and clinical indicators (Figure 4, Supplementary Figures 1, 2). Of all patients with axSpA (nr-axSpA and AS), the serum level of anti-Kaiso autoantibody was positively correlated with CRP ($r = 0.681$, $p < 0.01$) and BASDAI ($r = 0.47$, $p < 0.01$) (Figure 4). However, it was not significantly correlated with other activity measures such as ESR ($r = 0.131$, $p > 0.05$) and BASFI ($r = -0.178$, $p > 0.05$) (Supplementary Figure 1). When further analysis was performed, the results showed that the anti-Kaiso autoantibody level was negatively correlated with disease duration ($r = -0.485$, $p < 0.01$). Among nr-axSpA patients, the serum level of anti-Kaiso autoantibody was positively correlated with ALP ($r = 0.456$, $p < 0.01$) (Supplementary Figure 2). Moreover, logistic regression analysis showed that anti-Kaiso antibodies ($p < 0.05$), disease duration ($p < 0.05$), CRP ($p < 0.05$), and the BASDAI score ($p < 0.05$) could discriminate "nr-axSpA" from "AS."

3.5 Follow-up results of patients with nr-axSpA

Twenty-two of all the 50 patients with nr-axSpA progressed to AS over an 8-year period. According to Figure 5A, it was found that the anti-Kaiso autoantibodies of patients with nr-axSpA (7,233 ± 252.4 ng/ml) who progressed to AS (5,069 ± 178 ng/ml) were reduced to varying degrees overall. The AUC value for differentiating early and late stages of AS was 0.9 (cut-off value 5891.89 ng/ml, sensitivity 86.4%, specificity 86.4%) (Figure 5).

10.3389/fimmu.2023.1156350

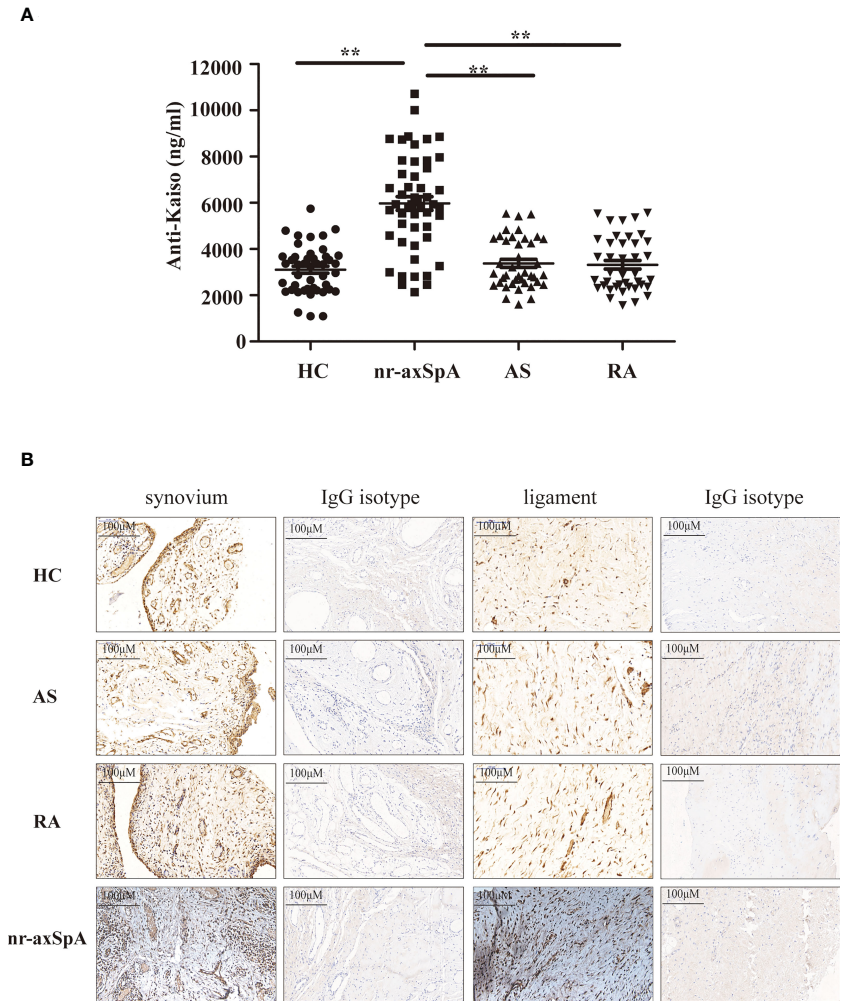

FIGURE 2
Validation levels of anti-Kaiso autoantibodies in the serum using the Meso Scale Discovery (MSD) assay system and the expression of Kaiso in the tissues detected using immunohistochemistry (IHC). **(A)** MSD analysis of anti-Kaiso autoantibodies in the serum of patients with nr-axSpA (n = 50), AS (n = 40), and RA (n = 40) and healthy controls (HC, n = 45). **(B)** Synovial and ligament tissues of HC, AS, RA, and nr-axSpA were stained with the anti-Kaiso antibody. Data are presented as mean ± SEM. **P <0.01 compared to patients with nr-axSpA. All IHC images are shown at ×100 magnification and are representative of images from three independent experiments.

4 Discussion

The identification of biomarkers for early axSpA diagnosis and therapy is the current focus of research. By screening the serum of patients with nr-axSpA and controls using human proteome microarrays, we identified seven candidate autoantibodies that were present specifically in the serum of those with nr-axSpA. Considering the potential role of Kaiso protein in the inflammation and new bone formation processes of AS, an anti-Kaiso autoantibody was selected for further validation studies. The results demonstrated that serum levels of anti-Kaiso autoantibodies were higher in patients with nr-axSpA than in controls. We also found that anti-Kaiso autoantibodies were highly accurate in diagnosing nr-axSpA. Moreover, serum levels of anti-Kaiso autoantibodies were positively correlated with CRP, BASDAI, and ALP levels and negatively correlated with disease duration.

Autoantibodies are immunological hallmarks of several autoimmune diseases and can be used as diagnostic biomarkers (22, 23). AxSpA was long assumed to be a seronegative disease, and antibodies were not considered a hallmark of this disease. Recently, an increasing number of autoantibodies have been recognized as potential diagnostic biomarkers for AS (5). In this study, we demonstrated that Kaiso-specific autoantibodies are present in the serum of healthy individuals but at higher levels in the nr-axSpA. Interestingly, autoantibody levels returned to normal in AS. This phenomenon implies that the serum anti-Kaiso level may be correlated with the bone deformation stage in AS. We also found a positive correlation between the concentration of serum anti-Kaiso autoantibody and ALP among nr-axSpA in our study, which is supported by previous reports showing its relationship with structural damage (24). Moreover, Kaiso, an antigen of the anti-Kaiso autoantibody in tissues, may participate in the regulation of osteoblast differentiation. Therefore, both *in vivo* and *in vitro* experiments were designed to investigate the role of Kaiso in osteogenesis. The experiments indicated that Kaiso could inhibit osteoblast differentiation *via the* Itga10/PI3K/AKT signaling pathway. In addition, we discovered that the expression of Kaiso decreased the

10.3389/fimmu.2023.1156350

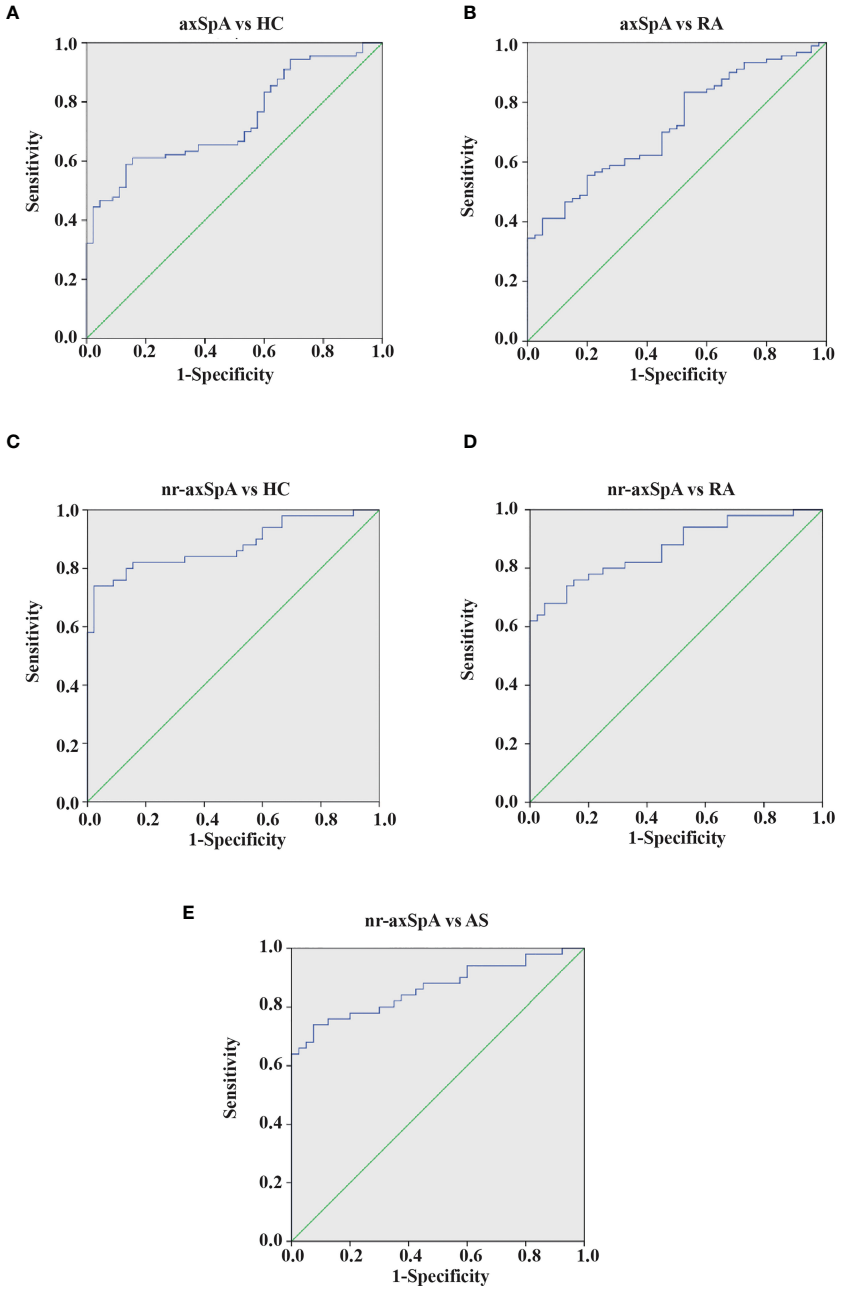

FIGURE 3
ROC curves of anti-Kaiso autoantibody for the discrimination of patients with axSpA from controls. **(A)** Patients with AxSpA (nr-axSpA and AS) versus healthy controls. **(B)** Patients with AxSpA versus RA. **(C)** Patients with nr-axSpA versus healthy controls. **(D)** Patients with nr-axSpA versus those with RA. **(E)** Patients with nr-axSpA versus those with AS.

osteogenic differentiation of MC3T3–E1 cells and BMSCs through downregulating Itga10 (21). The higher expression of Kaiso in nr-axSpA patients also indicates its potential function. The likely reason is that, in the later stage of this disease, the previously normal target joints and surrounding tissues were gradually replaced by ossified tissue, which was associated with reduced expression of Kaiso. We also discovered that some other diseases are characterized by the disappearance of autoantigens during disease progression. For instance, Guillain–Barré syndrome (25), Hashimoto's thyroiditis (26), and type 1 diabetes (27) are all autoimmune-related. As the disease progresses, its pathology is characterized by atrophy and necrosis of the target organs and tissues attacked by the immune system, which is accompanied by a reduction of some special autoantigens existing in them. These results may help to explain why anti-Kaiso autoantibodies were reduced in the AS stage. The following analysis revealed that serum anti-Kaiso autoantibody could be a potential diagnostic biomarker for differentiating nr-axSpA from other groups (AS, RA, and healthy controls). We further explored the diagnostic value of serum anti-Kaiso autoantibodies in the early stages of AS. We selected 22 patients with nr-axSpa who progressed to AS over 8 years and analyzed their change and clinical diagnosis value of anti-Kaiso autoantibodies. The results showed that the serum anti-Kaiso

10.3389/fimmu.2023.1156350

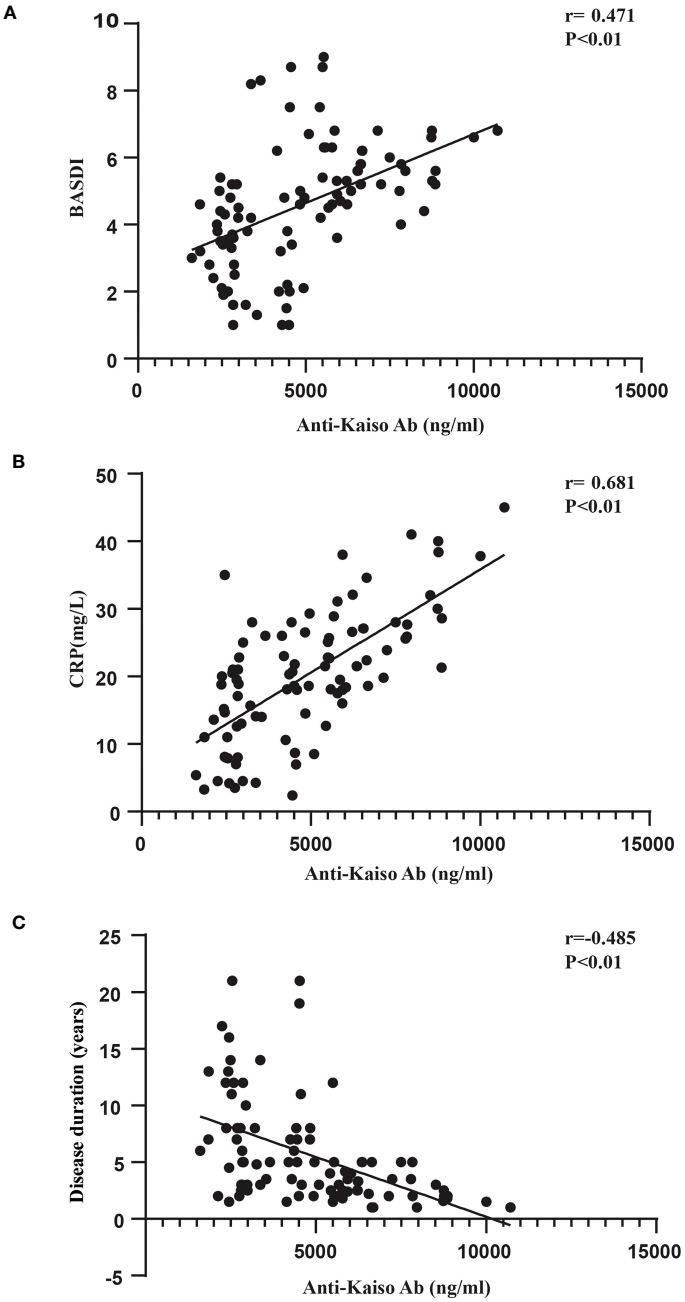

FIGURE 4
Correlation between anti-Kaiso autoantibody levels, BASDAI scores **(A)**, CRP **(B)**, and disease duration **(C)** in patients with axSpA.

autoantibody level significantly decreased among patients with nr-axSpa with radiographic progression, which is suggested to be related to the progression of AS disease. However, most patients with AS have used biological agents, while those with nr-axSpA have not. Owing to different drug use in different groups, biological agents may have an impact on the immune process. Therefore, it is not known whether biological agents affect antibody production. However, this requires further experimental validation.

Several autoantibodies have been reported to be involved in osteoblast mineralization and bone formation in AS (9, 28). Kaiso (also known as zinc finger and BTB domain containing 33), a unique member of the poxvirus and zinc finger (POZ) family, exhibits dual-specificity DNA binding to methylated CpG dinucleotides or a non-methylated sequence known as the Kaiso binding site (KBS) (29, 30). Kaiso regulates inflammation and cell proliferation in various diseases (31–33). In addition, several studies have revealed that Kaiso affects Wnt signaling, which is essential for the regulation of bone homeostasis (34). Moreover, the zinc finger and BTB domain containing gene 16 (ZBTB16), which is also a member of the POZ-zinc finger family, regulates osteoblast differentiation (35, 36). Thus, we hypothesized that Kaiso plays an important role in axSpA structural damage. Bone destruction occurs prior to new bone formation in the pathological process of axSpA (8); therefore, it is possible that bone destruction in the focal axial joint during the early stage of axSpA is associated with

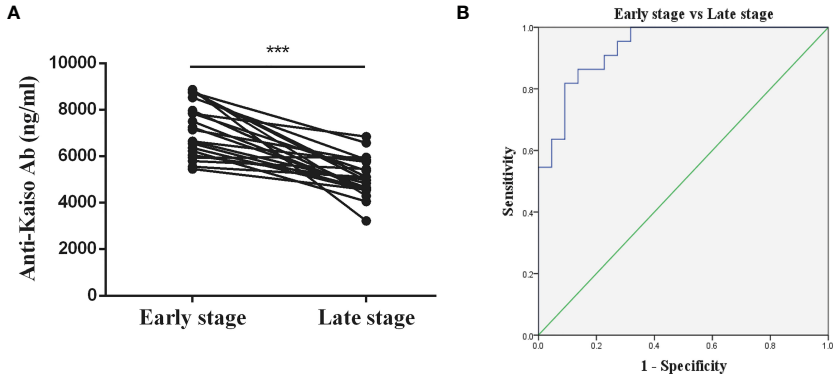

FIGURE 5
Diagnostic value of anti-Kaiso autoantibody in patients with AS. **(A)** Levels of anti-Kaiso autoantibody in patients with nr-axSpA progressing to AS over an 8-year period. **(B)** ROC curves of anti-Kaiso autoantibody for the discrimination of patients with nr-axSpA from those with AS. ***P <0.001

increased Kaiso protein expression in the skeletal and connective tissues, and that the resulting increase in exposure to the immune system leads to increased levels of anti-Kaiso autoantibodies. The relative reduction in Kaiso expression in AS may contribute to the limited bone destruction and progressive new bone formation observed in these patients. Furthermore, immunohistochemical analysis revealed that the expression of Kaiso in synovial and ligament tissues of nr-axSpA patients were higher than that of AS, RA, and controls. However, no different expression of Itga10 was found between them. The possible reason was that anti-Kaiso autoantibodies interacted with Kaiso and interfered with its regulation of Itga10 expression. Thus, anti-Kaiso autoantibodies may represent a biomarker of nr-axSpA, although these findings have yet to be validated in more patients.

In addition to the anti-Kaiso autoantibody tested in this study, additional novel autoantibodies, including MYLK, EIF2C1, and SUGT1, are also potential biomarkers for nr-axSpA. MYLK gene activity can be induced by TNF-α, an essential inflammatory factor in AS (37). Additionally, EIF2C1 participates in angiogenesis (38, 39), whereas SUGT1 regulates inflammatory activity (40). Thus, all processes regulated by these genes appear to engage in distinct aspects of axSpA pathogenesis. Additional experiments are required to verify the role of these autoantibodies in axSpA.

In summary, the anti-Kaiso autoantibody can be a biomarker for nr-axSpA (especially in the early AS stage) and a potential therapeutic target. Further studies with larger sample sizes are required to validate our findings.

Data availability statement

The original contributions presented in the study are included in the article/Supplementary Material. Further inquiries can be directed to the corresponding author.

Ethics statement

The studies involving human participants were reviewed and approved by Ethics Committee of Shanghai Changhai Hospital. The patients/participants provided their written informed consent to participate in this study.

Author contributions

YX and SZ collected the clinical data. XF and WT performed the experimental work and statistical analysis. XF and JL drafted the manuscript. WX designed the study and revised the manuscript. All authors contributed to the article and approved the submitted version.

Funding

This research was supported by the National Natural Science Foundation of China (82172390, 81901654, 81601412) and the Shanghai Sailing Program (22YF1459400).

Acknowledgments

We would like to thank Editage (www.editage.cn) for English language editing.

Conflict of interest

The authors declare that the research was conducted in the absence of any commercial or financial relationships that could be construed as a potential conflict of interest.

Publisher's note

All claims expressed in this article are solely those of the authors and do not necessarily represent those of their affiliated organizations, or those of the publisher, the editors and the reviewers. Any product that may be evaluated in this article, or

claim that may be made by its manufacturer, is not guaranteed or endorsed by the publisher.

Supplementary material

The Supplementary Material for this article can be found online at: https://www.frontiersin.org/articles/10.3389/fimmu.2023.1156350/full#supplementary-material

SUPPLEMENTARY FIGURE 1
Correlation between anti-Kaiso autoantibody levels, BASFI scores **(A)**, ESR **(B)** in patients with axSpA.

SUPPLEMENTARY FIGURE 2
Correlation between anti-Kaiso autoantibody levels and serum ALP activity in patients with nr-axSpA.

SUPPLEMENTARY FIGURE 3
IHC staining of Itga10 in tissues of HC, nr-axSpA, AS, and RA.

References

1. Sieper J, Poddubnyy D. Axial spondyloarthritis. *Lancet* (2017) 390:73–84. doi: 10.1016/S0140-6736(16)31591-4

2. Feldtkeller E, Khan MA, van der Heijde D, van der Linden S, Braun J. Age at disease onset and diagnosis delay in HLA-B27 negative vs. positive patients with ankylosing spondylitis. *Rheumatol Int* (2003) 23:61–6. doi: 10.1007/s00296-002-0237-4

3. Wanders A, Heijde D, Landewe R, Behier JM, Calin A, Olivieri I, et al. Nonsteroidal antiinflammatory drugs reduce radiographic progression in patients with ankylosing spondylitis: a randomized clinical trial. *Arthritis Rheum* (2005) 52:1756–65. doi: 10.1002/art.21054

4. Pal B. Ankylosing spondylitis, a seronegative spondarthritis. *Practitioner* (1987) 231:785–93.

5. Quaden DH, De Winter LM, Somers V. Detection of novel diagnostic antibodies in ankylosing spondylitis: An overview. *Autoimmun Rev* (2016) 15:820–32. doi: 10.1016/j.autrev.2016.06.001

6. Wright C, Sibani S, Trudgian D, Fischer R, Kessler B, Labaer J, et al. Detection of multiple autoantibodies in patients with ankylosing spondylitis using nucleic acid programmable protein arrays. *Mol Cell Proteomics* (2012) 11:M9 00384. doi: 10.1074/mcp.M9.00384

7. Baerlecken NT, Nothdorft S, Stummvoll GH, Sieper J, Rudwaleit M, Reuter S, et al. Autoantibodies against CD74 in spondyloarthritis. *Ann Rheum Dis* (2014) 73:1211–4. doi: 10.1136/annrheumdis-2012-202208

8. Maksymowych WP. Disease modification in ankylosing spondylitis. *Nat Rev Rheumatol* (2010) 6:75–81. doi: 10.1038/nrrheum.2009.258

9. Kim YG, Sohn DH, Zhao X, Sokolove J, Lindstrom TM, Yoo B, et al. Role of protein phosphatase magnesium-dependent 1A and anti-protein phosphatase magnesium-dependent 1A autoantibodies in ankylosing spondylitis. *Arthritis Rheumatol* (2014) 66:2793–803. doi: 10.1002/art.38763

10. Sieper J, van der Heijde D, Landewe R, Brandt J, Burgos-Vagas R, Collantes-Estevez E, et al. New criteria for inflammatory back pain in patients with chronic back pain: a real patient exercise by experts from the assessment of SpondyloArthritis international society (ASAS). *Ann Rheum Dis* (2009) 68:784–8. doi: 10.1136/ard.2008.101501

11. Van Der Linden S, Valkenburg HA, Cats A. Evaluation of diagnostic criteria for ankylosing spondylitis. a proposal for modification of the new York criteria. *Arthritis Rheum* (1984) 27:361–8. doi: 10.1002/art.1780270401

12. Arnett FC, Edworthy SM, Bloch DA, Mcshane DJ, Fries JF, Cooper NS, et al. The American rheumatism association 1987 revised criteria for the classification of rheumatoid arthritis. *Arthritis Rheum* (1988) 31:315–24. doi: 10.1002/art.1780310302

13. Creemers MC, Franssen MJ, Van't Hof MA, Gribnau FW, Van De Putte LB, Van Riel PL. Assessment of outcome in ankylosing spondylitis: an extended radiographic scoring system. *Ann Rheum Dis* (2005) 64:127–9. doi: 10.1136/ard.2004.020503

14. Hu CJ, Pan JB, Song G, Wen XT, Wu ZY, Chen S, et al. Identification of novel biomarkers for behcet disease diagnosis using human proteome microarray approach. *Mol Cell Proteomics* (2017) 16:147–56. doi: 10.1074/mcp.M116.061002

15. Pan J, Song G, Chen D, Li Y, Liu S, Hu S, et al. Identification of serological biomarkers for early diagnosis of lung cancer using a protein array-based approach. *Mol Cell Proteomics* (2017) 16:2069–78. doi: 10.1074/mcp.RA117.000212

16. Brudek T, Winge K, Folke J, Christensen S, Fog K, Pakkenberg B, et al. Autoimmune antibody decline in parkinson's disease and multiple system atrophy; a step towards immunotherapeutic strategies. *Mol Neurodegener* (2017) 12:44. doi: 10.1186/s13024-017-0187-7

17. Yu L, Miao D, Scrimgeour L, Johnson K, Rewers M, Eisenbarth GS. Distinguishing persistent insulin autoantibodies with differential risk: nonradioactive bivalent proinsulin/insulin autoantibody assay. *Diabetes* (2012) 61:179–86. doi: 10.2337/db11-0670

18. Kim SW, Park JI, Spring CM, Sater AK, Ji H, Otchere AA, et al. Non-canonical wnt signals are modulated by the kaiso transcriptional repressor and p120-catenin. *Nat Cell Biol* (2004) 6:1212–20. doi: 10.1038/ncb1191

19. Liu Y, Dong QZ, Wang S, Xu HT, Miao Y, Wang L, et al. Kaiso interacts with p120-catenin to regulate beta-catenin expression at the transcriptional level. *PLoS One* (2014) 9:e87537. doi: 10.1371/journal.pone.0087537

20. Lee YS, Schlotzhauer T, Ott SM, Van Vollenhoven RF, Hunter J, Shapiro J, et al. Skeletal status of men with early and late ankylosing spondylitis. *Am J Med* (1997) 103:233–41. doi: 10.1016/S0002-9343(97)00143-5

21. Tong W, Li J, Feng X, Wang C, Xu Y, He C, et al. Kaiso regulates osteoblast differentiation and mineralization via the Itga10/PI3K/AKT signaling pathway. *Int J Mol Med* (2021) 47. doi: 10.3892/ijmm.2021.4874

22. Agmon-Levin N, Damoiseaux J, Kallenberg C, Sack U, Witte T, Herold M, et al. International recommendations for the assessment of autoantibodies to cellular antigens referred to as anti-nuclear antibodies. *Ann Rheum Dis* (2014) 73:17–23. doi: 10.1136/annrheumdis-2013-203863

23. Fujii T. Direct and indirect pathogenic roles of autoantibodies in systemic autoimmune diseases. *Allergol Int* (2014) 63:515–22. doi: 10.2332/allergolint.14-RAI-0801

24. Kang KY, Hong YS, Park SH, Ju JH. Increased serum alkaline phosphatase levels correlate with high disease activity and low bone mineral density in patients with axial spondyloarthritis. *Semin Arthritis Rheum* (2015) 45:202–7. doi: 10.1016/j.semarthrit.2015.03.002

25. Uchibori A, Chiba A. Autoantibodies in Guillain-barre syndrome. *Brain Nerve* (2015) 67:1347–57. doi: 10.11477/mf.1416200305

26. Pyzik A, Grywalska E, Matyjaszek-Matuszek B, Rolinski J. Immune disorders in hashimoto's thyroiditis: what do we know so far? *J Immunol Res* (2015) 2015:979167. doi: 10.1155/2015/979167

27. Knip M, Siljander H, Ilonen J, Simell O, Veijola R. Role of humoral beta-cell autoimmunity in type 1 diabetes. *Pediatr Diabetes* (2016) 17 Suppl 22:17–24. doi: 10.1111/pedi.12386

28. Bougault C, El Jamal A, Briolay A, Mebarek S, Boutet MA, Garraud T, et al. Involvement of sphingosine kinase/sphingosine 1-phosphate metabolic pathway in spondyloarthritis. *Bone* (2017) 103:150–8. doi: 10.1016/j.bone.2017.07.002

29. Daniel JM, Spring CM, Crawford HC, Reynolds AB, Baig A. The p120(ctn)-binding partner kaiso is a bi-modal DNA-binding protein that recognizes both a sequence-specific consensus and methylated CpG dinucleotides. *Nucleic Acids Res* (2002) 30:2911–9. doi: 10.1093/nar/gkf398

30. Buck-Koehntop BA, Stanfield RL, Ekiert DC, Martinez-Yamout MA, Dyson HJ, Wilson IA, et al. Molecular basis for recognition of methylated and specific DNA sequences by the zinc finger protein kaiso. *Proc Natl Acad Sci U.S.A.* (2012) 109:15229–34. doi: 10.1073/pnas.1213726109

31. Chaudhary R, Pierre CC, Nanan K, Wojtal D, Morone S, Pinelli C, et al. The POZ-ZF transcription factor kaiso (ZBTB33) induces inflammation and progenitor cell differentiation in the murine intestine. *PLoS One* (2013) 8:e74160. doi: 10.1371/journal.pone.0074160

32. Pozner A, Terooatea TW, Buck-Koehntop BA. Cell-specific kaiso (ZBTB33) regulation of cell cycle through cyclin D1 and cyclin E1. *J Biol Chem* (2016) 291:24538–50. doi: 10.1074/jbc.M116.746370

33. Jones J, Wang H, Zhou J, Hardy S, Turner T, Austin D, et al. Nuclear kaiso indicates aggressive prostate cancers and promotes migration and invasiveness of prostate cancer cells. *Am J Pathol* (2012) 181:1836–46. doi: 10.1016/j.ajpath.2012.08.008

34. Baron R, Kneissel M. WNT signaling in bone homeostasis and disease: from human mutations to treatments. *Nat Med* (2013) 19:179–92. doi: 10.1038/nm.3074

35. Felthaus O, Gosau M, Klein S, Prantl L, Reichert TE, Schmalz G, et al. Dexamethasone-related osteogenic differentiation of dental follicle cells depends on ZBTB16 but not Runx2. *Cell Tissue Res* (2014) 357:695–705. doi: 10.1007/s00441-014-1891-z

36. Onizuka S, Iwata T, Park SJ, Nakai K, Yamato M, Okano T, et al. ZBTB16 as a downstream target gene of osterix regulates osteoblastogenesis of human multipotent mesenchymal stromal cells. *J Cell Biochem* (2016) 117:2423–34. doi: 10.1002/jcb.25634

37. Ye D, Ma TY. Cellular and molecular mechanisms that mediate basal and tumour necrosis factor-alpha-induced regulation of myosin light chain kinase gene activity. *J Cell Mol Med* (2008) 12:1331–46. doi: 10.1111/j.1582-4934.2008.00302.x

38. Eswarappa SM, Potdar AA, Koch WJ, Fan Y, Vasu K, Lindner D, et al. Programmed translational readthrough generates antiangiogenic VEGF-ax. *Cell* (2014) 157:1605–18. doi: 10.1016/j.cell.2014.04.033

39. Chen Z, Lai TC, Jan YH, Lin FM, Wang WC, Xiao H, et al. Hypoxia-responsive miRNAs target argonaute 1 to promote angiogenesis. *J Clin Invest* (2013) 123:1057–67. doi: 10.1172/JCI65344

40. Mayor A, Martinon F, De Smedt T, Petrilli V, Tschopp J. A crucial function of SGT1 and HSP90 in inflammasome activity links mammalian and plant innate immune responses. *Nat Immunol* (2007) 8:497–503. doi: 10.1038/ni1459

frontiers | Frontiers in Immunology

TYPE Original Research
PUBLISHED 06 July 2023
DOI 10.3389/fimmu.2023.1191536

Check for updates

OPEN ACCESS

EDITED BY
Lei Zhang,
The First Affiliated Hospital of Shandong First Medical University, China

REVIEWED BY
Daniel W.D. West,
University Health Network, Canada
Franka Klatte-Schulz,
Charité Medical University of Berlin, Germany
Finosh Thankam,
Western University of Health Sciences, United States

*CORRESPONDENCE
Xinjie Wu
wuxinjie@pku.edu.cn
Aisha S. Ahmed
aisha.ahmed@ki.se

RECEIVED 22 March 2023
ACCEPTED 16 June 2023
PUBLISHED 06 July 2023

CITATION
Wu X, Chen J, Sun W, Hart DA, Ackermann PW and Ahmed AS (2023) Network proteomic analysis identifies inter-alpha-trypsin inhibitor heavy chain 4 during early human Achilles tendon healing as a prognostic biomarker of good long-term outcomes.
Front. Immunol. 14:1191536.
doi: 10.3389/fimmu.2023.1191536

COPYRIGHT
© 2023 Wu, Chen, Sun, Hart, Ackermann and Ahmed. This is an open-access article distributed under the terms of the Creative Commons Attribution License (CC BY). The use, distribution or reproduction in other forums is permitted, provided the original author(s) and the copyright owner(s) are credited and that the original publication in this journal is cited, in accordance with accepted academic practice. No use, distribution or reproduction is permitted which does not comply with these terms.

Network proteomic analysis identifies inter-alpha-trypsin inhibitor heavy chain 4 during early human Achilles tendon healing as a prognostic biomarker of good long-term outcomes

Xinjie Wu[1,2]*, Junyu Chen[2], Wei Sun[3], David A. Hart[4], Paul W. Ackermann[2] and Aisha S. Ahmed[2,5]*

[1]Division of Spine Surgery, Department of Orthopaedic Surgery, Nanjing Drum Tower Hospital, The Affiliated Hospital of Nanjing University Medical School, Nanjing, China, [2]Department of Molecular Medicine and Surgery, Center for Molecular Medicine, Karolinska Institutet, Stockholm, Sweden, [3]Department of Orthopedic Surgery, China-Japan Friendship Hospital, Beijing, China, [4]Department of Surgery, Faculty of Kinesiology and the McCaig Institute for Bone & Joint Health, University of Calgary, Calgary, AB, Canada, [5]Department of Physiology, University of Helsinki, Helsinki, Finland

The suboptimal or protracted regeneration of injured connective tissues often results in significant dysfunction, pain, and functional disability. Despite the prevalence of the condition, few studies have been conducted which focused on biomarkers or key molecules involved in processes governing healing outcomes. To gain insight into injured connective tissue repair, and using the Achilles tendon as a model system, we utilized quantitative proteomic and weighted co-expression network analysis of tissues acquired from Achilles tendon rupture (ATR) patients with different outcomes at 1-year postoperatively. Two modules were detected to be associated with prognosis. The initial analysis identified inter-alpha-trypsin inhibitor heavy chain 4 (ITIH4) as a biomarker or hub protein positively associated with better healing outcomes. Additional analysis identified the beneficial role of ITIH4 in inflammation, cell viability, apoptosis, proliferation, wound healing, and for the synthesis of type I collagen in cultured fibroblasts. Functionally, the effects of ITIH4 were found to be mediated by peroxisome proliferator-activated receptor gamma (PPARγ) signaling pathways. Taken together, these findings suggest that ITIH4 plays an important role in processes of connective tissue repair and advocate for the potential of ITIH4 as a therapeutic target for injured connective tissue repair.

Trial registration: http://clinicaltrials.gov, identifiers NCT02318472, NCT01317160.

KEYWORDS

connective tissue, Achilles tendon rupture, ITIH4, prognosis, biomarker, therapeutic target

Introduction

Connective tissues such as tendon and ligament play a wide variety of functions in the joint (1). Moreover, mature connective tissues display impaired capability of regeneration, predisposing joints to degenerative diseases (2). The limited regenerative capability is mainly attributed to a paucity of cells and the relatively avascular or aneuronal nature of the adult tissues, leading to variable and often poor prognosis (3). While the above general perspective of connective tissue healing applies, some patients appear to heal with better outcomes than others (3). Despite such recent advancements, details regarding the pathways and biomarkers governing optimal healing after connective tissue injuries, are mostly unknown and remain to be elucidated.

The healing of connective tissue generally involves the contribution of a variety of cells infiltrating into the site of injury such as macrophages, fibroblasts, as well mesenchymal stem cells (4). Among these, fibroblasts play a crucial role from the early inflammatory to late regenerative healing phase by regulating inflammatory responses, extracellular matrix (ECM) deposition and remodeling as well as specific collagen (Coll) synthesis (5, 6). Collagens are the main component of the ECM and higher collagen type I (Col1) levels at the site of injury are reported as an indicator of better healing after connective tissue injuries (7).

Although connective tissue injuries can occur anywhere in the body, acute Achilles tendon rupture (ATR) is a frequent injury. ATR injuries are becoming more common and with a considerable long associated sick-leave and low frequency of players returning to their previous level of sports activity (8).

In recent years, significant progress has been made in exploring the underlying mechanisms of injured connective tissue healing (9). By using mass spectrometry (MS) based advanced proteomic techniques, our research group has recently identified elongation factor-2 (eEF2) at the early inflammatory healing phase and complement factor D (CFD) at the proliferative healing phase, as potential healing biomarkers predictive of patient outcomes with ATR (3). These biomarkers exhibited differential expression patterns among good and poor outcome patient subgroups. These studies are continuous, using diverse bioinformatic approaches for analysis of the proteomic data.

In the present study, we used a weighted co-expression network analytical approach with the MS proteomic data collected from tissue samples taken at the time of surgery to further characterize the basis for the differences in outcomes between patient subsets. The network-based co-expression analysis of proteomic data approach identifies modules specifically related to the prognosis and subsequently detected prognostic biomarkers or hub proteins. Identified biomarkers/hub proteins were further subjected to Gene ontology (GO) enrichment and Kyoto Encyclopedia of Genes and Genomes (KEGG) pathway analysis to ascertain their biological functions and specific signaling pathways leading to tissue repair. Thus, employing the network proteomic approach may provide new insights regarding specific molecules that may be contributing to more optimal outcomes after endogenous healing of the Achilles tendon.

Materials and methods

This study was conducted after approval from the Regional Ethical Review Committee in Sweden (Reference no. 2009/2079-31/2: 2013/1791-31/3) and followed all guidelines according to the Declaration of Helsinki. The written informed consent was acquired from all patients.

Subjects and sampling

Following the inclusion and exclusion criteria as described previously (10), 40 patients with acute ATR who underwent reconstruction surgery with the same surgical protocol were consecutively included in the present study. During the surgery, tendon biopsies were taken from the ruptured area and stored at minus 80^{o} C until proteomic analysis was performed. All the samples were collected within 2-7 days of the ATR injury. Postoperatively, all patients received the same rehabilitation program.

Patient reported outcomes

Patient-reported outcomes were evaluated 1-year postoperatively using validated questionnaires: Achilles Tendon Total Rupture Score (ATRS). The ATRS consists of 10 sub-scales such as strength in tendon, tiredness in the tendon, stiffness in tendon, pain in tendon, limitations in activity of daily life (ADL) assessing limitations on uneven surface, stairs, running, jumping and loss in physical work (11). Each sub scale ranges from 0 to 10 where 0 = worst and 10 = best outcome with no limitation. The maximum ATRS is 100, and a score higher than 80 was regarded as indication of a good outcome (10).

Functional outcomes

The functional outcomes were measured using the Heel-rise Test (HRT) at 1-year post-surgery. HRT is a validated test, indicating the outcome of strength and endurance of the affected gastrocnemius-soleus complex (12, 13). The HRT was performed on one leg with the patient standing on a box with a 10° incline. Patients were instructed to perform as many maximal height heel-rises as possible and as many heel-rise repetitions as possible. All the results, including the number of heel-rises, the height of every single heel-rise, the total work in joules (total distance × body weight), the time and the power (work/time) were recorded for analysis. The Limb Symmetry Index (LSI) was used to show the ratio between the injured and contralateral uninjured leg and results are presented in a percentage (injured/contralateral × 100).

Mass spectrometry

Protein extraction and digestion of tissue samples

The methods used were the same as reported previously (3). Frozen samples were powdered by Mikro-dismembrator (B. Braun

Biotech International, Germany) on dry ice. Powdered tissue samples were solubilized in 8M urea and 100 mM NaCl with 1% ProteaseMAX (Promega) in 100 mM ammonium bicarbonate (AmBic) and mixed vigorously. Low binding silica beads (400 µm, Ops Diagnostics, Lebanon NJ) were added to each sample and vortexed at high speed. Subsequently, samples were subjected twice to disruption on a Vortex Genie disruptor for 2 min before addition of AmBic, urea and NaCl. Following centrifugation, the 50 mM AmBic was added and vortexed vigorously. Proteins were then reduced with 100 mM dithiothreitol in 50 mM AmBic, incubated at 37°C and alkylated with 100 mM iodoacetamide in 50 mM AmBic. The reaction was stopped with formic acid and the samples were then cleaned on a C18 Hypersep plate (bed volume of 40 µL, Thermo Scientific) and dried in a vacuum concentrator (miVac, Thermo Scientific).

Reversed phase liquid chromatographic-MS/MS analysis

Briefly, RPLC of peptides were performed on a C18 EASY-spray and C18 trap columns connected to an Ultimate 3000 UPLC system (ThermoFisher). Mass spectra were acquired on an Q Exactive HF mass spectrometer (ThermoFisher), targeting 5 x 10^6 ions with maximum injection time of 100 ms, followed by data-dependent higher-energy collisional dissociation (HCD) fragmentations from precursor ions with a charge state.

Proteomic data analysis, protein identification and quantification

Raw files were imported to Proteome Discoverer v2.3 (ThermoFisher) and analyzed using the SwissProt protein database with the Mascot v 2.5.1 (MatrixScience Ltd., UK) search engine. MS/MS spectra were matched with The Human Uniport database (last modified: 3 September 2020; ID: UP000005640; 75,777 proteins) using the MSFragger database engine. Protein abundance was calculated based on normalized spectrum intensity (LFQ intensity), and an intensity-based absolute quantification (iBAQ) algorithm was used for normalization.

Weighed co–expression network analysis

Following previously described procedures of WGCNA (14), a weighted protein co-expression network was generated using the protein abundance network of unique proteins. The soft power applied for gene modules identification was selected to 7. Correlation coefficients between the modules and traits were calculated using Pearson's method. Prognosis-related protein modules were defined as those with a P value less than 0.05. All proteins from the selected modules were then visualized into a protein-protein interaction (PPI) network using the Cytoscape software (http://cytoscape.org/).

Functional enrichment analysis

Enrichment analysis of proteins was performed by the 'clusterProfiler' package (15). Gene ontology (GO) term analysis consists of biological processes (BP), cellular components (CC), molecular function (MF). Pathway enrichment analysis was conducted based on Kyoto Encyclopedia of Genes and Genomes (KEGG). $P < 0.05$ was considered statistically significant.

Identification of hub proteins

The hub proteins of a selected module were determined through an absolute value of the Module Membership (MM) > 0.8 and a Gene Significance (GS) > 0.1. Moreover, the hub proteins in selected modules were calculated and identified using the CytoHubba plugin in the Cytoscape software (16). The common hub proteins identified by the use of three different methods, WGCNA, MCC, and Degree, were investigated further.

Gene set enrichment analysis

Gene set enrichment analysis (GSEA) was performed by the 'clusterProfiler' package (15) to identify enriched hub protein-related signaling pathways and 'c2.cp.kegg.v7.0.symbols.gmt' was selected as the reference gene set. A false discovery rate (FDR) < 0.25 and $p < 0.05$ was considered as significant enrichment.

Antibodies and reagents

The antibodies used in the present study were as follows: anti-COL1A1 (72026) and anti-PPARγ (C26H12) from Cell Signaling Technologies (Boston, USA); and anti-ITIH4 (ab180139) from Abcam (Cambridge, UK). Secondary antibodies were either goat Alexa 488 (A-11008) or 594 (A-11012) obtained from ThermoFisher (Oxford, UK). Lipopolysaccharide (LPS, L2630) was purchased from Sigma (Steinheim, Germany).

Cell culture and treatment

The cells of the human dermal fibroblast cell line (fHDF/TERT166) were purchased from Evercyte (Vienna, Austria) and were cultured in Dulbecco's Modified Eagle Medium/Nutrient Mixture F-12 (DMEM/F-12, 10565018, Gibco) supplemented with 10% fetal bovine serum (FBS) and 1% antibiotics (penicillin-streptomycin) at 37 °CC in a 5% CO_2 humidified incubator. Different concentrations of LPS diluted in sterilized deionized water, varied from 0.01 µg/ml to 50 µg/ml, were used for cell activation experiments. Experiments were performed in triplicates and repeated at least three times independently.

Enzyme-linked immunosorbent assay

Enzyme-linked immunosorbent assays (ELISA) were used to investigate the synthesis of ITIH4 and interleukin-6 (IL-6). According to the instructions of the manufacturers, cell culture

supernatant levels for ITIH4 (DY8157-05, R&D) and IL-6 (BMS213-2, ThermoFisher) were assessed, respectively. The absorbance was measured at 450 nm using a microplate reader (SpectraMax iD3, Molecular Devices).

Cell viability assay

The PrestoBlue™ Cell Viability Reagent (A13261, ThermoFisher) was utilized to estimate cell viability at 24hr, 48hr, and 72 hr of culture. PrestoBlue™ solution (10 µL) was added to the cells in each well and incubated at 37 °C for 1 hr. The fluorescence of each well was subsequently evaluated at 560/590 nm using a microplate reader (SpectraMax iD3, Molecular Devices).

Cell proliferation assay

To confirm the changes in the proliferation rates, the EdU-488 Cell Proliferation Kit (C10337, ThermoFisher) was used according to the manufacturer's instructions. The results were assessed by fluorescence microscopy (ZOE Cell Imager, Bio-Rad). ImageJ software (NIH, Bethesda, MD, USA) was then used to analyze the cell proliferation rate.

Apoptosis and caspase activity assay

To determine whether cells were live (green) or dead (red), cells were stained with the LIVE/DEAD Cell Imaging kit (R37601, ThermoFisher) according to the manufacturer's instructions. Caspase activation was investigated using CellEvent™ Caspase3/7 detection reagent (C10423, ThermoFisher) per the manufacturer's instructions. Both assays were imaged using fluorescence microscopy (ZOE Cell Imager, Bio-Rad) and analyzed by ImageJ software (NIH, Bethesda, MD, USA).

In vitro model of wound healing

To observe the migration of the fibroblasts, the *in vitro* wound healing scratch assay was utilized (17). A scratch was created on a cell monolayer by using a 10 µL pipette tip. At 0 h and 24 h, the width of the scratch was assessed, and the rate of scratch recovery was determined. Migration activity was imaged under an optical microscope (ZOE Cell Imager, Bio-Rad) and analyzed by ImageJ software (NIH, Bethesda, MD, USA).

Immunofluorescence analysis

Briefly, for the immunofluorescence analysis, cells were fixed in 4% paraformaldehyde for 15 min. After permeabilization with 0.1% Triton X-100 for 15 min, the cells were then blocked with 3% bovine serum albumin for 1 hr and were subsequently, incubated with a primary antibody to COL1A1 or PPARγ overnight at 4 °C followed by incubation with fluorescent-conjugated secondary antibodies for 1 hr. The cell nuclei were stained by Hoechst 33342 (ThermoFisher) for 30 min. Images were captured under a fluorescence microscopy (ZOE Cell Imager, Bio-Rad) and analyzed by ImageJ software (NIH, Bethesda, MD, USA).

Cell transfection

The ITIH4 siRNA and negative controls were obtained from ThermoFisher (AM16708). Lipofectamine™ RNAiMAX Transfection Reagent (13778030, ThermoFisher) was used to introduce siRNA into fibroblasts according to the manufacturer's protocol. After transfection with ITIH4 siRNA, or scramble control siRNA, fibroblasts were stimulated with LPS.

Statistical analysis

All statistical analyses were performed using R software (version 4.0.4; R Core Team 2020, Vienna, Austria) or GraphPad Prism software (version 8.0; GraphPad Software Inc., La Jolla, CA, USA). Continuous variables were expressed as the mean ± SD values and compared with the Student's t-test or one-way analysis of variance. Categorical variables were expressed as frequencies and proportions and compared with the chi-square and Fisher exact tests. Univariate analysis of hub proteins was performed using Logistic regression models to determine the hub proteins associated with prognosis. Receiver Operating Characteristics (ROC) curve analysis and area under the ROC Curve (AUC) was performed and calculated. Meanwhile, the optimal cutoffs were identified by maximizing Youden's J index. Data with a P value < 0.05 was considered significant.

Results

Clinical parameters

The study included a total of 40 patients with ATR undergoing tendon reconstruction surgery. At one-year post-surgery during the follow-up, all patients were assessed for healing outcomes based on their ATRS. To explore the underlying mechanism of connective tissue repair, patients were divided into groups of good (ATRS > 80; n = 20) and poor healing outcomes (ATRS < 80; n = 20). No statistically significant differences were noted between the good and poor outcome groups regarding age, sex, and body mass index. However, the ATRS for the good outcome group (95.3±4.0) was significantly higher than the ATRS for the poor outcome group (61.5±9.67). The clinical parameters for all patients are presented in Table S1 and the study design is presented in Figure 1.

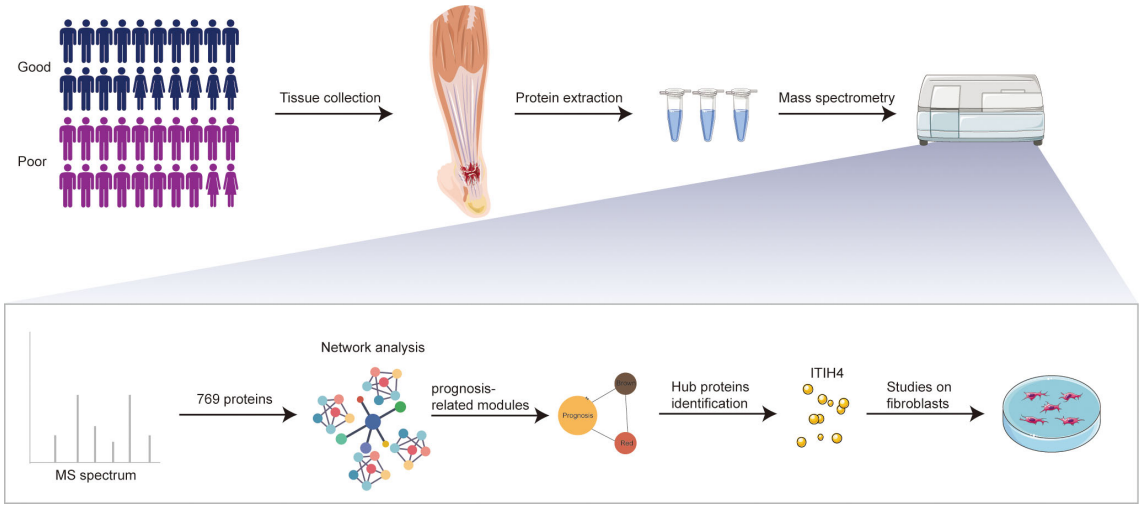

FIGURE 1
Schematic overview of experimental design. Quantitative proteomic analysis of the tendon tissues from ATR patients with different outcomes was performed based on RPLC-MS/MS, followed by network analysis and related *in vitro* studies on fibroblasts.

Proteomics and co–expression protein analysis

The use of RPLC-MS/MS analysis enabled the identification of a total of 855 unique proteins in all studied patients. These included 769 shared proteins across the good and poor outcome groups. A weighted co-expression network analysis was performed to identify the relationship between the protein abundance and clinical outcome. Using sample clustering to detect outliers, a β value of 7 as the first value that gave an R2 of ≥0.8, was selected as the soft-threshold to fulfill the scale-free approximation criterion (Figures 2A, B). A total of 14 strongly co-expressed modules were identified through the dynamic tree cutting method (Figures 2C, D). Among these, the brown and red modules were observed to be significantly related to prognosis (Figures 2E, F) and were highly expressed in good outcome patients (Figure 2G).

GO enrichment analysis and KEGG pathway analysis

In the next step, the brown and red modules were subjected to further bioinformatic analysis. The functional enrichment analysis revealed that most annotations in the brown module were involved in numerous biological and cellular processes such as inflammation, metabolism, regulation of protein activation, ECM metabolism as well in collagen-containing extracellular matrix and regulation of catalytic activity (Figure 3A). Further analysis by KEGG identified enriched signaling pathways which included the complement and coagulation cascades, peroxisome proliferator-activated receptors (PPAR) and cholesterol metabolism (Figure 3B).

The enrichment analysis of the red module revealed ECM organization and collagen-containing ECM as the most significant biological and cellular processes. The biological pathways highly enriched in the red module included ECM receptor interaction and focal adhesion. (Figures 3C, D).

Identification of relevant hub proteins and related pathways

Based on an absolute value of the module membership (MM) > 0.8 and gene significance (GS) > 0.1, 24 hub proteins from the brown and 23 from the red module were selected for further evaluation (Figures 4A, B). In the next step, the network was imported into the Cytoscape software and CytoHubba plugin was employed. By using the MCC and Degree methods, the top 10 hub proteins from the brown and red modules were detected along with their interaction as shown in Figures 4C, D. Subsequently, three common proteins, inter-alpha-trypsin inhibitor heavy chain 4 (ITIH4), Serpin family F member 1 (SERPINF1), and immunoglobulin lambda variable 1-47 (IGLV1-47), were detected (Figure 4E). Among these, the ITIH4 synthesis was found to be elevated in the good- compared to the poor outcome groups (Figure 4F). ITIH4, SERPINF1 and IGLV1-47 were further subjected to logistic regression analysis, which also identified a low odds-ratio 0.22 (0.04-0.92) of risk of poor prognosis with ITIH4 (Figure 4G). Moreover, the prognostic reliability of ITIH4, SERPINF1 and IGLV1-47 was studied by the ROC curve analysis which demonstrated ITIH4 with the highest area under the curve (AUC) value of 0.71 as a strong predictor of good clinical outcome (Figure 4H).

Through maximizing Youden's J index, the optimal cutoff was identified, and the patients were divided into two groups based on risk levels of poor prognosis (Figure 4I). As Col1 is the main collagen subtype of tissue repair, the relationship between ITIH4 and collagen type 1 A1 (COL1A1) was explored further. Our bioinformatic analysis showed elevated COL1A1 levels in the

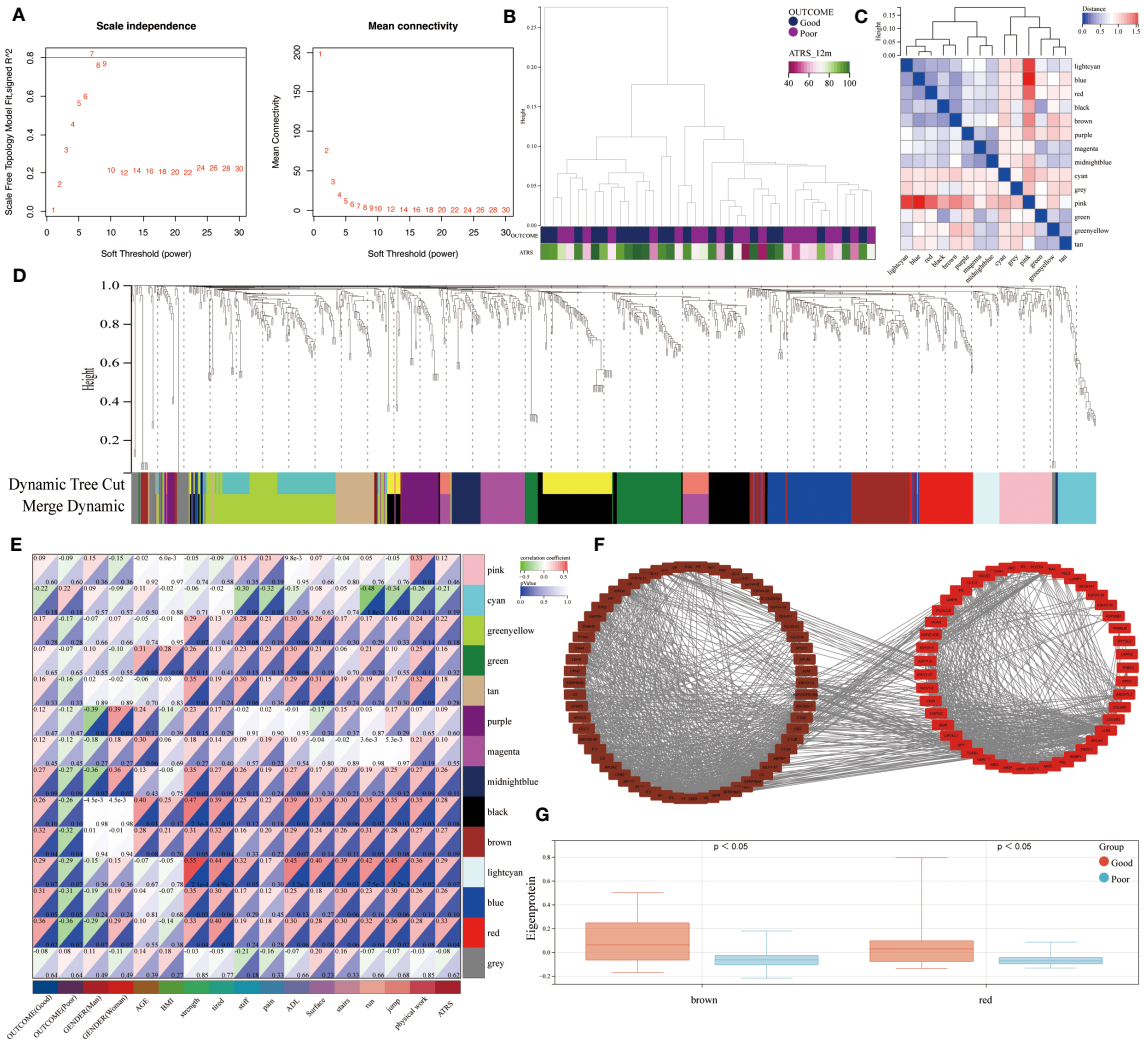

FIGURE 2
Identification of outcome-related modules and functional enrichment. **(A)** Scale-free topology index and the mean connectivity for each power value between 1 and 30. **(B)** Clustering dendrogram and clinical traits based the expression data between patients with different outcomes. **(C)** Eigengene adjacency heatmap of each module, representing the correlation between the modules. **(D)** Cluster dendrogram of the identified co-expression modules. **(E)** Heatmap of the correlation between modules and clinical traits. Each cell contains the corresponding correlation coefficient and p value. **(F)** Network of brown and red modules. **(G)** The module expressions between patients with different outcomes.

group with low compared to high-risk, indicating the positive effects of ITIH4 levels on collagen synthesis (Figure 4I).

To identify the potential pathways for connective tissue repair, GSEA was performed which selected PPAR as the highest ranked signaling pathway with an enrichment score of 0.84 (Figure 4J). Taken together, these analyses selected ITIH4 as the best predictive biomarker and PPAR as an associated signaling pathway, findings which were then subjected to further targeted investigations.

ITIH4 regulates inflammatory responses in human fibroblasts

The bioinformatic analysis identified inflammation as one of the crucial biological processes for connective tissue repair especially for annotations from the brown module. To study the role of ITIH4 in intracellular inflammatory processes, ITIH4 synthesis was knocked down by siRNA-ITIH4 in the human fibroblast cell line, fHDF/TERT166 (Supplementary Figures 1A, B). The effects of LPS on ITIH4 were then studied and it was observed that LPS treatment elevated ITIH4 levels in a dose-dependent manner (Figure 5A and Supplementary Figures 2 A-C). Notably, there was a decrease in ITIH4 after simulations of LPS at concentrations of 10 and 20µg/ml after 48 and 72h. This may be attributed to high concentrations of LPS treatment leading to an increase of cell death, which, in turn, decreased the secretion of ITIH4 after 48 and 72 h. In the next step, si-ITIH4 treated fibroblasts were stimulated with LPS and the synthesis of a classical marker of inflammation; IL-6 was assessed. Interestingly, dual effects were observed for both LPS and ITIH4 (Figure 5B, Supplementary Figures 3A, B) on IL-6 synthesis, highlighting a potential role of this biomarker during the early inflammatory stage of Achilles tendon repair.

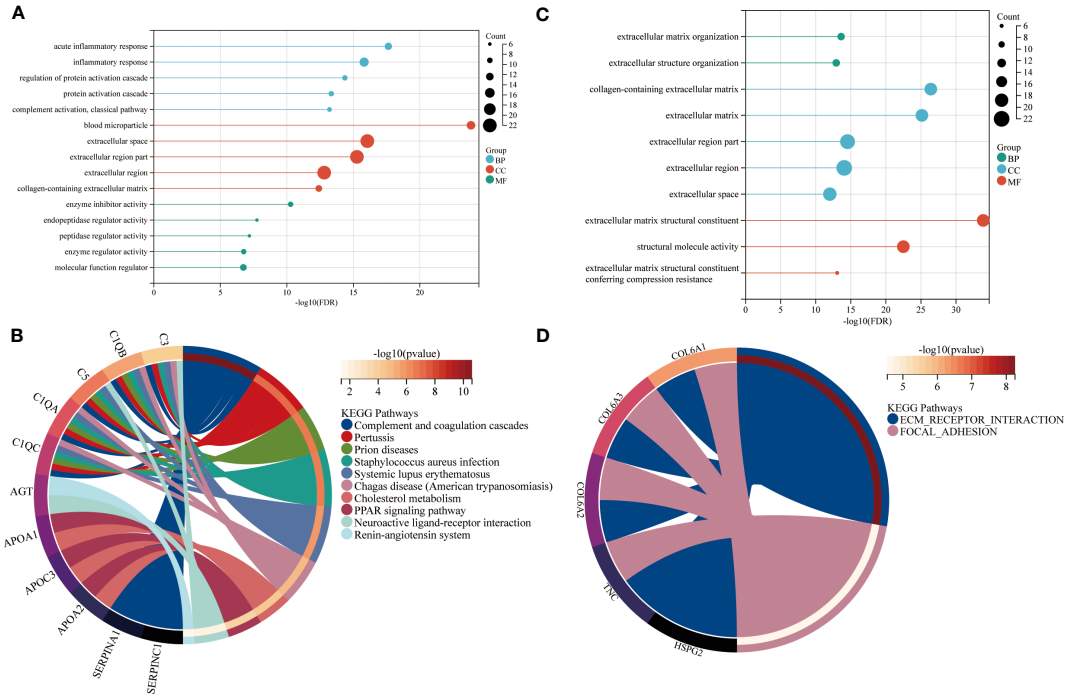

FIGURE 3
Functional enrichment of brown and red modules. GO and KEGG enrichment analysis of **(A, B)** brown and **(C, D)** red module. Enrichment factor indicating ratio of pathway related proteins in relation to all identified proteomes. Size of bubble represents the number of proteins with the related function. BP = biological process, CC = cellular component, MF = molecular function.

ITIH4 can regulate human fibroblast viability

Metabolic processes are crucial for cell survival as emphasized by the bioinformatic analysis. To determine the potential role of ITIH4 on metabolic activity, cell viability was assessed during LPS-induced inflammatory conditions on the human fibroblasts *in vitro*. The analysis revealed that acute inflammatory responses negatively impact cell viability, while relatively long-term (72 hr) inflammatory responses at lower doses (0.01-0.1 µg/ml) promote cell viability (Supplementary Figures 4A-C). Furthermore, the effects of ITIH4 on cell survival were investigated, and the results indicated that knockdown of ITIH4 alone significantly led to decreased cell viability of fibroblasts at 48 and 72 h (10-50 nM) (Supplementary Figures 4D-F). Additional analysis revealed that LPS-stimulated fibroblasts with ITIH4 knocked down led to further decreases in cell viability, highlighting a possible protective role for ITIH4 on cell survival and metabolism (Figure 5C).

ITIH4 may regulate connective tissue repair by influencing cell death and apoptosis

To explore a role for ITIH4 in apoptosis, the effect of si-ITIH4 treatment on LPS-induced apoptosis in human fibroblasts was evaluated. The analysis of activated Caspase-3/7 staining demonstrated that LPS alone or knockdown of ITIH4 promoted the activation of Caspase-3/7 in fibroblasts (Supplementary Figures 5A-D). During LPS treatments, knockdown of ITIH4 led to higher increases in activation of Caspase-3/7 in the treated fibroblasts than were observed in the LPS group with intact fibroblasts (Figures 5D, E). The results were confirmed further by live/dead assays, which showed that treating cells with LPS alone or following knockdown of ITIH4 leads to a decrease in the cell survival rate (Supplementary Figures 6A-D). Consistently, following LPS treatments, knockdown of ITIH4 resulted in a higher apoptosis rate (Figures 5F, G). Collectively, these results suggest that ITIH4 has a cytoprotective role in LPS-treated fibroblasts.

ITIH4 may influence inflammatory healing processes via modulation of cell proliferation

To assess the effect of ITIH4 on human fibroblast proliferative activity, the proliferation rate after ITIH4 knockdown and/or LPS treatment *via* EdU assays was investigated. The results suggested that LPS alone has a pro-proliferative effect in the long term (Supplementary Figures 7A, B). Conversely, knockdown of ITIH4 alone leads to reduction in the proliferation rate of the fibroblasts

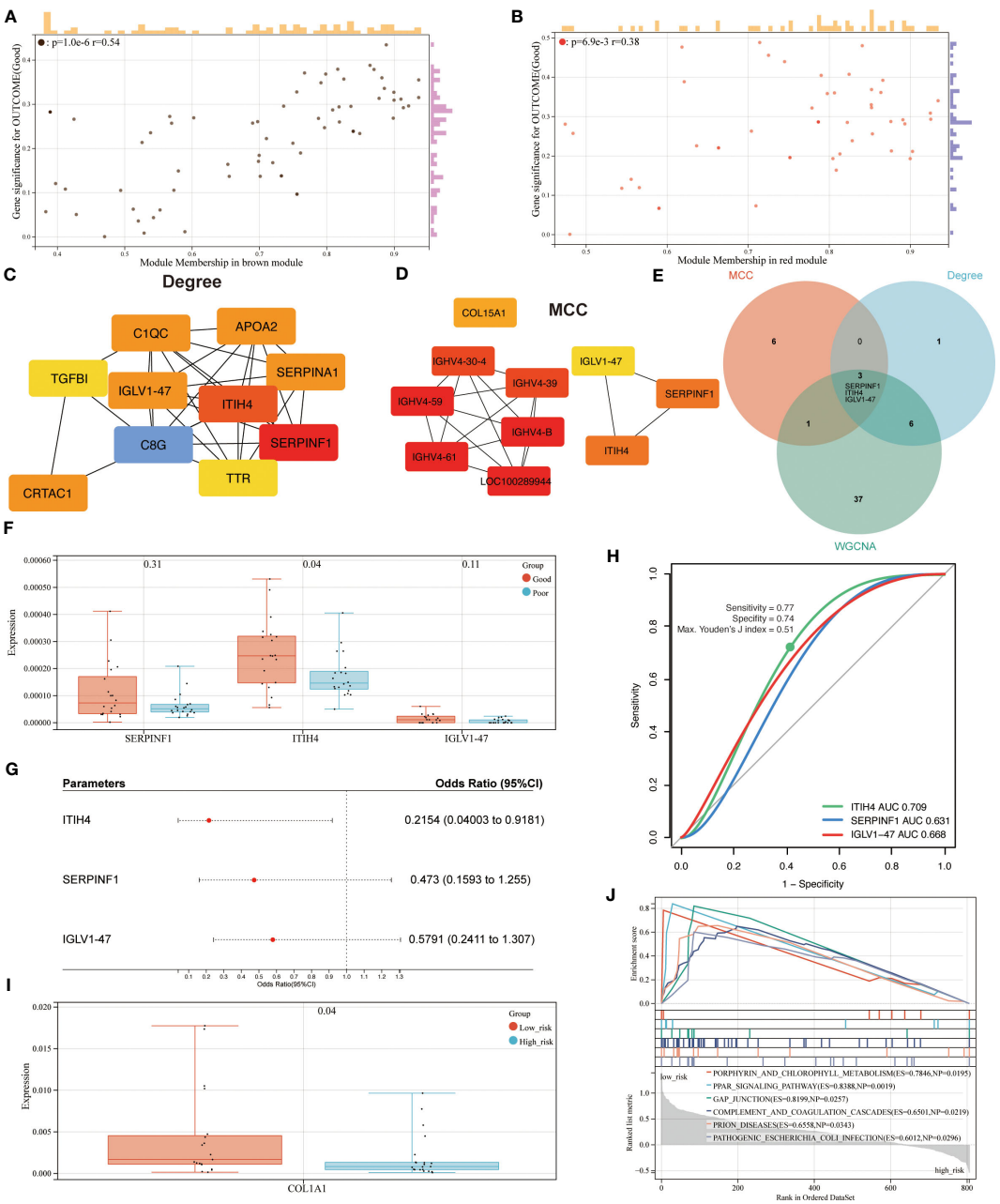

FIGURE 4
Identification of hub proteins and related pathways. **(A)** Scatterplot of gene significance (GS) versus module membership (MM) for the brown module. **(B)** Scatterplot of GS versus MM for the red module. **(C, D)** Top 10 hub proteins of two modules identified *via* Degree and MCC, respectively. **(E)** Venn diagram of common hub proteins *via* WGCNA, Degree, and MCC methods. **(F)** Synthesis of hub proteins between patients with different outcomes *via* mass spectrum. **(G)** Univariate analysis of hub proteins *via* Logistic regression models **(H)** ROC curve analysis of hub proteins. **(I)** Synthesis of COL1A1 between patients with different risks *via* mass spectrum. **(J)** GSEA analysis of enriched pathways between patients with different risks.

(Supplementary Figures 7C, D). Following LPS treatment at a relatively low concentration (0.1μg/ml), knockdown of ITIH4 inhibited the proliferative activity of the cells (Figures 6A, B). However, knockdown of ITIH4 enhanced cell proliferative activity when LPS was applied at relatively high concentrations (10-20 μg/ml) (Figures 6A, B). In general, the effect of ITIH4 on fibroblasts proliferation appears to dependent on the level of inflammation induced by LPS in this *in vitro* model.

ITIH4 may affect inflammatory healing processes via influencing cellular migration

Fibroblast migration at the site of injury is an essential process associated with wound healing (18). With the aim to assess the potential involvement of ITIH4 in this process, an inflammatory *in vitro* model of wound healing was used by creating a scratch in the LPS-stimulated monolayer cultures of the fibroblast cell line treated

10.3389/fimmu.2023.1191536

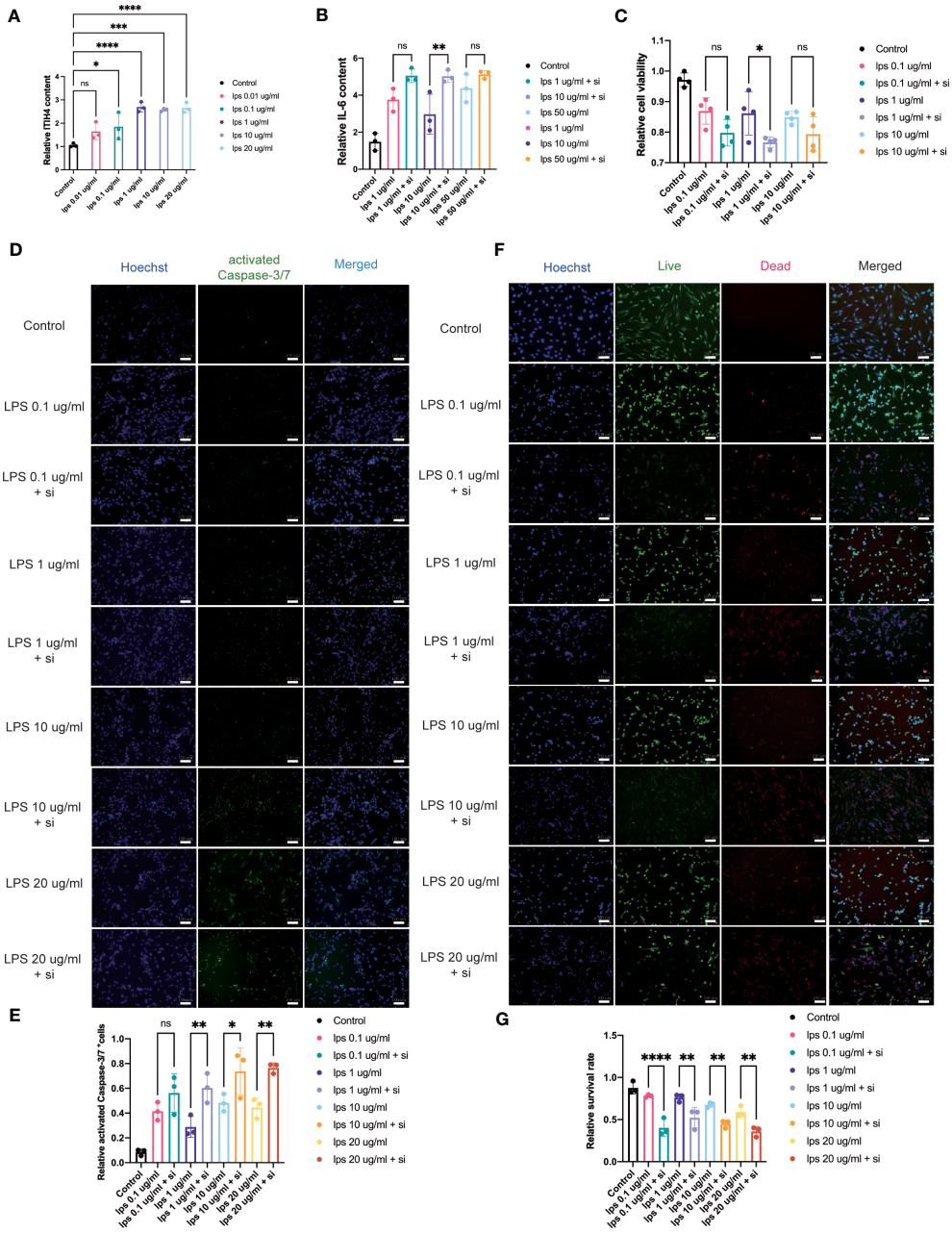

FIGURE 5
Influence of knockdown of ITIH4 on inflammation, cell viability, and apoptosis of fibroblasts treated with LPS. **(A)** Relative synthesis of ITIH4 investigated through ELISA analysis (n=3). Fibroblasts were transfected with 50 nM ITIH4 siRNA. At 24 h after transfection, fibroblasts were subjected to 24 h of LPS treatment with different concentrations. **(B)** Relative synthesis of IL-6 *via* ELISA analysis (n=3). **(C)** Cell viability assessed by the PrestoBlue™ Cell Viability Reagent (n= 4). **(D, E)** Representative images and quantitative analysis of Caspase-3/7 activation. (n=3). **(F, G)** Representative images and quantitative analysis of cell death assessed by live/dead assay. (n=3). Scale bar = 100 μm. ns, not significant; * P < 0.05; ** P < 0.01; *** P < 0.001; **** P < 0.0001.

with and without si-ITIH4. It was observed that LPS-stimulation can promote cell migration even at relatively low concentrations (0.1-10 μg/ml), whereas knockdown of ITIH4 inhibits the rate of cell migration (Supplementary Figures 8A-D). The experimental observations highlighted a reduced rate of cell migration in LPS-stimulated fibroblasts when treated with si-ITIH4 in comparison to untreated cells (Figures 6C, D). These findings further support a potential beneficial role for ITIH4 in wound healing during the inflammatory phase of healing.

ITIH4 can regulate collagen synthesis by human fibroblasts

Col1 is the main constituent of the connective tissue matrix and an essential component of the ECM organization. The bioinformatic analysis highlighted the process of collagen containing matrix production as one of the most enriched biological processes leading to a good healing outcome (Figures 3A, C). Additionally, patients with higher ITIH4

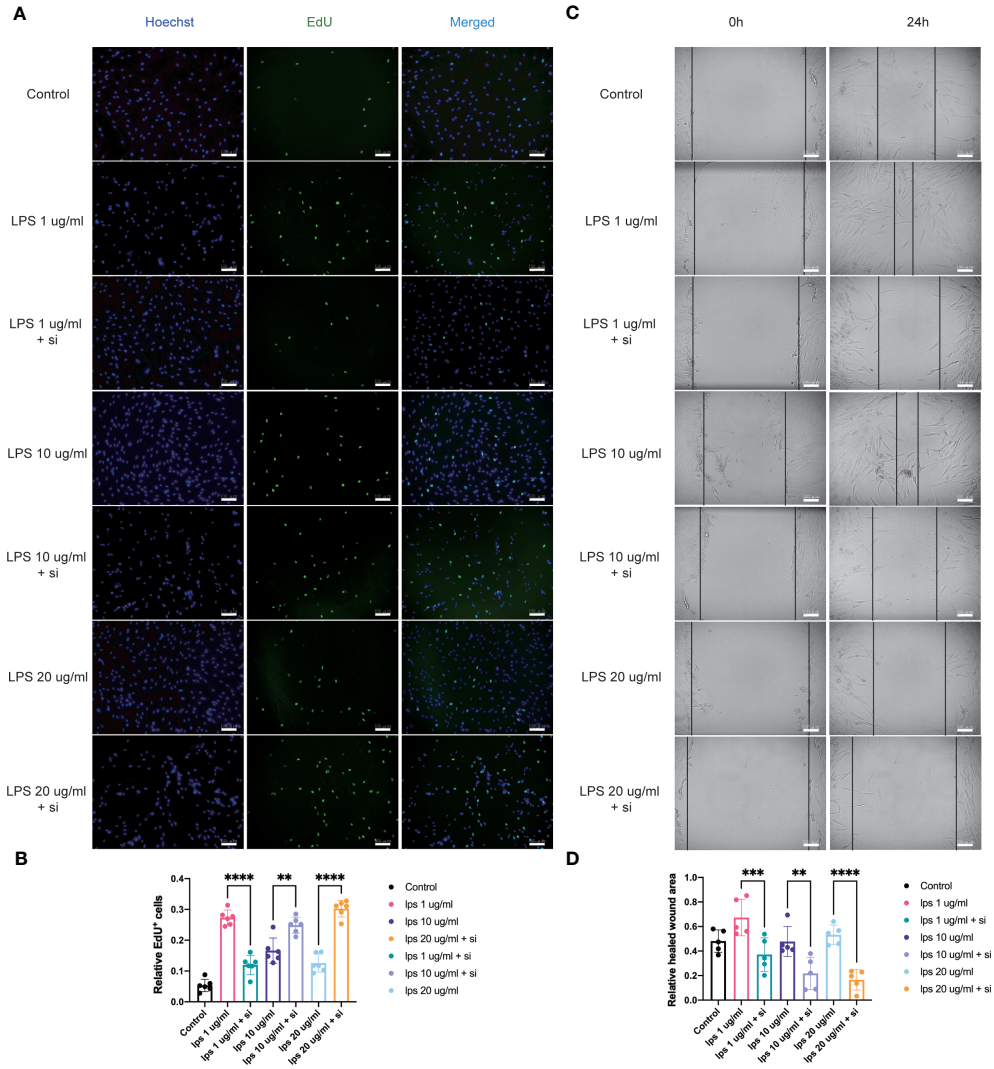

FIGURE 6
Influence of knockdown of ITIH4 on proliferation and migration of fibroblasts treated with LPS. Fibroblasts were transfected with 50 nM ITIH4 siRNA. At 8 h after transfection, fibroblasts were subjected to 72 h of LPS treatment with different concentrations. **(A, B)** Representative images and quantitative analysis of proliferation rate assessed by EdU assay. (n=6). At 24 h after transfection, a scratch was created, and fibroblasts were subjected to 24 h of LPS treatment with different concentrations. **(C, D)** Representative images and quantitative analysis of cell migration rate assessed *via* a wound healing assay. (n=5). Scale bar = 100 μm. ns, not significant; * P < 0.05; ** P < 0.01; *** P < 0.001; **** P < 0.0001.

synthesis exhibited elevated COL1A1 levels in surgical biopsies (Figure 4I). To further evaluate the effect of ITIH4 on Col1 synthesis during the inflammatory stage of healing, analysis of anti-Col1 staining using immunofluorescence was performed. The results indicated that relatively, low grade inflammation induced by LPS (0.1-20 μg/ml) can lead to an upregulation of COL1A1 synthesis whereas higher LPS concentrations (50 μg/ml) has a negative impact on COL1A1 synthesis (Supplementary Figures 9A, B). Interestingly, ITIH4 knockdown by si-ITIH4 alone was observed to reduce COL1A1 synthesis (Supplementary Figures 9C, D). Following LPS treatments, knockdown of ITIH4 suppressed the beneficial effects of LPS, leading to a downregulation of COL1A1 synthesis (Figures 7A, B). Thus, ITIH4 synthesis is positively correlated with Col1A1 synthesis in these cells.

Association between ITIH4 and the PPAR signaling pathway

The bioinformatic analysis identified PPAR as the most highly ranked signaling pathway associated with good healing outcomes after ATR. To confirm a potential association between PPAR and ITIH4 synthesis, immunofluorescence analysis with anti-ITIH4 and anti-PPAR-gamma was used with LPS-stimulated fibroblasts in the presence or absence of ITIH4. The results showed that LPS treatment alone downregulated the synthesis of PPARγ at relatively low concentrations (1-10 μg/ml), while at a relatively high concentration (50 μg/ml) it upregulated PPARγ synthesis. However, the knockdown of ITIH4 by si-ITIH4 significantly increased PPARγ synthesis in LPS-stimulated fibroblasts

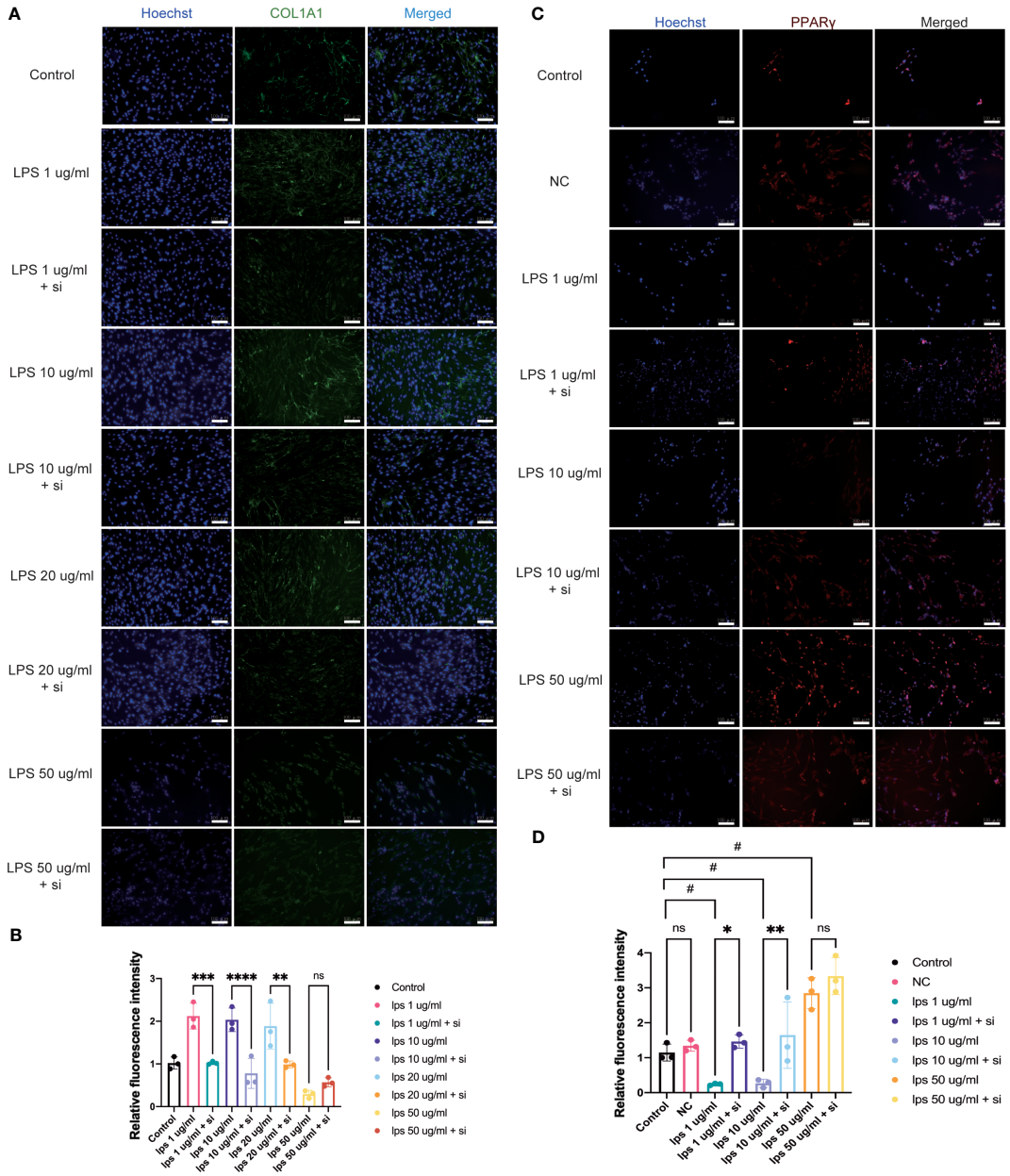

FIGURE 7
Effect of knockdown of ITIH4 on levels of collagen I and PPARγ in fibroblasts treated with LPS. Fibroblasts were transfected with 50 nM ITIH4 siRNA. At 8 h after transfection, fibroblasts were subjected to 48 h of LPS treatment with different concentrations. **(A, B)** Representative images and quantitative analysis of synthesis of COL1A1 *via* immunofluorescence analysis. (n=3). **(C, D)** Representative images and quantitative analysis of synthesis of PPARγ via immunofluorescence analysis. (n=3). Scale bar = 100 μm. ns, not significant; *,# P < 0.05; ** P < 0.01; *** P < 0.001; **** P < 0.0001.

(Figures 7C, D). Thus, the presence or absence of ITIH4 can impact synthesis of components of the PPAR pathway.

Discussion

In the present studies, we have identified prognostic biomarkers and pathways of connective tissue repair by using in-depth proteomic and co–expression network analysis of MS data acquired from ruptured human Achilles tendon tissues early after injury. A total 14 modules were identified from which 2 were determined to be significantly related to healing prognosis after ATR. Further analysis of elements in these prognostic modules identified ITIH4 as a prominent biomarker associated with better patient-reported outcomes. Functionally, the beneficial effect of ITIH4 on Col1 synthesis were observed to be potentially mediated by the PPARγ signaling pathway.

The first major finding was that ITIH4, a 120 KDa glycoprotein that is a component of the inter-alpha trypsin inhibitor, is a potential biomarker and hub protein prognostic of long-term

Achilles tendon healing. Previously, prognostic roles for elevated ITIH4 synthesis have been identified in inflammatory and infectious diseases with an elevated ITIH4 synthesis (19). In addition, higher synthesis of ITIH4 in patients with chronic hepatitis B-virus or HBV-related hepatocellular carcinoma patients was reported to be related to good prognostic outcomes in these diseases (20, 21). Here, by using advanced MS techniques along with deep bioinformatics, a prognostic role for ITIH4 in human Achilles tendon healing with good sensitivity and specificity was identified.

Functionally, a role for ITIH4 has previously been reported in liver metabolic processes, as well in inflammatory processes and neutrophil migration in arthritic joints (19, 22–24). As well, ITIH4 has also been reported to be a serologic biomarker in rheumatoid arthritis (25). In these disorders, the role of ITIH4 as an acute phase protein has been highlighted. Recently, the function of ITIH4 as a protease inhibitor has been reported, leading to inhibition of a lectin pathway of complement (26). Interestingly, these biological functions were also found to be highly enriched in the identified red and brown modules of the current studies, two modules identified as prognosis-related from the present bioinformatic analysis.

The process of connective tissue repair is often divided into overlapping phases of inflammation, proliferation, provisional matrix deposition, and remodeling. Notably, in the present study, connective tissues from ATR patients could only be collected from the early inflammatory phase at the time of surgery due to ethical considerations. During this stage, higher synthesis levels for ITIH4 in injured tissues were indicative of better recovery outcomes. Interestingly, previous studies have shown that ITIH4 also has a close association with IL-6 and LPS (19, 22). Consistent with those studies, we have demonstrated that in LPS-stimulated fibroblasts, ITIH4 synthesis was increased in a dose-dependent manner. Meanwhile, the secretion of IL-6, was promoted by ITIH4 deficiency. These findings are also consistent with previous observations that higher IL-6 levels delay the healing processes and negatively impact tissue regeneration (27, 28). It was further demonstrated that knockdown of ITIH4 aggravated LPS-induced inflammation, reducing cell viability and apoptosis. Taken together, these findings support a beneficial role for ITIH4 in healing, in part, by regulating IL-6 synthesis during the acute inflammatory phase of connective tissue repair after injury.

A role for ITIH4 in cell growth and regeneration has also been demonstrated in recent publications (29, 30). Consistent with such roles, our bioinformatic analysis identified various proteins that were enriched with metabolism-related annotations. To confirm the bioinformatic analysis, EdU assays were utilized to investigate the effect of ITIH4 on cell proliferation. Moreover, the experimental findings indicated that LPS alone can promote cell proliferation in accordance with previous publications (31, 32). Interestingly, in fibroblasts treated with different concentrations of LPS, knockdown of ITIH4 showed opposing roles on cell proliferation. The results of our studies may potentially be attributed to the presence of different isoforms of ITIH4 which we could not identify from the current methodologic approach. A previous study demonstrated that two isoforms of ITIH4 possess different functions on cell proliferation (22). The authors revealed that the long isoform of ITIH4 significantly inhibits cell proliferation, whereas the short isoform had the opposite effect (22). Taken together, the effect of ITIH4 on cell proliferation may depend on the level of inflammation as well as the isoform of ITIH4 that is present at the site. However, this conclusion is still in need of further confirmation with regards to Achilles tendon healing.

To mimic the inflammatory phase of healing, an inflammatory *in vitro* wound healing model was used. In accordance with previous publications (33, 34), the results obtained also showed that LPS may promote wound healing in a dose-dependent manner. It has been demonstrated that LPS treatment can potentially affect the healing processes by accelerating the resolution of inflammation, increasing immune infiltration, and altering the secretion of a number of mediators (35, 36). However, the beneficial effects of relatively low concentrations of LPS could be reduced *via* knockdown of ITIH4. Thus, the present results revealed that ITIH4 can potentially have positive effects on early wound healing.

In patients with a connective tissue injury such as an ATR, there is an initial reduction of type I collagen, a molecule responsible in part for the reduced tensile strength of the new deposited scar tissues due to lack of molecular cross links (37) as well as the organization of the collagen (38). In the present studies, ECM and collagen-related annotations were highly enriched. In addition, the synthesis of COL1A1 was higher in patients with low risk compared to high risk regarding outcomes. In cultured fibroblasts treated with LPS, the synthesis of COL1A1 was regulated in a dose dependent manner. These results are consistent with previous studies (31). However, in the present studies, the beneficial effects induced by relatively low LPS-concentrations were weakened by knockdown of ITIH4. Interestingly, we found that ITIH4 knockdown did not only result in low synthesis but also different distributions of COL1A1. However, this should be explained with caution. Col I is both located in cytoplasm and extracellular compartments. This may be attributed to various time periods, which still need further research.

According to previous studies, ITIH4 also plays a crucial role in ECM stabilization (39, 40). Hence, the present findings confirm the potential effect of ITIH4 on ECM following exposure to inflammatory environments. These findings also highlight ITIH4 as an integral part of the network of proteins and pathways essential of good healing outcomes.

From the present proteomic studies, the PPAR signaling pathway is highly involved in prognosis for patients with different outcomes. The PPAR pathway is known to be involved in lipid catabolism, inflammation, survival, proliferation, as well as regeneration of the skin, bone and liver (41–43). It has been demonstrated to be an emerging target to promote wound healing and regeneration. PPARs consist of ligand-activated transcription factors belonging to the nuclear hormone receptor super-family (44). As an important member of the super-family, it has been reported that the synthesis of PPAR-gamma is increased following exposure to inflammation, and it significantly suppresses collagen production (45). Relevant to the present discussion, PPAR pathway regulating drugs have been reported to influence wound healing in preclinical models (46). In addition, PPAR-gamma agonists have

also recently been documented to regulate ECM production in human fibroblasts (47). In the present studies, the synthesis of PPAR-gamma was regulated by LPS in a dose-dependent manner. Moreover, the synthesis of ITIH4 was negatively correlated with PPAR-gamma in cultured fibroblasts. In the context of LPS-induced inflammation, ITIH4 may act as a negative regulator of PPAR. While moderate or low inflammation upregulate ITIH4 and collagen by downregulating PPAR signaling pathway. Taken together, these results suggest that ITIH4 could regulate type I collagen production *via* regulating the synthesis of PPAR-gamma in inflammatory environments. However, further studies are needed to clarify the association among ITIH4 and PPAR signaling pathway.

In summary, the findings presented provide several molecular and functional insights into the healing mechanisms after connective tissue injuries, and the long-term quality of specific molecules and pathways. Specifically, they provide substantial evidence that ITIH4 can participate in the regulation of inflammatory and proliferating healing processes most probably through PPAR as a signaling pathway. As such, ITIH4 may represent a prognostic biomarker and therapeutic target for effective connective tissue repair and regeneration. ITIH4 may be one of several biomarkers of good versus poor outcomes of healing as the processes are quite complex and application of different methodological approaches may identify different biomarkers. In the future, integration of the knowledge gained from the identification of multiple biomarkers of good outcomes will not only lead to better understanding of the healing processes, but will also enhance opportunities to intervene with those patients destined for a poor outcome to convert the healing process to yield an improved outcome, particularly since the basis for a poor outcome may be due to multiple variables.

Study limitations

The present study has several limitations. Firstly, due to the technic problem and relatively low expressions of unique proteins, only the common proteins between the two groups were investigated. Further research would be needed to identify and validate certain proteins solely synthesized in good or poor healers. Secondly, due to a relatively small sample size, only univariate analysis of hub proteins was performed using logistic regression models. Future studies with larger sample sizes cohorts should be performed to confirm the role of specific hub proteins and the biomarker identified in our present studies. Secondly, although the *in vitro* studies supported the bioinformatic findings, more advanced *in vivo* experiments based on animal models, or the primary cells extracted from patients with connective injuries, specifically human primary tenocytes, should be used to assess the potential roles of ITIH4 in the healing process. Thirdly, the opposing roles of ITIH4 on proliferation at different inflammatory levels are quite interesting and needs further exploration to elucidate the molecular mechanisms involved. In addition, several signaling pathways are involved in connective tissue healing, however, the PPAR signaling pathway was selected for further investigation due to its high enrichment score. Nevertheless, other pathways likely should also be further investigated for their contributions, investigation that may also provide new insights into connective tissue regenerative processes leading to better outcomes.

Data availability statement

The datasets presented in this study can be found in online repositories. The names of the repository/repositories and accession number(s) can be found below: PXD033163 (ProteomeXchange)".

Ethics statement

The studies involving human participants were reviewed and approved by Regional Ethical Review Committee in Sweden (Reference no. 2009/2079-31/2: 2013/1791-31/3). The patients/participants provided their written informed consent to participate in this study.

Author contributions

XW participated in the study design, interpretation of data, statistical analysis, experiments, manuscript writing and reviewing. JC performed part of experiments and participated in data collection. WS participated in reviewing of the manuscript. DAH participated in the interpretation of data and reviewed and revised the manuscript. PWA and ASA participated in the study concept and design, interpretation of data, reviewed, and revised the manuscript. All authors contributed to the article and approved the submitted version.

Funding

The work was supported by the Swedish Research Council (2017-00202) and the regional agreement on medical training and clinical research (ALF; SLL20180348) to PA. The Swedish National Centre for Sports Research (2022-0066; 2023-0060), Swedish Rheumatism Association (R-940565; R-968148) and King Gustav V Foundation (FAI-2018-0524; FAI-2019-0611) to AA. The funding agencies had no influence over or took part in the study design, data collection, and analysis, interpretation of data, manuscript writing or in the decision to submit the manuscript for publication.

Acknowledgments

The authors would like to thank LB for the collection and storage of tissue biopsies and Dr. AV at the Proteomics Biomedicum, Karolinska Institutet, Sweden for excellent help in MS data analysis and interpretation.

Conflict of interest

The authors declare that the research was conducted in the absence of any commercial or financial relationships that could be construed as a potential conflict of interest.

Publisher's note

All claims expressed in this article are solely those of the authors and do not necessarily represent those of their affiliated organizations, or those of the publisher, the editors and the reviewers. Any product that may be evaluated in this article, or claim that may be made by its manufacturer, is not guaranteed or endorsed by the publisher.

Supplementary material

The Supplementary Material for this article can be found online at: https://www.frontiersin.org/articles/10.3389/fimmu.2023.1191536/full#supplementary-material

References

1. Greising SM, Corona BT, Call JA. Musculoskeletal regeneration, rehabilitation, and plasticity following traumatic injury. *Int J Sports Med* (2020) 41:495–504. doi: 10.1055/a-1128-7128

2. Blaker CL, Zaki S, Little CB, Clarke EC. Long-term effect of a single subcritical knee injury: increasing the risk of anterior cruciate ligament rupture and osteoarthritis. *Am J Sports Med* (2021) 49:391–403. doi: 10.1177/0363546520977505

3. Chen J, Wang J, Hart DA, Ahmed AS, Ackermann PW. Complement factor d as a predictor of Achilles tendon healing and long-term patient outcomes. *FASEB J* (2022) 36(6):e22365. doi: 10.1096/fj.202200200RR

4. Thomopoulos S, Parks WC, Rifkin DB, Derwin KA. Mechanisms of tendon injury and repair: TENDON INJURY AND REPAIR. *J Orthop Res* (2015) 33:832–9. doi: 10.1002/jor.22806

5. Schuster R, Rockel JS, Kapoor M, Hinz B. The inflammatory speech of fibroblasts. *Immunol Rev* (2021) 302:126–46. doi: 10.1111/imr.12971

6. Tomasek JJ, Gabbiani G, Hinz B, Chaponnier C, Brown RA. Myofibroblasts and mechano-regulation of connective tissue remodelling. *Nat Rev Mol Cell Biol* (2002) 3:349–63. doi: 10.1038/nrm809

7. Nourissat G, Berenbaum F, Duprez D. Tendon injury: from biology to tendon repair. *Nat Rev Rheumatol* (2015) 11:223–33. doi: 10.1038/nrrheum.2015.26

8. Fahlström M, Björnstig U, Lorentzon R. Acute Achilles tendon rupture in badminton players. *Am J Sports Med* (1998) 26:467–70. doi: 10.1177/03635465980260032201

9. Chalidis B, Givissis P, Papadopoulos P, Pitsilos C. Molecular and biologic effects of Platelet-Rich Plasma (PRP) in ligament and tendon healing and regeneration: a systematic review. *Int J Mol Sci* (2023) 24:2744. doi: 10.3390/ijms24032744

10. Chen J, Svensson J, Sundberg C-J, Ahmed AS, Ackermann PW. FGF gene expression in injured tendons as a prognostic biomarker of 1-year patient outcome after Achilles tendon repair. *J Exp Orthop* (2021) 8:20. doi: 10.1186/s40634-021-00335-0

11. Nilsson-Helander K, Thomeé R, Silbernagel KG, Thomeé P, Faxén E, Eriksson BI, et al. The Achilles tendon Total Rupture Score (ATRS): development and validation. *Am J Sports Med* (2007) 35:421–6. doi: 10.1177/0363546506294856

12. Poulsen CB, Borup R, Nielsen FC, Borregaard N, Hansen M, Grønbaek K, et al. Microarray-based classification of diffuse large B-cell lymphoma. *Eur J Haematol* (2005) 74:453–65. doi: 10.1111/j.1600-0609.2005.00429.x

13. Augustsson J, Esko A, Thomeé R, Svantesson U. Weight training of the thigh muscles using closed vs. open kinetic chain exercises: a comparison of performance enhancement. *J Orthop Sports Phys Ther* (1998) 27:3–8. doi: 10.2519/jospt.1998.27.1.3

14. Langfelder P, Horvath S. WGCNA: an R package for weighted correlation network analysis. *BMC Bioinf* (2008) 9:559. doi: 10.1186/1471-2105-9-559

15. Yu G, Wang L-G, Han Y, He Q-Y. clusterProfiler: an R package for comparing biological themes among gene clusters. *OMICS* (2012) 16:284–7. doi: 10.1089/omi.2011.0118

16. Chin C-H, Chen S-H, Wu H-H, Ho C-W, Ko M-T, Lin C-Y. cytoHubba: identifying hub objects and sub-networks from complex interactome. *BMC Syst Biol* (2014) 8 Suppl 4:S11. doi: 10.1186/1752-0509-8-S4-S11

17. Liang C-C, Park AY, Guan J-L. *In vitro* scratch assay: a convenient and inexpensive method for analysis of cell migration *in vitro*. *Nat Protoc* (2007) 2:329–33. doi: 10.1038/nprot.2007.30

18. Bi H, Li H, Zhang C, Mao Y, Nie F, Xing Y, et al. Stromal vascular fraction promotes migration of fibroblasts and angiogenesis through regulation of extracellular matrix in the skin wound healing process. *Stem Cell Res Ther* (2019) 10:302. doi: 10.1186/s13287-019-1415-6

19. Ma Y, Li R, Wang J, Jiang W, Yuan X, Cui J, et al. ITIH4, as an inflammation biomarker, mainly increases in bacterial bloodstream infection. *Cytokine* (2021) 138:155377. doi: 10.1016/j.cyto.2020.155377

20. Nakamura N, Hatano E, Iguchi K, Sato M, Kawaguchi H, Ohtsu I, et al. Elevated levels of circulating ITIH4 are associated with hepatocellular carcinoma with nonalcoholic fatty liver disease: from pig model to human study. *BMC Cancer* (2019) 19:621. doi: 10.1186/s12885-019-5825-8

21. Noh C-K, Kim SS, Kim D-K, Lee H-Y, Cho HJ, Yoon SY, et al. Inter-alpha-trypsin inhibitor heavy chain H4 as a diagnostic and prognostic indicator in patients with hepatitis B virus-associated hepatocellular carcinoma. *Clin Biochem* (2014) 47:1257–61. doi: 10.1016/j.clinbiochem.2014.05.002

22. Li L, Choi B-C, Ryoo JE, Song S-J, Pei C-Z, Lee KY, et al. Opposing roles of inter-α-trypsin inhibitor heavy chain 4 in recurrent pregnancy loss. *EBioMedicine* (2018) 37:535–46. doi: 10.1016/j.ebiom.2018.10.029

23. Wen N, Zhao N, Xu H, Zhao Y, Ma J. Serum inter-alpha-trypsin inhibitor heavy chain 4 in patients with inflammatory bowel disease: correlation with disease risk, inflammation, activity, and its variation after treatment. *Ir J Med Sci* (2021) 191 (5):2105–2111. doi: 10.1007/s11845-021-02837-3

24. Osada A, Matsumoto I, Mikami N, Ohyama A, Kurata I, Kondo Y, et al. Citrullinated inter-alpha-trypsin inhibitor heavy chain 4 in arthritic joints and its potential effect in the neutrophil migration. *Clin Exp Immunol* (2021) 203:385–99. doi: 10.1111/cei.13556

25. He K, He S, Su M. Inter-alpha-trypsin inhibitor heavy chain 4: a serologic marker relating to disease risk, activity, and treatment outcomes of rheumatoid arthritis. *J Clin Lab Anal* (2022) 36:e24231. doi: 10.1002/jcla.24231

26. Pihl R, Jensen RK, Poulsen EC, Jensen L, Hansen AG, Thøgersen IB, et al. ITIH4 acts as a protease inhibitor by a novel inhibitory mechanism. *Sci Adv* (2021) 7: eaba7381. doi: 10.1126/sciadv.aba7381

27. Patel S, Maheshwari A, Chandra A. Biomarkers for wound healing and their evaluation. *J Wound Care* (2016) 25:46–55. doi: 10.12968/jowc.2016.25.1.46

28. Coates BA, McKenzie JA, Yoneda S, Silva MJ. Interleukin-6 (IL-6) deficiency enhances intramembranous osteogenesis following stress fracture in mice. *Bone* (2021) 143:115737. doi: 10.1016/j.bone.2020.115737

29. Liao Z, Li S, Lu S, Liu H, Li G, Ma L, et al. Metformin facilitates mesenchymal stem cell-derived extracellular nanovesicles release and optimizes therapeutic efficacy in intervertebral disc degeneration. *Biomaterials* (2021) 274:120850. doi: 10.1016/j.biomaterials.2021.120850

30. Thankam FG, Chandra I, Diaz C, Dilisio MF, Fleegel J, Gross RM, et al. Matrix regeneration proteins in the hypoxia-triggered exosomes of shoulder tenocytes and adipose-derived mesenchymal stem cells. *Mol Cell Biochem* (2020) 465:75–87. doi: 10.1007/s11010-019-03669-7

31. Xie Y, Qian Y, Wang Y, Liu K, Li X. Mechanical stretch and LPS affect the proliferation, extracellular matrix remodeling and viscoelasticity of lung fibroblasts. *Exp Ther Med* (2020) 20:1–1. doi: 10.3892/etm.2020.9133

32. Gu N, Xing S, Chen S, Zhou Y, Jiang T, Jiao Y, et al. Lipopolysaccharide induced the proliferation of mouse lung fibroblasts by suppressing FoxO3a/p27 pathway. *Cell Biol Int* (2018) 42:1311–20. doi: 10.1002/cbin.11016

33. Li X-J, Huang F-Z, Wan Y, Li Y-S, Zhang WK, Xi Y, et al. Lipopolysaccharide stimulated the migration of NIH3T3 cells through a positive feedback between β-catenin and COX-2. *Front Pharmacol* (2018) 9:1487. doi: 10.3389/fphar.2018.01487

34. Nishihara F, Nakagome K, Kobayashi T, Noguchi T, Araki R, Uchida Y, et al. Trans-basement membrane migration of eosinophils induced by LPS-stimulated neutrophils from human peripheral blood. *vitro. ERJ Open Res* (2015) 1:00003–2015. doi: 10.1183/23120541.00003-2015

35. Kostarnoy AV, Gancheva PG, Logunov DY, Verkhovskaya LV, Bobrov MA, Scheblyakov DV, et al. Topical bacterial lipopolysaccharide application affects inflammatory response and promotes wound healing. *J Interferon Cytokine Res* (2013) 33:514–22. doi: 10.1089/jir.2012.0108

36. Wang L, Song D, Wei C, Chen C, Yang Y, Deng X, et al. Telocytes inhibited inflammatory factor expression and enhanced cell migration in LPS-induced skin wound healing models *in vitro* and *in vivo*. *J Trans Med* (2020) 18:60. doi: 10.1186/s12967-020-02217-y

37. Li H-Y, Hua Y-H. Achilles Tendinopathy: current concepts about the basic science and clinical treatments. *BioMed Res Int* (2016) 2016:6492597. doi: 10.1155/2016/6492597

38. Chaudhuri S, Nguyen H, Rangayyan RM, Walsh S, Frank CB. A Fourier domain directional filtering method for analysis of collagen alignment in ligaments. *IEEE Trans BioMed Eng* (1987) 34:509–18. doi: 10.1109/tbme.1987.325980

39. Chandler KB, Brnakova Z, Sanda M, Wang S, Stalnaker SH, Bridger R, et al. Site-specific glycan microheterogeneity of inter-alpha-trypsin inhibitor heavy chain H4. *J Proteome Res* (2014) 13:3314–29. doi: 10.1021/pr500394z

40. Miyake Y, Tanaka K, Arakawa M. ITIH3 and ITIH4 polymorphisms and depressive symptoms during pregnancy in Japan: the Kyushu Okinawa maternal and child health study. *J Neural Transm (Vienna)* (2018) 125:1503–9. doi: 10.1007/s00702-018-1905-1

41. Magadum A, Engel FB. PPARβ/δ: linking metabolism to regeneration. *Int J Mol Sci* (2018) 19:E2013. doi: 10.3390/ijms19072013

42. Rayner MLD, Healy J, Phillips JB. Repurposing small molecules to target PPAR-γ as new therapies for peripheral nerve injuries. *Biomolecules* (2021) 11:1301. doi: 10.3390/biom11091301

43. de Mos M, Koevoet WJLM, Jahr H, Verstegen MMA, Heijboer MP, Kops N, et al. Intrinsic differentiation potential of adolescent human tendon tissue: an in-vitro cell differentiation study. *BMC Musculoskelet Disord* (2007) 8:16. doi: 10.1186/1471-2474-8-16

44. Mirza AZ, Althagafi II, Shamshad H. Role of PPAR receptor in different diseases and their ligands: physiological importance and clinical implications. *Eur J Med Chem* (2019) 166:502–13. doi: 10.1016/j.ejmech.2019.01.067

45. Honda K, Marquillies P, Capron M, Dombrowicz D. Peroxisome proliferator-activated receptor gamma is expressed in airways and inhibits features of airway remodeling in a mouse asthma model. *J Allergy Clin Immunol* (2004) 113:882–8. doi: 10.1016/j.jaci.2004.02.036

46. Valentin S, Rudolph J, Goertz O, Botteck N, Langer S, Schneider S. Effect of fenofibrate on microcirculation and wound healing in healthy and diabetic mice. *Eur J Med Res* (2009) 14:65. doi: 10.1186/2047-783X-14-2-65

47. Zhu H-Y, Li C, Zheng Z, Zhou Q, Guan H, Su L-L, et al. Peroxisome proliferator-activated receptor-γ (PPAR-γ) agonist inhibits collagen synthesis in human hypertrophic scar fibroblasts by targeting Smad3 *via* miR-145. *Biochem Biophys Res Commun* (2015) 459:49–53. doi: 10.1016/j.bbrc.2015.02.061

frontiers | Frontiers in Immunology

TYPE Review
PUBLISHED 10 July 2023
DOI 10.3389/fimmu.2023.1164137

Check for updates

OPEN ACCESS

EDITED BY
Yuehong Chen,
Sichuan University, China

REVIEWED BY
Yujie Liu,
Second Military Medical University, China
Song Wang,
Zhejiang Cancer Hospital, China

*CORRESPONDENCE
Juebao Li
lijuebao@hmc.edu.cn

†These authors have contributed equally to this work

RECEIVED 12 February 2023
ACCEPTED 14 June 2023
PUBLISHED 10 July 2023

CITATION
Zhao K, Ruan J, Nie L, Ye X and Li J (2023) Effects of synovial macrophages in osteoarthritis.
Front. Immunol. 14:1164137.
doi: 10.3389/fimmu.2023.1164137

COPYRIGHT
© 2023 Zhao, Ruan, Nie, Ye and Li. This is an open-access article distributed under the terms of the Creative Commons Attribution License (CC BY). The use, distribution or reproduction in other forums is permitted, provided the original author(s) and the copyright owner(s) are credited and that the original publication in this journal is cited, in accordance with accepted academic practice. No use, distribution or reproduction is permitted which does not comply with these terms.

Effects of synovial macrophages in osteoarthritis

Kun Zhao[1,2†], Jiaqi Ruan[2†], Liuyan Nie[3], Xiangming Ye[1] and Juebao Li[1*]

[1]Center for Rehabilitation Medicine, Rehabilitation and Sports Medicine Research Institute of Zhejiang Province, Department of Rehabilitation Medicine, Zhejiang Provincial People's Hospital (Affiliated People's Hospital, Hangzhou Medical College), Hangzhou, Zhejiang, China, [2]Zhejiang University School of Medicine, Hangzhou, Zhejiang, China, [3]Department of Rheumatology, Sir Run Run Shaw Hospital, Zhejiang University School of Medicine, Hangzhou, China

Osteoarthritis (OA) is a common degenerative disease in mammals. However, its pathogenesis remains unclear. Studies indicate that OA is not only an aging process that but also an inflammation-related disease. Synovitis is closely related to the progression of OA, and synovial macrophages are crucial participants in synovitis. Instead of being a homogeneous population, macrophages are polarized into M1 or M2 subtypes in OA synovial tissues. Polarization is highly associated with OA severity. However, the M1/M2 ratio cannot be the only factor in OA prognosis because intermediate stages of macrophages also exist. To better understand the mechanism of this heterogeneous disease, OA subtypes of synovial macrophages classified by gene expression were examined. Synovial macrophages do not act alone; they interact with surrounding cells such as synovial fibroblasts, osteoclasts, chondrocytes, lymphocytes and even adipose cells through a paracrine approach to exacerbate OA. Treatments targeting synovial macrophages and their polarization are effective in relieving pain and protecting cartilage during OA development. In this review, we describe how synovial macrophages and their different polarization states influence the progression of OA. We summarize the current knowledge of the interactions between macrophages and other joint cells and examine the current research on new medications targeting synovial macrophages.

KEYWORDS

osteoarthritis, macrophages, synovial, polarization, treatment, review

1 Introduction

Osteoarthritis (OA) is a degenerative joint disease caused by chronic inflammation in cartilage, subchondral bone and synovium. In osteoarthritic joints, major pathological changes include damage to articular cartilage, sclerosis and cystic degeneration of subchondral bone, and hyperplasia of the synovial membrane and articular capsule. As the most common joint disease, OA causes pain and disability and creates a substantial burden on individuals and society (1). Despite the major public burden posed by OA, effective medicine for its treatment remains insufficient. Current clinical drugs for OA, including local glucocorticoids and nonsteroidal anti-inflammatory drugs (NSAIDs), can

suppress the pain caused by OA but cannot stop its progression. Therefore, clarifying the mechanism of OA initiation and discovering useful treatments have become urgent tasks for scientists and researchers.

Osteoarthritis was used to be thought as a degenerative disease mostly caused by cartilage defects before accumulating research reveals the significant contribution of synovial inflammation in the progression of OA. Imaging studies coupled with histopathologic analyses have demonstrated that synovitis could facilitate the pathogenesis of OA (2). The normal synovium has two layers (Figure 1). The inner layer, which is also called the lining layer, is mainly composed of synovial macrophages and synovial fibroblasts and plays an important role in maintaining joint homeostasis. The outer layer of the synovium consists of different types of connective tissue that assist various joint functions. However, in the OA synovium, the number of lining layer cells, especially the number of synovial macrophages, is increased (3). Microscopically, the appearance of OA can be indistinguishable from that observed in RA. They both involve neovascularization and infiltration by fibroblasts and macrophages. However, their histological changes are different. In contrast to the synovial inflammation observed in rheumatoid arthritis (RA), synovial inflammation in OA is not a diffuse process: its distribution is patchy and confined to areas adjacent to sites of chondropathy (2). The accumulation of macrophages in OA is not caused by a single factor but arises from complicated interactions between joint cells such as chondrocytes, fibroblasts, and lymphocytes. Molecules such as soluble matrix degradation products (SMDPs) from cartilage, fibronectin, adipokines and some alarmins act as danger-associated molecular patterns (DAMPs), which activate macrophages to produce inflammatory cytokines and chemokines through surface pattern recognition receptors (PRRs), such as Toll-like receptors (TLRs), which are expressed on the surface of macrophages. Additionally, cytokines and chemokines such as interleukins (ILs), growth factors and monocyte chemotactic protein (MCP) produced by various cells in the joint also play a role in macrophage activation and accumulation by binding to the corresponding receptors and further activating the JAK-STAT pathway (4). Macrophages play a crucial role in OA synovitis, and their polarization correlates with the progression of OA. Macrophages can be divided into three phenotypes according to their function: unstimulated macrophages (M0), proinflammatory macrophages (M1) and anti-inflammatory macrophages (M2). M0 cells are resting and preactivated macrophages, which can transform into M1 or M2 macrophages under certain microenvironments. M1 macrophages, as an anti-pathogene soldier, can be induced by bacterial lipopolysaccharide (LPS) or Th1 cytokines such as interferon-γ (IFN-γ), TNF-α both *in vitro* and *in vivo*. Activated M1 macrophages could secrete proinflammatory cytokines such as TNF-α and IL-1. In contrast, M2 macrophages are polarized by IL-4 and IL-13 and exert anti-inflammatory effects and tissue

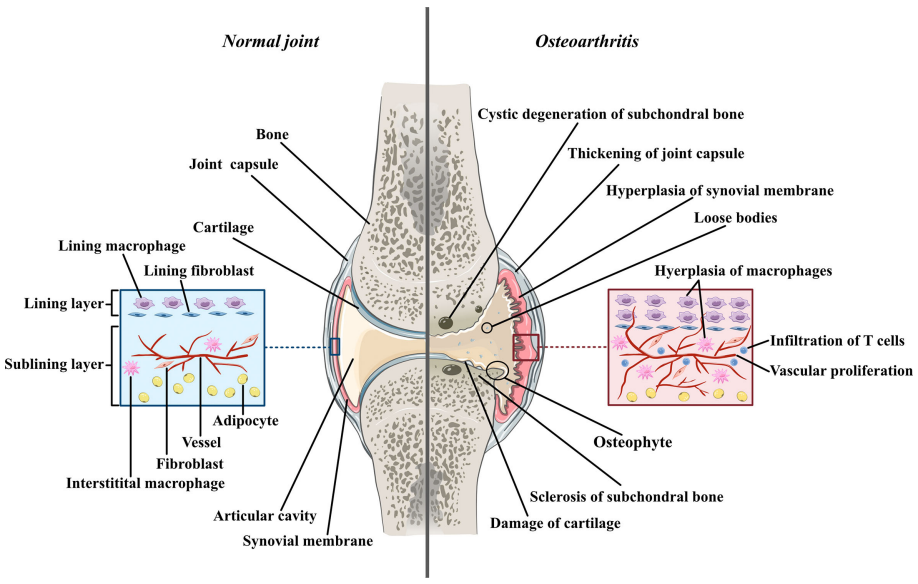

FIGURE 1
The comparison between normal joint and osteoarthritic joint Normal joint composed of joint cartilage, joint capsule, synovial membrane and articular cavity. Generally, synovial membrane has two layers. The inner layer, also called lining layer is mainly composed of synovial macrophage and synovial fibroblasts. The outer layer of synovial membrane also called sublining layer is connective tissue composed of blood vessels, collagens, interstitial macrophages, fibroblasts, adipocytes and a small number of lymphocytes. In osteoarthritic joint, the articular cartilage is damaged and the fragments of cartilage drift into articular cavity, forming loose bodies. The loss of cartilage leads to unevenly distributed loads on subchondral bones which can further cause osteoproliferation and sclerosis in the friction part as well as bone resorption and cystic degeneration in the periphery part. Moreover, both synovial membrane and articular capsule thicken in osteoarthritic joint due to inflammation. In hyperplastic synovial membrane, the most prominent changes are the hyperplasia of synovial and interstitial macrophages, the infiltration of T lymphocytes in sublining layer and the proliferation of blood vessels.

repair and remodeling functions (5). These macrophage inductors are still frequently used in *in vitro* experiments to induce M1/M2 and explore their effects in specific diseases, as well as in the main topic of our thesis -osteoarthritis. Despite all the knowledge about macrophage accumulation and polarization, the specific mechanism by which this occurs in OA joints has not been elucidated. Here, we aimed to share the current evidence of the role of synovial macrophages and their subsets in OA progression. We also summarized the current knowledge of interactions between macrophages and other joint cells, such as chondrocytes and fibroblasts. In this review, possible treatments for OA targeting polarized synovial macrophages are also summarized.

2 Synovial macrophages are activated and proliferate in OA

2.1 *In vitro* experiments

In 1991, the antigen-antibody technique was used to show that normal synovial lining cells expressed many macrophage-associated antigens, such as CD11b, CD16, CD14 and CD68 (6). Haywood L et al. collected synovial tissue samples from 104 OA patients in 2003 and found that angiogenesis and synovial lining thickness increased with increasing macrophage fractional areas (7). Afterward, Benito MJ showed significantly greater $CD14^+$ and $CD68^+$ cell infiltration, blood vessel formation and intercellular adhesion molecule-1 expression were detected in synovial tissue from OA patients than in normal individuals (3). In 2006, Bondeson J found that fewer proinflammatory cytokines, such as IL-1 and TNF-α, were produced in digested osteoarthritis synovium cultures after depleting $CD14^+$ cells (CD14 is expressed by classic mononuclear macrophages) using anti-CD14-conjugated magnetic beads. These results suggested that the number of macrophages was increased in the synovium of OA patients and that these proliferated synovial macrophages could exacerbate OA by producing proinflammatory cytokines such as TNF-α and IL-1. However, *in vitro* studies could not dynamically observe the activation of synovial macrophages in the body. Tracing the changes in synovial macrophages in the body was impossible until the discovery of the radionuclide labeling technique (8).

2.2 *In vivo* studies based on radionuclide-labeled folate

According to their distinct molecular phenotypes, monocytes can be divided into two subgroups: the $CD14^+CD16^-$ subgroup and the $CD14^-CD16^+$ subgroup. The first subgroup, which are called classic monocytes, has classic proinflammatory functions such as infiltration and macrophage transformation. The second subgroup is considered to have increased cytokine expression and antigen-presenting abilities (9, 10). It is frequently reported that folate receptor-β (FR-β) is specifically expressed on the surface of the classic $CD14^+CD16^-$ monocyte subgroup and derived macrophages. Therefore, radionuclide-labeled folate is frequently used to detect the quantity and distribution of activated macrophages *in vivo* (11).

In 2016, Kraus VB provided direct *in vivo* evidence for the connection between synovial macrophages and OA for the first time. Kraus VB injected radionuclide-labeled folate called 99mTc–EC20 (etarfolatide) into twenty-five individuals with symptomatic OA, after which SPECT-CT imaging of both knees and planar imaging of the whole body were used to detect activated macrophages *in vivo*. The results showed that activated macrophages were present in 76% of OA knees, and etarfolatide uptake was mainly detected in the synovium and joint capsule. Radiographic knee OA severity and joint symptoms significantly correlated with synovial and capsular etarfolatide uptake. In addition, whole-body planar imaging suggested that activated macrophages were localized to joints that were susceptible to OA, including hand finger joints, thumb bases, shoulders, great toes and ankles. Pain in these joints was also positively associated with the quantity of activated macrophages (12). These findings indicate that activated macrophages are increased in OA joints and that most of them accumulate in the synovium.

2.3 Modulating the quantity of synovial macrophages affects OA

After learning that synovial macrophages are increased in OA patients, researchers have tried to manipulate the quantity of synovial macrophages in animal models to further verify the connection between synovial macrophages and OA.

Clodronate-laden liposomes are toxic to all phenotypes of macrophages, and so they are commonly used to deplete macrophages. In 2004, van Lent PL injected clodronate-laden liposomes into mouse knee joints to selectively deplete synovial lining macrophages. Then, TGF-β was injected into knee joints to induce osteophyte formation. Van Lent PL found that osteophyte formation and the production of bone morphogenetic protein (BMP)-2 and BMP-4 were dramatically reduced after the depletion of synovial lining macrophages (13). Additionally, Takano S discovered that the expression of IL-1β, TNF-α and nerve growth factor (NGF, a cytokine associated with pain) in the synovium was reduced after depleting synovial macrophages in OA mice (14). Using a similar method, many other studies showed that the production of proinflammatory cytokines (IL-1β, TNF-α), the formation of osteophytes, and cartilage destruction were alleviated after selectively depleting synovial macrophages (15, 16). Despite these positive results, Wu CL's study showed conflicting findings. He found that OA was exacerbated after depleting synovial macrophages from transgenic obese mice with Fas-induced macrophage apoptosis using the small molecule AP20187. The author explained that it was possible that macrophages repopulated after AP20187 administration and that the repopulated macrophages contributed to the progression of OA. Another explanation was that synovial macrophages could protect against ox-LDL-induced inflammation, and so after macrophage depletion, this protection was no longer present (17).

10.3389/fimmu.2023.1164137

3 Macrophage polarization in the OA synovium

3.1 Discovery of M1/M2 macrophages in the OA synovium

Macrophages can be divided into multiple phenotypes. Among these phenotypes, the two most important subtypes are "classically activated macrophages" (M1 polarization) and "alternatively activated macrophages" (M2 polarization). M1 macrophages can be induced by IFN-γ and TNF-α *in vitro*. Characterized by CD80, CD86, and MHCII expression, these cells are known as proinflammatory macrophages due to their ability to produce proinflammatory cytokines such as TNF-α and IL-1. Moreover, they can release crucial inflammatory chemokines such as monocyte chemotactic protein-1 (MCP-1, also known as CCL2). Additionally, the high expression of the surface molecule MHCII contributes to their strong antigen presentation ability. M2 macrophages are induced by IL-4 or IL-10. Unlike M1 macrophages, these cells play a role in tissue repair and inflammation suppression by producing anti-inflammatory cytokines such as IL-10 and IL-1Ra. M2 macrophages express the scavenger receptor CD163 and mannose receptor CD206 and have higher levels of CD14 than M1 macrophages (5). The distribution and transformation of M1 and M2 macrophages play a vital role in the precise regulation of inflammation (Figure 2). The detailed characteristics of M1 and M2 polarization are shown in Table 1 (5, 18, 19).

TABLE 1 Characteristics of M1 and M2 macrophages.

	M1 macrophage	M2 macrophage
iNOS expression	+	–
MHCII expression	↑	↓
CD14	↓	↑
CD16/32	↑	↓
CD80	+	–
CD86	+	–
CD11c	+	–
CD163	–	+
CD206	–	+
CD209	–	+
TLR	TLR-2, TLR-4	TLR1, TLR-8
Stimulus	IFN-γ, LPS	IL-4, IL-13
Cytokines production	IL-1, IL-6, IL-12, TNF-α, CXCL9, CXCL10, CCL2	IL-4, IL-10, IL-13, IL-1Ra, TGF-β1, CCL17, CCL18, CXCL13, VEGF

"+" present. "-" absent. ↑high expression. ↓low expression.
IL, Interleukin; TLR, Toll-like receptors; TNF, Tumor Necrosis Factor; TGF, Transforming growth factor; LPS, Lipopolysaccharide; IFN, Interferon; CCL, Chemokine (C-C motif) ligand; VEGF, Vascular endothelial growth factor; CXCL, Chemokine (C-X-C motif) ligand.

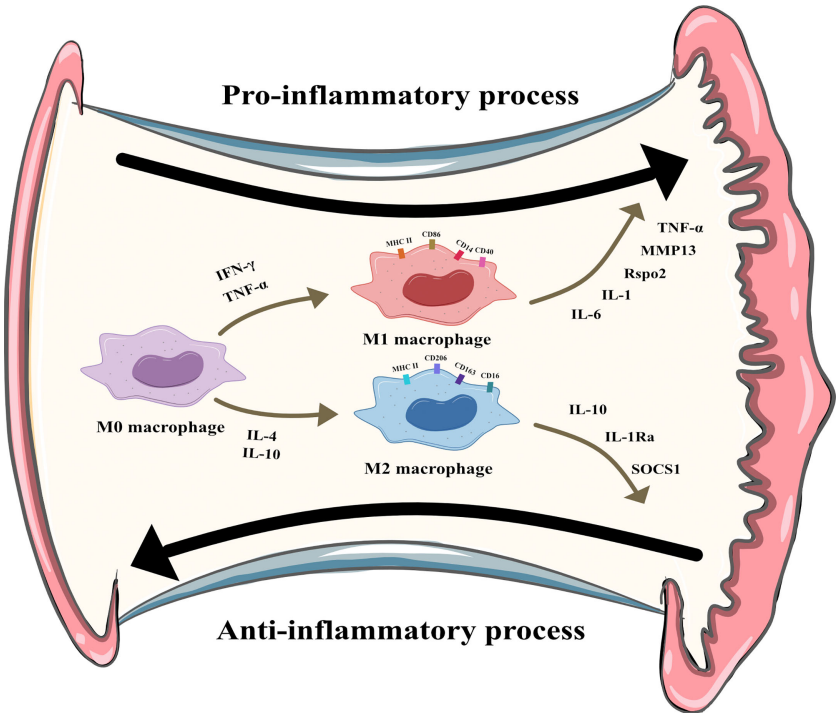

FIGURE 2
M1 and M2 polarization of synovial macrophages. M1 macrophages can be induced by Interferon-γ (IFN-γ) and tumor necrosis factor-α (TNF-α) and secret pro-inflammatory cytokines like interleukin (IL)-6, IL-1, R-spondin-2 (Rspo2), matrix metalloproteinase-13(MMP13), TNF-α. M2 macrophages can be induced by IL-4 and IL-10 and secret anti-inflammatory cytokines like IL-10, IL-1 receptor antagonist, suppressor of cytokine signaling 1 (SOCS1).

To investigate how macrophage polarization affects the progression of OA, van den Bosch MH used microarray analysis and immunohistochemistry (immunostaining for CD68 and CD163) and showed that compared to the normal synovium, the OA synovium overexpressed M1-like macrophage markers such as CD86 and M2-like macrophage markers such as CD206, IL-10, and IL-1Ra. Daghestani HN analyzed the concentrations of the M2 markers CD163 and CD14 in the synovial fluid (SF) of 25 OA patients and found that the concentrations of these markers were higher in OA patients. These findings indicated that M1 and M2 macrophages proliferated in the OA synovium, which might be caused by the increase in the total number of macrophages in the OA synovium. Interestingly, some studies have noted that compared with the total number of activated macrophages, the failure to transform from the M1 to M2 subtype may play a larger role in the progression of OA (4). Yarnall BW collected synovial samples from OA dogs and found that the ratio of M1-polarized cells to M2-polarized cells was higher in the OA synovium, which indicated that disordered macrophage polarization might contribute to OA initiation and progression (20). In 2018, Zhang H found that activated synovial macrophages in OA patients were mainly M1 macrophages rather than M2 macrophages. This finding suggests that the increase in M1 synovial macrophages caused by macrophage proliferation and abnormal polarization may be a crucial reason for OA exacerbation (21).

3.2 Modulating the M1/M2 ratio affects OA

Although two phenotypes of macrophages (M1 and M2) have been found in the OA synovium, the specific functions of these two subtypes remain unclear. Therefore, many scientists have tried to manipulate the M1/M2 ratio and determine how this change in the M1/M2 ratio affects OA and directly show the influence of macrophage polarization on OA.

In 2016, Utomo L described the direct influence of M1 and M2 macrophages on OA for the first time. Utomo L cultured OA cartilage tissue with M1 macrophages (induced by IFN-γ and TNF-α) or M2 macrophages (induced by IL-4/IL10) *in vitro*. Then, she found that M1 macrophages exacerbated cartilage inflammation by upregulating the expression of the proinflammatory factors IL1β, IL6, MMP13 and a disintegrin and metalloproteinase with thrombospondin motif-5 (ADAMTS5). M1 macrophages also suppressed the release of aggrecan (ACAN) and collagen type II (COL2A1) and stimulated cartilage cells to produce the inflammatory mediators nitric oxide (NO) and glycosaminoglycan (GAG). On the other hand, M2 macrophages (induced by IL-10) promoted the expression of IL-1β and suppressor of cytokine signaling-1 (SOCS1) (22).

Several reports have shown that mammalian target of rapamycin (mTORC1) can promote M1 polarization and reduce M2 polarization. Deleting the tuberous sclerosis complex 1 (TSC1) gene can constitutively activate mTORC1. In contrast, deleting the Ras homolog enriched in brain 1 (Rheb1) gene inhibits the function of mTORC1. Based on these findings, Zhang H used mice with Tsc1 or Rheb1 deletion to generate collagenase-induced OA and examined the role of macrophages and their polarization in OA. He found that TSC1-knockout mice had upregulated M1-like macrophage markers and exacerbated cartilage degeneration and osteophyte formation in experimental OA. Conversely, Rheb1-knockout mice exhibited downregulated M1-like macrophage markers, upregulated M2-like macrophage markers and attenuated experimental OA. This result proves that M1 macrophages promote synovial hyperplasia, synovial inflammation and OA progression, while M2 macrophages alleviate OA progression (21). As for the specific mechanism of how M1 or M2 macrophages affect OA, scientists found M1 macrophage play its pro-inflammatory role mainly through secret cytokines like IL-1 and TNF-α, which will be explained in detail in the following passage. However, studies concerning the corresponding pathways of M2 macrophage in OA remains insufficient. Some articles reported M2 may exert protective effects through its exosomes which mainly mediated by the PI3K/AKT/mTOR signal pathway (23).

3.3 Various factors activate M1/M2 polarization through JAK/STAT, NFκB/MAPK, STAT6 and ROS/NLRP3 pathways in OA

Because of the importance of macrophage polarization in OA progression, scientists have tried to determine the intrinsic factors that lead to the abnormal polarization of macrophages in OA patients. Studies showed that IFN-γ and TNF-α activate the JAK/STAT pathway, whereas LPS activates the NFκB and MAPK pathways in M1 polarization. IL4/IL13 activate STAT6 and regulate transcription factors, including IRF4, PPARγ, and KLF4 in M2 polarization. Other pathways including that from JNK, PI3K/Akt, Notch, TGF-β, and hypoxia-dependent intracellular pathways have been shown to be involved in the balance of M1/M2 polarization (4). In the pathogenesis and progression of OA, several regulatory mechanisms of macrophage polarization were also discovered. Wei Z et al. found that anti-citrullinated protein antibodies (ACPAs, an autoimmune antibody) could induce M1 polarization by upregulating the expression of interferon regulatory factor 5 (IRF5) in macrophages. However, this effect was more obvious in rheumatoid arthritis (RA) than in OA because autoimmune factors are a major cause of RA but not OA (24). Another possible factor resulting in M1 polarization in OA is soluble collagens. Under disease conditions, soluble degraded forms of collagens can be detected in synovial fluids. These soluble collagens act as self-antigens and can increase M1 polarization during OA pathogenesis. Fortunately, Pal S et al. showed that sulforaphane could block M1 macrophage polarization induced by soluble collagen and convert M1 macrophages into the M2 subtype (25). Recently, some new articles reported more pathways related to M1/M2 polarization in OA patients. It was found that inhibition of TRPV4 (transient receptor potential channel subfamily V member 4), an ion channel related to oxidative stress and inflammation, delays OA progression by inhibiting M1 synovial macrophage polarization through the

ROS/NLRP3 pathway (26). Another research found that MAGL (Monoacylglycerol lipase) could regulates synovial macrophage polarization vis inhibition of mitophagy. MAGL inhibition enhanced the mitophagy levels of M1 macrophages (27). However, the mechanism involved in regulating macrophage polarization by MAGL requires further study. Collectively, those studies showed the possible intrinsic factors that cause an imbalance in macrophage polarization in OA. Further studies are needed to clarify the detailed mechanisms of abnormal polarization states.

4 Synovial macrophages help distinguish the two OA subgroups

Although the discovery of M1 and M2 polarization in synovial macrophages was a huge breakthrough in understanding the pathogenesis of OA, this is not the only factor in the initiation and progression of this disease because many intermediate stage macrophages are present in the OA synovium despite these two extreme subtypes (18). To better understand the heterogeneity of this disease, scientists further classified OA based on the gene expression of total synovial macrophages. It was recently reported that knee OA can be divided into 2 subgroups based on the properties of activated synovial macrophages. After RNA sequencing of OA and inflammatory-arthritis (IA) synovial tissue macrophages, Wood MJ identified 2 distinct OA subgroups based on the hierarchical heatmap of the top 500 most variable genes. One OA group was distinct, and another OA group was more similar to IA. The distinct OA group was termed classical OA (cOA), and the IA-like OA group was termed inflammatory-like OA (iOA). Subsequently, synovial macrophage gene expression analysis and gene set enrichment analysis were performed to determine whether the two OA subtypes had different disease mechanisms. The results demonstrated that the iOA group overexpressed cell cycle-related genes such as MKI67 (the proliferation marker Ki67–encoding gene) compared to the cOA group. Consistent with this finding, flow cytometry proved that the synovial tissue of the iOA group contained a higher ratio of macrophages than that of the cOA group. In general, the heterogeneous gene expression signatures of OA synovial macrophages may represent different cellular disease mechanisms and be an important consideration in OA classification (18).

5 Synovial macrophages exacerbate OA by producing proinflammatory cytokines, affecting synovial fibroblasts and interacting with chondrocytes

5.1 OA synovial macrophages stimulate proinflammatory cytokines

Takano S found that synovial macrophages highly expressed TNF-α and IL-1 (14). Consistent with this finding, Bondeson J collected the supernatant of macrophage-depleted OA synovial tissue culture and found that the concentrations of IL1 and TNF-α declined (8). Zhang H performed mRNA sequencing on cultured macrophages from TSC1-knockout mice and found that the cytokines IL-1, IL-6 and TNF-α were upregulated. In addition to the two most well-known macrophage-derived cytokines (TNF-α and IL-1), many other cytokines and chemokines are directly or indirectly involved in macrophage-mediated OA progression. Zhang H found that R-spondin-2 (Rspo2) played an important role in OA. Interarticular injection of Rspo2 exacerbates OA, and the injection of Rspo2 antibodies reversed the exacerbation (21). Synovial macrophages can directly or indirectly induce the production of matrix-degrading enzymes such as MMPs by chondrocytes and synovial fibroblasts (28). Moreover, Takano S discovered that synoviocytes could produce NGF and cause pain in OA (14). Haywood L found that synovial macrophages secreted VEGF to exacerbate synovial angiogenesis (7). Another interesting cytokine is TGF-β. Synovial macrophages can induce osteophyte formation in OA *via* the production of TGF-β, BMP-2, and BMP-4 (13). Chemokines that can mediate macrophage accumulation are also crucial participants in synovitis. Synovial macrophages not only produce chemokines such as CCL2 but also stimulate other tissue cells to secrete chemokines that further enhance macrophage accumulation (5, 29).

5.2 OA synovial macrophages interact with synovial fibroblasts

After Bondeson J removed macrophages from OA synovial cultures, the macrophage-derived cytokines IL1 and TNF-α decreased, and the fibroblast-derived cytokines IL-6, IL-8, and MMPs were also reduced (8). In addition, after stimulating synovial fibroblasts with TNF-α and IL1, Takano S observed a strong increase in NGF (related to OA pain) (14). *In vitro* coculture experiments indicated that macrophages triggered the emergence of proinflammatory fibroblasts that expressed not only the typical fibroblast-derived proinflammatory mediator IL-6 but also mediators of cartilage degradation, such as MMPs. These cells could also produce collagens that exacerbate synovial fibrosis. The activation of functional synovial fibroblasts also impacts the function and phenotype of macrophages. Synovial fibroblasts send attraction signals to macrophages through the mechanical movement of ECM fibers caused by the contraction of fibroblasts. Moreover, fibroblasts have also been shown to produce macrophage colony stimulating factor (M-CSF) and granulocyte-macrophage colony stimulating factor (GM-CSF), two conventional mediators that stimulate the mononuclear phagocyte system (30) (Figure 3A).

5.3 OA synovial macrophages interact with chondrocytes

Aberrant hyperplasia and differentiation of chondrocytes are crucial for OA initiation and progression. It has been reported that the severity of synovitis is closely related to the severity of joint dysfunction due to the interaction between cartilage and the synovium (3). MMPs are a group of matrix-degrading enzymes that mediate

10.3389/fimmu.2023.1164137

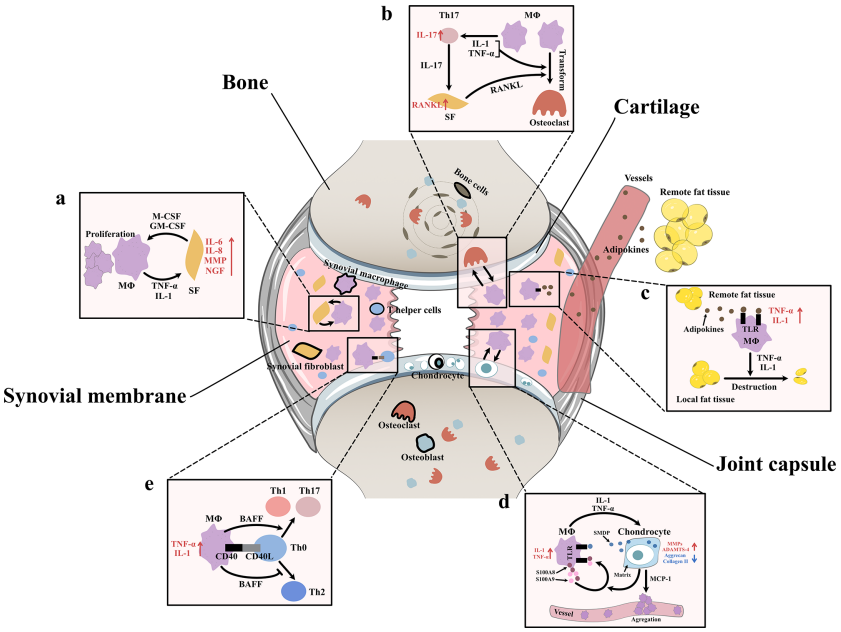

FIGURE 3
Interaction between synovial macrophages and other cells **(A)** Synovial macrophages and synovial fibroblasts: Synovial macrophages release interleukin (IL)-1, tumor necrosis factor-α (TNF-α) to increase the expression of IL-6, IL-8, matrix metalloproteinases (MMPs), nerve growth factor (NGF) in synovial fibroblasts. Fibroblasts stimulate macrophage proliferation by producing macrophage colony stimulating factor (M-CSF) and granulocyte-macrophage colony stimulating factor (GM-CSF) **(B)** Synovial macrophages and osteoclast: Macrophages can transform into osteoclast when stimulated by IL-1, TNF-α, and especially receptor activator of nuclear factor κB ligand (RANKL). It is found synovial macrophages indirectly elevate RANKL level through CD4+ T cells and synovial fibroblast cells. Macrophages secret TNF-α and IL-1 to stimulate the differentiation of Th17 cells, which subsequently release IL-17 to induce the RANKL production of synovial fibroblasts. **(C)** Synovial macrophage and adipocytes: Fat tissues outside the joint secret adipokines like leptin, adiponectin and visfatin into blood circulation. Then adipokines get into synovial membrane and activate macrophage TLR to increase TNF-α, IL-1 expression. These macrophage-derived cytokines, in turn, lead to destruction and remodeling of local joint adipose tissue, which is a protective factor of osteoarthrosis. **(D)** Synovial macrophages and chondrocytes: Synovial macrophages release IL1, TNF-α to upregulate the expression of MMPs, A Disintegrin and Metalloproteinase with Thrombospondin-4 (ADAMTS-4) while downregulate Aggrecan and collagen II. In turn, injured cartilage produces soluble matrix degradation products (SMDP) and monocyte chemotactic protein-1 (MCP-1). It also leads to increased levels of two autocrine proteins S100A8 and S100A9 in macrophages. Both SMDP and S100A8/S100A9 function through activating Toll-like receptor (TLR) expressed on macrophages. MCP-1 functions by promoting macrophage aggregation. **(E)** Synovial macrophages and CD4+T cells: Synovial macrophages secret B cell Activating Factor (BAFF) to promote pro-inflammatory Th1 cells and Th17 cells while suppress anti-inflammatory Th2 response. Meanwhile, CD4+T cells also contribute to macrophage activation through CD40/CD40L co-stimulatory pathways.

cartilage erosion, and several of them have been suggested to participate in OA. VDIPEN, an MMP-generated neoepitope, is positively associated with cartilage breakdown. In 2007, synovial macrophages were removed using clodronate-laden liposomes prior to the creation of a mouse OA model, and Blom AB proved that synovial macrophages affected cartilage function through MMPs. He found that the expression of MMP-3 and MMP-9 in synovial tissue but not cartilage tissue was significantly decreased in macrophage-depleted mice, indicating that synovial macrophages could directly affect cartilage by producing MMPs. A dramatic decrease in the expression of VDIPEN was also noticed (28). In 2018, Zhang H found that the expression of the chondrogenesis regulator gene sry-box transcription factor 9 (*Sox9*) and the chondrocyte marker genes *Col2a1* and *Acan* was decreased, while the expression of *Col10a1* and runt-related transcription factor 2 (*Runx2*), which are associated with chondrocyte differentiation, was enhanced in OA mice with increased M1 polarization. A high level of cartilage matrix mineralization was also observed, indicating that activated synovial macrophages could promote abnormal chondrocyte maturation and differentiation through cytokines/enzymes (21). It was later discovered that activated synovial macrophages could secrete TNF-α and IL-1 to increase cartilage expression of proinflammatory cytokines such as MMPs and ADAMTS-4 and decrease protein levels of ACAN and collagen II (31–33). Another newly-discovered mediator of this macrophage–cartilage communication was extracellular vehicles (EVs). EVs are cell-derived membrane vesicles containing numerous types of bioactive molecules, including proteins, lipids, mRNAs, microRNAs and DNA. In an *in vitro* study, scientists found when EVs secreted by M1 reached chondrocytes, they transferred their cargos into chondrocytes and caused significant increase in the expression of IL-6, MMP13, and ADAMTS5 which further led to cartilage degeneration (34). The stimulation effect between cells is mutual. Synovial macrophages also expressed increased IL-1β and VEGF when cultured with abnormal cartilage cells from OA joints (33). Further study showed that the underlying mechanism of the proinflammatory effect of injured cartilage may be associated with SMDPs and MCP-1 (also known as CCL2). When articular cartilage is injured, molecular fragments of cartilage, such as SMDPs, irritate the synovium and bind with TLRs expressed on synovial macrophages to increase the expression of multiple proinflammatory cytokines that further exacerbate cartilage injury (35–37). MCP-1 is an important leukocyte chemotactic factor that is expressed by injured cartilage cells

and can promote macrophage accumulation (29, 38). Damage to the cartilage could also lead to increased levels of the alarmins S100A8 and S100A9, two autocrine proteins produced by synovial macrophages that act on themselves to induce proinflammatory cytokines such as IL and TNF through TLRs (39). These results indicated the mutual effects of activated synovial macrophages and OA cartilage (Figure 3D).

5.4 OA synovial macrophages interact with T cells

As mentioned before, another important change in the OA synovium is the increase in CD4+ T cells. Instead of acting alone, these lymphocytes interact with synovial macrophages in multiple ways. For instance, the level of B-cell activating factor (BAFF), which is a cytokine produced mainly by macrophages, is elevated in OA synovial fluid (40). As a member of the TNF family, BAFF can not only support the survival and proliferation of B cells but also play a role in T-cell activation. BAFF can promote proinflammatory Th1 cells and Th17 cells while suppressing the anti-inflammatory Th2 response, which may serve as evidence of the interplay between macrophages and T cells (41). When macrophages trigger a specific immune response, T cells also contribute to macrophage activation through the CD40/CD40L costimulatory pathways. CD40 is a member of the TNF receptor family that is mainly expressed on the surface of antigen-presenting cells such as macrophages, and its ligand CD40L is almost exclusively expressed by activated $CD4^+$ T cells. When CD40 and CD40L interact, it leads to macrophage activation and B-cell differentiation (42, 43). In turn, activated macrophages further enhance cellular and humoral immune responses, which result in proinflammatory positive feedback. CD40L mRNA levels are elevated in the synovium during the early onset of OA (40) (Figure 3E).

5.5 OA synovial macrophages cause bone destruction through osteoclastogenesis

As specialized phagocytes, osteoclasts play an important role in the metabolic balance of bone tissue. An equivalent level of osteoclasts and osteoblasts is a key factor in healthy bone remodeling. However, in OA joints, osteoclasts are aberrantly activated, which leads to typical subchondral bone destruction and absorption (44). Notably, this activation of osteoclasts may involve synovial macrophages. CD14+ macrophages extracted from the synovial fluid of OA patients can transform into functional osteoclasts when stimulated by receptor activator of nuclear factor κB ligand (RANKL, an osteoclast differentiation factor), IL-1α and TNF-α (44). In addition to direct transformation, macrophages can also indirectly promote osteoclast activation through CD4+ T cells and synovial fibroblasts. In rheumatoid arthritis (RA), cytokines such as TNF-α and IL-1 secreted by macrophages stimulate the differentiation of Th17 cells, which subsequently release IL-17 to induce RANKL production in synovial fibroblasts (45). In OA, osteoclastogenesis induced by CD4+ T cells has also been discovered; however, whether the mechanism of this change is identical to that in RA has not yet been clarified (46) (Figure 3B).

5.6 OA synovial macrophages interact with adipocytes

Obesity is not only a risk factor for OA occurrence but also an exacerbating factor in OA development. Animal experiments have shown that a high-fat diet (HFD) can exacerbate synovitis in OA mice, which is characterized by increased infiltration of synovial macrophages and partial loss of joint adipose tissue (47). It is assumed that fat tissues outside the joint rather than those inside the joint are responsible for the exacerbation of synovitis. Fat tissues outside the joint may secrete adipokines such as leptin, adiponectin and visfatin to remotely control the number and function of macrophages in the synovium *via* blood circulation. Markedly elevated blood adipokines and an increased number of synovial macrophages and TNF-α and IL-1 expression were found in HFD-fed OA mice (47). Among adipokines, visfatin was recently shown to be capable of inducing inflammatory responses by activating Toll-like receptor 4 (TLR4) expressed on monocytes and macrophages and subsequently inducing the secretion of TNF and IL1 (48, 49). Leptin and adiponectin are also closely related to the nonspecific immune response (50). Local fat tissue in OA joints, on the other hand, is thought to protect against OA progression. A study of OA synoviocytes cultured with microfragmented adipose tissue (MF) showed that MF reduced the release of CCL2 and MMPs, downregulated TLR4 and increased tissue inhibitor of metalloproteinases (TIMP-1, an MMP-9 inhibitor) in synoviocytes (51). Another clinical study of 977 OA patients showed that the infrapatellar fat pad (a part of local fat tissue) is beneficially associated with radiographic OA, MRI structural pathology and knee pain (52). It is worth mentioning that the relationship between macrophages and adipocytes is mutual. Macrophage-derived proinflammatory cytokines contribute to the destruction and remodeling of local joint adipose tissue (47) (Figure 3C).

6 Drugs targeting macrophages and macrophage-associated inflammatory pathways

6.1 Drugs targeting macrophage-associated inflammatory cytokines (TNF-α, IL-1)

Recent studies have shown that the IL-1 receptor antagonist (IL-1Ra) anakinra exerts positive effects on articular inflammatory diseases such as rheumatoid arthritis and systemic juvenile idiopathic arthritis (53). In some animal experiments, it has been proven that IL-1Ra can prevent the progression of experimental OA by inhibiting the generation and activity of IL-1 (54, 55). However, different conclusions were drawn by two RCTs in which no significant clinical improvements in OA were detected after interarticular injection of the IL-1Ra anakinra or the IL-1 receptor antibody AMG108 (56, 57) (Table 2). Overall, the mechanism and clinical application of IL-1Ra in OA treatment require further research.

TNF-α is a crucial proinflammatory mediator in the initiation of OA. Therefore, anti-TNF therapy has become a hot spot of research in recent years. In 2006, Grunk M reported that a 68-year-old male patient with bilateral OA of the knees gained remarkable pain relief after subcutaneous injection of the TNF antibody adalimumab. This case report indicated exciting medical efficacy of TNF antibody on OA human beings rather than animals for the first time (58). Subsequently, Magnano MD carried out a pilot study in which 12 patients with hand OA were treated with adalimumab (40 mg/2 w) for 12 weeks. The treatment group had statistically significant improvements in the number of swollen joints and improvements in the number of tender joints, grip strength, disability and pain (59). In another pilot study, 10 women with bilateral OA of the hand were enrolled. The participants were treated with interarticular injections of the TNF antibody infliximab in one hand and an equal amount of saline in the other hand. After 12 months of treatment, the hands treated with infliximab exhibited more significant pain relief and radiographic alleviation than those treated with saline (60). Although these case reports and pilot studies demonstrated that TNF antibodies could

TABLE 2 Characteristics of studies researching macrophage-targeting drugs for OA treatment.

First Author, Year	Study Type	Country	Population	Experimental environment	Interference
Drugs targeting macrophage-derived inflammatory cytokines					
IL-1 antagonist					
Pelletier JP, 1997[54]	Animal study	Canada	17 dogs	*In vivo + in vitro*	Surgery induced knee OA + intra-articular injection of autologous cells transduced with the IL-1Ra gene
Caron JP, 1996[55]	Animal study	Canada	16 dogs	*In vivo*	Surgery induced knee OA + intra-articular injection of recombinant human IL-1Ra
Chevalier X, 2009[56]	RCT	USA	170 knee OA patients	*In vivo*	Anakinra (an IL-1Ra) intra-articular injection
Cohen SB, 2011[57]	RCT	USA	228 knee OA patients	*In vivo*	AMG 108 (a fully human monoclonal antibody to IL-1R) subcutaneously or intravenously injection
TNF blockade					
Grunke M, 2006[58]	Case report	Germany	a 68 year old male knee OA patient	*In vivo*	Adalimumab (human TNF antibody) subcutaneously injection
Magnano MD, 2007[59]	Pilot trial	USA	12 hands OA patients	*In vivo*	Adalimumab intra-articular injection
Fioravanti A, 2009[60]	Pilot trial	Italy	10 hands OA patients	*In vivo*	Infliximab (TNF-α antagonist) intra-articular injections
Chevalier X, 2015[61]	RCT	France	99 hands OA patients	*In vivo*	Adalimumab subcutaneous injections
Aitken D, 2018[62]	RCT	Australia	51 hands OA patients	*In vivo*	Adalimumab subcutaneous injections every other week
Drugs inducing M2 polarization					
Dai M, 2018[63]	Animal study	China	Rats	*In vivo + in vitro*	Surgery-induced knee OA+ SCII intra-articular injections
Shu CC, 2020[64]	Animal study	Australia	Mice	*In vivo*	Surgery induced knee OA+ intra-articular injection of Hymovis (a hyaluronan hexadecylamide derivative)
Manferdini C, 2017[65]	In vitro test	Italy	12 human OA synovial tissues	*In vitro*	M1 macrophages from OA tissues were co-cultured with ASC
Cherian JJ, 2015[66]	RCT	USA	102 knee OA patients	*In vivo*	GEC-TGF-β1 intra-articular injection
Ha CW, 2015[67]	RCT	South Korea	27 knee OA patients	*In vivo*	GEC-TGF-β1 intra-articular injection (high dose)
Cho JJ, 2017[68]	RCT	South Korea	27 knee OA patients	*In vivo*	GEC-TGF-β1 intra-articular injection (high dose)
Cho J, 2016[69]	RCT	South Korea	156 knee OA patients	*In vivo*	Invossa™ intra-articular injection
Lee H; 2018[70]	Animal study	South Korea	Rats	*In vivo*	Surgery-induced knee OA+ Invossa™ intra-articular injection

(Continued)

10.3389/fimmu.2023.1164137

TABLE 2 Continued

First Author, Year	Study Type	Country	Population	Experimental environment	Interference
Drugs inhibiting M1 polarization					
Wang H, 2021[71]	Animal study	China	Mice	*In vivo*	Collagenase-induced OA+ Frugoside intra-articular injection

First Author, Year	Drug Name	Outcome	Result	Mechanism
Drugs targeting macrophage-derived inflammatory cytokines				
IL-1 antagonist				
Pelletier JP, 1997[54]	Autologous cells transduced with the IL-1Ra gene	Macroscopic and microscopic changes	IL-1Ra suppressed early experimental osteoarthritis	Block IL-1 receptor
Caron JP, 1996[55]	Recombinant human IL-1Ra	Macroscopic and microscopic changes; RNA expression	IL-1Ra suppressed experimental osteoarthritis	Block IL-1 receptor
Chevalier X, 2009[56]	Anakinra	WOMAC score; Adverse events	Anakinra didn't improve joint pain and function	Block IL-1 receptor
Cohen SB, 2011[57]	AMG 108	WOMAC score; Adverse events	AMG 108 didn't improve joint pain and function	Block IL-1 receptor
TNF blockade				
Grunke M, 2006[54]	Adalimumab	Self-reported joint function and pain; MRI	Adalimumab improved joint function and pain	Bind with TNF
Magnano MD, 2007[59]	Adalimumab	ACR response; Adverse events	Adalimumab leaded to pain relief and radiographic alleviation	Bind with TNF
Fioravanti A, 2009[60]	Infliximab	Radiographs changes; VAS pain score	Infliximab leaded to pain relief and radiographic alleviation	Bind with TNF
Chevalier X, 2015[61]	Adalimumab	Number of people with 50% of VAS improvement;	Adalimumab didn't improve joint pain and function	Bind with TNF
Aitken D, 2018[62]	Adalimumab	VAS pain score; AUSCAN pain score; MRI	Adalimumab didn't improve joint pain and function	Bind with TNF
Drugs inducing M2 polarization				
Dai M, 2018[63]	SCII	Macroscopic and microscopic changes; RNA expression	SCII significantly improved the structural integrity of the cartilage tissue in OA rats	SCII increases M2-polariation of macrophages; SCII inhibites chondrocyte apoptosis
Shu CC, 2020[64]	Hymovis	Macroscopic and microscopic changes; RNA expression	Hymovis reduces allodynia at an early but not late stage of OA	Hymovis increased M2- macrophages.
Manferdini C, 2017[65]	ASC	Microscopic changes; RNA expression	M1-like macrophage markers downregulated while M2-like macrophage markers upregulated when cultured with ASC	ASC activates M2-macrophages while inhibits M1-macrophages
Cherian JJ, 2015[66]	GEC-TGF-β1	IKDC score; VAS pain; Adverse events	GEC-TGF-β1 patients had improved scores	TGF-β induces osteogenesis and chondrogenesis; TGF-β increase M2 polarization
Ha CW, 2015[67]	GEC-TGF-β1	IKDC score; WOMAC score; VAS pain;	GEC-TGF-β1 patients had improved scores	TGF-β induces osteogenesis and chondrogenesis; TGF-β increase M2 polarization
Cho JJ, 2017[68]	GEC-TGF-β1	MRI	GEC-TGF-β1 patients had improved MRI assessment parameters	TGF-β induces osteogenesis and chondrogenesis; TGF-β increase M2 polarization

(Continued)

TABLE 2 Continued

First Author, Year	Drug Name	Outcome	Result	Mechanism
Cho J, 2016[69]	Invossa™	IKDC score; WOMAC score; VAS pain; KOOS score	Invossa™ patients had improved scores	TGF-β induces osteogenesis and chondrogenesis; TGF-β increase M2 polarization
Lee H; 2018[70]	Invossa™	Pain behavior; Histological staining; RNA expression	Invossa™ rats showed pain relief, cartilage regeneration. It encouraged M2 polarization and inhibit M1 polarization	TGF-β induces osteogenesis and chondrogenesis; TGF-β increase M2 polarization
Drugs inhibiting M1 polarization				
Wang H, 2021[71]	Frugoside	Histological staining; RNA expression; Protein level;	Frugoside attenuates synovial inflammation and delays the development of OA	Frugoside inhibits macrophage M1 polarization

RCT, randomized control trial; OA, osteoarthrosis; IL-1Ra, Interleukin-1 receptor antagonis; WOMAC, Western Ontario and McMaster Universities Osteoarthritis Index; ACR, American College of Rheumatology; VAS, Visual Analogue Scale; AUSCAN, Australian/Canadian Hand OA Index; SCII, squid type II collagen; ASC, adipose mesenchymal stromal cell; GEC-TGF-β1, genetically engineered chondrocytes virally transduced with TGF-β1; IKDC, International Knee Documentation Committee; KOOS, Knee Injury and Osteoarthritis Outcome Score.

prevent the progression of OA, several RCTs yielded opposite conclusions. A randomized controlled crossover trial enrolled 43 patients with erosive hand OA and treated them with adalimumab or saline. Another RCT enrolled 85 hand OA participants and treated them with adalimumab or saline. Both RCTs showed similar pain scores and radiographic scores between the groups (61, 62).

6.2 Drugs that induce M2 polarization

Since M2 synovial macrophages play an anti-inflammatory role in OA, drugs that induce M2 polarization might be a promising strategy for the treatment of OA. In this section, we will summarize several drugs that increase M2 macrophages.

Dai M found that squid type II collagen (SCII) could increase the production of collagen type II and GAG and promote cartilage repair *in vitro* by increasing the ratio of M2 macrophages and the levels of chondrogenic cytokines (TGF-β1 and TGF-β3) in synovial fluid. Additionally, the glycine in SCII could activate the glycine receptor on chondrocytes to decrease intracellular calcium concentrations, resulting in the inhibition of chondrocyte apoptosis. *In vivo* experiments using a rat model of OA also proved that SCII could induce M2 polarization, increase chondrogenic cytokines and inhibit chondrocyte apoptosis and MMP13 production (63).

Shu CC found that OA mice treated with Hymovis® (a hyaluronan derivative) showed significantly higher ratios of M2 macrophages. This may explain the longer-term effect of Hymovis® on pain relief and the decrease in joint cystic fibrosis (64).

Manferdini C found that adipose mesenchymal stromal cells (ASCs) could transform M1 macrophages into M2 macrophages through PGE2. In cocultures containing ASCs and M1 macrophages, the M1 macrophage factors IL1β, TNFα, IL6, MIP1α/CCL3, S100A8 and S100A9 were downregulated, while the M2 markers IL10, CD163 and CD206 were upregulated. This change could be blocked by a PGE2 receptor antagonist. This result indicates that ASCs can be a promising OA treatment (65).

TGF-β may have anti-inflammatory and immunosuppressive properties. The cytokine TGF-β can induce osteogenesis and chondrogenesis and plays a role in cell growth, differentiation and extracellular matrix protein synthesis. In addition, TGF-β can promote proteoglycan synthesis and chondrocyte proliferation. Multiple clinical trials have proven that interarticular injection of genetically engineered allogeneic human chondrocytes expressing TGF-β1 (GEC-TGF-β1) can alleviate pain and articular deterioration in OA patients (66–68). Based on the efficacy of TGF-β, INVOSSA-K was discovered. As a novel cell and gene therapy for OA, INVOSSA-K contains nontransformed human chondrocytes and GEC-TGF-β1. In a phase III clinical trial, the pain scores and function scores of OA patients significantly improved at the 1-year follow-up after a single injection of Invossa™ (69). To investigate how Invossa™ alleviates OA, Lee H injected Invossa™ into a rat OA model. Using RT-PCR and histological staining, he found that INVOSSA-K increased the number of M2 macrophages and decreased the number of M1 macrophages, indicating that INVOSSA-K might play an anti-inflammatory role by manipulating macrophage polarization (70). Though from a scientific point of view, the principals of INVOSSA-K treatment is interesting, it is still need to note that this treatment is not available to most western countries yet because the manufacture mislabeled the ingredients used (Table 2).

6.3 Drugs that inhibit M1 polarization

Frugoside (FGS) is isolated from *Calotropis gigantea* and possesses a special cardenolide structure. It was recently discovered that cardiac glycosides are beneficial for the cardiovascular system and can alleviate inflammatory symptoms. In 2021, Wang H found that FGS could delay the development of OA by inhibiting the M1 polarization of synovial macrophages. The expression of iNOS, F4/80, Col2α1, MMP13 and M1 macrophage

factors was analyzed by RT-PCR, WB, flow cytometry and immunofluorescence staining after injecting FGS into the damaged joints of collagenase-induced OA (CIOA) mice. The results demonstrated that FGS inhibited M1 macrophage polarization, which subsequently decreased the secretion of IL-6 and TNF-α. Further results showed that FGS could inhibit M1 macrophage polarization by partially downregulating the expression of miR-155 (71) (Table 2).

7 Conclusions

Our review summarizes the role of synovial macrophages in the onset and progression of OA. Current evidence indicates that OA synovitis mainly arises from the proliferation and activation of synovial macrophages. The accumulation of M1 macrophages and imbalanced M1/M2 ratio promote OA development. M1 macrophages exacerbate inflammation by secreting multiple proinflammatory cytokines and activate surrounding tissue cells. The crosstalk between macrophages and these surrounding cells is summarized in this review. Drugs targeting macrophages and macrophage-associated inflammatory pathways are also summerized in this review. IL-1 receptor antagonists and TNF-α receptor antagonists might be able to ameliorate OA. New therapies such as SCII, Hymovis®, ASC, INVOSSA and Frugoside can either enhance M2 polarization or inhibit M1 polarization, which subsequently reduces the inflammatory response in OA patients.

Author contributions

KZ and JQR contributed equally as co-first author. All authors contributed to the article and approved the submitted version.

Conflict of interest

The authors declare that the research was conducted in the absence of any commercial or financial relationships that could be construed as a potential conflict of interest.

Publisher's note

All claims expressed in this article are solely those of the authors and do not necessarily represent those of their affiliated organizations, or those of the publisher, the editors and the reviewers. Any product that may be evaluated in this article, or claim that may be made by its manufacturer, is not guaranteed or endorsed by the publisher.

References

1. Hiligsmann M, Cooper C, Arden N, Boers M, Branco JC, Luisa Brandi M, et al. Health economics in the field of osteoarthritis: an expert's consensus paper from the European society for clinical and economic aspects of osteoporosis and osteoarthritis (ESCEO). *Semin Arthritis Rheumatol* (2013) 43(3):303–13. doi: 10.1016/j.semarthrit.2013.07.003

2. Sellam J, Berenbaum F. The role of synovitis in pathophysiology and clinical symptoms of osteoarthritis. *Nat Rev Rheumatol* (2010) 6(11):625–35. doi: 10.1038/nrrheum.2010.159

3. Benito MJ, Veale DJ, FitzGerald O, van den Berg WB, Bresnihan B. Synovial tissue inflammation in early and late osteoarthritis. *Ann Rheum Dis* (2005) 64(9):1263–7. doi: 10.1136/ard.2004.025270

4. Zhang H, Cai D, Bai X. Macrophages regulate the progression of osteoarthritis. *Osteoarthritis Cartilage* (2020) 28(5):555–61. doi: 10.1016/j.joca.2020.01.007

5. Yao Y, Xu XH, Jin L. Macrophage polarization in physiological and pathological pregnancy. *Front Immunol* (2019) 10:792. doi: 10.3389/fimmu.2019.00792

6. Athanasou NA, Quinn J. Immunocytochemical analysis of human synovial lining cells: phenotypic relation to other marrow derived cells. *Ann Rheum Dis* (1991) 50 (5):311–5. doi: 10.1136/ard.50.5.311

7. Haywood L, McWilliams DF, Pearson CI, Gill SE, Ganesan A, Wilson D, et al. Inflammation and angiogenesis in osteoarthritis. *Arthritis Rheumatol* (2003) 48 (8):2173–7. doi: 10.1002/art.11094

8. Bondeson J, Wainwright SD, Lauder S, Amos N, Hughes CE. The role of synovial macrophages and macrophage-produced cytokines in driving aggrecanases, matrix metalloproteinases, and other destructive and inflammatory responses in osteoarthritis. *Arthritis Res Ther* (2006) 8(6):R187. doi: 10.1186/ar2099

9. Ziegler-Heitbrock L. The CD14+ CD16+ blood monocytes: their role in infection and inflammation. *J Leukoc Biol* (2007) 81(3):584–92. doi: 10.1189/jlb.0806510

10. Xie J, Huang Z, Yu X, Zhou L, Pei F. Clinical implications of macrophage dysfunction in the development of osteoarthritis of the knee. *Cytokine Growth Factor Rev* (2019) 46:36–44. doi: 10.1016/j.cytogfr.2019.03.004

11. Shen J, Hilgenbrink AR, Xia W, Feng Y, Dimitrov DS, Lockwood MB, et al. Folate receptor-β constitutes a marker for human proinflammatory monocytes. *J Leukoc Biol* (2014) 96(4):563–70. doi: 10.1189/jlb.2AB0713-372R

12. Kraus VB, McDaniel G, Huebner JL, Stabler TV, Pieper CF, Shipes SW, et al. Direct *in vivo* evidence of activated macrophages in human osteoarthritis. *Osteoarthritis Cartilage* (2016) 24(9):1613–21. doi: 10.1016/j.joca.2016.04.010

13. van Lent PL, Blom AB, van der Kraan P, Holthuysen AE, Vitters E, van Rooijen N, et al. Crucial role of synovial lining macrophages in the promotion of transforming growth factor beta-mediated osteophyte formation. *Arthritis Rheumatol* (2004) 50 (1):103–11. doi: 10.1002/art.11422

14. Takano S, Uchida K, Inoue G, Miyagi M, Aikawa J, Iwase D, et al. Nerve growth factor regulation and production by macrophages in osteoarthritic synovium. *Clin Exp Immunol* (2017) 190(2):235–43. doi: 10.1111/cei.13007

15. Blom AB, van Lent PL, Holthuysen AE, van der Kraan PM, Roth J, van Rooijen N, et al. Synovial lining macrophages mediate osteophyte formation during experimental osteoarthritis. *Osteoarthritis Cartilage* (2004) 12(8):627–35. doi: 10.1016/j.joca.2004.03.003

16. Topoluk N, Steckbeck K, Siatkowski S, Burnikel B, Tokish J, Mercuri J. Amniotic mesenchymal stem cells mitigate osteoarthritis progression in a synovial macrophage-mediated *in vitro* explant coculture model. *J Tissue Eng Regener Med* (2018) 12 (4):1097–110. doi: 10.1002/term.2610

17. Wu CL, McNeill J, Goon K, Little D, Kimmerling K, Huebner J, et al. Conditional macrophage depletion increases inflammation and does not inhibit the development of osteoarthritis in obese macrophage fas-induced apoptosis-transgenic mice. *Arthritis Rheumatol* (2017) 69(9):1772–83. doi: 10.1002/art.40161

18. Wood MJ, Leckenby A, Reynolds G, Spiering R, Pratt AG, Rankin KS, et al. Macrophage proliferation distinguishes 2 subgroups of knee osteoarthritis patients. *JCI Insight* (2019) 4(2):e125325. doi: 10.1172/jci.insight.125325

19. Wu K, Yuan Y, Yu H, Dai X, Wang S, Sun Z, et al. The gut microbial metabolite trimethylamine n-oxide aggravates GVHD by inducing M1 macrophage polarization in mice. *Blood.* (2020) 136(4):501–15. doi: 10.1182/blood.2019003990

20. Yarnall BW, Chamberlain CS, Hao Z, Muir P. Proinflammatory polarization of stifle synovial macrophages in dogs with cruciate ligament rupture. *Vet Surg* (2019) 48 (6):1005–12. doi: 10.1111/vsu.13261

21. Zhang H, Lin C, Zeng C, Wang Z, Wang H, Lu J, et al. Synovial macrophage M1 polarisation exacerbates experimental osteoarthritis partially through r-spondin-2. *Ann Rheum Dis* (2018) 77(10):1524–34. doi: 10.1136/annrheumdis-2018-213450

22. Utomo L, Bastiaansen-Jenniskens YM, Verhaar JA, van Osch GJ. Cartilage inflammation and degeneration is enhanced by pro-inflammatory (M1) macrophages *in vitro*, but not inhibited directly by anti-inflammatory (M2) macrophages. *Osteoarthritis Cartilage* (2016) 24(12):2162–70. doi: 10.1016/j.joca.2016.07.018

23. Da-Wa ZX, Jun M, Chao-Zheng L, Sen-Lin Y, Chuan L, De-Chun L, et al. Exosomes derived from M2 macrophages exert a therapeutic effect via inhibition of the PI3K/AKT/mTOR pathway in rats with knee osteoarthritic. *BioMed Res Int* (2021) 2021:7218067. doi: 10.1155/2021/7218067

24. Zhu W, Li X, Fang S, Zhang X, Wang Y, Zhang T, et al. Anti-citrullinated protein antibodies induce macrophage subset disequilibrium in RA patients. *Inflammation.* (2015) 38(6):2067–75. doi: 10.1007/s10753-015-0188-z

25. Pal S, Konkimalla VB. Sulforaphane regulates phenotypic and functional switching of both induced and spontaneously differentiating human monocytes. *Int Immunopharmacol* (2016) 35:85–98. doi: 10.1016/j.intimp.2016.03.008

26. Sun H, Sun Z, Xu X, Lv Z, Li J, Wu R, et al. Blocking TRPV4 ameliorates osteoarthritis by inhibiting M1 macrophage polarization via the ROS/NLRP3 signaling pathway. *Antioxidants (Basel Switzerland)* (2022) 11(12):2315. doi: 10.3390/antiox11122315

27. Gu C, Chen M, Li X, Geng D, Wang C. MAGL regulates synovial macrophage polarization vis inhibition of mitophagy in osteoarthritic pain. *Mol Med Rep* (2023) 27 (6):117. doi: 10.3892/mmr.2023.13004

28. Blom AB, van Lent PL, Libregts S, Holthuysen AE, van der Kraan PM, van Rooijen N, et al. Crucial role of macrophages in matrix metalloproteinase-mediated cartilage destruction during experimental osteoarthritis: involvement of matrix metalloproteinase 3. *Arthritis Rheumatol* (2007) 56(1):147–57. doi: 10.1002/art.22337

29. Conti P, DiGioacchino M. MCP-1 and RANTES are mediators of acute and chronic inflammation. *Allergy Asthma Proc* (2001) 22(3):133–7. doi: 10.2500/108854101778148737

30. Schuster R, Rockel JS, Kapoor M, Hinz B. The inflammatory speech of fibroblasts. *Immunol Rev* (2021) 302(1):126–46. doi: 10.1111/imr.12971

31. Fernandes JC, Martel-Pelletier J, Pelletier JP. The role of cytokines in osteoarthritis pathophysiology. *Biorheology* (2002) 39(1-2):237–46.

32. Schlaak JF, Pfers I, Meyer Zum Büschenfelde KH, Märker-Hermann E. Different cytokine profiles in the synovial fluid of patients with osteoarthritis, rheumatoid arthritis and seronegative spondylarthropathies. *Clin Exp Rheumatol* (1996) 14 (2):155–62.

33. Samavedi S, Diaz-Rodriguez P, Erndt-Marino JD, Hahn MS. A three-dimensional chondrocyte-macrophage coculture system to probe inflammation in experimental osteoarthritis. *Tissue Eng Part A* (2017) 23(3-4):101–14. doi: 10.1089/ten.tea.2016.0007

34. Ebata T, Terkawi MA, Kitahara K, Yokota S, Shiota J, Nishida Y, et al. Noncanonical pyroptosis triggered by macrophage-derived extracellular vesicles in chondrocytes leading to cartilage catabolism in osteoarthritis. *Arthritis Rheumatol* (2023). doi: 10.1002/art.42505

35. Goldring MB. The role of cytokines as inflammatory mediators in osteoarthritis: lessons from animal models. *Connect Tissue Res* (1999) 40(1):1–11. doi: 10.3109/03008209909005273

36. Ayral X, Pickering EH, Woodworth TG, Mackillop N, Dougados M. Synovitis: a potential predictive factor of structural progression of medial tibiofemoral knee osteoarthritis – results of a 1 year longitudinal arthroscopic study in 422 patients. *Osteoarthritis Cartilage* (2005) 13(5):361–7. doi: 10.1016/j.joca.2005.01.005

37. Haubruck P, Pinto MM, Moradi B, Little CB, Gentek R. Monocytes, macrophages, and their potential niches in synovial joints - therapeutic targets in post-traumatic osteoarthritis? *Front Immunol* (2021) 12:763702. doi: 10.3389/fimmu.2021.763702

38. Yuan GH, Masuko-Hongo K, Sakata M, Tsuruha J, Onuma H, Nakamura H, et al. The role of c-c chemokines and their receptors in osteoarthritis. *Arthritis Rheumatol* (2001) 44(5):1056–70. doi: 10.1002/1529-0131(200105)44:5<1056::AID-ANR186>3.0.CO;2-U

39. van den Bosch MH, Blom AB, Schelbergen RF, Koenders MI, van de Loo FA, van den Berg WB, et al. Alarmin S100A9 induces proinflammatory and catabolic effects predominantly in the M1 macrophages of human osteoarthritic synovium. *J Rheumatol* (2016) 43(10):1874–84. doi: 10.3899/jrheum.160270

40. Yang L, Chen Z, Guo H, Wang Z, Sun K, Yang X, et al. Extensive cytokine analysis in synovial fluid of osteoarthritis patients. *Cytokine* (2021) 143:155546. doi: 10.1016/j.cyto.2021.155546

41. Chen M, Lin X, Liu Y, Li Q, Deng Y, Liu Z, et al. The function of BAFF on T helper cells in autoimmunity. *Cytokine Growth Factor Rev* (2014) 25(3):301–5. doi: 10.1016/j.cytogfr.2013.12.011

42. Elgueta R, Benson MJ, de Vries VC, Wasiuk A, Guo Y, Noelle RJ. Molecular mechanism and function of CD40/CD40L engagement in the immune system. *Immunol Rev* (2009) 229(1):152–72. doi: 10.1111/j.1600-065X.2009.00782.x

43. Soong RS, Song L, Trieu J, Lee SY, He L, Tsai YC, et al. Direct T cell activation via CD40 ligand generates high avidity CD8+ T cells capable of breaking immunological tolerance for the control of tumors. *PloS One* (2014) 9(3):e93162. doi: 10.1371/journal.pone.0093162

44. Adamopoulos IE, Sabokbar A, Wordsworth BP, Carr A, Ferguson DJ, Athanasou NA. Synovial fluid macrophages are capable of osteoclast formation and resorption. *J Pathol* (2006) 208(1):35–43. doi: 10.1002/path.1891

45. Takayanagi H. New developments in osteoimmunology. *Nat Rev Rheumatol* (2012) 8(11):684–9. doi: 10.1038/nrrheum.2012.167

46. Shen PC, Wu CL, Jou IM, Lee CH, Juan HY, Lee PJ, et al. T Helper cells promote disease progression of osteoarthritis by inducing macrophage inflammatory protein-1γ. *Osteoarthritis Cartilage* (2011) 19(6):728–36. doi: 10.1016/j.joca.2011.02.014

47. Larrañaga-Vera A, Lamuedra A, Pérez-Baos S, Prieto-Potin I, Peña L, Herrero-Beaumont G, et al. Increased synovial lipodystrophy induced by high fat diet aggravates synovitis in experimental osteoarthritis. *Arthritis Res Ther* (2017) 19(1):264. doi: 10.1186/s13075-017-1473-z

48. Kalaitzoglou E, Lopes EBP, Fu Y, Herron JC, Flaming JM, Donovan EL, et al. TLR4 promotes and DAP12 limits obesity-induced osteoarthritis in aged female mice. *JBMR Plus* (2019) 3(4):e10079. doi: 10.1002/jbm4.10079

49. Moschen AR, Kaser A, Enrich B, Mosheimer B, Theurl M, Niederegger H, et al. Visfatin, an adipocytokine with proinflammatory and immunomodulating properties. *J Immunol* (2007) 178(3):1748–58. doi: 10.4049/jimmunol.178.3.1748

50. Loffreda S, Yang SQ, Lin HZ, Karp CL, Brengman ML, Wang DJ, et al. Leptin regulates proinflammatory immune responses. *FASEB J* (1998) 12(1):57–65. doi: 10.1096/fsb2fasebj.12.1.57

51. Paolella F, Manferdini C, Gabusi E, Gambari L, Filardo G, Kon E, et al. Effect of microfragmented adipose tissue on osteoarthritic synovial macrophage factors. *J Cell Physiol* (2019) 234(4):5044–55. doi: 10.1002/jcp.27307

52. Han W, Cai S, Liu Z, Jin X, Wang X, Antony B, et al. Infrapatellar fat pad in the knee: is local fat good or bad for knee osteoarthritis? *Arthritis Res Ther* (2014) 16(4): R145. doi: 10.1186/ar4607

53. Burger D, Dayer JM, Palmer G, Gabay C. Is IL-1 a good therapeutic target in the treatment of arthritis? *Best Pract Res Clin Rheumatol* (2006) 20(5):879–96. doi: 10.1016/j.berh.2006.06.004

54. Pelletier JP, Caron JP, Evans C, Robbins PD, Georgescu HI, Jovanovic D, et al. *In vivo* suppression of early experimental osteoarthritis by interleukin-1 receptor antagonist using gene therapy. *Arthritis Rheumatol* (1997) 40(6):1012–9. doi: 10.1002/art.1780400604

55. Caron JP, Fernandes JC, Martel-Pelletier J, Tardif G, Mineau F, Geng C, et al. Chondroprotective effect of intraarticular injections of interleukin-1 receptor antagonist in experimental osteoarthritis. suppression of collagenase-1 expression. *Arthritis Rheumatol* (1996) 39(9):1535–44. doi: 10.1002/art.1780390914

56. Chevalier X, Goupille P, Beaulieu AD, Burch FX, Bensen WG, Conrozier T, et al. Intraarticular injection of anakinra in osteoarthritis of the knee: a multicenter, randomized, double-blind, placebo-controlled study. *Arthritis Rheumatol* (2009) 61 (3):344–52. doi: 10.1002/art.24096

57. Cohen SB, Proudman S, Kivitz AJ, Burch FX, Donohue JP, Burstein D, et al. A randomized, double-blind study of AMG 108 (a fully human monoclonal antibody to IL-1R1) in patients with osteoarthritis of the knee. *Arthritis Res Ther* (2011) 13(4):R125. doi: 10.1186/ar3430

58. Grunke M, Schulze-Koops H. Successful treatment of inflammatory knee osteoarthritis with tumour necrosis factor blockade. *Ann Rheum Dis* (2006) 65 (4):555–6. doi: 10.1136/ard.2006.053272

59. Magnano MD, Chakravarty EF, Broudy C, Chung L, Kelman A, Hillygus J, et al. A pilot study of tumor necrosis factor inhibition in erosive/inflammatory osteoarthritis of the hands. *J Rheumatol* (2007) 34(6):1323–7.

60. Fioravanti A, Fabbroni M, Cerase A, Galeazzi M. Treatment of erosive osteoarthritis of the hands by intra-articular infliximab injections: a pilot study. *Rheumatol Int* (2009) 29(8):961–5. doi: 10.1007/s00296-009-0872-0

61. Chevalier X, Ravaud P, Maheu E, Baron G, Rialland A, Vergnaud P, et al. Adalimumab in patients with hand osteoarthritis refractory to analgesics and NSAIDs: a randomised, multicentre, double-blind, placebo-controlled trial. *Ann Rheum Dis* (2015) 74(9):1697–705. doi: 10.1136/annrheumdis-2014-205348

62. Aitken D, Laslett LL, Pan F, Haugen IK, Otahal P, Bellamy N, et al. A randomised double-blind placebo-controlled crossover trial of HUMira (adalimumab) for erosive hand OsteoaRthritis - the HUMOR trial. *Osteoarthritis Cartilage* (2018) 26(7):880–7. doi: 10.1016/j.joca.2018.02.899

63. Dai M, Sui B, Xue Y, Liu X, Sun J. Cartilage repair in degenerative osteoarthritis mediated by squid type II collagen via immunomodulating activation of M2 macrophages, inhibiting apoptosis and hypertrophy of chondrocytes. *Biomaterials.* (2018) 180:91–103. doi: 10.1016/j.biomaterials.2018.07.011

64. Shu CC, Zaki S, Ravi V, Schiavinato A, Smith MM, Little CB. The relationship between synovial inflammation, structural pathology, and pain in post-traumatic osteoarthritis: differential effect of stem cell and hyaluronan treatment. *Arthritis Res Ther* (2020) 22(1):29. doi: 10.1186/s13075-020-2117-2

65. Manferdini C, Paolella F, Gabusi E, Gambari L, Piacentini A, Filardo G, et al. Adipose stromal cells mediated switching of the pro-inflammatory profile of M1-like macrophages is facilitated by PGE2: *in vitro* evaluation. *Osteoarthritis Cartilage* (2017) 25(7):1161–71. doi: 10.1016/j.joca.2017.01.011

66. Cherian JJ, Parvizi J, Bramlet D, Lee KH, Romness DW, Mont MA. Preliminary results of a phase II randomized study to determine the efficacy and safety of genetically engineered allogeneic human chondrocytes expressing TGF-β1 in patients with grade 3

chronic degenerative joint disease of the knee. *Osteoarthritis Cartilage* (2015) 23 (12):2109–18. doi: 10.1016/j.joca.2015.06.019

67. Ha CW, Cho JJ, Elmallah RK, Cherian JJ, Kim TW, Lee MC, et al. A multicenter, single-blind, phase IIa clinical trial to evaluate the efficacy and safety of a cell-mediated gene therapy in degenerative knee arthritis patients. *Hum Gene Ther Clin Dev* (2015) 26 (2):125–30. doi: 10.1089/humc.2014.145

68. Cho JJ, Totterman S, Elmallah RK, Kim TW, Lee B, Mont MA. An MRI evaluation of patients who underwent treatment with a cell-mediated gene therapy for degenerative knee arthritis: a phase IIa clinical trial. *J Knee Surg* (2017) 30(7):694–703. doi: 10.1055/s-0036-1597275

69. Cho J, Kim T, Park Y, Shin J, Kang S, Lee B. Invossa™(Tissuegene-c) in patients with osteoarthritis: a phase III trial. *Osteoarthritis Cartilage* (2016) 24:S190. doi: 10.1016/j.joca.2016.01.374

70. Lee H, Choi K, Kim H, Kim D, Lee Y, Lee B, et al. INVOSSA-K induces an anti-inflammatory environment in a rat mia model via macrophage polarization. *Osteoarthritis Cartilage* (2018) 26:S125. doi: 10.1016/j.joca.2018.02.272

71. Wang H, Zhang H, Fan K, Zhang D, Hu A, Zeng X, et al. Frugoside delays osteoarthritis progression via inhibiting miR-155-modulated synovial macrophage M1 polarization. *Rheumatol (Oxford)* (2021) 60(10):4899–909. doi: 10.1093/rheumatology/keab018

frontiers | Frontiers in Immunology

TYPE Original Research
PUBLISHED 20 July 2023
DOI 10.3389/fimmu.2023.1171150

Check for updates

OPEN ACCESS

EDITED BY
Rachel Elaine Hewitt,
University of Cambridge, United Kingdom

REVIEWED BY
Chuanju Liu,
New York University, United States
Jiaxiang Bai,
Soochow University, China

*CORRESPONDENCE
Yuhua Li
miraculously2020@163.com
Ben Liu
liubenqilu@gmail.com
Haichun Liu
sdulhc@163.com

†These authors have contributed equally to this work and share first authorship

RECEIVED 21 February 2023
ACCEPTED 22 June 2023
PUBLISHED 20 July 2023

CITATION
Yu R, Yuan Y, Liu Z, Liu L, Xu Z, Zhao Y, Jia C, Zhang P, Li H, Liu Y, Wang Y, Li W, Nie L, Sun X, Li Y, Liu B and Liu H (2023) Selenomethionine against titanium particle-induced osteolysis by regulating the ROS-dependent NLRP3 inflammasome activation via the β-catenin signaling pathway. *Front. Immunol.* 14:1171150. doi: 10.3389/fimmu.2023.1171150

COPYRIGHT
© 2023 Yu, Yuan, Liu, Liu, Xu, Zhao, Jia, Zhang, Li, Liu, Wang, Li, Nie, Sun, Li, Liu and Liu. This is an open-access article distributed under the terms of the Creative Commons Attribution License (CC BY). The use, distribution or reproduction in other forums is permitted, provided the original author(s) and the copyright owner(s) are credited and that the original publication in this journal is cited, in accordance with accepted academic practice. No use, distribution or reproduction is permitted which does not comply with these terms.

Selenomethionine against titanium particle-induced osteolysis by regulating the ROS-dependent NLRP3 inflammasome activation via the β-catenin signaling pathway

Ruixuan Yu[1†], Yongjian Yuan[1†], Zhicheng Liu[1,2†], Long Liu[3†], Zhaoning Xu[4], Yunpeng Zhao[1], Chunwang Jia[1], Pengfei Zhang[1], Hang Li[1], Yuhao Liu[1], Yi Wang[5,6], Weiwei Li[3], Lin Nie[1], Xuecheng Sun[7], Yuhua Li[1*], Ben Liu[1*] and Haichun Liu[1*]

[1]Department of Orthopaedics, Qilu Hospital of Shandong University, Jinan, Shandong, China, [2]The First Clinical Medical School, Shandong University, Jinan, Shandong, China, [3]Department of Pathology, Qilu Hospital, Cheeloo College of Medicine, Shandong University, Jinan, Shandong, China, [4]School of Nursing and Rehabilitation, Shandong University, Jinan, Shandong, China, [5]Department of Plastic and Burns Surgery, The Second Hospital of Shandong University, Jinan, Shandong, China, [6]Emergency Medicine Center, The Second Hospital of Shandong University, Jinan, Shandong, China, [7]Department of Orthopedic Trauma, Weifang People's Hospital, Weifang, Shandong, China

Wear debris-induced osteolysis, especially titanium (Ti) particles-induced osteolysis, is the most common cause of arthroplasty failure with no effective therapy. Previous studies have suggested that inflammation and impaired osteogenesis are associated with Ti particles -induced osteolysis. Selenium (Se) is an essential trace element in the human body, which forms selenomethionine (Se-Met) in nature, and selenoproteins has strong anti-inflammatory and antioxidant stress effects. In this study, the effects of Se-Met on Ti particles-induced osteolysis were observed and the potential mechanism was explored. We found that exogenous Se-Met relieved osteolysis induced by Ti particles in two animal models and MC3T3-E1 cells. We found that the addition of Se-Met effectively inhibited Ti particle-induced inflammation by regulating reactive oxygen species-dependent (ROS-dependent) NOD-like receptor protein 3 (NLRP3) inflammasome activation. These therapeutic effects were abrogated in MC3T3-E1 cells that had received a β-catenin antagonist, suggesting that Se-Met alleviates inflammatory osteolysis via the β-catenin signaling pathway. Collectively, these findings indicated that Se-Met may serve as a potential therapeutic agent for treating Ti particle-induced osteolysis.

KEYWORDS

selenomethionine, titanium particle-induced osteolysis, β-catenin, inflammatory osteolysis, NLRP3

1 Introduction

Total joint arthroplasty (TJA) is one of the most effective surgical procedures for treating terminal rheumatic arthritis and severe osteoarthritis, providing pain relief and improving the patients' quality of life. As the aging population is growing worldwide and the number of patients undergoing this surgery is increasing each year, the demand for TJAs is predicted to increase substantially (1). Therefore, the side effects of TJAs during long-term follow-up are a major concern, especially wear debris-induced osteolysis, which is considered to trigger implant loosening and affect the longevity of the implant (2, 3). It is mainly caused by a chronic inflammation reaction triggered by debris, including Ti particles (4), and disrupts bone homeostasis by stimulating various cell types, such as osteoblasts, osteoclasts, macrophages, and fibroblasts, to secrete proinflammatory cytokines, including IL-6, IL-1β, and tumor necrosis factor alpha (TNF-α) (5). Bone homeostasis is based on the balance between osteogenesis and bone resorption, and previous studies have focused on increased osteoclastic bone resorption (6), which has been mainly related to osteoclasts and macrophages (7), but the effect of osteoblasts is of great importance.

Se is an essential trace element in the human body and has been proven to exert biological functions in various systems (8), and Se-Met is one of the main natural forms of Se in living organisms (9). Selenoproteins is considered of great importance in inflammation and immunity, adequate levels of Se are necessary for initiating immunity (10), and previous studies have shown that Se treatment enhances the osteoblastic differentiation of bone marrow stromal cells (BMSCs) and inhibits the differentiation and formation of mature osteoclasts (11), facilitating osteogenic differentiation and bone healing. Selenium nanoparticles were recently found to suppress NLRP3 inflammasome activation in acute kidney injury mouse model (12), while a Se-deficient diet can suppress the expression of selenoprotein, which has an anti-oxidant function, and causes mitochondrial dysfunction and apoptosis of chondrocytes (13). Considering the physiological role of Se and selenoproteins in anti-oxidation and the detrimental effects of oxidative stress and inflammation in wear debris-induced osteolysis, whether Se can play a role in wear debris-induced inflammatory reactions and osteogenic inhibition remains unknown.

The NLRP3 inflammasome is a critical component of the innate immune system (14), and several studies have revealed that the NLRP3 inflammasome contributes to the pathogenesis of wear debris mediated inflammatory osteolysis (15) and is related to the induction of inflammatory mediators such as prostaglandin E2 (PGE2), TNF-α, and IL-1β (16), and Ti particle-induced reactive oxygen species production and structural changes in the mitochondria have been verified (17), thus providing proof of concept that pharmacological inhibition of the NLRP3 inflammasome is a viable therapeutic strategy. It has been reported that inflammation and osteogenesis inhibition are attenuated through activation of the β-catenin signaling pathway in Ti particle-induced osteolysis (18), and Se-Met has been shown to alleviate many inflammatory reactions (19–21).

This study aimed to investigate the role of Se-Met in Ti particle-induced osteolysis. In this study, we plan to determine the function of Se-Met in Ti particle-induced osteolysis in animals models and MC3T3-E1 cells, and we will explore the potential involvement and underlying mechanisms of NLRP3 inflammasome in the Ti particle-induced osteolysis following Se-Met treatment.

2 Methods

2.1 Preparation of Ti particles

Ti particles (catalog #IRMM531A) were purchased from Sigma Corporation (Sigma, St. Louis, MO, USA) and scanned using a scanning electron microscope, as shown in Figure 1E. The sizes and distributions of the Ti particles have been previously measured and reported. The average size of the Ti particle was 3.31 ± 2.38 μm. Ti particles were soaked in 75% alcohol for 24 h and then rinsed thrice with sterile water, heated at 180° for 8 h. Then, the Ti particles were immersed in sterile PBS. The imulus assay (LAL, Biowhittaker, USA) was used to detect the liquid in which the particles were soaked to ensure that the endotoxin levels were under 0.3 EU/ml. Titanium rods, 10 mm in length and 1 mm in diameter, were purchased from Sigma (St. Louis, MO, USA). After cleaning the rods thrice with 75% alcohol, the rods were sterilized by autoclaving and subsequently placed under sterile conditions until use.

2.2 Animals and Ti particles–induced osteolysis model

The experimental procedures were approved by the institutional Animal Care and Use Committee of Shandong University, and met the guidelines for the Care and Use of Laboratory Animals. Ten-week-old C57BL/6 wild-type (WT) mice were provided by the Experimental Animal Center of Shandong University. Twelve-week-old male Sprague-Dawley (SD) rats were provided by Vital River (Beijing, China). In summary, we constructed two animal models.

2.2.1 Cranial osteolysis models

The method used to establish cranial osteolysis models in mice has been described in our previous study. WT mice were divided into three groups (n = 7 per group): sham control group (CTL group), Ti particle only group (Ti group), and Ti particles + SE-MET treatment group (SE-MET group). All mice received an intraperitoneal (I.P.) injection of 1% pentobarbital sodium anesthesia at a dose of 50 mg/kg before surgery. Subsequently, each mouse underwent a 0.5-cm sagittal incision, and the periosteum remained intact. To simulate Ti particle-induced osteolysis, 100 μl of 0.1 mg/ml titanium particle suspension was injected directly into the skull and periosteum using a sterile technique in the Ti group and Se-Met treatment group. In contrast, in the sham group, no other intervention was performed, and the full-thickness skin was then sutured. Se-Met (Cat: HY-B1000) was purchased from MCE (Monmouth Junction, NJ, USA), and it was

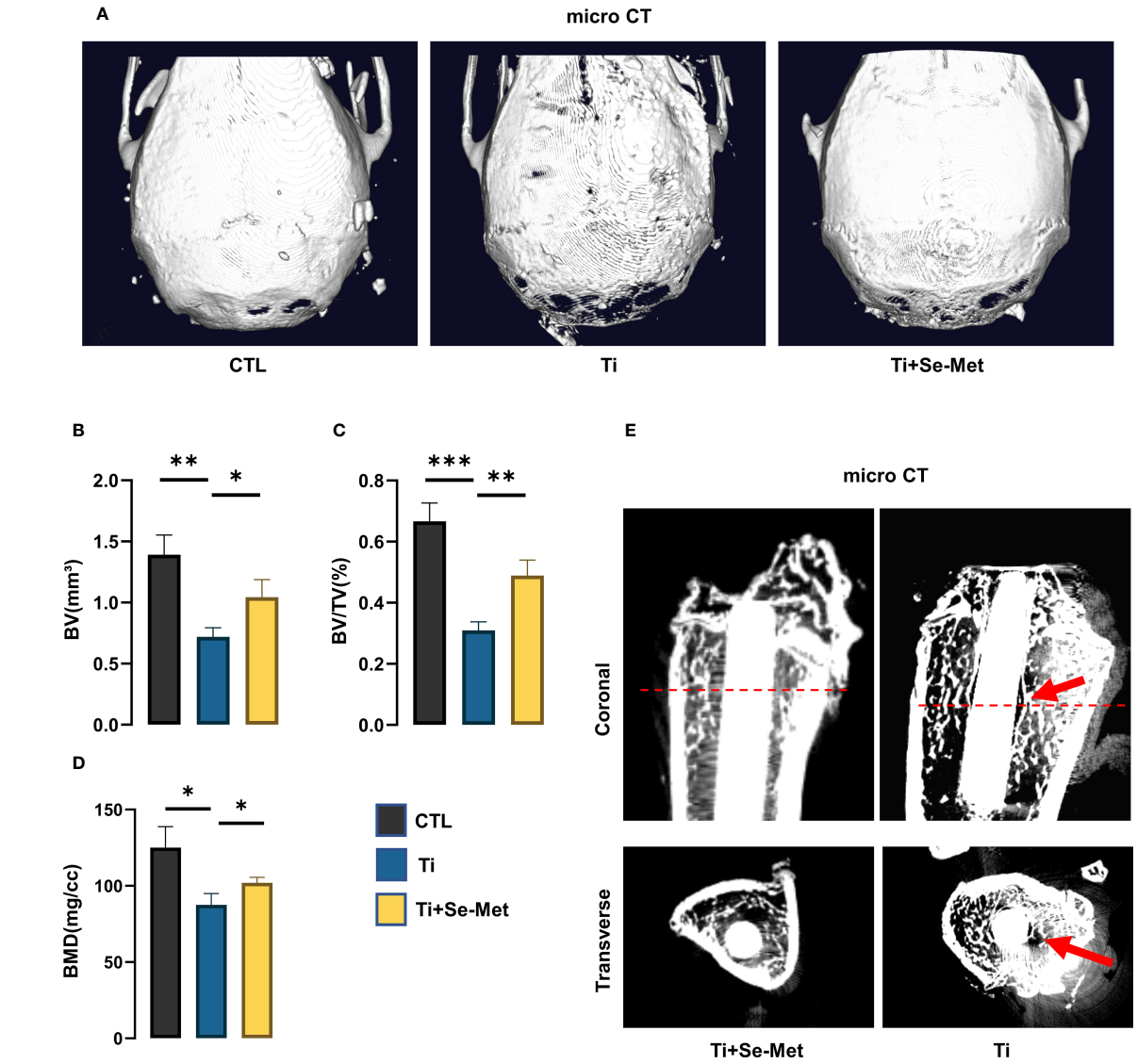

FIGURE 1
Se-Met attenuated Ti-particle-induced osteolysis. **(A)** Representative images of 3D reconstruction of mouse cranial bones; **(B-D)** quantitative analysis of BV, BV/TV (%), BMD (mg/cc); **(E)** Representative images of rat femurs, identified with red arrows showing osteolysis area. *P < 0.05, **P < 0.01, ***P < 0.001.

dissolved in sterilized treated drinking water to make an aqueous solution of 1mg/L. The SE-MET group (both rats and mice) was treated with 1 mg/L SE-MET solution instead of normal drinking water, and the mice in the CTL and Ti groups were treated with normal drinking water. The duration of Ti particle-induced osteolysis induction was 4 weeks (22).

2.2.2 Intramedullary nail osteolysis models

Fourteen SD rats with an average weight of 300 ± 30 g were randomly divided into two groups (n = 7 per group): the Ti particle only group (Ti group) and the Ti particles + SE-MET treatment group (SE-MET group). Before surgery, all rats were anesthetized by I.P. injection of 1% sodium pentobarbital at a dose of 40 mg/kg. The knee joint was disinfected and the knee capsule was dissected until the articular surface was exposed. A hole was punched in the intercondylar fossa. Before the Ti rod was implanted, 100 µL of 0.1 mg/ml Ti particle suspension was injected into the bone marrow cavity, and then the rod was inserted into the hole. Residual Ti particles in the joint cavity were cleaned with sterile saline and then closed (23).

2.3 Micro-CT Assessment

Femurs with Ti rods and calvarial tissues were initially fixed in formalin and subsequently examined by micro-CT with a Skyscan1176 scanner and associated analysis software (SkyScan, Aartselaar, Belgium). The scanning parameters were set as follows: 18 µm per layer, under a voltage of 50 kV and a current of 500 µA. Cone Beam Reconstruction software (SkyScan) was used for the reconstruction of three-dimensional (3D) images and to

evaluate different histomorphometric measurements: BMD (mg/mm2), BV (mm3), and BV/TV (%).

2.4 Histological and immunohistochemical analysis

Paraffin-embedded sections were prepared. Morphological characteristics of the rat femurs were observed using hematoxylin and eosin (H&E) staining. Masson staining (Salorbio, China) was used to stain new immature collagen in the blue zone by tissue coloration. Immunohistochemical staining for osteocalcin (OCN) (ab93876, Abcam, USA), COX2 (ab179800, Abcam, USA), and NLRP3 (ab263899, Abcam, USA) was also performed. Images were obtained using a light microscope.

2.5 Cell culture

MC3T3-E1 cells were obtained from the Cell Bank of the Chinese Academy of Sciences (Shanghai, China). MC3T3-E1 cells were maintained in α-MEM (Gibco, Brooklyn, NY) containing 10% FBS, 100 μg/ml streptomycin, and 100 U/ml penicillin in a 5% CO2 humidified atmosphere at 37°C, adherent cells were cultured until the cells reached approximately 90% confluence. The osteogenic medium was α-MEM supplemented with 10% FBS, 10 mM β-glycerophosphate, 0.5 mM vitamin C, and 0.1 μM dexamethasone. The induction time of Osteogenesis was induced for 14 d. Osteolysis was induced by adding 10 μg/cm^2 Ti particles. Cells were cultured in 6-well plates at a density of 1 × 10^5 cells/well in an incomplete medium and stimulated with 10 μg/cm^2 Ti particles solution, with or without Se-Met (5 μM) for 24 h. The culture medium and cells were collected for further experiments.

2.6 CCK-8 assay

To perform the Cell Counting Kit-8 (CCK-8) assay, MC3T3-E1 cells were seeded in 96-well plates at a density of 5000 cells per well. After allowing the cells to adhere for 12 h, different concentrations of the experimental drug were added to the wells and incubated for 24 h. Following this, 10μL of CCK-8 reagent was added to each well and incubated for another 15 min. The absorbance was measured at 450nm using a microplate reader. The data obtained was then used to calculate cell viability and compare the effects of the experimental drug on cellular proliferation.

2.7 Red S staining

After being cultured in osteogenic medium for 2 weeks, MC3T3-E1 cells were washed with PBS, fixed in 4% paraformaldehyde for 20 min, and stained for 30 min with 1% Alizarin Red Staining Solution (Servicebio. Nanjing. China). After the staining, the remaining dye solution was rinsed with distilled water. Stained calcified nodules were observed and photographed under a light microscope.

2.8 ALP staining

To assess Alkaline phosphatase (ALP) activity, MC3T3-E1 cells were cultured in osteogenic medium for a week and then fixed in 4% paraformaldehyde for 15 minutes. Following this, the cells were rinsed three times with PBS and stained with BCIP/NBT working solution in the dark for 60 minutes. Microscopic analysis was performed to examine the staining results.

2.9 Protein isolation and Western blotting analysis

Total protein was isolated from MC3T3-E1 with RIPA Lysis Buffer (Servicebio Corporation, Nanjing. China). Then the total protein was centrifuged at 12000 RPM for 6 min at 4°, and protein concentrations were measured using the BCA Protein Assay Kit (Beyotime Biotechnology Corporation). Equal amounts of the extracted proteins were electrophoresed on SDS-PAGE gels and transferred onto polyvinylidene difluoride membrane. Subsequently, 5% BSA was used to block the membranes for 1 h at room temperature and membranes were then washed thrice in TBST and incubated with primary antibodies overnight at 4°C, including anti-NLRP3 (1:1000 dilution, SC06-23, ThermoFisher Corporation, USA), anti-iNOS (1:1000 dilution, ab15323, Abcam Corporation, USA), anti-COX2 (1:2000 dilution, 12375-1-AP, Proteintech Corporation, USA), anti-COL1 (1:1000 dilution, 14695-1-AP, Proteintech Corporation, USA), anti-Osteopontin (OPN) (1:1000 dilution, ab214050, Abcam Corporation, USA), anti-RUNX2 (1:1000 dilution, #12556S, Cellsignal Corporation, USA), anti-β-Catenin (1:1000 dilution, 17565-1-AP, Proteintech Corporation, USA), anti-β-tubulin (1:2000 dilution, 10094-1-lg, Proteintech Corporation, USA), and anti-GADPH (1:2500 dilution, ab9485, Abcam Corporation, USA). After washing thrice with TBST buffer, the membranes were incubated with HRP-conjugated anti-goat IgG, anti-mouse IgG, or anti-rabbit IgG as secondary antibodies. The DNR Bio-Imaging System was used to detect protein levels on the membrane.

2.10 Real-time quantitative PCR

Total mRNA was isolated from MC3T3-E1 cells using the TRIzol reagent. Complementary DNA was synthesized from total mRNA using the PrimeScript RT Reagent Kit. RNA PCR kit (Servicebio. Nanjing. China) was used for the real-time PCR analysis. All procedures were performed per the manufacturer's instructions. Table 1 lists the PCR primer sequences.

2.11 Immunofluorescence

MC3T3-E1 cells were seeded on coverslips containing osteogenic medium in 24-well plates. The cells were then fixed with 4% paraformaldehyde and permeabilized with 0.2% Triton X-100 (Servicebio. Nanjing. China) for 15 min. They were then blocked

TABLE 1 Primers used for quantitative real-time PCR.

Source	Target	Forward primer, 5′-3′	Reverse primer, 3′-5′
Mouse	COX-2	GGAACTTTCTGGTCCCTTCAG	TGTGTTTGGAGTGGGTTTCA
	iNOS	GCCAAGCTGAAATTGAATGAGGA	TTCTGTGCCGGCAGCTTTAAC
	RUNX-2	TTGACCTTTGTCCCAATGC	AGGTTGGAGGCACACATAGG
	Caspase-3	CTCGCTCTGGTACGGATGTG	TCCCATAAATGACCCCTTCATCA
	β-Catenin	ACGGTGCCGCGCCGCTTATA	TAGCCATTGTCCACGCAGCGG
	GADPH	AGCAGTCCCGTACACTGGCAAAC	TCTGTGGTGATGTAAATGTCCTCT

with a blocking buffer for 60 min. Next, primary antibodies, including anti-NLRP3 (1:50), anti-COX2 (1:150), anti-OCN (1:200), and anti-β-catenin (1:400), were added to each well and incubated at 4°C for 12 h. Subsequently, the cells were rinsed and incubated for 60 min in the dark with the corresponding secondary fluorescent antibodies (Alexa Fluor®488 or 647 (Abcam). Fluorescently stained cells were counterstained with DAPI for 15 min. Cover slides were placed on microscope slides with a fluorescent anti-fade solution (Beyotime) and observed under a fluorescence microscope (Zeiss). Fluorescence intensity was measured using ImageJ software.

2.12 Flow cytometry

Briefly, Mc3t3-e1 cells from each group were analyzed using flow cytometry. Cells were stained with annexin V-FITC and propidium iodide for 20 min at room temperature in the dark, according to the manufacturer's protocol. Apoptosis was detected by CytoFLEX S flow cytometry (Beckman Coulter, Indianapolis, IN, USA). The measured data were analyzed using FlowJo software. The measured data were analyzed using FlowJo software.

2.13 ROS assay

To detect intracellular ROS, we used a ROS assay kit. All procedures were performed per the manufacturer's instructions. Briefly, after washing twice with sterile PBS, MC3T3-E1 cells were stained with 10 μM DCFDA at 37°C for 20 min in the dark and mixed every 4 min. The MC3T3-E1 cells were then washed with serum-free culture medium thrice to reduce interference from excess DCFDA. DCFDA fluorescence intensity in each group was measured using an LSM780 laser scanning confocal microscope (ZEISS, Germany).

2.14 Transmission electron microscopy

MC3T3-E1 cells were collected by trypsinization, transferred into 2 mL centrifuge tubes, and fixed with fixative solution (Servicebio, G1102) for 2 h at 4°C. Cells were post-fixed in 1% osmium tetroxide in 0.1 M phosphate buffer (pH 7.4) for 2 h at room temperature (20°C). MC3T3-E1 cells were dehydrated in a graded ethanol series (50%, 70%, 80%, 90%, 95%, 100%, and 100%) for 15 min, and then infiltrated into the embedding solution with propylene oxide overnight. Ultrathin sections (50 nm) were obtained using an EM UC7 ultramicrotome, post-stained with uranyl acetate and lead citrate, and visualized using transmission electron microscopy (24).

2.15 Enzyme-linked immunosorbent assay

After culturing MC3T3-E1 cells with different interventions, the medium was collected for enzyme-linked immunosorbent assay (ELISA). IL-1β levels were assayed by ELISA using a commercial kit (Elabscience, Wuhan, China) according to the manufacturer's instructions.

2.16 RNA-seq

The total RNA of MC3T3-E1 cells was obtained using TRIzol Reagent. The extracts were screened, amplified by PCR, and sequenced using an MGI T7 instrument. For bioinformatics analysis, raw reads that contained the adapter or had low quality (Q-value ≤20) were deleted and then located in the mouse-related genome using HISAT2 (version 2.1.0). Samtools was used to sequence the resulting files, and HTSeq (version 0.9.0) analysis was performed to determine the count of each gene. Gene Ontology (GO) and Kyoto Encyclopedia of Genes and Genomes (KEGG) pathway analyses were performed.

2.17 Statistical analysis

The data are presented as the mean ± standard deviation and were analyzed using GraphPad Prism (GraphPad Software Inc., USA). The software was used for the statistical analyses. Student's t-test or one-way analysis of variance (ANOVA) was used to determine the statistical significance of differences. Statistical significance was set at $P < 0.05$

3 Results

3.1 Se-Met suppresses the severity of Ti particle-induced osteolysis *in vivo*

Ti particle-induced osteolysis has been widely reported in the literature. To investigate the role of Se-Met in Ti particle-induced osteolysis, we established a cranial osteolysis model in mice and an intramedullary nail osteolysis model in rats. We then performed CT

scans on both models and analyzed the 3D reconstruction images of the mouse cranial bone lysis model, which showed that the periprosthetic bone mass was significantly damaged in the titanium group, the cranial thickness was thinner than that in the sham control group, and the bone mass was significantly destroyed (Figure 1A). However, after the intervention with Se-Met, the bone loss was alleviated significantly, and the quantitative analysis of bone parameters (Figures 1B–D) showed that BV/TV, BMD, and BV were significantly higher than those in the Ti group. In the 2D reconstructed images of the rat intramedullary nail osteolysis model, osteolysis around the Ti rod was evident. Compared to the Ti group, osteolysis was significantly reduced in the Se-Met treatment group (Figure 1E).

Consistently, H&E and Masson staining and immunohistochemistry confirmed the suppression of periprosthetic osteolysis by treatment with Se-Met in Ti particle-induced osteolysis in mouse and rat models. H&E staining of rat femurs showed absorption of bone structure in the Ti group, and inflammatory infiltration was found in the bone absorption area, while the bone destruction areain the Se-Met group was significantly decreased, and the number of inflammatory cells was also reduced (Figure 2A). To further explore the components of inflammatory infiltration, Masson staining of rat femurs showed a large amount of disordered fibrous tissue in the inflammatory infiltration area of osteolysis (Figure 2B), which was restored by adding Se-Met. Masson's trichrome staining was performed using the mouse osteolysis model. It was confirmed that Se-Met alleviated inflammatory fibrous tissue infiltration induced by Ti particles (Figure 2C).

3.2 Effects of Se-Met on inhibition of inflammatory osteolysis *in vivo*

To test the hypothesis that Se-Met may have an inhibitory role in periprosthetic osteolysis, immunohistochemical staining was performed for each group in the mouse skulls. The results showed that the expression of OCN in the Ti particle group was reduced, which could be completely reversed after treatment with Se-Met (Figure 3A). The same result was observed in the OCN staining of rat femurs (Figures 3B, C). According to previous studies, inflammatory responses play a critical role in Ti particle-induced osteolysis, and inhibition of inflammation in osteoblasts can exert a positive effect on osteolysis. We performed immunohistochemical staining of COX2 and found that the expression of COX2 in the Ti group of mouse skulls was significantly increased compared with the CTL group, while it was reduced in the Se-Met treatment group (Figure 3D), and similarly in the COX2 staining of rat femurs (Figures 3E, F).

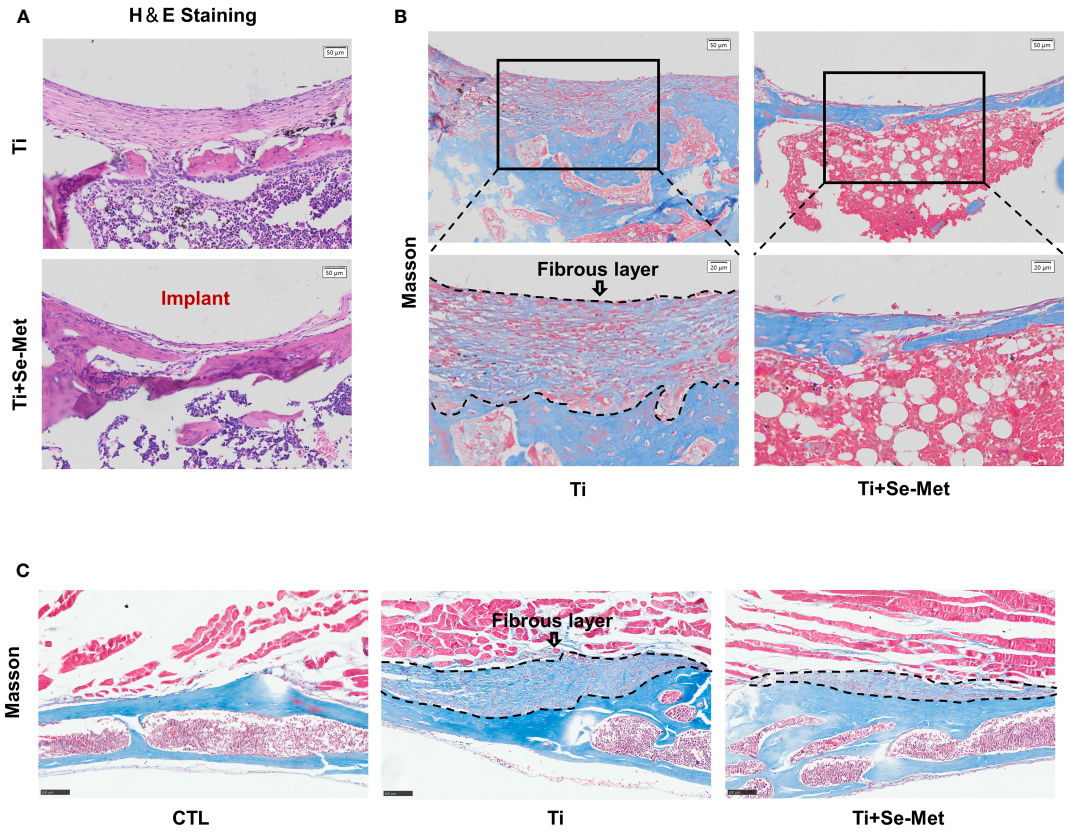

FIGURE 2
Se-Met rescued Ti-particle-induced osteolysis. **(A)** H&E staining of rat femurs; **(B, C)** Masson staining of rat femurs and mouse cranial bones, the areas marked by black dashed lines are inflammatory fibrous layers.

3.3 Se-Met attenuates inflammatory osteolysis induced by Ti particles *in vitro*

As mentioned above, we found that Se-Met rescued osteogenesis inhibition and reduced local inflammation caused by Ti particles *in vivo*, to further verify the conclusion we conducted *in vitro* experiments, osteoblast-related factors, including RUNX-2, OPN, and COL 1, were examined through western blotting, the results showed that osteogenic markers were significantly upregulated in the Se-Met treated group compared with the Ti group, indicating that Se-Met treatment alleviated the Ti particle-induced osteogenesis reduction (Figures 4A–D). In addition, the real-time PCR results were consistent with those of western blotting (Figure 4E). Immunofluorescence detection showed that OCN expression in the Ti group was significantly lower than that in the CTL group, whereas OCN expression in the Se-Met group was higher than that in the Ti group, which was consistent with the above results (Figures 4F, G). We induced osteogenic differentiation

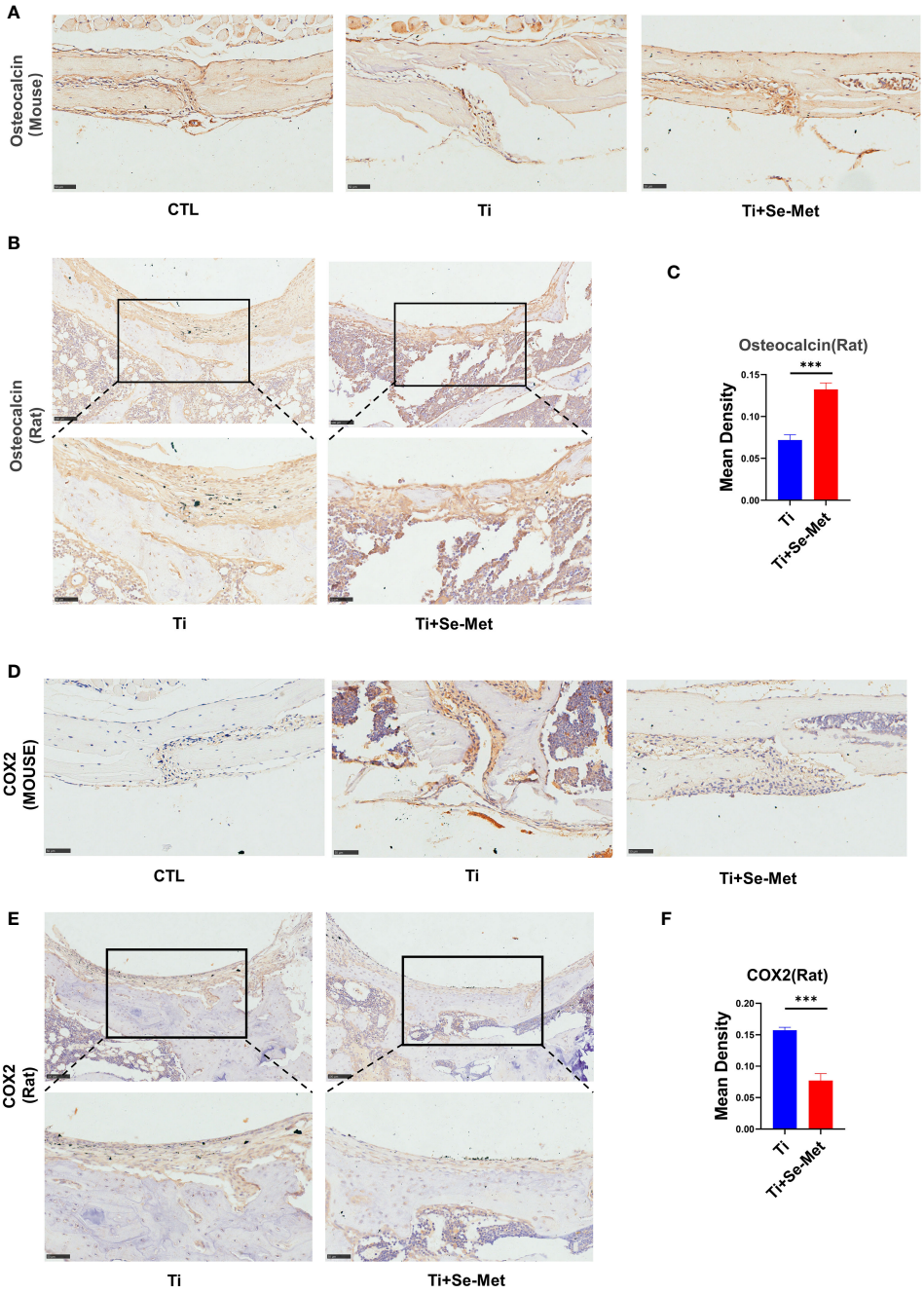

FIGURE 3
Se-Met rescued Ti-particle-induced osteolysis in Immunohistochemistry. **(A-C)** Immunohistochemical results showed that Se-Met rescued the decreased secretion of OCN induced by Ti particle stimulation; **(D-F)** The results of immunohistochemistry showed that Se-Met inhibited the increase of COX2 expression induced by Ti particles ***P < 0.001.

of MC3T3-E1 cells stimulated with Ti particles. ALP staining was performed after 7 days, and the results showed that Ti particles could reduce the ALP activity *in vitro*, and Se-Met could restore it (Figure 4H). Alizarin red staining was performed after 14 d, and the results showed that Se-Met alleviated the reduction in the mineralization rate caused by Ti stimulation (Figure 4I).

It is well known that inhibiting the inflammation extent in osteoblasts can exert a positive effect on osteolysis treatment. To further determine whether Se-Met exerts an effect on osteoblasts in inflammatory osteolysis, MC3T3E1 cells were stimulated with Ti particles and cultured in the presence or absence of Se-Met, proteins were collected for western Blotting assay and the results showed that Ti particles stimulation significantly elevated INOS COX2 expression, especially NLRP3, while the additional application of Se-Met substantially recovered their secretion, indicating a lower severity of inflammatory osteolysis (Figures 5A–D), COX2 expression was also detected by Immunofluorescence, and the results showed that the increased COX2 expression caused by Ti particles stimulation could be suppressed by Se-Met treatment (Figures 5E, F). mRNA was extracted for qPCR to validate the above results (Figures 5G, H).

3.4 Se-Met antagonizes mitochondrial ROS-dependent NLRP3 inflammasome activation *in vitro*

Given the fact that inflammatory reactions have detrimental effects on wear debris-induced osteolysis and that the NLRP3 inflammasome plays a critical role in inflammatory responses,

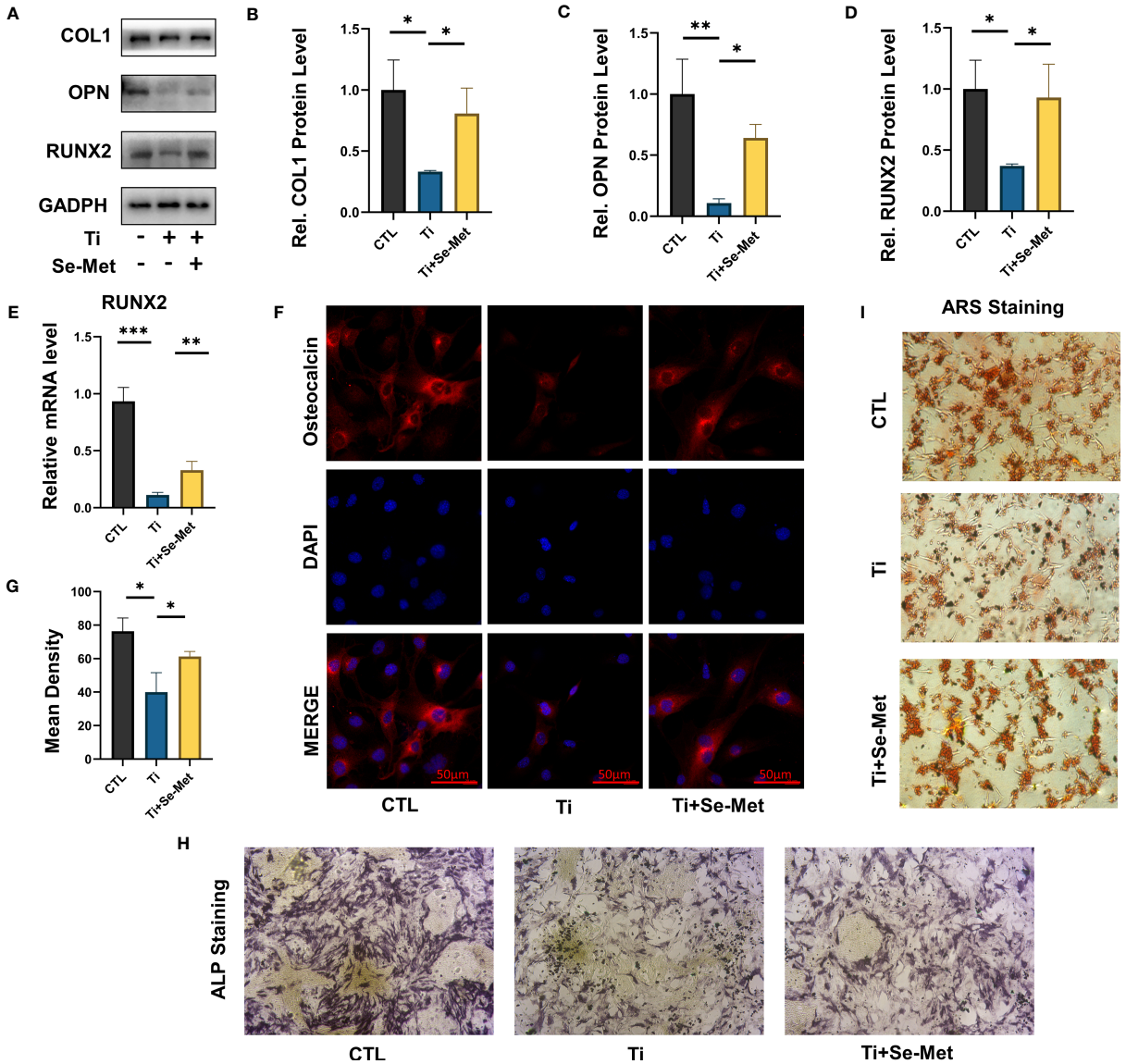

FIGURE 4
Se-Met has a protective effect on osteoblast dysfunction induced by Ti particles. **(A-D)** Western blot results showed that Se-Met significantly rescued the decreased expression of osteoblast-related factors Col 1, RUNX-2, and OPN caused by Ti particles stimulation; **(E)** Real-time PCR results showed that Se-Met effectively relieves the RUNX2 expression decreased caused Ti particles; **(F, G)** Se-Met treatment rescued Ti particle-induced OCN expression in MC3T3-E1 cells, as assayed by cell immunostaining; **(H)** Representative images of ALP staining at 7 d; **(I)** Representative images of ARS staining at 21 d. * P < 0.05, **P < 0.01, ***P < 0.001.

we sought to determine whether Se-Met exerts an inhibitory effect on NLRP3 inflammasome activation in inflammatory osteolysis. We evaluated the NLRP3 inflammasome expression in mouse cranial bone through immunohistochemical staining, which showed a significant increase in NLRP3 inflammasome expression in the Ti-stimulated group and a decrease with Se-Met treatment (Figure 6A). The rat femur samples also demonstrated that Se-Met reduced the NLRP3 inflammasome expression *in vivo* (Figure 6B). The NLRP3 inflammasome expression level *in vitro* was also examined by western blotting, which indicated that NLRP3 inflammasome expression enhancement by stimulation of Ti particles was suppressed by adding Se-Met (Figure 6C). We also extracted protein from cells and assayed it by western blotting, which showed that Se-Met treatment reduced the Ti particle-induced elevation in NLRP3 expression (Figure 6D). ROS levels were detected using the DCFDA assay (Figures 6E, F), which showed that Ti particles enhanced ROS levels, whereas adding Se-Met largely attenuated this effect. Flow cytometry was performed to determine the proportion of apoptotic cells. As shown in (Figures 6G, H), the ratio of apoptotic MC3T3-E1 cells increased after stimulation with Ti particles, whereas the addition of Se-Met prevented this effect. Real-time PCR also demonstrated that caspase-3, an apoptosis indicator, was significantly increased by Ti particle stimulation, and se-met treatment alleviated this effect (Figure 6I). It is well known that increased ROS generation is closely associated with impaired mitochondrial function. To verify the potential interaction between Se-Met and mitochondrial function, we performed transmission electron microscopy (TEM), high-field images of swollen mitochondria in the MC3T3E1 cells with Ti stimulated showed that the mitochondria surrounded the nucleus, indicating accelerated mitochondrial damage, and these changes were reduced in MC3T3E1 cells with Se-Met treatment (Figure 6J). Furthermore, ELISA to detect IL-1β indicated that the enhanced NLRP3 inflammasome production and function induced by Ti particles was alleviated by Se-Met treatment (Figure 6K).

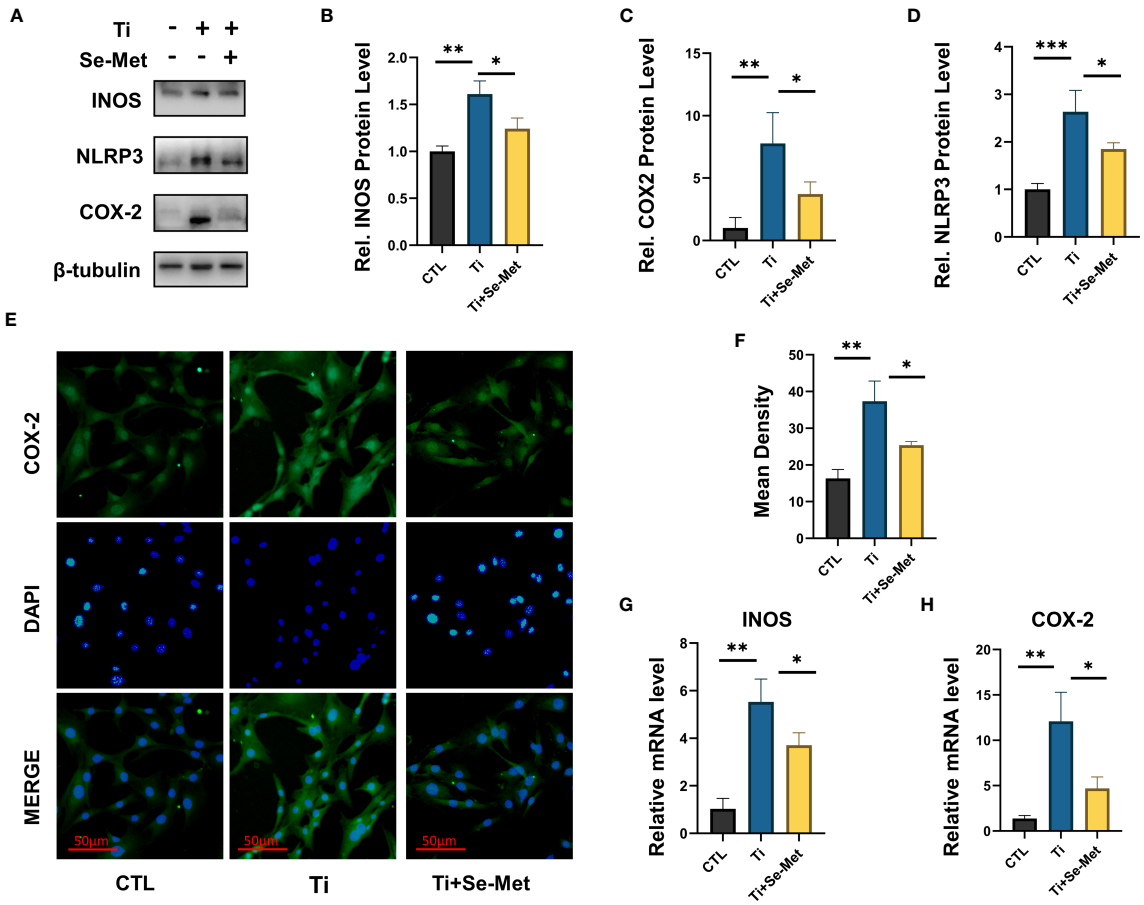

FIGURE 5
Se-Met has an inhibitory effect on the inflammatory response induced by Ti particles. **(A-D)** Se-Met inhibited the expression of inflammatory cytokines, such as iNOS, COX-2, and NLRP3, which were enhanced with Ti particle stimulation, as indicated by western blot. **(E, F)** Se-Met treatment inhibited Ti particle-induced COX2 expression in MC3T3-E1 cells, as assayed by cell immunostaining. **(G, H)** Se-Met significantly inhibits the upregulation of COX2 and INOS induced by Ti particle stimulation, as shown by real-time fluorescent PCR results. *P < 0.05, **P < 0.01, ***P < 0.001.

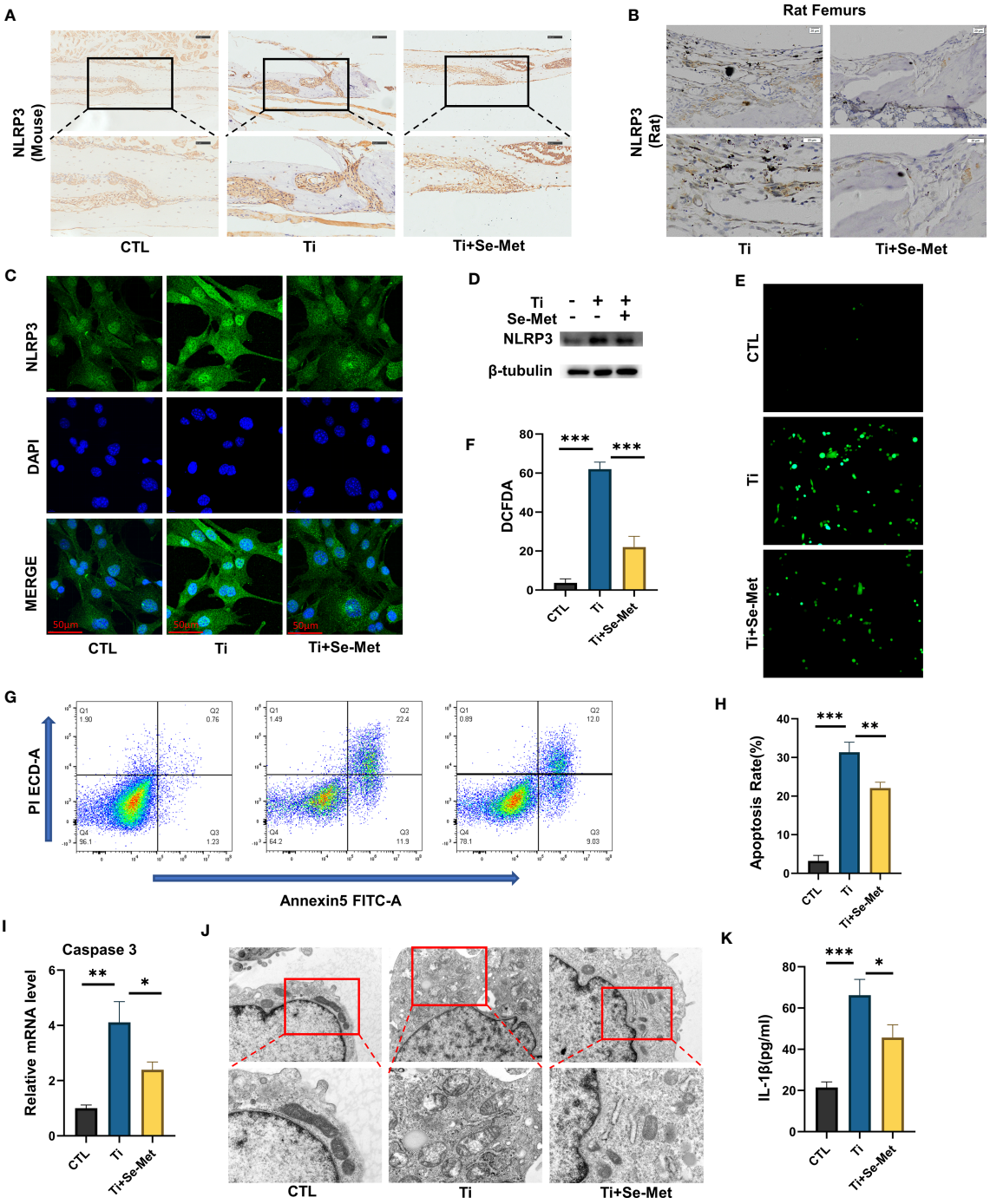

FIGURE 6
Se-Met antagonizes mitochondrial ROS-dependent NLRP3 inflammasome activation *in vitro*. **(A, B)** Representative images of IHC staining, which showed Se-Met inhibited the up-regulation of NLRP3 expression stimulated by Ti particles *in vivo*; **(C)** Representative images of immunofluorescence staining, which showed treatment of Se-Met inhibited the up-regulation of NLRP3 expression in MC3T3-E1 cells; **(D)** Western blot showed that Se-Met inhibited the rise of NLRP3; **(E, F)** Se-Met antagonized the Ti particle–mediated production of ROS, as detected by the DCFDA assay; **(G, H)** The effect of Ti particles on apoptosis rate of MC3T3-E1 cells was tested by flow cytometry; **(I)** The mRNA were collected from each group, followed by real-time PCR to measure caspase-3 levels; **(J)** Representative TEM images of mitochondria in MC3T3-E1 cells of each group; **(K)** The expression of IL-1β in the culture media of groups of MC3T3-E1, as detected by ELISA. *P < 0.05, **P < 0.01, ***P < 0.001.

10.3389/fimmu.2023.1171150

3.5 Se-Met exerts an effect in inflammatory osteolysis induced by Ti particles through the β-catenin signaling pathway

To gain additional insights into the mechanism responsible for the regulation of inflammation and bone formation by Se-Met, we isolated the total mRNA of MC3T3-E1 osteoblasts after stimulation with Ti particles for 24 h, and RNA-seq was analyzed using the MGI T7 platform to generate mRNA profiles. A heat map was plotted, and cluster analyses were performed (Figure 7A). The differentially expressed genes (DEGs) were annotated using GO categories (Figure 7B) and KEGG pathway analysis (Figure 7C). Heat map and cluster analysis of inflammatory osteolysis-related genes showed significant differences between the control group and the Ti particle-stimulated group. The results indicated a decrease in osteogenesis biomarkers in the Ti particle-stimulated group, while the addition of

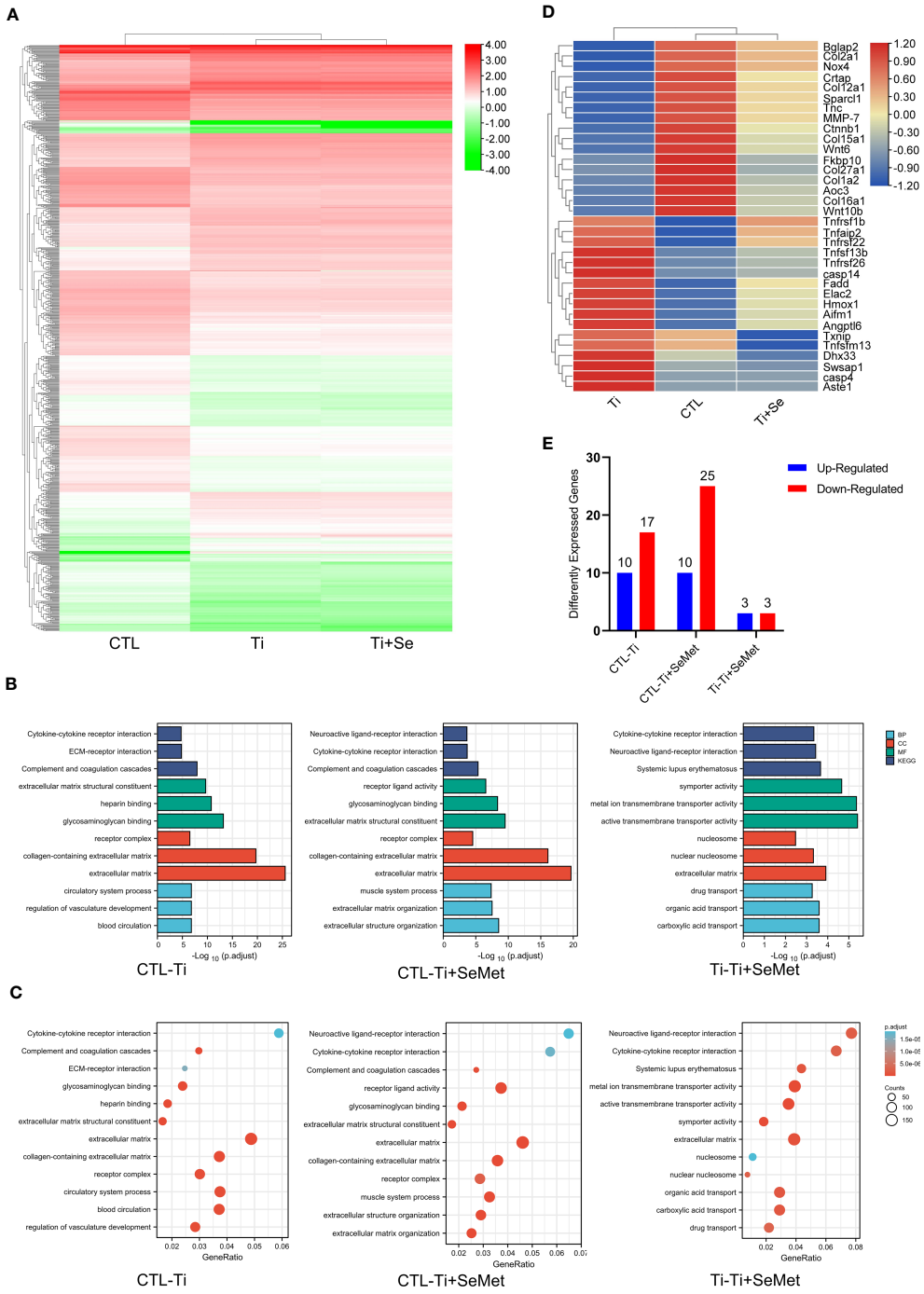

FIGURE 7
RNA-seq analysis showed that Se-Met rescued osteolysis induced by Ti particles, which was related to the β-Catenin pathway. **(A)** Heat map and cluster analysis; **(B, C)** Significant pathway of GO Enrichment analysis; **(D)** Cluster analysis of osteolysis-related genes; **(E)** Number of differentially expressed novel genes.

Se-Met prevented this effect, and we noticed increased β-catenin levels in the Se-Met treatment group, which is consistent with the results of real-time PCR and western blotting (Figures 7D, 8A-C). Moreover, the statistics of the number of differential new genes detected are shown in Figure 7E. We further performed Immunofluorescence in MC3T3E1 cells, which showed that the inhibition of β-catenin expression by stimulation with Ti particles was relieved by adding Se-Met (Figures 8D, E). These data illustrate

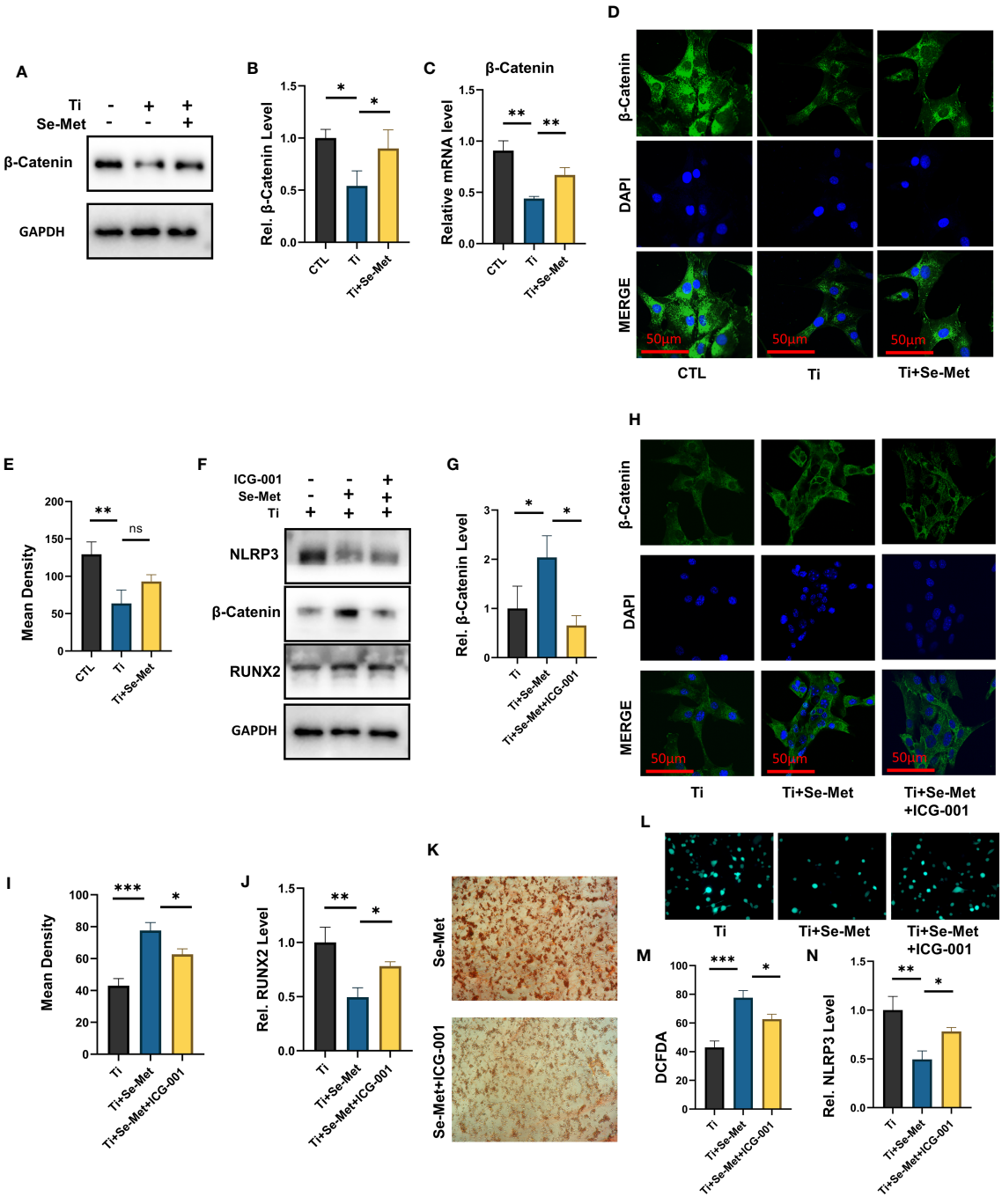

FIGURE 8
Se-Met antagonizes Ti-particle-induced osteolysis by activating the β-catenin signaling pathway. **(A-C)** The mRNA and total protein were collected from each group, followed by real-time PCR and immunoblotting to measure β-Catenin levels; **(D, E)** Immunofluorescence results showed that Ti decreased the expression of β-Catenin, which was alleviated by Se-Met; **(F)** The total proteins of each group were extracted and detected by Western blot; **(G)** The protective effect of Se-Met against the decrease in β-Catenin induced by Ti stimulation was inhibited by ICG-001; **(H, I)** Immunofluorescence results showed that the addition of SE-met alleviated the decrease of β-Catenin induced by Ti particles, while ICG-001 inhibited this effect; **(J)** WB results showed that the expression of RUNX2 decreased by ICG-001 stimulation; **(K)** Representative images of ARS staining at 21 d, show that ICG-001 inhibited the mineralization rate of MC3T3-E1 cells; **(L, M)** ICG-001 attenuated the ROS inhibitory effect of Se-Met, as detected by the DCFDA assay; **(N)** Western blot results showed that ICG-001 attenuated the down-regulation effect of Se-Met on NLRP3 inflammasome. *P < 0.05, **P < 0.01, ***P < 0.001.

that β-catenin signaling may be involved in the protective effects of Se-Met on Ti particle-induced osteogenic inhibition.

Bearing in mind that indocyanine green-001 (ICG-001) is a targeted β-catenin signaling inhibitor, we used it to pretreat MC3T3E1 cells. Western blotting showed that ICG-001 eliminated the effect of Se-Met in upregulating β-catenin (Figures 8F, G). Immunofluorescence results showed that the addition of SE-met alleviated the decrease in β-catenin induced by Ti particles, while ICG-001 inhibited this effect (Figures 8H, I). The results showed that the application of Se-Met substantially enhanced RUNX2 secretion, an osteoblast-related factor, whereas adding ICG001 substantially inhibited this effect (Figures 8F, J). Alizarin red staining showed that ICG-001 significantly reduced the mineralization rate of MC3T3E1 cells after 21 d of osteogenic induction (Figure 8K). Analysis of ROS levels in each group by the DCFDA assay also showed that ICG-001 eliminated the therapeutic effect of Se-Met (Figures 8L, M). Western blotting showed that the inhibitory effect of Se-Met on NLRP3 expression was attenuated by ICG-001 (Figures 8F, N). These collective results suggest that ICG-001 blocks the beneficial effects of Se-Met in Ti particle-induced osteogenic reduction through the NLRP3 inflammasome-regulated β-catenin signaling pathway.

4 Discussion

Wear debris-induced osteolysis is due to an imbalance in bone homeostasis between bone resorption and formation (25), which involves many cells including macrophages, lymphocytes, fibroblasts, osteoclasts, and osteoblasts (26), Previous research has claimed that bone regeneration inhibition is fundamental in osteolysis initiation (27), and the inflammation response in osteoblasts is demonstrated to be related to attenuated osteogenesis (28), Therefore, treatment of inflammation and promotion of osteogenic differentiation can be an effective method for the prevention and curation of wear debris-induced bone loss after TJA.

Se is an essential trace element in animals and humans and is generally taken up from the diet through food or other forms of external supplementation (29). Plants mainly convert Se into Se-Met and incorporate it into proteins instead of methionine (Met) (9). Selenoproteins are anti-oxidants and can regulat redox balance (10, 30), suggesting that Se-Met might be a candidate for treating wear debris-induced osteolysis. However, whether Se-Met is involved in wear debris-induced osteolysis is poorly understood. This study aimed to demonstrate whether Se-Met represents a promising treatment for alleviating wear debris-induced osteolysis *in vivo*. We found that Ti particle-induced osteolysis was significantly reduced by treatment with Se-Met, which also increased the expression of OCN in femoral slices. We aimed to further explore whether Se-Met mediates its pharmacological effect via suppressing inflammation and osteogenic inhibition in MC3T3E1 cells cocultured with Ti particles. We discovered an enhancement of inflammatory cytokines including INOS COX-2 and NLRP3 inflammasome and downregulation of osteogenic biomarkers including RUNX2 COL-1 and OPN with the addition of Ti particles, the application of Se-Met has been found to exert positive effects in both inhibiting inflammatory cytokines and promoting osteogenesis in MC3T3E1 cells.

The NLRP3 inflammasome plays a detrimental role in inflammation and apoptosis in osteoblasts and contributes to wear debris-induced osteolysis (23), and promoting NLRP3 inflammasome in BMSCs can suppress osteogenic differentiation (31). McCall et al. reported that the functional expression of NLRP3 in osteoblasts is possibly related to apoptotic cell death (32), and previous research has verified the ability of Se-Met to decrease the ROS levels and apoptosis rate in the N2A-SW cell model (33), and mitochondria of cells contribute to the NLRP3 inflammasome activation through several mechanisms. In this study, Se-Met treatment suppressed Ti particle-induced ROS and elevated NLRP3 inflammasome expression in osteoblasts, while inflammatory cytokines and apoptosis were downregulated upon Se-Met treatment. Collectively, these findings strongly suggest that Se-Met inhibits Ti particle-induced apoptosis and inflammation by suppressing the NLRP3 inflammasome.

The β-catenin signaling pathway is closely implicated in osteoblastic differentiation and mineralization (34, 35). Previous research has shown that the β-catenin signaling pathway has a crucial effect on inflammatory osteolysis pathogenesis (36), while Se has been reported to promote the migration and osteogenic differentiation of BMSCs (11), and the ability of Se-Met to reduce oxidative stress has been demonstrated (13). In our study, β-catenin levels decreased after stimulation with Ti particles, which could be upregulated by Se-Met treatment. Intriguingly, Se-Met was shown to elevate the expression of osteogenic biomarkers, including OPN, RUNX2, and COL1, and downregulate the NLRP3 inflammasome and ROS expression. To further explore whether Se-Met exerts the function of promoting osteogenesis by regulating the ROS-dependent NLRP3 inflammasome activation via the β-catenin signaling pathway, ICG-001, a targeted β-catenin signaling pathway inhibitor, was applied to coculture with MC3T3E1 cells. Our study showed that osteoblastic differentiation and bone formation were reduced, and the expression of ROS and NLRP3 inflammasome was elevated, indicating that the rescue effect of Se-Met was alleviated by ICG-001 administration. These results suggest that Se-Met antagonizes the inhibitory effect of Ti particles on bone regeneration with the help of β-catenin signaling pathway activation. The NLRP3 inflammasome is a critical component of the innate immune system that mediates caspase-1 activation and the secretion of proinflammatory cytokines IL-1β/IL-18 in response to cellular damage (14), and Se-Met could regulate the activation of the NLRP3 inflammasome, which suggests the great potential of Se-Met in anti-inflammation treatment. Study has demonstrated that biological macromolecules displayed protective effects against intestinal barrier dysfunction (37), which offer important insights on Se-Met in nonimmunogenicity and safety compared with bioactive molecular mimics.

However, there are some limitations exist in our current study. First of all, metal implants may release metal ions into the surroundings and blood *in vivo*, and their side effects need to be

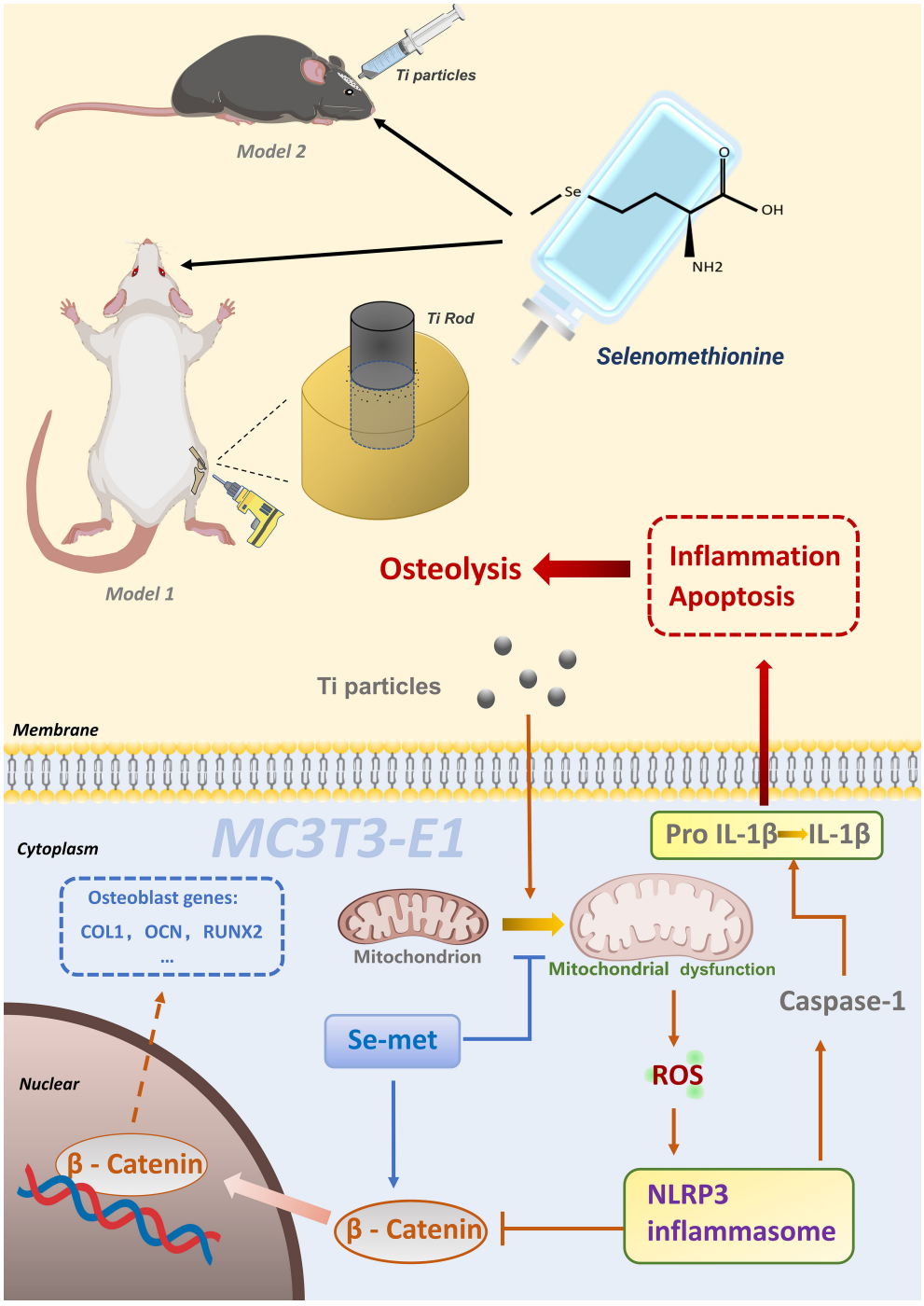

FIGURE 9
Schematic model of Se-Met in Ti particleinduced osteolysis.

considered (38). However, ultra-high molecular weight polyethylene (UHMWPE) wear particles do not have this effect, and UHMWPE wear particles can be used to establish osteolysis models in subsequent studies (39). Second, we constructed two small animal models and lack of biomechanical analysis. Subsequent studies could be performed in a large animal model to verify the protective effect of Se-Met on osteolysis. Finally, the safety assessment of Se-Met supplementation is lacking, and the safety of ingestion of large amounts of Se-Met for the treatment of osteolysis needs to be further investigated (40).

5 Conclusion

Collectively, it appears that Se-Met plays a protective role in Ti particle-induced disorganization of osteoblasts and impairment of

bone formation during osteolysis by suppressing inflammatory cytokine secretion, reducing apoptosis, and promoting bone formation, which might be associated with the activation of the ROS-dependent NLRP3 inflammasome via the β-catenin signaling pathway in osteoblasts (Figure 9). In conclusion, the present study sheds light on the prevention and treatment of wear debris–induced prosthetic loosening in the clinic.

Data availability statement

The data presented in the study are deposited in the GEO repository, accession number GSE236911.

Ethics statement

The animal study was reviewed and approved by Institutional Animal Care and Use Committee of Shandong University.

Author contributions

RY, YY, ZL, and LL contributed equally to this work as first authors. They designed and performed experiments, analyzed data, and wrote the manuscript. ZX, YZ, CJ, PZ, HLi, YuhL, YW, WL and LN provided technical assistance in experiments and data analysis. YuhL and BL supervised the project and provided guidance throughout the study. HLiu contributed to the manuscript revision and final approval. All authors discussed the results and contributed to the final manuscript.

Funding

National Natural Science Foundation of China (grant No. 82072478 to Yunpeng Zhao, grant No. 82073437 to Weiwei Li), Shandong Provincial Natural Science Foundation (grant No. ZR2020YQ54 to Yunpeng Zhao).

Acknowledgments

The authors thank the Translational Medicine Core Facility of Shandong University and Laboratory of Basic Medical Sciences of Qilu Hospital of Shandong University for the consultation and instrument availability that supported this work.

Conflict of interest

The authors declare that the research was conducted in the absence of any commercial or financial relationships that could be construed as a potential conflict of interest.

Publisher's note

All claims expressed in this article are solely those of the authors and do not necessarily represent those of their affiliated organizations, or those of the publisher, the editors and the reviewers. Any product that may be evaluated in this article, or claim that may be made by its manufacturer, is not guaranteed or endorsed by the publisher.

References

1. Sharkey PF, Lichstein PM, Shen C, Tokarski AT, Parvizi J. Why are total knee arthroplasties failing today–has anything changed after 10 years? *J Arthroplasty* (2014) 29(9):1774–8. doi: 10.1016/j.arth.2013.07.024

2. Wang Z, Deng Z, Gan J, Zhou G, Shi T, Wang Z, et al. TiAl6V4 particles promote osteoclast formation via autophagy-mediated downregulation of interferon-beta in osteocytes. *Acta Biomater.* (2017) 48:489–98. doi: 10.1016/j.actbio.2016.11.020

3. Dyskova T, Gallo J, Kriegova E. The role of the chemokine system in tissue response to prosthetic by-products leading to periprosthetic osteolysis and aseptic loosening. *Front In Immunol* (2017) 8:1026. doi: 10.3389/fimmu.2017.01026

4. Wang Y, Yan Y, Su Y, Qiao L. Release of metal ions from nano CoCrMo wear debris generated from tribo-corrosion processes in artificial hip implants. *J Mech Behav BioMed Mater* (2017) 68:124–33. doi: 10.1016/j.jmbbm.2017.01.041

5. Zhang L, Haddouti EM, Welle K, Burger C, Wirtz DC, Schildberg FA, et al. The effects of biomaterial implant Wear debris on osteoblasts. *Front Cell Dev Biol* (2020) 8:352. doi: 10.3389/fcell.2020.00352

6. Li N, Li X, Zheng K, Bai J, Zhang W, Sun H, et al. Inhibition of sirtuin 3 prevents titanium particle-induced bone resorption and osteoclastsogenesis via suppressing ERK and JNK signaling. *Int J Biol Sci* (2021) 17(5):1382–94. doi: 10.7150/ijbs.53992

7. Tian B, Jiang T, Shao Z, Zhai Z, Li H, Fan Q, et al. The prevention of titanium-particle-induced osteolysis by OA-14 through the suppression of the p38 signaling pathway and inhibition of osteoclastogenesis. *Biomaterials* (2014) 35(32):8937–50. doi: 10.1016/j.biomaterials.2014.06.055

8. Ying H, Zhang Y. Systems biology of selenium and complex disease. *Biol Trace Elem Res* (2019) 192(1):38–50. doi: 10.1007/s12011-019-01781-9

9. Tapiero H, Townsend DM, Tew KD. The antioxidant role of selenium and seleno-compounds. *Biomed Pharmacother* (2003) 57(3-4):134–44. doi: 10.1016/S0753-3322(03)00035-0

10. Huang Z, Rose AH, Hoffmann PR. The role of selenium in inflammation and immunity: from molecular mechanisms to therapeutic opportunities. *Antioxid Redox Signal* (2012) 16(7):705–43. doi: 10.1089/ars.2011.4145

11. Li C, Wang Q, Gu X, Kang Y, Zhang Y, Hu Y, et al. Porous Se@SiO2 nanocomposite promotes migration and osteogenic differentiation of rat bone marrow mesenchymal stem cell to accelerate bone fracture healing in a rat model. *Int J Nanomed* (2019) 14:3845–60. doi: 10.2147/IJN.S202741

12. Wang S, Chen Y, Han S, Liu Y, Gao J, Huang Y, et al. Selenium nanoparticles alleviate ischemia reperfusion injury-induced acute kidney injury by modulating GPx-1/NLRP3/Caspase-1 pathway. *Theranostics* (2022) 12(8):3882–95. doi: 10.7150/thno.70830

13. Chi Q, Luan Y, Zhang Y, Hu X, Li S. The regulatory effects of miR-138-5p on selenium deficiency-induced chondrocyte apoptosis are mediated by targeting SelM. *Metallomics: Integrated Biometal Science.* (2019) 11(4):845–57. doi: 10.1039/c9mt00006b

14. Kelley N, Jeltema D, Duan Y, He Y. The NLRP3 inflammasome: an overview of mechanisms of activation and regulation. *Int J Mol Sci* (2019) 20(13). doi: 10.3390/ijms20133328

15. Wu Y, Teng Y, Zhang C, Pan Y, Zhang Q, Zhu X, et al. The ketone body beta-hydroxybutyrate alleviates CoCrMo alloy particles induced osteolysis by regulating NLRP3 inflammasome and osteoclast differentiation. *J Nanobiotechnol* (2022) 20(1):120. doi: 10.1186/s12951-022-01320-0

16. Burton L, Paget D, Binder NB, Bohnert K, Nestor BJ, Sculco TP, et al. Orthopedic wear debris mediated inflammatory osteolysis is mediated in part by NALP3 inflammasome activation. *J Orthop Res* (2013) 31(1):73–80. doi: 10.1002/jor.22190

17. Wang N, Maskomani S, Meenashisundaram GK, Fuh JYH, Dheen ST, Anantharajan SK. A study of titanium and magnesium particle-induced oxidative stress and toxicity to human osteoblasts. *Mater Sci Eng C Mater Biol Appl* (2020) 117:111285. doi: 10.1016/j.msec.2020.111285

18. Ping Z, Hu X, Wang L, Shi J, Tao Y, Wu X, et al. Melatonin attenuates titanium particle-induced osteolysis via activation of wnt/beta-catenin signaling pathway. *Acta Biomater.* (2017) 51:513–25. doi: 10.1016/j.actbio.2017.01.034

19. Wellenstein MD, Coffelt SB, Duits DEM, van Miltenburg MH, Slagter M, de Rink I, et al. Loss of p53 triggers WNT-dependent systemic inflammation to drive breast cancer metastasis. *Nature* (2019) 572(7770):538–42. doi: 10.1038/s41586-019-1450-6

20. George SJ. Wnt pathway: a new role in regulation of inflammation. *Arterioscler Thromb Vasc Biol* (2008) 28(3):400–2. doi: 10.1161/ATVBAHA.107.160952

21. Li X, Xiang Y, Li F, Yin C, Li B, Ke X. WNT/beta-catenin signaling pathway regulating T cell-inflammation in the tumor microenvironment. *Front Immunol* (2019) 10:2293. doi: 10.3389/fimmu.2019.02293

22. Cao J, Ma X, Liu L, Zhang G, Wu Y, Fu Y, et al. Cortistatin attenuates titanium particle-induced osteolysis through regulation of TNFR1-ROS-caspase-3 signaling in osteoblasts. *Ann New York Acad Sci* (2022) 1513(1):140–52. doi: 10.1111/nyas.14774

23. Zheng K, Bai J, Li N, Li M, Sun H, Zhang W, et al. Protective effects of sirtuin 3 on titanium particle-induced osteogenic inhibition by regulating the NLRP3 inflammasome via the GSK-3beta/beta-catenin signalling pathway. *Bioact Mater* (2021) 6(10):3343–57. doi: 10.1016/j.bioactmat.2021.02.039

24. Zhao Y, Qiu C, Wang W, Peng J, Cheng X, Shangguan Y, et al. Cortistatin protects against intervertebral disc degeneration through targeting mitochondrial ROS-dependent NLRP3 inflammasome activation. *Theranostics* (2020) 10(15):7015–33. doi: 10.7150/thno.45359

25. Alhasan H, Terkawi MA, Matsumae G, Ebata T, Tian Y, Shimizu T, et al. Inhibitory role of annexin A1 in pathological bone resorption and therapeutic implications in periprosthetic osteolysis. *Nat Commun* (2022) 13(1):3919. doi: 10.1038/s41467-022-31646-0

26. Purdue PE, Koulouvaris P, Potter HG, Nestor BJ, Sculco TP. The cellular and molecular biology of periprosthetic osteolysis. *Clin Orthop Relat Res* (2007) 454:251–61. doi: 10.1097/01.blo.0000238813.95035.1b

27. Goodman SB, Ma T, Chiu R, Ramachandran R, Smith RL. Effects of orthopaedic wear particles on osteoprogenitor cells. *Biomaterials* (2006) 27(36):6096–101. doi: 10.1016/j.biomaterials.2006.08.023

28. Tsai C-F, Chen J-H, Wu C-T, Chang P-C, Wang S-L, Yeh W-L. Induction of osteoclast-like cell formation by leptin-induced soluble intercellular adhesion molecule secreted from cancer cells. *Ther Adv Med Oncol* (2019) 11:1758835919846806. doi: 10.1177/1758835919846806

29. Rayman MP. Selenium and human health. *Lancet* (2012) 379(9822):1256–68. doi: 10.1016/S0140-6736(11)61452-9

30. Xie Y, Liu Q, Zheng L, Wang B, Qu X, Ni J, et al. Se-Methylselenocysteine ameliorates neuropathology and cognitive deficits by attenuating oxidative stress and metal dyshomeostasis in Alzheimer model mice. *Mol Nutr Food Res* (2018) 62(12): e1800107. doi: 10.1002/mnfr.201870070

31. Wang L, Chen K, Wan X, Wang F, Guo Z, Mo Z. NLRP3 inflammasome activation in mesenchymal stem cells inhibits osteogenic differentiation and enhances adipogenic differentiation. *Biochem Biophys Res Commun* (2017) 484(4):871–7. doi: 10.1016/j.bbrc.2017.02.007

32. McCall SH, Sahraei M, Young AB, Worley CS, Duncan JA, Ting JP-Y, et al. Osteoblasts express NLRP3, a nucleotide-binding domain and leucine-rich repeat region containing receptor implicated in bacterially induced cell death. *J Bone Miner Res* (2008) 23(1):30–40. doi: 10.1359/jbmr.071002

33. Chen C, Chen Y, Zhang ZH, Jia SZ, Chen YB, Huang SL, et al. Selenomethionine improves mitochondrial function by upregulating mitochondrial selenoprotein in a model of alzheimer's disease. *Front Aging Neurosci* (2021) 13:750921. doi: 10.3389/fnagi.2021.750921

34. Jian J, Sun L, Cheng X, Hu X, Liang J, Chen Y. Calycosin-7-O-β-d-glucopyranoside stimulates osteoblast differentiation through regulating the BMP/WNT signaling pathways. *Acta Pharm Sin B* (2015) 5(5):454–60. doi: 10.1016/j.apsb.2015.06.005

35. Yun HM, Park KR, Quang TH, Oh H, Hong JT, Kim YC, et al. 2,4,5-trimethoxyldalbergiquinol promotes osteoblastic differentiation and mineralization via the BMP and wnt/β-catenin pathway. *Cell Death Disease.* (2015) 6:e1819. doi: 10.1038/cddis.2015.185

36. Qu R, Chen X, Yuan Y, Wang W, Qiu C, Liu L, et al. Ghrelin fights against titanium particle-induced inflammatory osteolysis through activation of beta-catenin signaling pathway. *Inflammation* (2019) 42(5):1652–65. doi: 10.1007/s10753-019-01026-w

37. Kai L, Zong X, Jiang Q, Lu Z, Wang F, Wang Y, et al. Protective effects of polysaccharides from atractylodes macrocephalae koidz. against dextran sulfate sodium induced intestinal mucosal injury on mice. *Int J Biol Macromolecules.* (2022) 195:142–51. doi: 10.1016/j.ijbiomac.2021.12.042

38. Savarino L, Granchi D, Ciapetti G, Cenni E, Nardi Pantoli A, Rotini R, et al. Ion release in patients with metal-on-metal hip bearings in total joint replacement: a comparison with metal-on-polyethylene bearings. *J BioMed Mater Res* (2002) 63 (5):467–74. doi: 10.1002/jbm.10299

39. Sobieraj M, Marwin S. Ultra-High-Molecular-Weight polyethylene (UHMWPE) in total joint arthroplasty. *Bull Hosp Jt Dis (2013).* (2018) 76(1):38–46.

40. Vinceti M, Filippini T, Jablonska E, Saito Y, Wise LA. Safety of selenium exposure and limitations of selenoprotein maximization: molecular and epidemiologic perspectives. *Environ Res* (2022) 211:113092. doi: 10.1016/j.envres.2022.113092

frontiers | Frontiers in Immunology

TYPE Original Research
PUBLISHED 21 July 2023
DOI 10.3389/fimmu.2023.1149686

Check for updates

OPEN ACCESS

EDITED BY
Chuan-ju Liu,
New York University, United States

REVIEWED BY
Renpeng Zhou,
New York University, United States
Guiwu Huang,
New York University, United States
Debasis Sahu,
Ubioquitos Inc, Canada

*CORRESPONDENCE
Yang Cao
yang9yue8ri@163.com
Meng Liu
13764723430@163.com

†These authors have contributed equally to this work and share first authorship

RECEIVED 22 January 2023
ACCEPTED 26 June 2023
PUBLISHED 21 July 2023

CITATION
Yang L, Yu X, Liu M and Cao Y (2023) A comprehensive analysis of biomarkers associated with synovitis and chondrocyte apoptosis in osteoarthritis.
Front. Immunol. 14:1149686.
doi: 10.3389/fimmu.2023.1149686

COPYRIGHT
© 2023 Yang, Yu, Liu and Cao. This is an open-access article distributed under the terms of the Creative Commons Attribution License (CC BY). The use, distribution or reproduction in other forums is permitted, provided the original author(s) and the copyright owner(s) are credited and that the original publication in this journal is cited, in accordance with accepted academic practice. No use, distribution or reproduction is permitted which does not comply with these terms.

A comprehensive analysis of biomarkers associated with synovitis and chondrocyte apoptosis in osteoarthritis

Ling Yang[1,2†], Xueyuan Yu[3†], Meng Liu[4*] and Yang Cao[1*]

[1]Department of Hematology, The First People's Hospital of Changzhou, Third Affiliated Hospital of Soochow University, Changzhou, China, [2]Department of Traditional Chinese Medicine, Xinhua Hospital Affiliated to Shanghai Jiao Tong University School of Medicine, Shanghai, China, [3]Department of Plastic, Aesthetic and Maxillofacial Surgery, The First Affiliated Hospital of Xi'an Jiao Tong University, Xi'an, China, [4]Department of Clinical Laboratory,The First Affiliated Hospital of Xi'an Jiao Tong University, Xi'an, China

Introduction: Osteoarthritis (OA) is a chronic disease with high morbidity and disability rates whose molecular mechanism remains unclear. This study sought to identify OA markers associated with synovitis and cartilage apoptosis by bioinformatics analysis.

Methods: A total of five gene-expression profiles were selected from the Gene Expression Omnibus database. We combined the GEO with the GeneCards database and performed Gene Ontology and Kyoto Encyclopedia of Genes and Genome analyses; then, the least absolute shrinkage and selection operator (LASSO) algorithm was used to identify the characteristic genes, and a predictive risk score was established. We used the uniform manifold approximation and projection (UMAP) method to identify subtypes of OA patients, while the CytoHubba algorithm and GOSemSim R package were used to screen out hub genes. Next, an immunological assessment was performed using single-sample gene set enrichment analysis and CIBERSORTx.

Results: A total of 56OA-related differential genes were selected, and 10 characteristic genes were identified by the LASSO algorithm. OA samples were classified into cluster 1 and cluster 2 subtypes byUMAP, and the clustering results showed that the characteristic genes were significantly different between these groups. MYOC, CYP4B1, P2RY14, ADIPOQ, PLIN1, MFAP5, and LYVE1 were highly expressed in cluster 2, and ANKHLRC15, CEMIP, GPR88, CSN1S1, TAC1, and SPP1 were highly expressed in cluster 1. Protein–protein interaction network analysis showed that MMP9, COL1A, and IGF1 were high nodes, and the differential genes affected the IL-17 pathway and tumor necrosis factor pathway. The GOSemSim R package showed that ADIPOQ, COL1A, and SPP1 are closely related to the function of 31 hub genes. In addition, it was determined that mmp9 and Fos interact with multiple transcription factors, and the ssGSEA and CIBERSORTx algorithms revealed significant differences in immune infiltration between the two OA subtypes. Finally, a qPCR experiment was performed to explore the important genes in rat cartilage and synovium tissues; the qPCR results showed that COL1A and IL-17A were both highly expressed in synovitis tissues and cartilage tissues of OA rats, which is consistent with the predicted results.

Discussion: In the future, common therapeutic targets might be found forsimultaneous remissions of both phenotypes of OA.

KEYWORDS

osteoarthritis, synovitis, cartilage apoptosis, immune infiltration, bioinformatics analysis

1 Introduction

Osteoarthritis (OA), the most common form of arthritis, is characterized by chronic pain and high incidence (1) and disability (2) rates. OA arises from a complex process involving the cartilage, bone, synovium, ligaments, infrapatellar fat pads, meniscus, and muscles (3). Among them, the representatives that are most often studied are two significantly altered hallmarks, cartilage apoptosis and synovitis, whose discovery has often been considered a breakthrough in research on optimal treatment strategies for OA. Synovial inflammation usually occurs in the early stage of OA. Synovial inflammation can lead to the infiltration of inflammatory cells and the release of inflammatory factors, which can lead to cartilage destruction and joint dysfunction (4). However, unambiguous therapeutic targets and the correlation between the two phenotypes remain to be discovered, and we hoped in this research to identify genes or pathways significantly related to both synovitis and cartilage apoptosis to further interrogate the mechanism and effective therapeutic targets.

Clinical basic and systems biology studies have been performed to detect the pathogenesis of OA (5). Many OA-related protein markers or pathways play a role in the development and progression of OA, including endoplasmic reticulum, stress marker glucose-regulated protein 78 (*GRP78*), and Bcl2-associated athanogene 1 (*bag1*) (6). Transient receptor potential vanilloid 1 (*TRPV1*) is closely related to pain perception by OA patients (7). What is more? The roles of disintegrin and metalloproteinase with thrombospondin motif 5 (*ADAMTS5*) and follistatin-like protein 1 (*FSTL1*) in OA diagnosis and prognosis (8) have been reported. As for pathways, the Ca^{2+}/CaMKII/Nrf2 signaling pathway could inhibit M1 macrophage polarization to attenuate synovium in OA (7), and a promotional effect of the *JUNB*/*FBXO21*/*ERK* axis on cartilage degeneration in osteoarthritis by autophagy inhibition (9) was also reported. However, the studies above only explored the mechanism or potential target from the perspective of a single phenotype, and their sample numbers were limited. A systematic high-throughput analysis of targets and pathways associated with two or more phenotypes of OA is needed.

Some systematic bioinformatic analyses have partly improved on the defects above. The *FoxO* and *IL-17* signaling pathways are likely to regulate OA progression according to Kyoto Encyclopedia of Genes and Genomes (KEGG) enrichment, and ubiquitylation was found to be a key bioactive reaction in OA after analyzing the molecular function and protein–protein interaction (PPI) results (9). Abnormally methylated differentially expressed genes (DEGs) in OA such as *COL3A1*, *LUM*, and *MMP2* are potential methylation biomarkers of OA, and *THBS2* might play a role in the end stage of the disease (10). However, these studies all have defects as they lack multi-omics analyses and are pending multi-dimensional validation. Recently, a bioinformatics-led investigation used the Gene Ontology (GO) and KEGG databases, the CIBERSORTx method, and the ConsensusClusterPlus R package to perform enrichment and immune infiltration analyses before ultimately differentiating immunity patterns into two clusters and validating the expressions of *TCA1*, *TLR7*, *MMP9*, *CXCL10*, *CXCL13*, *HLA-DRA*, *ADIPOQ*, and *SPP1* using qPCR in chondrocytes (5). However, a synovitis analysis was not performed in this comprehensive and systematic research. Therefore, a systematic, multi-dimensional analysis covering multiple phenotypes should be performed.

In this study, we combined genes from the Gene Expression Omnibus and GeneCards databases to find OA-related genes, then constructed a risk model and used the receiver operating characteristic (ROC) curve to screen out and evaluate 10 characteristic genes. Network analysis and functional analysis of two subtypes were performed to estimate the degrees of immune infiltration, and the results were finally validated by qRT-PCR in rats' tissues.

2 Methods

2.1 Data download

We first downloaded the following five datasets associated with osteoarthritis from the Gene Expression Omnibus (GEO) database: GSE55457 (11), GSE12021 (GPL96) (12), GSE55235 (11), GSE12021 (GPL97) (12), and GSE82107 (13). Among these, the GSE55457, GSE12021 (GPL96), and GSE55235 datasets were used as osteoarthritis diagnostic model training sets, whereas the GSE12021 (GPL97) and GSE82107 datasets were used as osteoarthritis diagnostic model validation sets.

The osteoarthritis diagnostic model training sets were created by extracting and merging a common expression profile from GSE55457, GSE12021 (GPL96), and GSE55235, which contain 10 osteoarthritic synovial tissue samples and 10 control synovial tissue samples, 10 osteoarthritic synovial tissue samples and 9 control synovial tissue samples, and 10 osteoarthritic synovial tissue samples and 10 control synovial tissue samples, respectively. We used the "Combat" function in the sva R package (14) to correct a batch effect of merged data of 30 osteoarthritic synovial tissue samples and 29 control synovial tissue samples. The distribution of

target gene-expression levels before and after the correction was visualized by box plot.

GSE12021 contains 10 osteoarthritic synovial tissue samples and 4 control synovial tissue samples, whereas GSE82107 contains 10 and 7 samples, respectively. All the samples are of human origin, and all the datasets are from the GPL97 platform (Table 1).

2.2 Identification of OA DEGs

We input the keywords "synovitis" and "chondrocyte apoptosis" into the GeneCards database to obtain synovitis-related and chondrocyte apoptosis-related genes (15) (Supplementary Table 1). Then, we defined osteoarthritis-related genes by taking the intersection of synovitis-related genes, chondrocyte apoptosis-related genes, and osteoarthritis diagnostic model training sets. The results are shown using Venn diagrams.

To estimate the impact of osteoarthritis-related gene-expression levels on the severity of osteoarthritis, differential gene-expression analysis of OA and control samples of integrated datasets was performed using the limma R package (16). A differential gene was defined by a threshold of |fold change (FC)| > 1.5 and $p< 0.05$; genes with FC > 1.5 and $p< 0.05$ were considered up-regulated genes and those with FC< -1.5 and $p< 0.05$ were considered down-regulated genes. We took the intersection of differential genes and x1-related genes and obtained differentially expressed osteoarthritis-related genes. The results are visualized using volcano plots.

2.3 Constructing a forest model and nomogram model

We used the least absolute shrinkage and selection operator (LASSO) analysis method to perform dimension reduction analysis and obtained the characteristic genes from differentially expressed osteoarthritis-related genes. For normalized gene-expression values of weighted coefficients penalty of the characteristic genes, we established a risk score formula and visualized them by forest maps.

$$\text{riskScore} = \sum_i \text{Coefficient}(\text{gene}_i) * \text{mRNA Expression}(\text{gene}_i)$$

A nomogram was constructed according to selected characteristic genes to forecast the prevalence of OA. Then, the model's accuracy was tested using an independent validation dataset.

2.4 The molecular subtype of OA

Uniform manifold approximation and projection (UMAP), a non-linear dimensionality-reduction algorithm, was used to partition and compress a group of patients into clusters based on the given feature. Then, the characteristic genes provided the basis to identify these patients' subtypes using the umap R package (17).

2.5 The assessment of biological characteristics among subtypes of OA patients

Gene function enrichment could be performed by GO enrichment analysis from different dimensions and levels, i.e., biological process, molecular function, and cellular component categories (18). The KEGG database extensively includes related genomes, biological pathways, drugs and diseases, and so on (19). We used the clusterProfiler R package (20, 21) to perform GO functional annotation and KEGG pathway enrichment to identify the significantly enriched biological processes of DEGs of different subtypes in OA patients, with the significance threshold of enrichment analysis set at $p< 0.05$.

Gene set enrichment analysis (GSEA) could confirm whether a group of pre-defined genes was statistically different between two biological states; this approach is commonly used to estimate a sample's pathway and biological process activity (22). To analyze the differences in biological processes of different subtypes of OA patients, we downloaded "c5.go.v7.4.entrez.gmt" and "c2.cp.kegg.v7.4.entrez.gmt" based on gene-expression profile data (23). Then, GSEA was performed with the clusterProfiler R package to analyze enrichment and visualize the dataset.

Gene set variation analysis (GSVA) is a non-parametric unsupervised analysis method able to convert a gene's expression matrix to a gene set's expression matrix between different samples to estimate gene set enrichment in order to assess metabolic pathway enrichment among samples (24). To study the variation in biological processes among different subtypes, we used the GSVA R package (24) on account of the gene-expression profile of different samples of OA subtypes. The reference dataset "h.all.v7.4.symbols.gmt" was downloaded from the MSigDB database (23) to calculate a single sample's enrichment score for each hallmark.

2.6 PPI analysis

There are universal inter-relationships between genes, especially between those able to regulate the same biological process. To reveal

TABLE 1 The datasets are from the GEO database.

GSE	GPL	Species	Tissue Source	OA sample number	Control sample number
GSE55457	GPL96	Homo sapiens	Synovium	10	10
GSE12021	GPL96	Homo sapiens	Synovium	10	9
GSE55235	GPL96	Homo sapiens	Synovium	10	10
GSE12021	GPL97	Homo sapiens	Synovium	10	4
GSE82107	GPL570	Homo sapiens	Synovium	10	7

the connection between patients with different subtypes of OA, we constructed PPI networks on account of their DEGs. We obtained PPI data from STRING (25), using a score of 700 points as the threshold. After exporting PPI data, we conducted a further analysis using Cytoscape (Institute for Systems Biology, Seattle, WA, USA) (26), which contains the following 12 algorithms (27): Betweenness, BottleNeck, Closeness, ClusteringCoefficien, Degre, DMN, EcCentricity, EPC, MCC, MNC, Radiality, and Stress. We calculated the top 30 nodes in each algorithm and defined the "hub node" as the gene that appeared in at least five algorithms. Hub nodes have a greater level of connection with others and are extremely important in regulating all biological processes.

MicroRNA (miRNA) is a type of non-coding single-stranded RNA molecule coded by endogenous genes that measure 19-25 nt in length and play important roles in regulating biological evolution. MiRNA can influence the expression of target genes by post-transcriptional regulation during the processes of tumor incidence and development, biological development, organogenesis, epigenetic regulation, virus resistance, and so on. MiRNA and target genes usually exist in a one-to-many or many-to-one "regulate or be regulated" relationship (28). To analyze the connection between hub genes and miRNAs, we obtained hub gene–related miRNAs from Starbase (http://starbase.sysu.edu.cn/), which can provide predictions from a total of seven prediction procedures (TargetScan, microT, miRmap, picTar, RNA22, PITA, and miRanda), and we chose the relationships between miRNAs and messenger RNAs (mRNAs) that could be found in at least two of the procedures. We then constructed mRNA–miRNA regulatory networks and visualized them using Cytoscape.

Transcription factors (TFs) can control gene expression by interacting with target genes. We examined the relationships between TFs and hub genes from the MIRNet network to contrast hub gene–TF networks and analyze hub genes' regulatory reactions. The hub gene–TF networks were then visualized by Cytoscape.

2.7 Identification and correlation analysis of immune cell infiltration among different subtypes in OA patients

The immune microenvironment is an integrated system that encompasses immune cells, inflammatory cells, fibroblasts, the mesenchyme, and various cytokines and chemokines. The analysis of immune cell infiltration in samples could play an important role in disease research and treatment prognosis. Single-sample GSEA (ssGSEA) is an extension of the GSEA method. In this research, we used ssGSEA to calculate the concentrations of 28 kinds of immune cells (29), then visualized the immune cell composition by box plot. Differences in immune cell proportions were estimated by the Wilcoxon test, and $p< 0.05$ was seen as statistically significant. CIBERSORx is based on machine learning and could extend this algorithm framework to analyze gene-expression profiles specific to certain cell types without the cells' physical dissociation. RNA sequencing data were used to estimate the immune cell abundance (30). We estimated the abundance of 22 kinds of immune cells in OA patients of different subtypes from the dataset with the CIBERSORTx algorithm and drew a heatmap of immune cell infiltration correlation using the Corrplot R package (31).

The quantification of immune activity levels in tumor samples and the reflection of stromal and immune gene signatures by ESTIMATE analysis is a gene expression-based algorithm. The difference in immune scores of patients was estimated using the "estimate" R package (32) to calculate the hub genes' correlations with immune scores.

2.8 Animal experiments

We bought three-month-old male-specific pathogen–free Sprague–Dawley rats from the Shanghai Institute of Planned Parenthood Research–BK Laboratory Animals Co., Ltd. (Shanghai, China) and divided them into two groups (n = 6 each). All procedures and protocols used in this study were approved by the ethical committee of Xin Hua Hospital, which is affiliated with the Shanghai Jiao Tong University School of Medicine (approval no. XHEC-F-2022-014). The rats were treated according to the 3R principles and housed at a temperature of 22 ± 2°C, under a 12-h light/dark cycle and humidity of 40-70%. All rats were intraperitoneally injected with 3% sodium pentobarbital (0.1 mL/100 g; Sigma-Aldrich, USA). Additionally, in the OA group, we injected 0.1ml of MIA (30 mg/mL; Aladdin Biochemical Technology Co., Shanghai, China) in the right knee joint space, whereas the control group received an equivalent volume of normal saline 0.9%. Each rat was reared for 4 weeks; then, we extracted cartilage tissues and synovial tissues after euthanasia. Next, the genes in the tissues were detected by qRT-PCR. As stated in the above results, MMP9, COL1A, and IGF1 were identified as high nodes interacting with 53, 47, and 4 genes, respectively. While MMP9 and FOS as hub genes interacted with 33 and 32 TFs, respectively. What is more? The PPI results showed that the differential genes may be enriched in the IL-17 pathway and other pathways. So, we chose MMP9, COL1A, IGF1, and IL-17 pathway-related proteins (IL-17A, Jak 2, JNK, MAPK 1, and STAT 3) to verify the expression of them. The primer sequences of each gene are shown in Table 2.

2.9 Statistical analysis

Data processing and analysis were completed in the R statistical language (version 4.1.1; R Foundation for Statistical Computing, Vienna, Austria). Continuous variables were compared between two groups by independent *t*-test to estimate normally distributed variables' statistical significance, while two separate sets of variables were compared by Wilcoxon rank-sum test to estimate non-normally distributed variables' statistical significance. Pearson correlation was used to calculate different genes' correlation coefficients. The partial ROC (pROC) R package (33) was used for ROC curve analysis, and the area under the ROC curve (AUC) calculation was performed to evaluate the diagnostic model's accuracy. All two-sided p values< 0.05 were considered statistically significant.

TABLE 2 The primer sequences.

Gene	Forward primer sequence	Reverse primer sequence
Gapdh	TCACTGCCACTCAGAAGACT	ACATTGGGGGTAGGAACACG
mmp9	GGTCCCCCTACTGCTGGTCCT	CGAGAACTTCCAATACCGACC
FOS	GGAGGACCTTATCTGTGCGT	TGCGGTTGCTTTTGATTTTT
COL1A	TATGTATCACCAGACGCAGAAGT	GCAAAGTTTCCTCCAAGACC
IGF1	ACGGGCATTGTGGATGAGTG	TGTGTCGATAGGGGCTGGGA
JNK	GGAGGAGCGAACTAAGAATGG	ACTGCTGTCTGTATCCGAGGC
JAK2	CCCTGGCTGTCTATAACTCC	TCTGTACCTTATCCGCTTCC
stat3	TTAACATTCTGGGCACGAAC	TCAGTGACAATCAAGGAGGC
IL-17A	CTACCTCAACCGTTCCACTT	ACTTCTCAGGCTCCCTCTTC
MAPK1	GGGCAGTTCTGGTCGTAGTGG	GGAAGGATTCAGGGCAGGGA

3 Results

3.1 Expression of OA-related genes in OA patients

As shown in the flow chart (Figure 1), we first merged three datasets—GSE55457, GSE12021 (GPL96), and GSE55235—into a consolidated data set then removed significant batch effects (Figures 2A, C) between two groups of data to obtain gene-expression profiling data with consistent expression levels (Figures 2B, D). The consolidated data included 30 OA samples and 29 control samples. To screen OA-related genes, we searched keywords "synovitis" and "chondrocyte apoptosis" and found 795 synovitis-related genes and 3,353 chondrocyte apoptosis-related

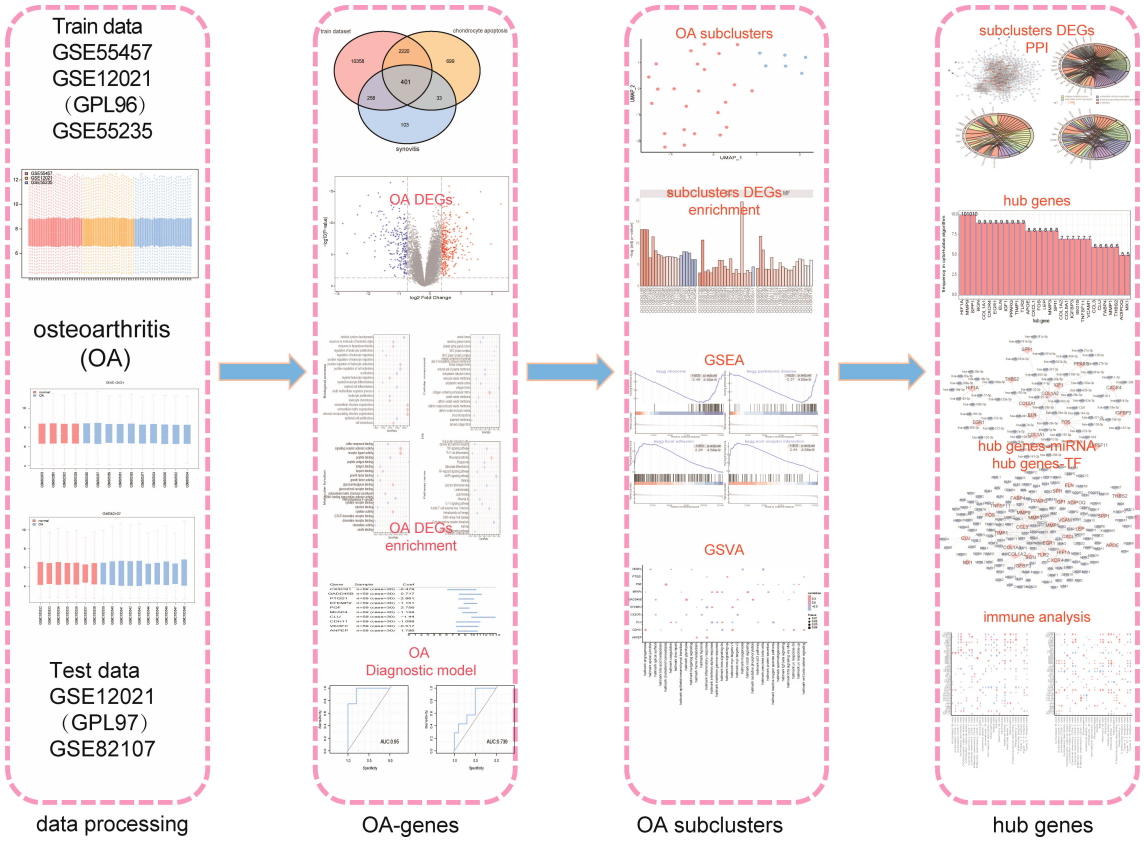

FIGURE 1
The flow chart.

genes in GeneCards (14) then took the intersection with the consolidated gene-expression profiling data and obtained 401 OA-related genes (Figure 2E).

The variance analysis between OA samples and control samples obtained 577 differential genes, which included 338 up-regulated genes and 239 down-regulated genes (Figure 3A). To analyze the two groups' functional differences, we assessed the impacts of DEGs on the related biological functions of patients. For functional annotation of DEGs, GO enrichment analysis showed highly significant enrichment in the "myeloid leukocyte migration", "leukocyte chemotaxis", and "extracellular matrix" biological processes (Figure 3B); in the "collagen-containing extracellular matrix" and "endoplasmic reticulum lumen MHC protein complex" cellular components (Figure 3C); and in the "glycosaminoglycan binding", "cytokine activity", "receptor ligand activity", and "signaling receptor activator activity" molecular functions (Figure 3D). These genes were also enriched in "rheumatoid arthritis", "tumor necrosis factor (TNF) signaling pathway", "IL-17 signaling pathway," and "osteoclast differentiation" pathways in KEGG (Figure 3E). Taking the intersection of DEGs and OA-related genes, they yielded 56 differentially expressed OA-related genes (Figure 3F), including 27 up-regulated genes and 29 down-regulated genes. The RCircos R package was used to annotate up- or down-regulated genes on chromosomes (34) and showed that these genes appeared in a similar position (Figures 3G, H).

3.2 Risk model construction

At this point, we performed ssGSEA to measure per-sample immune cell infiltration levels of control and OA groups, and the

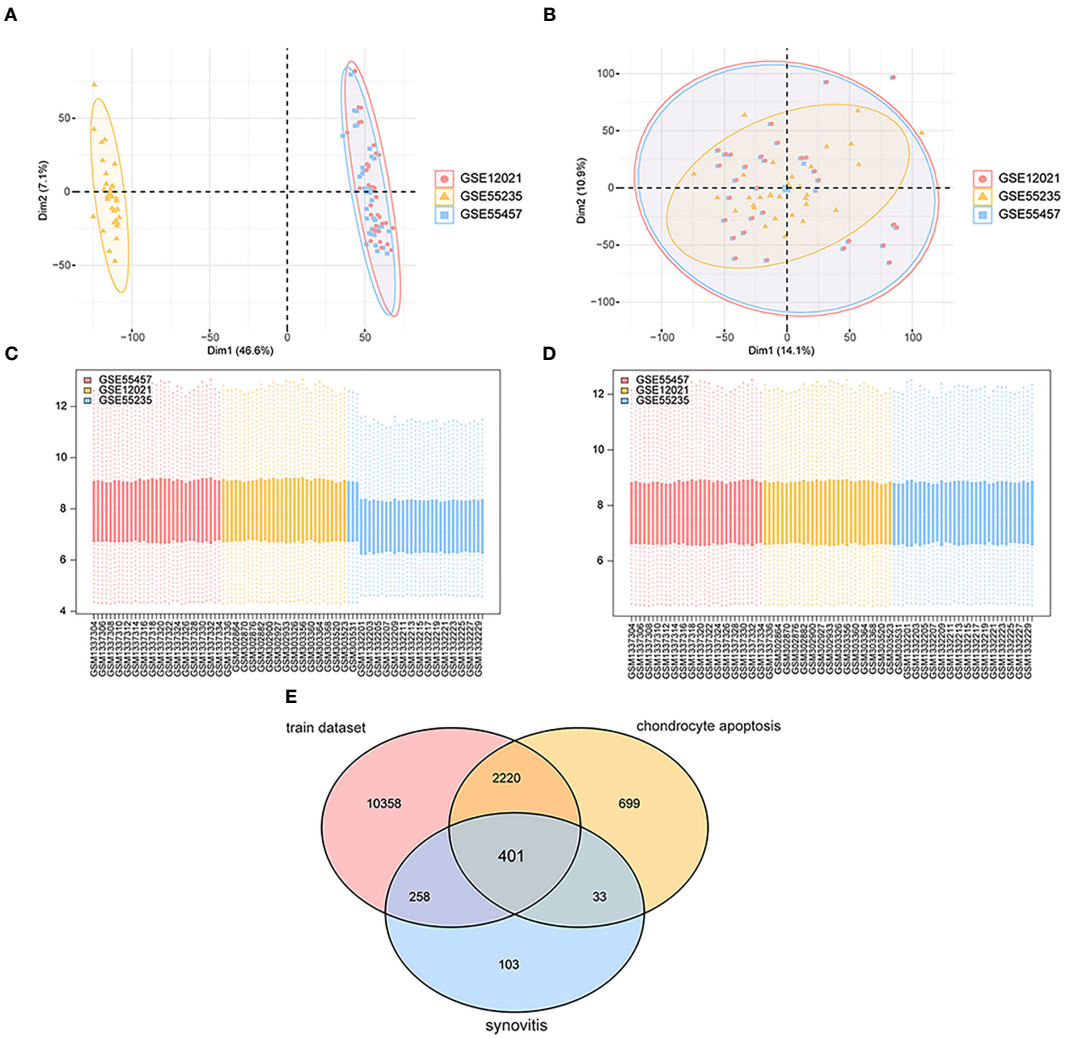

FIGURE 2
Data sets integration. **(A, C)** The maps of gene expression levels of integrated samples; the horizontal axis is the samples, and the vertical axis is the gene expression levels. **(B, D)** The maps of gene expression levels of integrated samples after the batch effects were removed; the horizontal axis is the samples, and the vertical axis is the gene expression levels. **(E)** The Venn map of OA-related genes; pink represents gene expression data in the training set, yellow means chondrocyte apoptosis-related genes, and blue means synovitis-related genes.

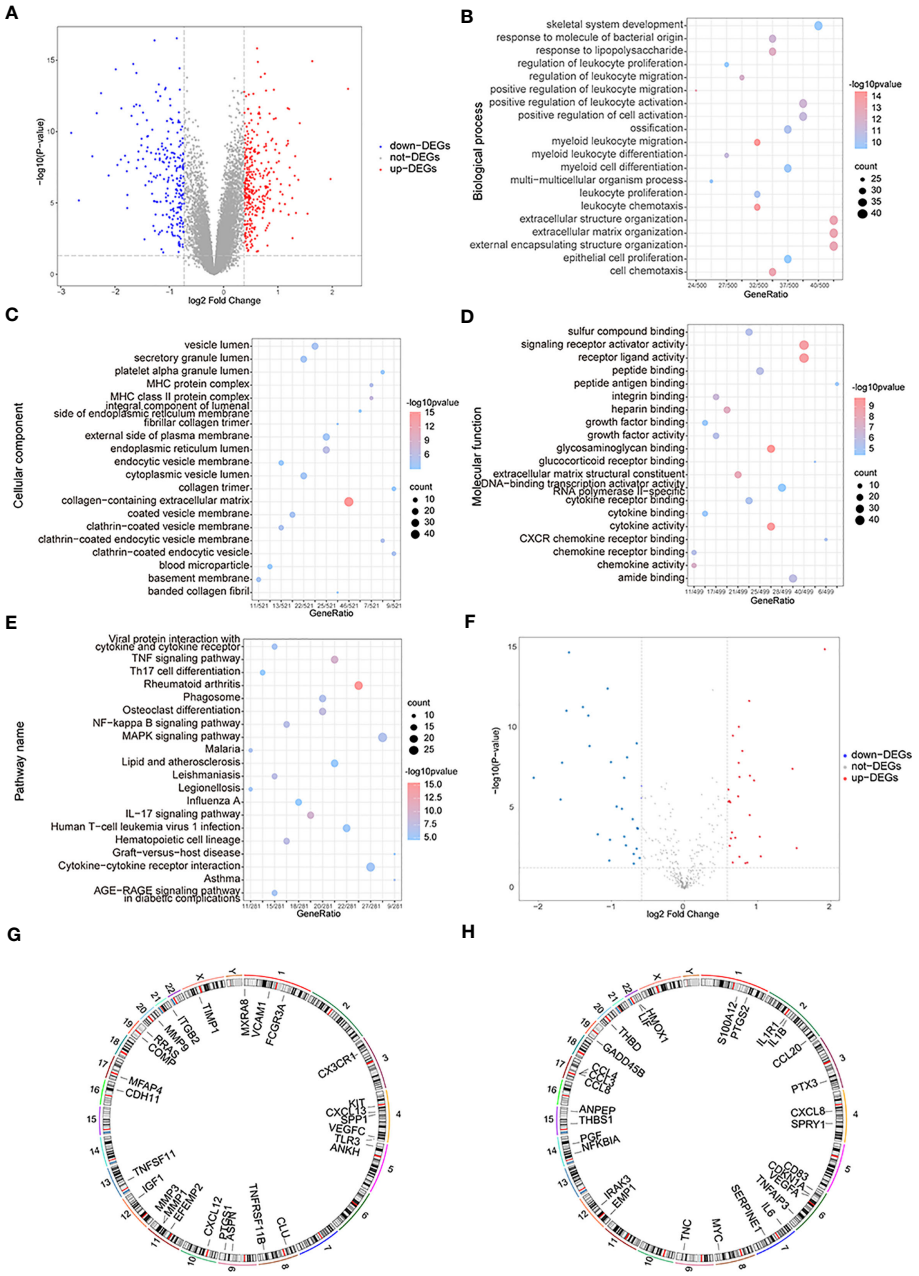

FIGURE 3
The functional enrichment analysis of differentially expressed genes (DEGs). **(A)** The volcano map of DEGs; the horizontal axis is log2FoldChange and the vertical axis is -log10(P-value); red nodes represent the up-regulated DEGs, blue nodes represent the down-regulated differentially expressed genes, and grey nodes mean the genes with no significant differences in expression level. **(B–E)** The BP, CC, MF, and KEGG analysis in GO terms of DEGs; the horizontal axis is gene ratio, the vertical axis is GO terms, the node sizes mean the genes' numbers under each GEO term, and the color of the nodes means the significance level. **(F)** The volcano map of differentially expressed OA-related genes; the horizontal axis is log2FoldChange and the vertical axis is -log10(P-value); red nodes represent the up-regulated differentially expressed genes, blue nodes represent the down-regulated differentially expressed genes, and grey nodes means the genes with no significant differences in expression level. **(G, H)** The chromosome annotation of up or down-regulated differentially expressed genes. (KEGG, Kyoto Encyclopedia of Genes and Genome; GO, the Gene Ontology; BP, biological process; CC, cellular component; MF, molecular function).

results showed that multiple immune cells' infiltration levels were different between these two groups ($p< 0.05$) (Figure 4A). Specifically, the concentrations of gamma delta T-cells, immature B-cells, immature dendritic cells, and macrophages of OA samples were higher than those of the control samples.

We then analyzed the correlation in expression levels of 27 up-regulated genes and 29 down-regulated genes among the OA group and control group. The results showed that in the normal group, the expression levels of up-regulated (Figure 4B) and down-regulated (Figure 4D) genes were mostly positively correlated ($p<0.05$). In the OA sample group, the expression levels of up-regulated (Figure 4C) and down-regulated (Figure 4E) genes were mostly negatively correlated ($p<0.05$).

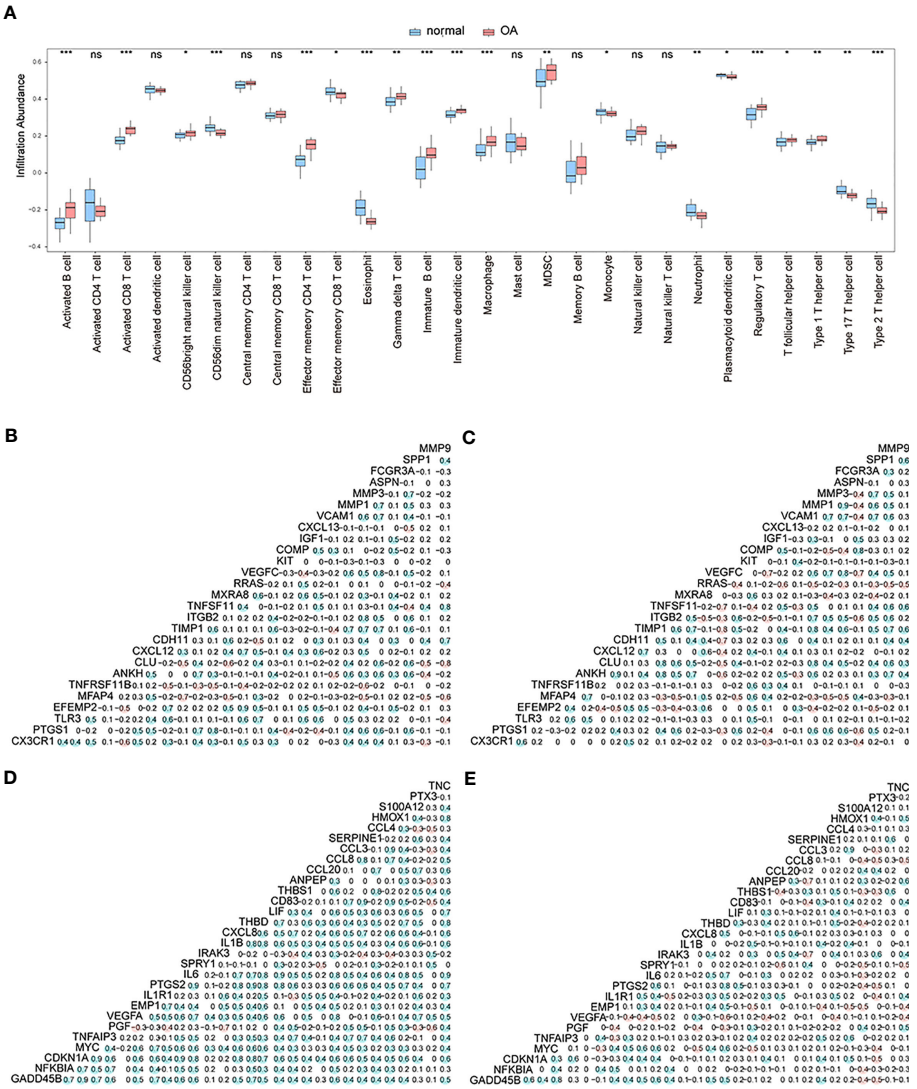

FIGURE 4
The correlation analysis. **(A)** The different enrichment levels of immune cells between OA samples and control samples; the horizontal axis is the immune cell, and the vertical axis is the enrichment level; *means the significant p-value was less than 0.05, **means the p-value was less than 0.01, and ***means the p-value was less than 0.001. **(B–C)** Correlation analysis of gene expression levels of up-regulated differentially expressed OA-related genes in both the control group and OA group; blue means positive correlation and red means negative correlation. **(D–E)** Correlation analysis of gene expression levels of down-regulated differentially expressed OA-related genes in both the control group and OA group; blue means positive correlation and red means negative correlation.

To estimate differentially expressed OA-related genes' impact on OA patients, we used the LASSO algorithm to identify the following 10 characteristic genes with a great impact on OA among 56 differentially expressed OA-related genes: *CX3CR1*, *GADD45B*, *PTGS1*, *EFEMP2*, *PGF*, *MFAP4*, *CLU*, *CDH11*, *VEGFC*, and *ANPEP* (Figures 5A, B). An OA predictive risk score was estimated by multiplying and adding the 10 characteristic genes' coefficients and gene-expression values. Each normalized expression value of the weighted penalty coefficient of characteristic genes was expressed by forest mapping (Figure 5C), and the predicted risk score of each sample was calculated to draw the ROC curve. The results included an AUC of 0.965 in the training set (Figure 5D). We then performed model validation involving the independent test data sets GSE12021 (GPL97) and GSE82107, and the AUCs were 0.95 and 0.736 (Figures 5E, F), which indicated that the model prediction is good for OA patients. Similarly, the 10 characteristic genes were analyzed to predict OA ROC curves separately, and the results showed that all these genes had good predictive efficacy (Figure 5G).

Considering patients' predicted risk scores and the 10 characteristic genes, we built a nomogram model to predict OA patients' prevalence rates and correct the nomogram model (Figures 6A, B). To assess the predictive model's accuracy and predict the net benefits of patients who received intervention according to the model, we divided both OA samples and control samples into two groups, where the first group contained 15 OA samples and 15 control samples and the second group contained 15 OA samples and 14 control samples. The ggDCA R package (35) was used for decision curve analysis, and the predicted lines lying

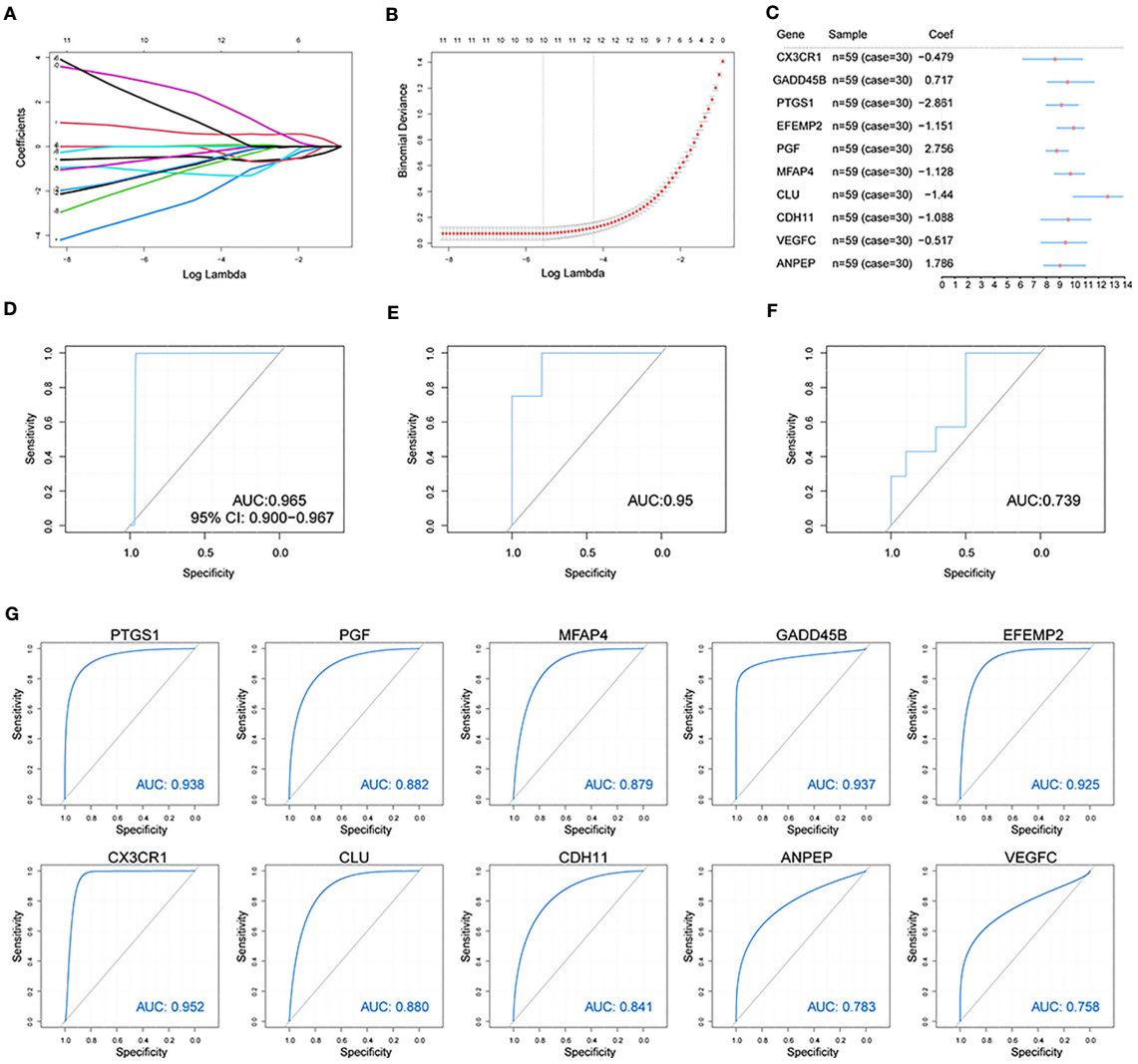

FIGURE 5
Construction of the osteoarthritis model. **(A, B)** The LASSO analysis was used to identify the characteristic genes. **(C)** The characteristic genes' forest map of OA patients. **(D)** The ROC curve of predicted risk scores was used on the OA training set. **(E)** The ROC curve of predicted risk scores was used on the OA test set GSE12021(GPL97). **(F)** The ROC curve of predicted risk scores was used on the OA test set GSE82107. **(G)** The ROC curve of the 10 characteristic genes in OA diagnosis.

above the standard line indicate that the decision of the nomogram model might be beneficial for OA diagnosis (Figures 6C–F).

3.3 Identifying different OA subtypes according to characteristic genes

Considering the 10 OA-related genes, a pair of OA subtypes, cluster 1 and cluster 2, were identified by the UMAP algorithm (Figure 7A), with 24 samples in cluster 1 and 6 samples in cluster 2. The clustering results showed significant differences in characteristic genes between the two groups (Figure 7B). The expression levels of differentially expressed OA-related genes of both subtypes in the control and OA groups were measured, and the results showed that most differentially expressed OA-related genes in the two groups were also differentially expressed in both subtypes (Figure 7C).

3.4 Enrichment analysis and network analysis

To detect the biological differences between patients with the two different OA subtypes, we first obtained 355 DEGs by analyzing both groups of patients' gene-expression profiles. We performed GO annotation of these DEGs and found these genes are involved in many biological processes (Figure 8A; Supplementary Table 2-go). Specifically, the results showed that these genes were mainly enriched in biological processes such as extracellular matrix organization, extracellular structure organization, extracellular encapsulating structure organization, and ossification (Figure 8B); cellular components such as collagen-containing extracellular matrix, endoplasmic reticulum lumen, platelet alpha granule, and fibrillar collagen trimer (Figure 8C); and molecular functions such as extracellular matrix structural constituent, glycosaminoglycan binding, integrin binding, and amide binding (Figure 8D).

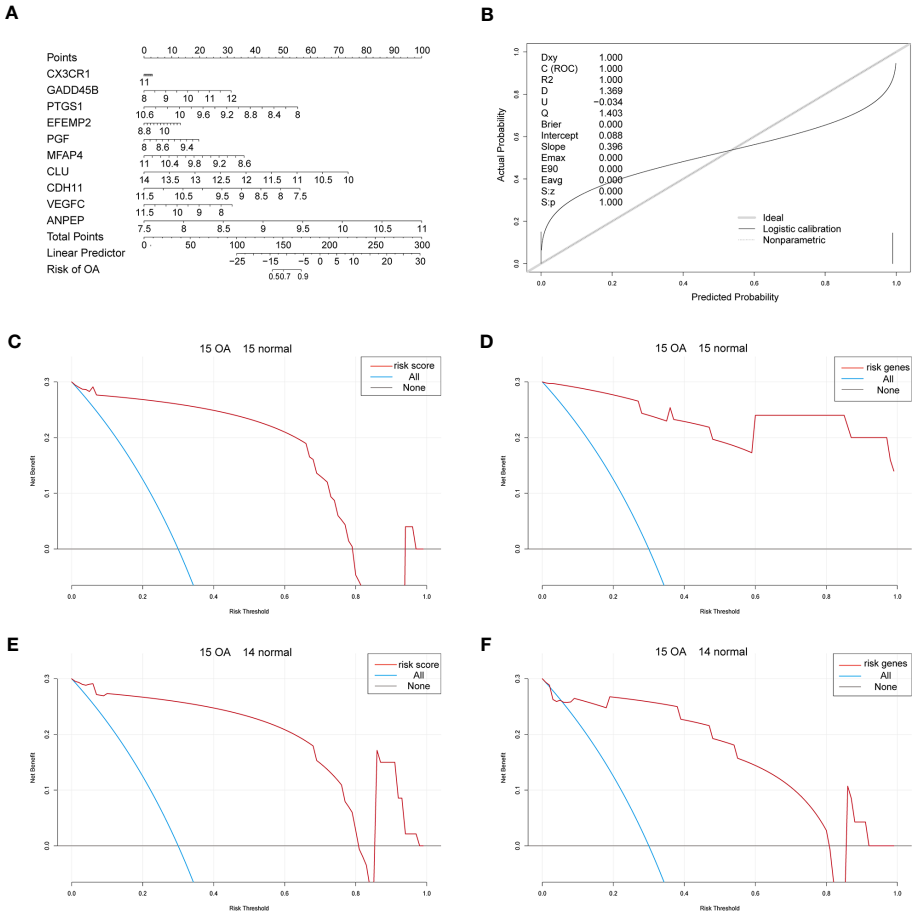

FIGURE 6
The nomogram. **(A)** The nomogram of the 10 characteristic genes in OA diagnosis. **(B)** The nomogram-corrected curve. **(C)** The DCA curve of predicted risk scores in the first group; blue means immediate diagnosis and pink represents the score risk model. **(D)** The DCA curve of the characteristic genes in the first group; blue means immediate diagnosis and pink means the combination of the characteristic genes. **(E)** The DCA curve of predicted risk scores in the second group; blue means immediate diagnosis and pink represents the score risk model. **(F)** The DCA curve of the characteristic genes in the second group; blue means immediate diagnosis and pink means the combination of the characteristic genes.

Enrichment in KEGG pathways such as rheumatoid arthritis, PPAR signaling pathway, protein digestion and absorption, and osteoclast differentiation was also noted (Figure 8E; Supplementary Table 2-kegg).

We then performed GSEA considering both subtypes of OA patients and found that biological processes such as GO structural constituents of ribosomes, GO oxidoreductase activity acting on NAD pH quinone or a similar component as an acceptor, GO mitochondrial respiratory chain complex assembly, GO ribosomal subunit, and GO ATP synthesis-coupled electron transport could be inhibited in patients from cluster 1 (Figure 9A), while biological processes such as GO endoplasmic reticulum lumen, GO collagen fibril organization, GO endoderm formation, and GO neuroinflammatory response were promoted (Figures 9B, C; Supplementary Table 3-gsea-go). The pathway activity of patients from the two subtype groups was analyzed, and the results showed that pathways such as the ribosome, Parkinson's disease, drug metabolism cytochrome p450, and metabolism of xenobiotics by cytochrome p450 were inhibited in cluster 1 patients (Figure 9D), while pathways such as ECM receptor interaction, lysosome, focal adhesion, and *Leishmania* infection were promoted (Figures 9E, F; Supplementary Table 3-gsea-kegg).

To further explore the functional differences between the two subtypes, we used GSVA and found that biological processes such as hallmark hypoxia, hallmark interleukin-2 STAT5 signaling, hallmark interleukin-6 JAK/STAT3 signaling, and hallmark inflammatory response were significantly activated in cluster 1 patients (Figure 10A). Concurrently, most of the other biological processes, such as hallmark notch signaling, hallmark oxidative phosphorylation, hallmark p53 pathway, and hallmark pancreas beta cells, showed significant differences between the two groups of patients (Figure 10A). We also analyzed the correlation between patients' characteristic genes and hallmark biological processes, and the results showed that MFAP4 and hallmark TGF beta signaling, hallmark epithelial-mesenchymal transition, or hallmark angiogenesis were significantly positively correlated ($p< 0.05$), while EFEMP2 and hallmark heme metabolism, PGF and hallmark spermatogenesis, hallmark UV response dn, and hallmark pancreas beta cells were significantly negatively correlated ($p< 0.05$) (Figure 10B).

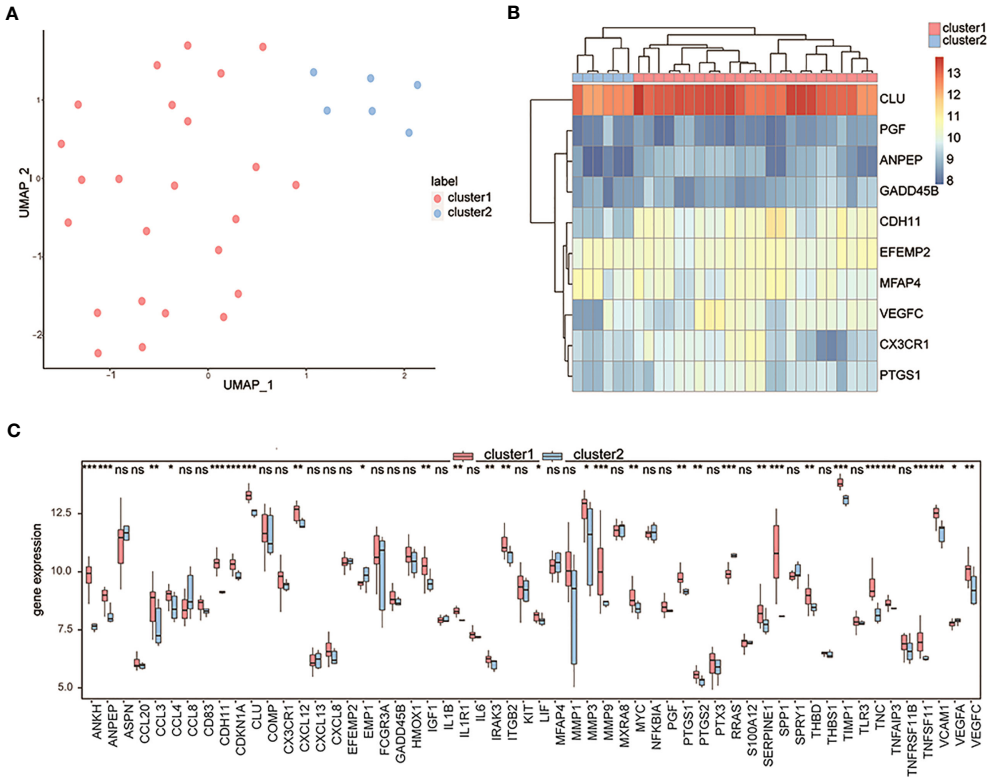

FIGURE 7
Clustering OA patients by the characteristic genes. **(A)** The UMAP clustering results; pink means cluster 1 and blue means cluster 2. **(B)** The expression heatmap of characteristic genes in two clusters; pink means cluster 1 and blue means cluster 2. **(C)** The expression differences of differentially expressed OA-related genes between cluster 1 and cluster 2; the horizontal axis is the characteristic gene, and the vertical axis is the gene expression level. ns means P≥0.05 with no statistical significance; * means P<0.05; ** means P<0.01; *** means P<0.001.

3.5 Network analysis between two subtypes of patients

To analyze the impact of the two subtypes of patients' DEGs on osteoarthritis patients' biological functions, we first built subtypes of patients' DEGs-related PPI networks and visualized the results using Cytoscape. The PPI networks contained 451 interaction pairs and 349 DEGs, with an average node degree of 2.58, an average local clustering coefficient of 0.404, and a PPI enrichment *p*-value< 1.0 (15). Among them, mmp9, COL1A, and IGF1 were high-degree nodes that interacted with 53, 47, and 4 genes, respectively (Figure 11A). To analyze the effects of genes in the PPI network on osteoarthritis, we performed enrichment analysis involving genes from the network and determined that these genes mainly affected biological processes like ossification, collagen metabolic process, and extracellular matrix organization (Figure 11B); cellular components like collagen-containing extracellular matrix, endoplasmic reticulum lumen, and fibrillar collagen trimer (Figure 11C); cell functions like extracellular matrix structural constituent, platelet-derived growth factor binding, and receptor-ligand activity (Figure 11D); and signaling pathways like rheumatoid arthritis, lipid and atherosclerosis, the A signaling pathway, and the TNF signaling pathway (Figure 11E).

We used 12 algorithms of CytoHubba to calculate the top 30 nodes in each algorithm and extracted 31 genes we called hub nodes from at least five algorithms (Figure 11F). Then, the GOSemSim R package was used to analyze the hub genes' GO semantic similarity (36), and the results showed that RPL19, RPS11, and RPL10A had greater functional correlations with multiple genes (Figure 11G).

We built a hub gene mRNA–miRNA network. The network contained 97 interactions, which included 14 mRNAs and 68 miRNAs, in which COL1A1 and COL1A2 hub genes could both interact with 14 miRNAs (Figure 11H). The hub genes' mRNA–TF network was also built and contained 29 miRNAs and 167 TFs; among these, hub genes mmp9 and Fos could interact with 33 and 32 miRNAs, respectively (Figure 11I).

3.6 Differences in immune characteristics between RNA modification patterns

CIBERSORTx and ssGSEA were used to compare immune cell infiltration levels between osteoarthritis patients of two subtypes. ssGSEA showed that patients' concentrations of central memory $CD4^+$ T-cells, central memory $CD8^+$ T-cells, effector memory $CD4^+$ T-cells, effector memory $CD8^+$ T-cells, natural killer cells, and natural killer T-cells in cluster 1 were significantly higher than those in cluster 2 (Figure 12A). We computed the correlation of characteristic genes and immune cells between cluster 1 and cluster 2 patients, and the results indicated that activated $CD8^+$ T-cells and

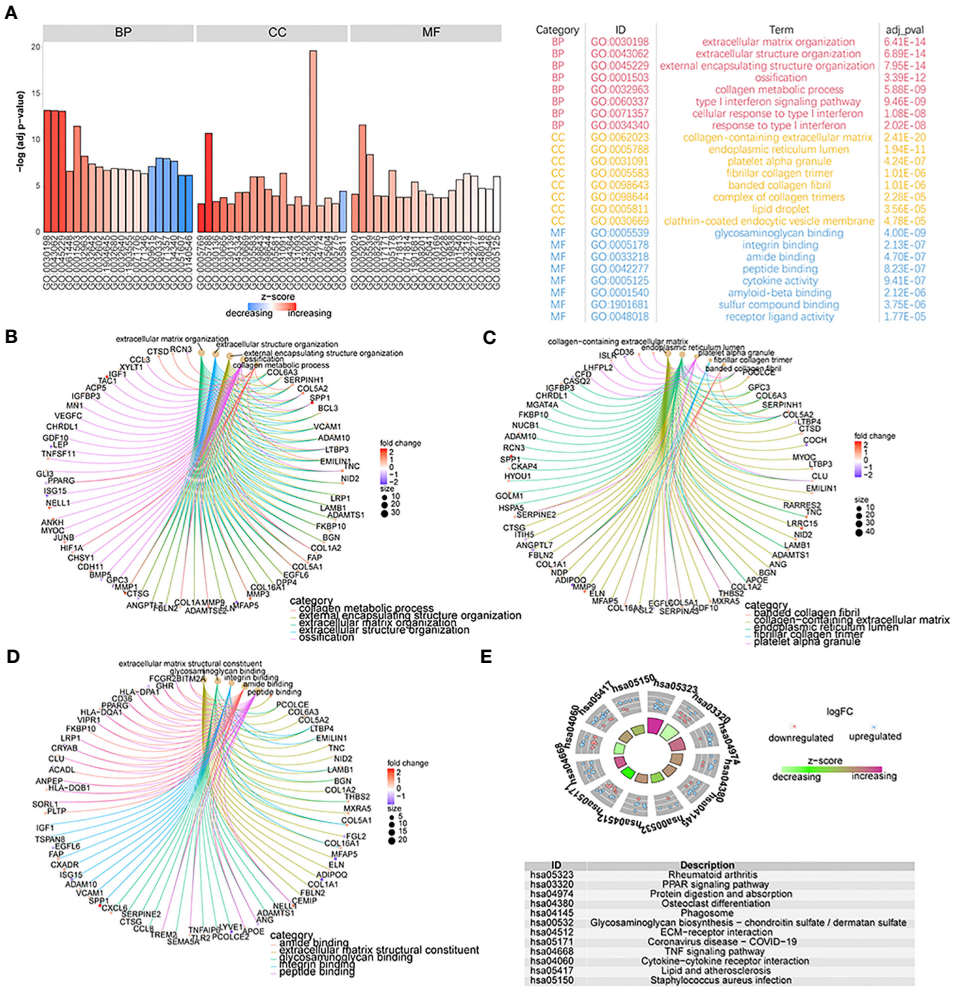

FIGURE 8
The functional analysis of DEGs. **(A)** GO functional enrichment analysis of DEGs; the horizontal axis is GO terms and the vertical axis is the significance of enrichment results. **(B–D)** The results of the first five items of BP, CC, and MF analysis; the node size means the genes' number which was enriched under each term; different line colors mean different biological functions. **(E)** The KEGG enrichment analysis; different node colors mean different gene expression levels and the quadrilateral color means the Z-score of KEGG pathways.

activated dendritic cells were significantly correlated with multiple characteristic genes' expression levels ($p< 0.05$) (Figure 12B) in cluster 1, while in cluster2, activated B-cells were significantly related to the characteristic genes' expression levels ($p< 0.05$) (Figure 12C). The correlations of hub genes and immune cells in cluster 1 and cluster 2 were respectively calculated, and we found that hub gene *PPARG* showed a stronger correlation with multiple immune cells in cluster 1 ($p< 0.05$) (Figure 12D), while hub genes *MMP1* and *MMP3* were highly related to multiple immune cells in cluster 2 ($p< 0.05$) (Figure 12E). We also estimated the correlation among various immune cells of both groups of patients and found that the correlations were weak in cluster 1 (Figure 12F), while in cluster 2, type 1 T helper cells, activated $CD8^+$ T-cells, macrophages, immature B-cells, activated $CD4^+$ T-cells, MDSCs, regulatory T-cells, activated dendritic cells, memory B-cells, central memory $CD8^+$ T-cells, natural killer T-cells, natural killer cells, central memory $CD4^+$ T-cells, type 17 T helper cells, and activated B-cells were positively correlated; however, there were negative correlations among T follicular helper cells, type 2 T helper cells, and most other immune cells (Figure 12G).

Next, CIBERSORTx was used to compare immune cell infiltration levels between the two subtypes of patients, and the results showed that the correlation of various immune cell concentrations between cluster 1 and cluster 2 was significantly different ($p< 0.05$) (Figures 13A, B). We then calculated the correlations of 31 hub genes and immune cell contents separately and found that M1 macrophages and dendritic cells were significantly negatively correlated with multiple hub genes (Figure 13C), while gamma delta T-cells and M0 macrophages were significantly positively correlated with the same genes (Figure 13D).

We compared immune scores between OA samples and control samples and found that the OA samples' scores were significantly higher than those of the control samples ($p< 0.05$) (Figure 14A). Then, the correlations of hub genes' expression levels and immune scores were calculated, and the results showed that hub genes such

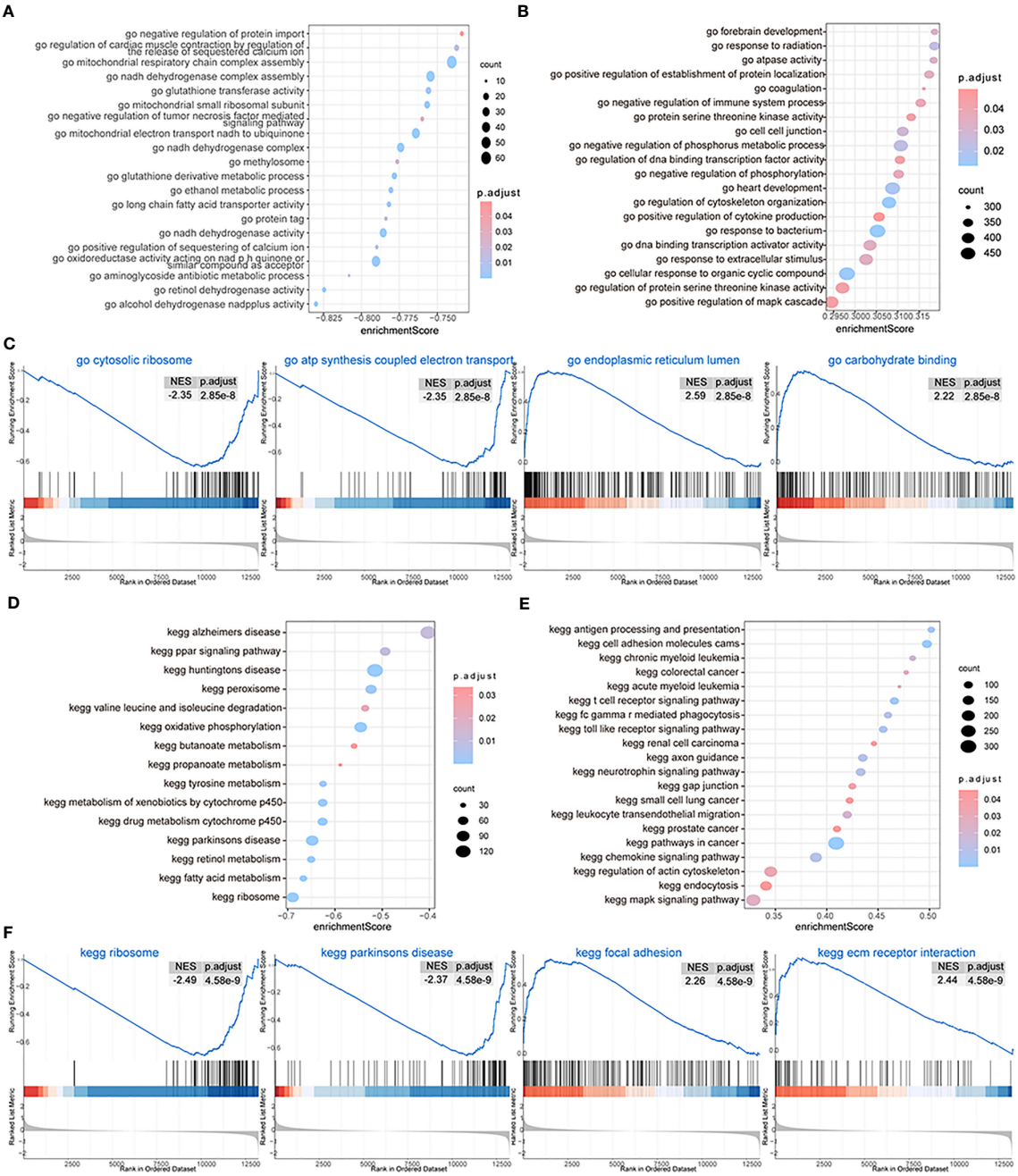

FIGURE 9
GSEA. **(A, B)** The GSEA-GO analysis; the biological process is inhibited **(A)** and the biological process is activated **(B)** in cluster 1; the horizontal axis is the enrichment score, and the vertical axis is GO terms. The color means the p-value and the node size means the enriched genes' number. **(C)** The first four items of GO terms. **(D, E)** The GSEA-KEGG analysis; the biological process is inhibited **(D)** and the biological process is activated **(E)** in cluster 1; the horizontal axis is the enrichment score, and the vertical axis is KEGG terms. The color means the p-value and the node size means the enriched genes' number. **(F)** The first four items of KEGG terms.

as *FABP4*, *EGR1*, *ADIPOQ*, *PPARG*, and *LEP* were negatively correlated with immune scores, while hub genes such as COL1A2, *MMP1*, *TIMP1*, *BGN*, and COL1A1 were positively correlated with them ($p < 0.05$) (Figure 14B). To estimate the ability to distinguish the two subtypes of OA according to hub genes, we computed the AUC score using the ROC curve and found that genes such as *TNFSF11*, *VCAM1*, *CCL3*, *CLU*, *FABP4*, and *THBS2* could distinguish between the two subtypes very well (Figure 14C).

3.7 RT-qPCR validation results

As mentioned above, we used 2-month-old SD rats for the following studies. After KOA modeling, the same batch of rats were randomly selected for knee joint staining to verify the success of KOA model (Supplementary Figure 1). After KOA modeling, cartilage tissue, and synovial tissue were collected from two groups of rats for PCR verification. The expression levels of the

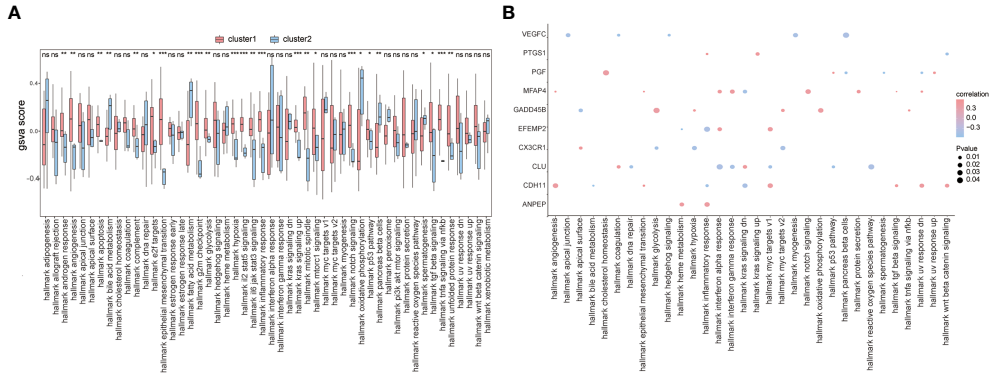

FIGURE 10
GSVA. **(A)** The difference in hallmark between the two subtypes of patients; the horizontal axis is the hallmark, and the vertical axis is GSVA scores; pink means cluster 1 and blue means cluster 2, *means the significant p-value was less than 0.05, **means the p-value was less than 0.01, and ***means the p-value was less than 0.001. **(B)** The correlation of characteristic genes and hallmark; the horizontal axis is hallmark, and the vertical axis is characteristic genes; the node size means the significance level and the node color means the correlation level.

COL1A, Fos, IGF1, mmp9, IL-17A, Jak2, JNK, MAPK1, and STAT3 nodes were verified in PCR rats' tissues, and the results are shown in Figure 15. All the genes tested were different in the OA group, but this trend was not completely consistent. Only COL1A and IL-17A were highly expressed in cartilage and synovium, which is consistent with the bioinformatics prediction.

4 Discussion

Osteoarthritis (OA) is the most common joint disease and shows an increased incidence with age (37). An imbalance in the catabolism and anabolism of cartilage (38) and pain-related synovitis (39) could affect the development of OA, and synovium might induce an early response in OA by regulating cartilage development and proteolysis (40). Thus, both synovium and cartilage are important in OA progression and could underly the therapeutic potential in OA. Synovial inflammation can induce articular cartilage injury, while cartilage injury can further aggravate synovial inflammation (41). To date, however, no well-defined target or treatment mechanism exists for either phenotype, so we performed a bioinformatics analysis on the results of microarray and high-throughput technology, identified and validated *in vivo* the DEGs associated with both synovitis and cartilage apoptosis, then analyzed immune cell infiltration and subtype classification for an in-depth understanding of the mechanisms of OA.

The present study considered 577 differently expressed genes and 401 synovitis or chondrocyte apoptosis-related genes whose intersection revealed 56 differential expressed OA-related genes. Several biological processes, cellular components, and molecular functions were enriched categories in the GO analysis of DEGs, while KEGG analysis revealed the DEGs were involved in the TNF signaling pathway, IL-17 signaling pathway, and other pathways. TNF-α transmits signals through TNF receptor 1 (TNF1) and TNF receptor 2 (TNF2) in the TNF pathway (42), and TNF-α can also be released by adipose tissue to negatively regulate by promoting matrix metalloproteinase generation and inhibiting proteoglycans or type II collagen synthesis (43). Intra-articular injection of IL-17-neutralizing antibodies could decrease the expression of joint-degeneration markers (44), and a holistic study showed that hub genes in OA were significantly enriched in the IL-17 signaling pathway (45). These conclusions are consistent with the results of our analysis and the fact that pathway protein interleukin-1A was highly expressed in the synovium and cartilage of OA rats.

The levels of multiple immune cells in OA samples, such as gamma delta T-cells, immune B-cells, immature dendritic cells, and macrophages, were higher than those in the control group according to ssGSEA, and 10 characteristic genes were identified from 56 differential expressed OA-related genes by LASSO algorithms, i.e., *CX3CR1*, *GADD45B*, *PTGS1*, *EFEMP2*, *PGF*, *MFAP4*, *CLU*, *CDH11*, *VEGFC*, and *ANPEP*. We then calculated predictive risk scores and used ROC curves to obtain results showing that these genes have good predictive abilities; moreover, the nomogram model decisions, which were made based on the predicting risk scores and 10 characteristic genes, might be beneficial to OA diagnosis.

We then used UMAP methods to divide OA patients into cluster 1 and cluster 2. Notably, most of the genes differentially expressed between OA and control samples were also differentially expressed between these two clusters, such as *IGF1*, *MMP9*, and *CX3CR1*. Also, a PCR experiment in rats' tissues showed that the level of IGF1 in OA rats' synovium was higher than that in control rats, but the trend was exactly opposite in the cartilage, while the trends of MMP9 were the same in both tissues with low expression in OA samples and high expression in control samples, contrary to the bioinformatic analysis results. Insulin-like growth factor 1 (IGF-1) can promote longitudinal bone growth (46) and support chondrocyte survival, proliferation, or cartilage matrix synthesis *via* PI3K/AKT, MAPK, and NF-kB pathways (47, 48); however, whether its expression level will change with OA progression and tissue type and finally lead to the difference between rats and human patients and between cartilage and synovium needs to be elaborated. Still, the differentially expressed level of insulin-like growth factor 1 in the synovium of OA was first mentioned in this

10.3389/fimmu.2023.1149686

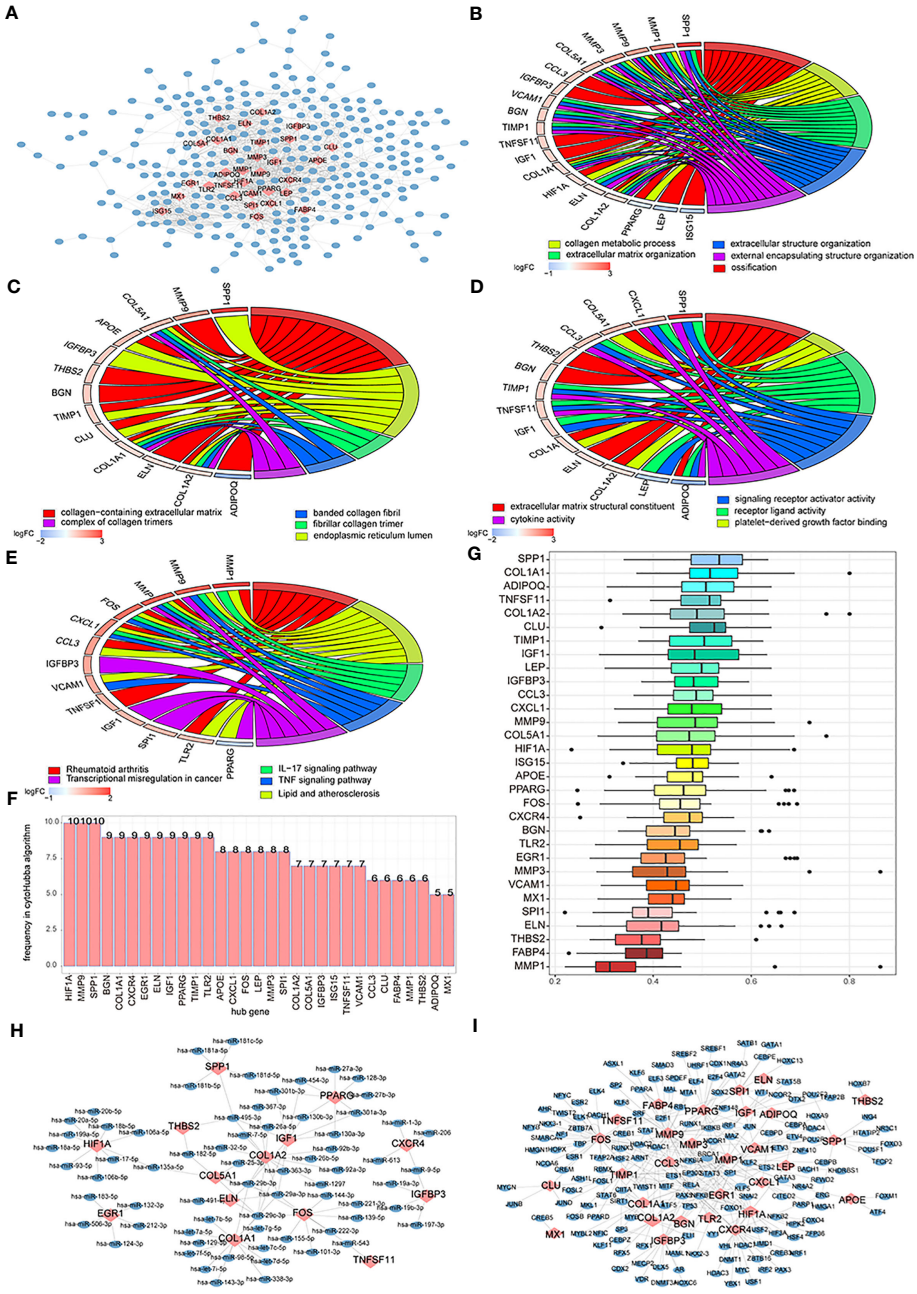

FIGURE 11
The differentially expressed genes (DEGs)-associated networks. **(A)** DEGs' protein-protein interaction (PPI) network; the blue node represents DEG, and the pink node means hub genes. **(B–E)** The BP, CC, MF, and KEGG analysis of genes' GO terms in the PPI network; the node color means genes' expression level, and the different line color means different biological functions. **(F)** The genes frequency tables of 12 algorithms; the horizontal axis is genes, and the vertical axis is frequency. **(G)** The GO semantic similarity scores of hub genes in DEGs' PPI network; the horizontal axis is the similarity level, and the vertical axis is the gene. **(H)** Hub genes' mRNA-miRNA network; the pink node means hub genes and the blue node means miRNA. **(I)** Hub genes' mRNA-TF network; the pink node means hub genes and the blue node means TF.

study and might be a new therapeutic target in synovitis in early-stage OA. Additionally, studies focusing on OA showed that it may be a potential diagnostic marker of OA given the higher levels recorded in OA cartilage tissue than in control cartilage tissue (49, 50) and with its leading role in the intima layer's macrophages in early-stage OA synovitis (51). Our analysis concerning MMP9 also found an expression difference between OA and control samples, but the trends were totally different and remain to be further investigated by different experimental or modeling methods.

A total of 355 DEGs were identified from the expression profiles of the two OA subtypes and subsequently enriched using GO, KEGG, and GSEA. Then, functional differences between the two subtypes were analyzed using GSVA. Subsequently, we constructed a PPI network of DEGs among OA subtypes and identified three

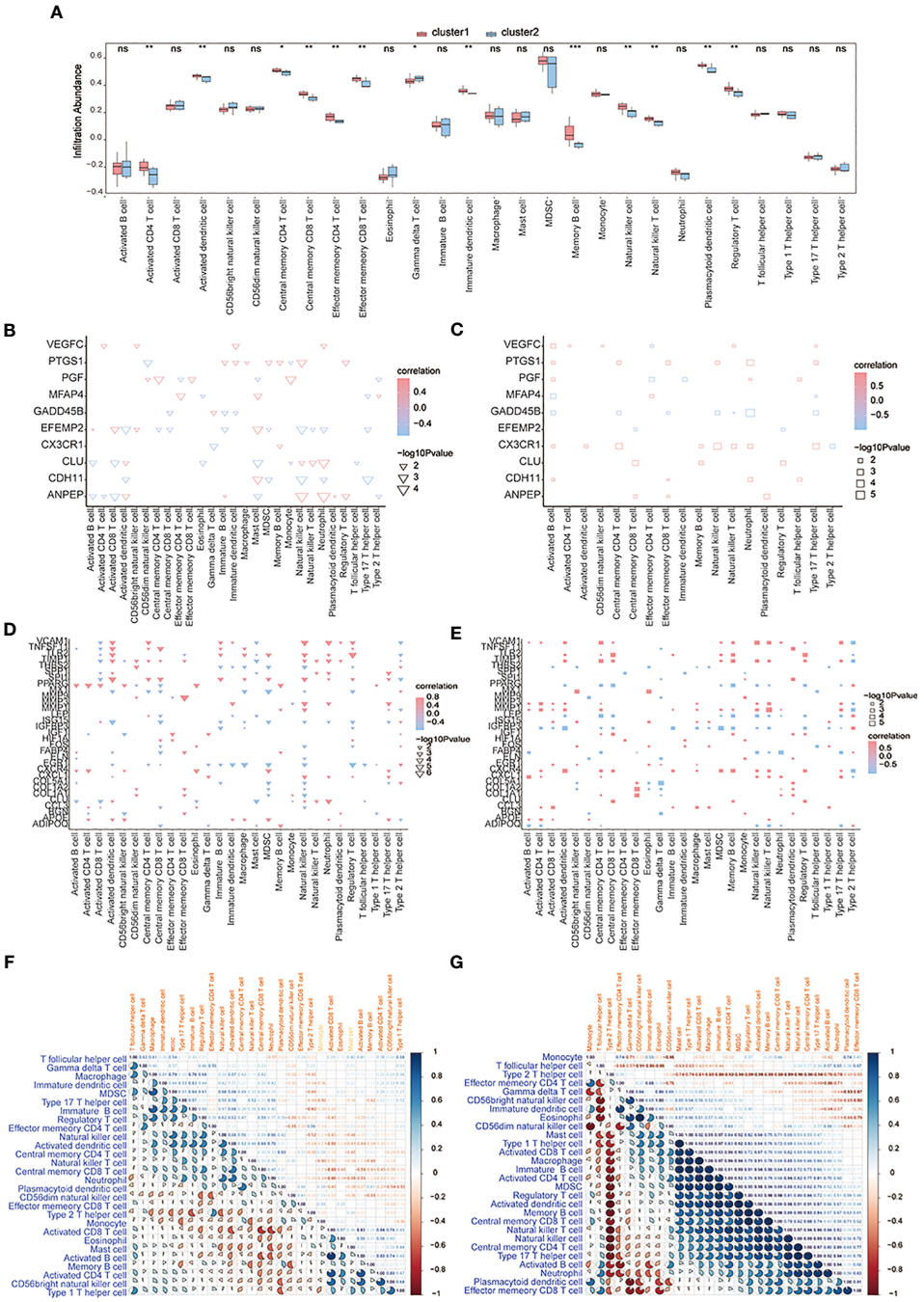

FIGURE 12
The immune characteristics-ssGSEA between two subtypes of OA patients. **(A)** The content histogram of immune cells between cluster 1 and cluster 2 patients; the blue means cluster 2 sample while the pink one means cluster 1 sample; the horizontal axis is the immune cell, and the vertical axis is cell content. **(B, C)** The correlation of characteristic genes and immune cells between cluster 1 and cluster 2; the node size means significance and the node color means correlation; the horizontal axis is the immune cell and the vertical axis is characteristic genes. **(D, E)** The correlation of hub genes and immune cells between cluster 1 and cluster 2; the node size means significance and the node color means correlation; the horizontal axis is the immune cell, and the vertical axis is the hub gene. **(F, G)** The correlation analysis of immune cells in cluster 1 and cluster 2; red means negative correlation while blue means positive correlation. ns means P≥0.05, with no statistical significance; * means P<0.05; ** means P<0.01; *** means P<0.001.

highly connected nodes: MMP9, COL1A, and IGF1. The results of the gene-enrichment analysis showed that these genes were mainly enriched in the IL-17 pathway, TNF pathway, and other signaling pathways. Both MMP9 and IGF1 have been discussed previously, while COL1A is often considered a marker of osteoblast differentiation (52), and the polymorphism of the transcription factor SP1 binding site is closely related to bone mass and fracture (53). Simultaneously, as a fibrosis mark, COL1A could also promote articular cartilage repair after injury (54). The PCR results in rat tissues showed that the expression level of COL1A in the OA group was higher than that in the control group both in cartilage tissues and synovial tissues, which indicated that the repair mechanisms in

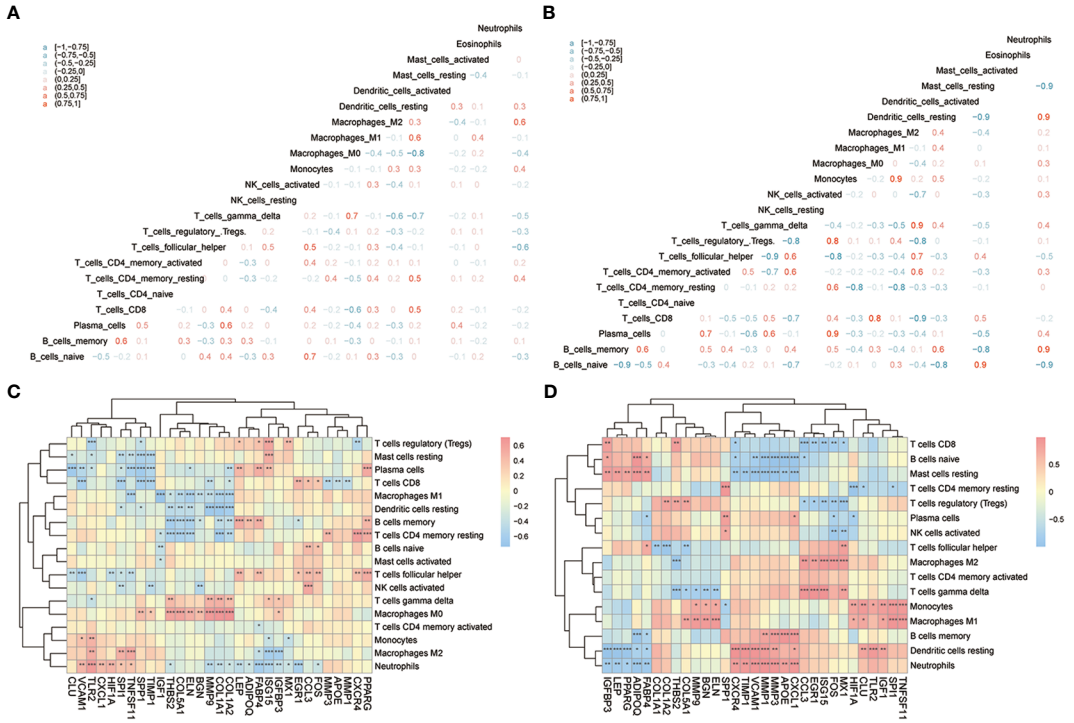

FIGURE 13
The immune characteristics-CIBERSORTX between two subtypes of OA patients. **(A, B)** The correlation of immune cells' content between cluster 1 and cluster 2 patients; pink means positive correlation while blue means negative correlation. **(C, D)** The correlation of immune cells and hub genes between cluster 1 and cluster 2 patients; the horizontal axis is the hub gene, and the vertical axis is the immune cell; red means positive correlation while blue means negative correlation. The node size means significance and the node color means correlation. *means the significant p-value was less than 0.05, **means the p-value was less than 0.01, and ***means the p-value was less than 0.001.

the cartilage of OA rats might be activated, while synovium might also undergo fibrosis. We also first looked at the effect of COL1A on synovitis in OA.

A total of 31 hub genes were found and the GOSemSim R package showed that *ADIPOQ*, *COL1A1*, and *SPP1* were closely related to the function of several genes. Adiponectin (*ADIPOQ*) is released from adipose tissue and plays an important role in bone formation and resorption (55); it is involved in the inflammatory response and triggers cartilage damage by up-regulating the expression of cytokines, matrix-degrading enzymes, and chemokines in chondrocytes and synovial fibroblasts (56). Phosphoprotein 1 (*SPP1*) is an extracellular matrix adhesion molecule that plays important roles in bone mineralization, immune response, tumor metastasis, inflammation, and angiogenesis (57), and it has also been identified to be a regulator of the PI3K/AKT pathway and could influence chondrocyte status

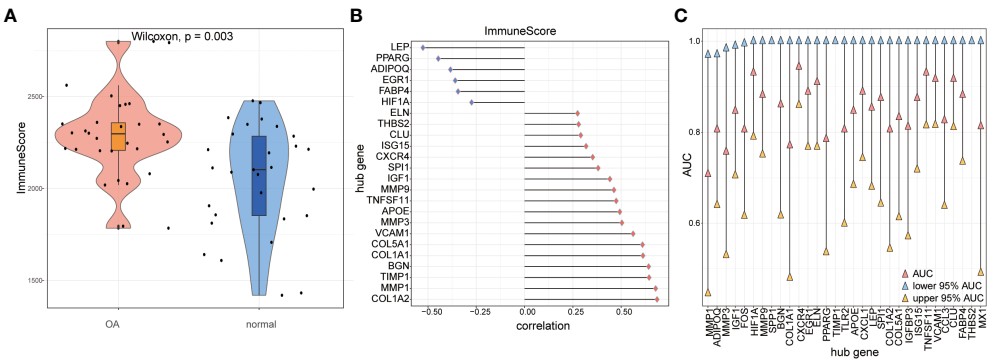

FIGURE 14
The immune score calculation. **(A)** The immune score of OA samples and control samples; red means OA samples while blue means control samples; the vertical axis is the immune score. **(B)** The correlation of immune score and hub genes in all the OA samples; the horizontal axis is the correlation, and the vertical axis is hub genes. **(C)** AUC and 95% AUC in the ROC curve of hub genes, the blue node means lower 95% AUC, yellow means upper 95% AUC, pink means AUC, the horizontal axis is hub genes, and the vertical axis is AUC values.

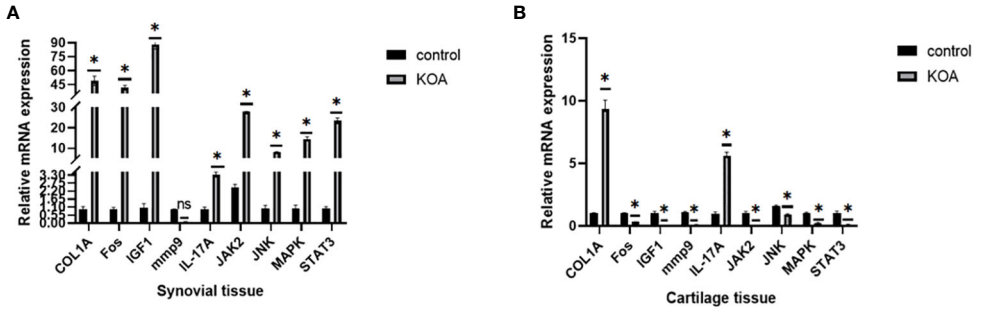

FIGURE 15
PCR results. **(A)** Expression levels of related proteins in cartilage tissues. **(B)** Expression levels of related proteins in synovial tissues (ns: p>0.05, *: p<0.05).

in OA (58). These findings are consistent with the results of our analysis, but experimental verification of *ADIPOQ* and *SPP1* is lacking in the present study.

We constructed mRNA-miRNA and mRNA-TF networks of hub genes and found that *COL1A1* and *COL1A2* interacted with 14 miRNAs, respectively, while *MMP9* and *Fos* interacted with 33 and 32 TFs, respectively. During rat tissue's PCR validation, the expression of *Fos* was increased in synovium but decreased in cartilage from the OA group compared to the control group. *C-fos* could form a heterodimeric *AP-1* complex with *C-Jun* (59). Previous studies have shown that *C-fos* could promote osteoclast fusion and accelerate osteoclastogenesis *via* the *ERK/C-Fos/NFATc1* pathway (60), and *C-Fos/AP-1* could also drive synovial mesenchymal stem cells to generate pannus, invade the cartilage and bone, and release interleukin-1β (61), which eventually activates downstream matrix metalloproteinase and induces cartilage destruction *via C-Fos/AP-1* (62). Therefore, the synovium of our OA rats might be activated by *C-Fos*, while the cartilage might be in the compensatory stage of repair after injury. The conclusion needs to be further verified.

Finally, we used ssGSEA and CIBERSORTx algorithms to compare the immune status between the two subtypes. The results showed that there were differences in the concentrations of immune cells, the correlation between characteristic genes and immune cells, the correlation between hub genes and immune cells, and the correlation between the content of immune cells between cluster 1 and cluster 2 patients. What is more? The results of ROC curve analysis and AUC scores showed that *TNFSF11*, *VCAM1*, *CCL3*, *CLU*, *FABP4*, and *THBS2* could effectively distinguish the two subtypes of OA. This analysis helps to further the understanding of the immune status contrast between OA and control samples and between the two subtypes of OA.

However, there were limitations in this study; for example, *in vivo* verification experiments were only performed on synovium and cartilage tissues of MIA-intervened OA rats, without the use of different modeling methods or other species. In addition, only qRT-PCR was used to verify the bioinformatics analysis results, and no other experiments, such as western blotting, immunofluorescence, or immunohistochemistry, were used to validate at the cell or tissues level, so the validation results are limited, while further validation of 10 key genes could also provide more information for our research on OA, which is also the shortcoming of the study.

In summary, the present study screened several genes and pathways closely related to synovitis and cartilage degradation in OA through bioinformatics analysis. Notable genes include *CX3CR1*, *GADD45B*, *PTGS1*, *EFEMP2*, *PGF*, *MFAP4*, *CLU*, *CDH11*, *VEGFC*, *ANPEP*, *MMP9*, *COL1A*, *Fos*, *IGF1*, *ADIPOQ*, and *SPP1*. Key pathways include the *IL-17* signaling pathway, TNF signaling pathway, and *p53* pathway. The expression levels of *MMP9*, *COL1A*, *Fos*, *IGF1*, and *IL-17* pathway-related proteins *IL-17A*, *ERK1*, *JAK2*, *JNK*, *MAPK1*, and *STAT3* were confirmed by RT-PCR in rats' tissues, with *IL-17A* highly expressed in both synovium and cartilage of KOA rats and with lower expressions of MMP9 in both tissues; the former two findings are consistent with the prediction, while the latter finding is the exact opposite. These results suggest that chondrocyte repair or synovial fibrosis might exist in OA rats, and the *IL-17* pathway might also be activated in OA rats. The *IL-17A*, *COL1A*, and *MMP9* screening performed in this study might yield therapeutic targets for synovitis and cartilage apoptosis in OA.

Data availability statement

The datasets presented in this study can be found in online repositories. The names of the repository/repositories and accession number(s) can be found in the article/Supplementary Material.

Ethics statement

The animal study was reviewed and approved by Xin Hua Hospital, which is affiliated with Shanghai Jiao Tong University School of Medicine (Approval No. XHEC-F-2022-014).

Author contributions

LY: Experimental operation, Data management and analysis; XY: Experimental operation, Writing manuscript, Writing-review and editing; ML: Supervision, Writing-review; YC: Conceptualization, methodology, supervision, Writing-review and editing. All authors contributed to the article and approved the submitted version.

Funding

This study has been supported by Changzhou Sci & Tech Program (Grant No. CJ20210075), Young Talent Development Plan of Changzhou Health Commission (CZQM2020023), Top Talent of Changzhou The 14th Five-Year Plan High-Level Health Talents Training Project (No. 2022260).

Conflict of interest

The authors declare that the research was conducted in the absence of any commercial or financial relationships that could be construed as a potential conflict of interest.

Publisher's note

All claims expressed in this article are solely those of the authors and do not necessarily represent those of their affiliated organizations, or those of the publisher, the editors and the reviewers. Any product that may be evaluated in this article, or claim that may be made by its manufacturer, is not guaranteed or endorsed by the publisher.

Supplementary material

The Supplementary Material for this article can be found online at: https://www.frontiersin.org/articles/10.3389/fimmu.2023.1149686/full#supplementary-material

References

1. Schell J, Scofield RH, Barrett JR, Kurien BT, Betts N, Lyons TJ. Strawberries improve pain and inflammation in obese adults with radiographic evidence of knee osteoarthritis. *Nutrients.* (2017) 9(9):949. doi: 10.3390/nu9090949

2. S, Lee K, Ju JH. Recent updates of diagnosis, pathophysiology, and treatment on osteoarthritis of the knee. *Int J Mol Sci* (2021) 22(5):2619. doi: 10.3390/ijms22052619

3. Katz JN, Arant KR, Loeser RF. Diagnosis and treatment of hip and knee osteoarthritis: a review. *JAMA* (2021) 325(6):568–78. doi: 10.1001/jama.2020.22171

4. Hu Y, Gui Z, Zhou Y, Xia L, Lin K, Xu Y. Quercetin alleviates rat osteoarthritis by inhibiting inflammation and apoptosis of chondrocytes, modulating synovial macrophages polarization to M2 macrophages. *Free Radic Biol Med* (2019) 145:146–60. doi: 10.1016/j.freeradbiomed.2019.09.024

5. Hu X, Ni S, Zhao K, Qian J, Duan Y. Bioinformatics-led discovery of osteoarthritis biomarkers and inflammatory infiltrates. *Front Immunol* (2022) 13:871008. doi: 10.3389/fimmu.2022.871008

6. Feng K, Chen Z, Pengcheng L, Zhang S, Wang X. Quercetin attenuates oxidative stress-induced apoptosis *via* SIRT1/AMPK-mediated inhibition of ER stress in rat chondrocytes and prevents the progression of osteoarthritis in a rat model. *J Cell Physiol* (2019) 234(10):18192–205. doi: 10.1002/jcp.28452

7. Lv Z, Xu X, Sun Z, Yang YX, Guo H, Li J, et al. TRPV1 alleviates osteoarthritis by inhibiting M1 macrophage polarization *via* Ca2+/CaMKII/Nrf2 signaling pathway. *Cell Death Dis* (2021) 12(6):504. doi: 10.1038/s41419-021-03792-8

8. Elsadek BEM, Abdelghany AA, Abd El-Aziz MA, Madkor HR, Abd Elrady Ahmed A, Abd-Elghaffar SK. Validation of the diagnostic and prognostic values of ADAMTS5 and FSTL1 in osteoarthritis rat model. *Cartilage* (2021) 13 (2_suppl):1263S–73S. doi: 10.1177/1947603519852405

9. Lin Z, Miao J, Zhang T, He M, Wang Z, Feng X. JUNB-FBXO21-ERK axis promotes cartilage degeneration in osteoarthritis by inhibiting autophagy. *Aging Cell* (2021) 20(2):e13306. doi: 10.1111/acel.13306

10. Zheng L, Chen W, Xian G, Pan B, Ye Y, Gu M. Identification of abnormally methylated-differentially expressed genes and pathways in osteoarthritis: a comprehensive bioinformatic study. *Clin Rheumatol* (2021) 40(8):3247–56. doi: 10.1007/s10067-020-05539-w

11. Woetzel D, Huber R, Kupfer P, Pohlers D, Pfaff M, Driesch D, et al. Identification of rheumatoid arthritis and osteoarthritis patients by transcriptome-based rule set generation. *Arthritis Res Ther* (2014) 16(2):R84. doi: 10.1186/ar4526

12. Huber R, Hummert C, Gausmann U, Pohlers D, Koczan D, Guthke R, et al. Identification of intra-group, inter-individual, and gene-specific variances in mRNA expression profiles in the rheumatoid arthritis synovial membrane. *Arthritis Res Ther* (2008) 10(4):R98. doi: 10.1186/ar2485

13. Broeren MG, de Vries M, Bennink MB, van Lent PL, van der Kraan PM, Koenders MI, et al. Functional tissue analysis reveals successful cryopreservation of human osteoarthritic synovium. *PLoS One* (2016) 11(11):e0167076. doi: 10.1371/journal.pone.0167076

14. Leek JT, Johnson WE, Parker HS, Jaffe AE, Storey JD, et al. The sva package for removing batch effects and other unwanted variation in high-throughput experiments. *Bioinformatics* (2012) 28(6):882–3. doi: 10.1093/bioinformatics/bts034

15. Stelzer G, Rosen N, Plaschkes I, Zimmerman S, Twik M, Fishilevich S, et al. The GeneCards suite: from gene data mining to disease genome sequence analyses. *Curr Protoc Bioinf* (2016) 54:1 30 1–1 30. doi: 10.1002/cpbi.5

16. Ritchie ME, Phipson B, Wu D, Hu Y, Law CW, Shi W, et al. Limma powers differential expression analyses for RNA-sequencing and microarray studies. *Nucleic Acids Res* (2015) 43(7):e47. doi: 10.1093/nar/gkv007

17. Milosevic D, Medeiros AS, Stojković Piperac M, Cvijanović D, Soininen J, Milosavljević A, et al. The application of uniform manifold approximation and projection (UMAP) for unconstrained ordination and classification of biological indicators in aquatic ecology. *Sci Total Environ* (2022) 815:152365. doi: 10.1016/j.scitotenv.2021.152365

18. Ashburner M, Ball CA, Blake JA, Botstein D, Butler H, Cherry JM, et al. Gene ontology: tool for the unification of biology. the gene ontology consortium. *Nat Genet* (2000) 25(1):25–9. doi: 10.1038/75556

19. Kanehisa M, Goto S. KEGG: kyoto encyclopedia of genes and genomes. *Nucleic Acids Res* (2000) 28(1):27–30. doi: 10.1093/nar/28.1.27

20. Yu G, Wang LG, Han Y, He QY, et al. clusterProfiler: an r package for comparing biological themes among gene clusters. *OMICS* (2012) 16(5):284–7. doi: 10.1089/omi.2011.0118

21. Wu T, Hu E, Xu S, Chen M, Guo P, Dai Z, et al. clusterProfiler 4.0: a universal enrichment tool for interpreting omics data. *Innovation (N Y)* (2021) 2(3):100141. doi: 10.1016/j.xinn.2021.100141

22. Subramanian A, Tamayo P, Mootha VK, Mukherjee S, Ebert BL, Gillette MA, et al. Gene set enrichment analysis: a knowledge-based approach for interpreting genome-wide expression profiles. *Proc Natl Acad Sci U S A* (2005) 102(43):15545–50. doi: 10.1073/pnas.0506580102

23. Liberzon A, Birger C, Thorvaldsdóttir H, Ghandi M, Mesirov JP, Tamayo P. The molecular signatures database (MSigDB) hallmark gene set collection. *Cell Syst* (2015) 1 (6):417–25. doi: 10.1016/j.cels.2015.12.004

24. Hanzelmann S, Castelo R, Guinney J. GSVA: gene set variation analysis for microarray and RNA-seq data. *BMC Bioinf* (2013) 14:7. doi: 10.1186/1471-2105-14-7

25. von Mering C, Huynen M, Jaeggi D, Schmidt S, Bork P, Snel B, et al. STRING: a database of predicted functional associations between proteins. *Nucleic Acids Res* (2003) 31(1):258–61. doi: 10.1093/nar/gkg034

26. Shannon P, Markiel A, Ozier O, Baliga NS, Wang JT, Ramage D, et al. Cytoscape: a software environment for integrated models of biomolecular interaction networks. (2003) 13(11):2498–504. doi: 10.1101/gr.1239303

27. Chin C-H, Chen SH, Wu HH, Ho CW, Ko MT, Lin CY. cytoHubba: identifying hub objects and sub-networks from complex interactome. *BMC Syst Biol* (2014) 8(4):1–7. doi: 10.1186/1752-0509-8-S4-S11

28. Lu TX, Rothenberg ME. MicroRNA. *J Allergy Clin Immunol* (2018) 141 (4):1202–7. doi: 10.1016/j.jaci.2017.08.034

29. Barbie DA, Tamayo P, Boehm JS, Kim SY, Moody SE, Dunn IF, et al. Systematic RNA interference reveals that oncogenic KRAS-driven cancers require TBK1. *Nature* (2009) 462(7269):108–12. doi: 10.1038/nature08460

30. Newman AM, Steen CB, Liu CL, Gentles AJ, Chaudhuri AA, Scherer F, et al. Determining cell type abundance and expression from bulk tissues with digital cytometry. *Nat Biotechnol* (2019) 37(7):773–82. doi: 10.1038/s41587-019-0114-2

31. Wei T, Huang G, Gao M, Huang J, Li H, Xia H, et al. Package 'corrplot'. *Statistician* (2017) 56(316):e24. doi: 10.1155/2022/8307975

32. Yoshihara K, Shahmoradgoli M, Martínez E, Vegesna R, Kim H, Torres-Garcia W, et al. Inferring tumour purity and stromal and immune cell admixture from expression data. *Nat Commun* (2013) 4:2612. doi: 10.1038/ncomms3612

33. Robin X, Turck N, Hainard A, Tiberti N, Lisacek F, Sanchez JC, et al. pROC: an open-source package for r and s+ to analyze and compare ROC curves. *BMC Bioinf* (2011) 12:77. doi: 10.1186/1471-2105-12-77

34. Zhang H, Meltzer P, Davis S. RCircos: an r package for circos 2D track plots. *BMC Bioinf* (2013) 14:244. doi: 10.1186/1471-2105-14-244

35. Vickers AJ, Elkin EB. Decision curve analysis: a novel method for evaluating prediction models. *Med Decis Making* (2006) 26(6):565–74. doi: 10.1177/0272989X06295361

36. Yu G. Gene ontology semantic similarity analysis using GOSemSim. *Methods Mol Biol* (2020) 2117:207–15. doi: 10.1007/978-1-0716-0301-7_11

37. Mandl LA. Osteoarthritis year in review 2018: clinical. *Osteoarthritis Cartilage* (2019) 27(3):359–64. doi: 10.1016/j.joca.2018.11.001

38. Fujii Y, Liu L, Yagasaki L, Inotsume M, Chiba T, Asahara H. Cartilage homeostasis and osteoarthritis. *Int J Mol Sci* (2022) 23(11):6316. doi: 10.3390/ijms23116316

39. Sanchez-Lopez E, Coras R, Torres A, Lane NE, Guma M. Synovial inflammation in osteoarthritis progression. *Nat Rev Rheumatol* (2022) 18(5):258–75. doi: 10.1038/s41584-022-00749-9

40. Ayturk UM, Sieker JT, Haslauer CM, Proffen BL, Weissenberger MH, Warman ML. Proteolysis and cartilage development are activated in the synovium after surgical induction of post traumatic osteoarthritis. *PLoS One* (2020) 15(2):e0229449. doi: 10.1371/journal.pone.0229449

41. Sellam J, Berenbaum F. The role of synovitis in pathophysiology and clinical symptoms of osteoarthritis. *Nat Rev Rheumatol* (2010) 6(11):625–35. doi: 10.1038/nrrheum.2010.159

42. Yang S, Wang J, Brand DD, Zheng SG. Role of TNF-TNF receptor 2 signal in regulatory T cells and its therapeutic implications. *Front Immunol* (2018) 9:784. doi: 10.3389/fimmu.2018.00784

43. Wang T, He C. Pro-inflammatory cytokines: the link between obesity and osteoarthritis. *Cytokine Growth Factor Rev* (2018) 44:38–50. doi: 10.1016/j.cytogfr.2018.10.002

44. Faust HJ, Zhang H, Han J, Wolf MT, Jeon OH, Sadtler K. IL-17 and immunologically induced senescence regulate response to injury in osteoarthritis. *J Clin Invest* (2020) 130(10):5493–507. doi: 10.1172/JCI134091

45. Cai W, Li H, Zhang Y, Han G. Identification of key biomarkers and immune infiltration in the synovial tissue of osteoarthritis by bioinformatics analysis. *PeerJ* (2020) 8:e8390. doi: 10.7717/peerj.8390

46. Jimi E, Fei H, Nakatomi C. NF-κB signaling regulates physiological and pathological chondrogenesis. *Int J Mol Sci* (2019) 20(24):6275. doi: 10.3390/ijms20246275

47. Geiger BC, Wang S, Padera RFJr, Grodzinsky AJ, Hammond PT. Cartilage-penetrating nanocarriers improve delivery and efficacy of growth factor treatment of osteoarthritis. *Sci Transl Med* (2018) 10(469):eaat8800. doi: 10.1126/scitranslmed.aat8800

48. Hossain MA, Adithan A, Alam MJ, Kopalli SR, Kim B, Kang CW. IGF-1 facilitates cartilage reconstruction by regulating PI3K/AKT, MAPK, and NF-kB signaling in rabbit osteoarthritis. *J Inflammation Res* (2021) 14:3555–68. doi: 10.2147/JIR.S316756

49. Li S, Wang H, Zhang Y, Qiao R, Xia P, Kong Z. COL3A1 and MMP9 serve as potential diagnostic biomarkers of osteoarthritis and are associated with immune cell infiltration. *Front Genet* (2021) 12:721258. doi: 10.3389/fgene.2021.721258

50. Luo S, Li W, Wu W, Shi Q. Elevated expression of MMP8 and MMP9 contributes to diabetic osteoarthritis progression in a rat model. *J Orthop Surg Res* (2021) 16(1):64. doi: 10.1186/s13018-021-02208-9

51. Ostojic M, Zevrnja A, Vukojevic K, Soljic V. Immunofluorescence analysis of NF-kB and iNOS expression in different cell populations during early and advanced knee osteoarthritis. *Int J Mol Sci* (2021) 22(12):6461. doi: 10.3390/ijms22126461

52. Maurotti S, Mare R, Pujia R, Ferro Y, Mazza E, Romeo S. Hemp seeds in post-arthroplasty rehabilitation: a pilot clinical study and an *In vitro* investigation. *Nutrients.* (2021) 13(12):4330. doi: 10.3390/nu13124330

53. Gerdhem P, Brändström H, Stiger F, Obrant K, Melhus H, Ljunggren O. Association of the collagen type 1 (COL1A 1) Sp1 binding site polymorphism to femoral neck bone mineral density and wrist fracture in 1044 elderly Swedish women. *Calcif Tissue Int* (2004) 74(3):264–9. doi: 10.1007/s00223-002-2159-2

54. Ma K, Zhu B, Wang Z, Cai P, He M, Ye D. Articular chondrocyte-derived extracellular vesicles promote cartilage differentiation of human umbilical cord mesenchymal stem cells by activation of autophagy. *J Nanobiotechnology* (2020) 18 (1):163. doi: 10.1186/s12951-020-00708-0

55. Smitka K, Marešová D. Adipose tissue as an endocrine organ: an update on pro-inflammatory and anti-inflammatory microenvironment. *Prague Med Rep* (2015) 116:87–111. doi: 10.14712/23362936.2015.49

56. Jiang L, Zhu X, Rong J, Xing B, Wang S, Liu A. Obesity, osteoarthritis and genetic risk: the rs182052 polymorphism in the ADIPOQ gene is potentially associated with risk of knee osteoarthritis. *Bone Joint Res* (2018) 7(7):494–500. doi: 10.1302/2046-3758.77.BJR-2017-0274.R1

57. Frank JW, Seo H, Burghardt RC, Bayless KJ, Johnson GA. ITGAV (alpha v integrins) bind SPP1 (osteopontin) to support trophoblast cell adhesion. *Reproduction* (2017) 153(5):695–706. doi: 10.1530/REP-17-0043

58. Lin Z, Tian XY, Huang XX, He LL, Xu F. microRNA-186 inhibition of PI3K-AKT pathway *via* SPP1 inhibits chondrocyte apoptosis in mice with osteoarthritis. *J Cell Physiol* (2019) 234(5):6042–53. doi: 10.1002/jcp.27225

59. Fujii T, Murata K, Mun SH, Bae S, Lee YJ, Pannellini T. MEF2C regulates osteoclastogenesis and pathologic bone resorption *via* c-FOS. *Bone Res* (2021) 9(1):4. doi: 10.1038/s41413-020-00120-2

60. Fang C, Guo JW, Wang YJ, Li XQ, Zhang H, Cui J. Diterbutyl phthalate attenuates osteoarthritis in ACLT mice *via* suppressing ERK/c-fos/NFATc1 pathway, and subsequently inhibiting subchondral osteoclast fusion. *Acta Pharmacol Sin* (2022) 43(5):1299–310. doi: 10.1038/s41401-021-00747-9

61. Shiozawa S, Tsumiyama K, Yoshida K, Hashiramoto A. Pathogenesis of joint destruction in rheumatoid arthritis. *Arch Immunol Ther Exp (Warsz)* (2011) 59(2):89–95. doi: 10.1007/s00005-011-0116-3

62. Motomura H, Seki S, Shiozawa S, Aikawa Y, Nogami M, Kimura T. A selective c-Fos/AP-1 inhibitor prevents cartilage destruction and subsequent osteophyte formation. *Biochem Biophys Res Commun* (2018) 497(2):756–61. doi: 10.1016/j.bbrc.2018.02.147

frontiers | Frontiers in Immunology

TYPE Original Research
PUBLISHED 16 August 2023
DOI 10.3389/fimmu.2023.1247355

Check for updates

OPEN ACCESS

EDITED BY
Lei Zhang,
The First Affiliated Hospital of Shandong First Medical University, China

REVIEWED BY
Bettina Grötsch,
University of Erlangen Nuremberg, Germany
Weiwei Li,
Shandong University, China

*CORRESPONDENCE
Tengbo Yu
ytb1970@163.com
Tianrui Wang
wangtr@qdu.edu.cn

†These authors have contributed equally to this work and share first authorship

RECEIVED 26 June 2023
ACCEPTED 31 July 2023
PUBLISHED 16 August 2023

CITATION
Yan M, Sun Z, Wang J, Zhao H, Yu T, Zhang Y and Wang T (2023) Single-cell RNA sequencing reveals distinct chondrocyte states in femoral cartilage under weight-bearing load in Rheumatoid arthritis.
Front. Immunol. 14:1247355.
doi: 10.3389/fimmu.2023.1247355

COPYRIGHT
© 2023 Yan, Sun, Wang, Zhao, Yu, Zhang and Wang. This is an open-access article distributed under the terms of the Creative Commons Attribution License (CC BY). The use, distribution or reproduction in other forums is permitted, provided the original author(s) and the copyright owner(s) are credited and that the original publication in this journal is cited, in accordance with accepted academic practice. No use, distribution or reproduction is permitted which does not comply with these terms.

Single-cell RNA sequencing reveals distinct chondrocyte states in femoral cartilage under weight-bearing load in Rheumatoid arthritis

Mingyue Yan[1,2†], Zewen Sun[1,2†], Junjie Wang[1,2], Haibo Zhao[1,2], Tengbo Yu[2,3*†], Yingze Zhang[4] and Tianrui Wang[1*†]

[1]Department of Orthopedics, The Affiliated Hospital of Qingdao University, Qingdao, Shandong, China, [2]Institute of Sports Medicine and Health, Qingdao University, Qingdao, Shandong, China, [3]Department of Orthopedic Surgery, Qingdao Hospital, University of Health and Rehabilitation Sciences (Qingdao Municipal Hospital), Qingdao, Shandong, China, [4]Department of Orthopedics, The Third Hospital of Hebei Medical University, Shijiazhuang, Hebei, China

Introduction: Rheumatoid arthritis (RA) is a common autoimmune joint disease, the pathogenesis of which is still unclear. Cartilage damage is one of the main manifestations of the disease. Chondrocytes are the main functional component of articular cartilage, which is relevant to disease progression. Mechanical loading affects the structure and function of articular cartilage and chondrocytes, but the effect of weight bearing on chondrocytes in rheumatoid arthritis is still unclear.

Methods: In this paper, single-cell RNA sequencing (scRNA-seq) was performed on collected cartilage from the weight-bearing region (Fb group) and non-weight-bearing region (Fnb group) of the femur, and the differences between the Fb and Fnb groups were analyzed by cell type annotation, pseudotime analysis, enrichment analysis, cell interactions, single-cell regulatory network inference and clustering (SCENIC) for each cell type.

Results: A total of 87,542 cells were analyzed and divided into 9 clusters. Six chondrocyte subpopulations were finally identified by cellular annotation, and two new chondrocyte subtypes were annotated as immune-associated chondrocytes. The presence of each chondrocyte subpopulation and its distribution were verified using immunohistochemical staining (IHC). In this study, the atlas of femoral cartilage in knee rheumatoid arthritis and 2 new immune-related chondrocytes were validated using scRNA-seq and IHC, and chondrocytes in the weight-bearing and non-weight-bearing regions of the femur were compared. There might be a process of macrophage polarization transition in MCs in response to mechanical loading, as in macrophages.

Conclusion: Two new immune-associated chondrocytes were identified. MCs have contrasting functions in different regions, which might provide insight into the role of immune and mechanical loading on chondrocytes in the development of knee rheumatoid osteoarthritis.

KEYWORDS

Rheumatoid arthritis, chondrocyte, single-cell RNA sequencing, weight-bearing region, immune

1 Background

Rheumatoid arthritis (RA) is a common chronic progressive autoimmune joint disease, the onset and progression of which are closely related to immune cells, synoviocytes, and osteoclasts (1), and the pathogenesis has not been fully investigated. Knee rheumatoid arthritis is characterized by knee pain and limited mobility, with the main pathological features including synovitis, progressive bone erosion, and cartilage damage (2). It has been shown that chondrocyte proliferation, apoptosis, and autophagy are associated with the progression of RA disease (3), suggesting that a deeper understanding of cartilage would facilitate a better exploration of the pathogenesis of RA.

Articular cartilage is an important connective tissue on the joint surface, with a smooth and elastic surface that reduces joint friction and motion shock. Cartilage tissue is mainly composed of chondrocytes and secreted extracellular matrix, but abnormal mechanical loading can affect the metabolic balance of chondrocytes and have an impact on the catabolism of the cartilage extracellular matrix (4). It has also been demonstrated that mechanical overload not only affects chondrocyte proliferation but also induces chondrocyte apoptosis (5, 6). At the same time, stress stimulation from joint motion is one of the important external factors regulating cartilage growth and development, and lack of stress stimulation increases chondrocyte IL-4 or IL-10 levels, which in turn exacerbates cartilage breakdown (7). In this study, cartilage damage was found to be more severe in the weight-bearing region of the femur during knee replacement surgery in RA patients, and it was hypothesized that assessment of chondrocytes in both weight-bearing and non-weight-bearing regions might provide further insight into the function of chondrocytes and facilitate an in-depth exploration of the pathogenesis of RA.

Single-cell RNA sequencing (scRNA-seq) enables the analysis of cells in tissues at single-cell resolution, filling the gap of high-throughput transcriptome technologies that cannot be sequenced precisely to cell type. This technique has been widely used in autoimmune diseases to reveal cellular heterogeneity and identify pathogenic cell subpopulations in a wide range of immune inflammation-related tissues (8). A study found that the proportion of helper T cells and activated T cells in the synovium of rheumatoid arthritis is higher than that of osteoarthritis(OA) (9). Up to now, single-cell studies in RA have mostly focused on tissues such as peripheral blood and synovium (10, 11), and relatively few studies have been conducted on chondrocytes. Tang et al. performed the first single-cell sequencing of chondrocytes in OA and identified subpopulations of chondrocytes such as fibrocartilage chondrocyte (FC), effector chondrocyte (EC), homeostatic chondrocyte (HomC), regulatory chondrocyte (RegC) and cartilage progenitor cells (CPC) (12). Our team's previous single-cell study of healthy cartilage in the ankle joint also identified two new subpopulations of chondrocytes, which were named metal ion related chondrocytes (MirCs) and splicing chondrocytes (SpCs) (13).

Mehmet et al. proposed that analysis of differential genes between damaged and undamaged cartilage could help determine the exact cause of focal cartilage damage (14). Therefore, in this study, cartilage from the weight-bearing and non-weight-bearing regions of the femur of RA patients was taken separately and sequenced with scRNA-seq to explore the function of chondrocyte subpopulations as well as to complement and validate the previously identified chondrocyte subtypes. This study hopefully provides insight into the effects of mechanical loading and immunological factors on chondrocytes and offers a reference for further exploration of the pathogenesis and genetic markers of RA.

2 Methods

2.1 Volunteers screening and samples selection

The flow chart of the study is shown in Figure 1A. In this study, the volunteers were taken from patients who had no history of knee trauma and were diagnosed with RA, with proposed knee replacement in our hospital. We took cartilage from the weight-bearing and non-weight-bearing regions of the joint on the discarded femur from the knee replacement surgery. The locations of the obtained cartilage samples are shown as red circles in Figure 1A (2), with region A being the weight-bearing region and region B being the non-weight-bearing region. We cumulatively obtained a total of 7 groups of surface cartilage from the weight-bearing region of the femur (called the Fb group) and the non-weight-bearing region (called the Fnb group) from 7 patients, and performed scRNA-seq on 4 groups (8 samples) and immunohistochemical staining (IHC) analysis on 3 groups (6 samples). The study was approved by the Institutional Ethics Review Committee of the Affiliated Hospital of Qingdao University(QYFY WZLL 27403), and all donor patients signed a written informed consent.

2.2 Cartilage zoning, segmentation, and single-cell suspension preparation

All cartilage tissue was isolated within 3 hours of the knee replacement osteotomy, and two experienced clinicians evaluated the cartilage and positioned the weight-bearing and non-weight-bearing regions. The surgically discarded bone tissue was then placed in sterile saline and transferred to an ultra-clean table to segment the cartilage tissue, ensuring that the excised cartilage tissue did not retain any subchondral bone. The cartilage tissue was then transferred to sterile Petri dishes placed on ice in phosphate-buffered saline (PBS). Each tissue sample was approximately 0.25 × 1 × 2 cm in size and weighed approximately 0.5 ~ 0.6 g. The cartilage samples were cut into 0.5 mm^3 and rinsed twice with PBS. The digestion solution (0.2% collagenase II and 0.25% EDTA-trypsin) was preheated in a water bath at 37°C, into which the tissue blocks were shaken at 100 rpm for 20 min at 37°C to obtain a single cell suspension. Afterward, PBS containing 10% fetal bovine serum was added to stop the digestion. The obtained cell suspension was filtered through a 70 μm cell strainer and centrifuged at 300 × g

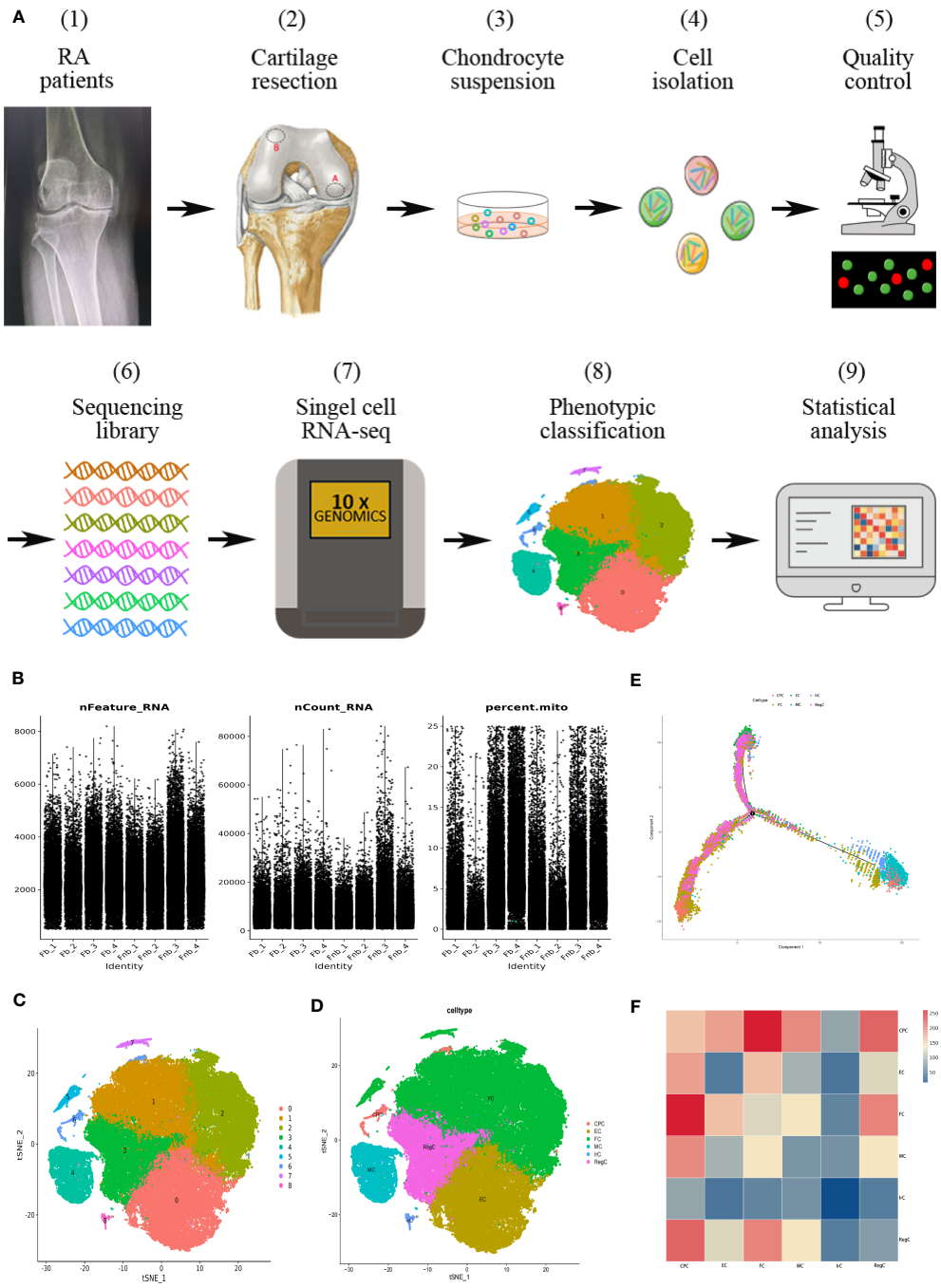

FIGURE 1
Single-cell RNA-seq of human RA cartilage chondrocytes. **(A)** Schematic workflow of the experimental strategy. The circles represented the location of the cartilage samples taken, with region A being the weight-bearing region and region B being the non-weight-bearing region. **(B)** Quality control conditions. **(C)** Clustering results. **(D)** Cell type annotation results. **(E)** Pseudotime analysis of each cell type using the Moncle function. Trajectory analysis was performed for the entire development line, and the color of each point represented the order of cell growth and differentiation. **(F)** The interaction strength of intercellular communication between cell types. The color of the rectangle represented the probability of the role. CPC, cartilage progenitor cells; EC, effector chondrocyte; FC, fibrocartilage chondrocyte; IrC, inflammatory related chondrocyte; MC, macrophage chondrocyte; RegC, regulatory chondrocyte; RA, rheumatoid arthritis; t-SNE, t-distributed stochastic neighbor embedding.

for 5 min at 4°C. Dead cells were removed using the Miltenyi® kit (MACS 130-090-101). Finally, the cell suspension was resuspended by centrifugation at 300 × g for 3 min at 4°C 2 times. The overall cell viability was confirmed over 85% using Tissue Blue and the cells in the single-cell suspension were counted by an automated cell counter at a density of 700 - 1200 cells/μl.

2.3 10× Genomics scRNA-seq library preparation and cell clustering

The prepared single-cell suspensions were added to 10x chromium, and the single cells were extracted and amplified according to the instructions of the 10X Genomics Chromium

Single-Cell 3 kit (V3). The cDNA library was constructed following standard procedures. The library was sequenced on an Illumina NovaSeq 6000 sequencing system with a minimum of 20,000 reads per cell by LC-Bio Technology Co.Ltd (Hangzhou, China).

Sequencing files were converted to a FASTQ format by Illumina bcl2fastq software (version 2.20), and the sample data were processed and counted using the Cell Ranger pipeline (version 4.0.3). The scRNA-seq data were decoded using the Ensembl GRCh38/GRCm38 reference genome, and the output data were then loaded into the SeuratR package (version 3.1.1) for normalization, reduction, and clustering. Genes expressed in less than 3 cells were not incorporated into the analysis. In this program, the number of genes expressed in a single cell should be more than 500, and the proportion of genes of mitochondrial DNA origin should be less than 25%. Since the presence of ribosomal genes affects the results of cell clustering, we used the Rsubread, edgeR, and scater packages to remove the sequences of ribosomal genes. The samples were integrated using the RunHarmony in Seurat. Perform dimensionality reduction and visualization analysis of the data using the RunTSNE in Seurat. The FindMarkers in Seurat was used to identify marker genes expressed in more than 10% of cells in each cluster and to screen for differentially expressed genes (DEGs) between the Fb and Fnb groups. Use the featureplot to visualize the expression levels of marker genes in the t-SNE plot. The ggplot2 R package was used to visualize the results of the DEG analysis.

2.4 Gene ontology and Kyoto encyclopedia of genes and genomes pathway enrichment analyses

GO enrichment analysis is a commonly used bioinformatics tool to determine whether a set of genes is enriched in a biological process or function, which is used to annotate genes and analyze their biological processes. The KEGG analysis based on the KEGG database is commonly used for functional annotation and enrichment analysis of genes and metabolic pathways, which helps to understand the interactions between biomolecules and metabolic pathways. We performed GO and KEGG enrichment analysis using Metascape (http://metascape.org/gp/#/main/step1) to gain insight into the biological function of each cluster, with a P value < 0.05 indicating significant results.

2.5 Identification of different cell types

DEGs with high log2FC values and high specificity were selected as marker genes for each cluster. The marker genes were normalized for each cell type using the pheatmap package, after which they were clustered and heatmaps were drawn. The analyzed marker genes were compared with the list of already validated marker genes to identify the cell types (12, 13). The results of GO and KEGG pathway enrichment analysis were also taken into account when annotating cell types. The results of the enrichment analysis were visualized using the ggplot2 package.

2.6 Protein-protein interaction network construction and hub gene identification

Search Tool for the Retrieval of Interacting Genes (STRING; http://string-db.org)(version 11.5) is an online tool for analyzing gene coding protein interactions. Cytoscape (version 3.9.1) is an open-source network analysis software that can be used for biological network analysis and visualization of the results. We used STRING to construct a PPI network of DEGs between the Fb and Fnb groups. The information obtained from STRING was imported into Cytoscape, and the top 10 hub genes were identified by cytoHubba.

2.7 Pseudotime analysis

Seurat objects with annotations were converted to readable cds objects. Cells were aligned along the simulated cell developmental trajectory, and the orderCells function was used to show cells' presumed position in the Monocle. Different colors represented different cell subpopulations.

2.8 Cell-cell interactions

We use the CellChat R package to analyze cellular interaction networks and to calculate probability values for cell-cell interactions by combining single-cell expression profiles with known ligands and receptors. Seurat objects with annotations need to be converted to CellChat objects. Over-expressed ligands or receptors in one cell type were identified using the IdentifyOverExpressedGenes function. Then, gene-expression data are projected into the protein interaction network using the projectData function in CellChat. Use the function of IdentifyExpressedInteractionCellChat to screen for ligand-receptor interactions when either the ligand or its receptor was overexpressed.

2.9 Single-cell regulatory network inference and clustering

SCENIC is a single-cell RNA sequencing analysis tool for resolving transcriptome data from individual cells to characterize transcription factor activity in individual cells. Seurat objects with annotations were imported to run Scenic (version 0.9.1). Use GENIE3 to extrapolate gene regulatory networks from gene expression data. The TF targeting relationship with the gene was verified with the help of RcisTarget software. Then, cells with active gene regulatory networks were identified using AUCell software, and regulons were scored for their Area Under Curve (AUC) by binarizing specific regulons. The RSS score of the TF was obtained by the calcRSS and ranked by value to determine the Top TF for each cell type. The differentially expressed transcription factors were visualized using the pheatmap function.

2.10 Statistical analysis

The Wilcoxon rank sum test and independent samples t-test were selected for data analysis of the number of different cell subpopulations between groups according to the characteristics of the data format. R packages stats and car were used to compare the differences in cell numbers between the Fb and Fnb groups, and the data were visualized with the ggplot2 package. P values < 0.05 were considered statistically significant.

2.11 IHC

Immunohistochemical staining(IHC) was performed as follows. Distal femoral cartilage tissue was trimmed and then incubated in 4% buffered paraformaldehyde fixative for 48h. The tissues were then incubated in EDTA for 3 months for decalcification, and the decalcification effect was detected using a needle. Afterward, the tissues were embedded in paraffin, and the paraffin samples were dewaxed and rehydrated with xylene and ethanol. Subsequently, samples were incubated in 3% hydrogen peroxide for 10 minutes to block endogenous peroxidase activity. Antigen repair was performed by treatment with 3% bovine serum albumin at room temperature for 30 min and digestion with pepsin. Later, the samples were incubated with primary antibodies (specific names of these primary antibodies are mentioned in the results section) for 12 h at 4°C, followed by secondary antibody administration for 50 min at room temperature. Finally, the samples were counterstained with DAB and hematoxylin nuclei for about 3 min. The stained sections were visualized and imaged with a vertical microscope (Nikon Eclipse Ci) and an imaging system (Nikon Digital Sight DS-FI2) with white light. IHC staining of cartilage sections was scored blindly by experienced pathologists using a light microscope. The widely accepted German semi-quantitative scoring system was used, taking into account the range of staining strength and staining area. Staining intensity: 0, no coloring; 1, light yellow; 2, brown-yellow; 3, brown-brown. Stained area: 0, <5%; 1, 5%-25%; 2, 25%-50%; 3, 51%-75%; 4, >75%. These two scores were multiplied together as the final score. Comparative analysis of IHC staining scores for each layer of cartilage tissue was performed using the Kruskal-Wallis test for within-group differences and the Wilcoxon rank sum test for between-group differences. R package ggplot2 was used for data visualization.

3 Results

3.1 Single-cell profiling of human RA cartilage chondrocytes

Ultimately, 87,542 cells were analyzed and divided into cluster0-8. The basic quality control conditions were as shown in Figure 1B. Figure 1C displayed the clustering results and summary results of the cell type annotation. 9 cell clusters were combined and annotated into 6 chondrocyte subpopulations, including CPC, EC, FC, IrC(inflammatory related chondrocyte), MC(macrophage chondrocyte), and RegC (Figure 1D). The results of the pseudotime analysis were shown in Figure 1E. EC was selected as the initial stage according to its distribution. The results of cellular interactions were shown in Figure 1F, indicating that there might be strong interactions between CPC and FC, and RegC. The results of cell interactions were provided in Supplementary Data (Supplemental Data Table 1).

3.2 Identification of human RA cartilage chondrocyte populations and TF regulation

We collated the Top10 DEGs for different cell types (Supplemental Data Table 2) and plotted the gene expression heat map (Figure 2A). Gene expression clustering plots (Figure 2B) and DotPlot plots (Figure 2C) showed the specific distribution of marker genes. The cell interactions (Figure 2D) show the Top5 TF of each cell subpopulation, showing that KLF7 mainly affects CPC, SOX9 mainly affects EC, NFATC4 has some specificity in FC, MAF is more significant in MC, IRF3 is mainly associated with IrC and DLX4 has a greater effect on RegC.

IHC was performed to validate the gene markers in different chondrocyte types (Figure 3). FCs were distributed throughout the cartilage, slightly more in the middle layer and less in the weight-bearing region. RegCs were visible in all layers of cartilage, but there were relatively fewer in the weight-bearing region. ECs were similarly distributed throughout the cartilage, with fewer in the weight-bearing region, and the differences were mainly in the deep layer. CPCs were primarily found in the middle layer of cartilage, with significantly less in the middle and deep layers of the weight-bearing region. MCs were present throughout the cartilage, and there were higher concentrations in the middle layer. In the weight-bearing region, there were significantly fewer MCs in the middle and deep layers compared to the non-weight-bearing region. IrCs were more abundant in all layers of cartilage, similar to the distribution of MCs, with significantly lower numbers in the middle and deep layers of the weight-bearing region compared to the non-weight-bearing region.

We performed GO/KEGG pathway enrichment analysis for each cell subpopulation of DEGs, and the detailed results were shown in Supplemental Data Tables 3, 4. The bubble plots showed the results of GO and KEGG enrichment analysis (Figures 4A–F). CPC was mainly associated with nuclear division, chromosomes, extracellular matrix structural constituents, and cell cycle. EC-related genes were mostly enriched in the collagen-containing extracellular matrix, ossification, and focal adhesion. FC was mainly enriched in extracellular structure organization and ECM-receptor interaction. RegC was mainly associated with cartilage development, collagen-containing extracellular matrix. Cluster4 was mainly associated with antigen processing and presentation, MHC class II protein complex, immune receptor activity, and KEGG suggesting a close relationship with phagosome and Rheumatoid arthritis. Cluster8 was enriched to the regulation of leukocyte cell-cell adhesion, immunological synapse, cytokine activity, and cytokine-cytokine receptor interaction. Our team combined the GO/KEGG enrichment results and marker gene annotated by Wang et al. on immune cells (15). The macrophage subpopulation(APOC1) was more matched with Cluster4 (Supplemental Data Figure 1). The function of cluster 8 was not

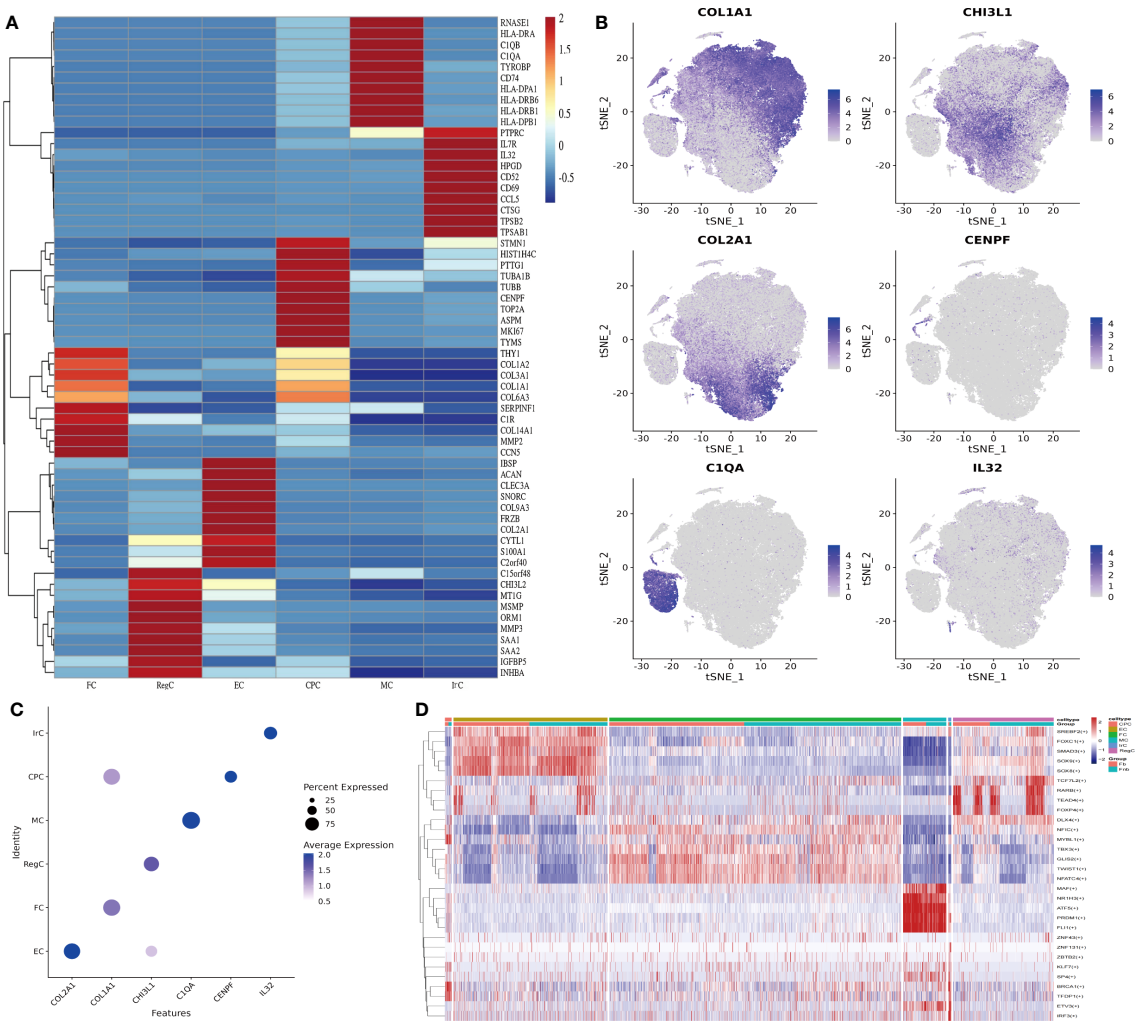

FIGURE 2
Identification of chondrocyte subpopulations. **(A)** Heatmap revealing the scaled expression of differentially expressed genes for each cell type. Specific representative genes in each chondrocyte subset were highlighted along the right margin. The color scheme is based on z-scores. **(B)** Clustering plots of Marker genes in cell subpopulations. **(C)** DotPlot of cell Marker genes. **(D)** Differences in transcription factor expression between different groups and cell types, with colors indicating transcription factor AUC values in different cells. Fb, femur weight-bearing region; Fnb, femur non-weight-bearing region. CPC, cartilage progenitor cells; EC, effector chondrocyte; FC, fibrocartilage chondrocyte; IrC, inflammatory related chondrocyte; MC, macrophage chondrocyte; RegC, regulatory chondrocyte; RA, rheumatoid arthritis; t-SNE, t-distributed stochastic neighbor embedding.

clearly indicated, and we tentatively found that it was related to inflammatory processes such as leukocyte adhesion and cytokine receptors. Therefore, Cluster4 was named macrophage chondrocyte (MC), and cluster8 was named inflammatory related chondrocyte(IrC).

We also calculated and compared the proportion of each cell type and cluster in the Fb and Fnb groups (Figure 5A; Supplemental Data Figure 2). We used the Wilcoxon rank sum test to compare the number of each cell subpopulation between the two groups (Figure 5B), and the characteristics of the data format were in Supplemental Data Tables 5, 6. The Fnb group had more RegCs, but this was not statistically significant. Based on the DEGs between the two groups (Supplemental Data Table 7). The volcano plot of DEGs between Fb and Fb was shown in Supplemental Data Figure 3. The DEGs were imported into String, an online tool for PPI network analysis (Figure 5C; Supplemental Data Table 8), after which the data were imported into Cytoscape, and the Top 10 Hub genes were identified using the cytoHubba plugin (Figure 5D). DEGs of MC between Fb and Fb were also analyzed (Supplemental Data Table 9). Figure 5E showed a volcano plot of DEGs in MC between Fb and Fb. GO and KEGG enrichment analyses were performed. (Figures 5F, G; Supplemental Data Table 10). The results showed that the MCs in the Fb group were mainly associated with antigen processing and presentation and MHC class II protein complex binding; while the MCs in the Fnb group were mainly enriched to cartilage development and extracellular matrix organization.

3.3 Identification of chondrocyte populations in MC and IrC

The two immune-related cell subpopulations, MC and IrC, were reclustered and 5981 cells were retained to obtain a total of 4

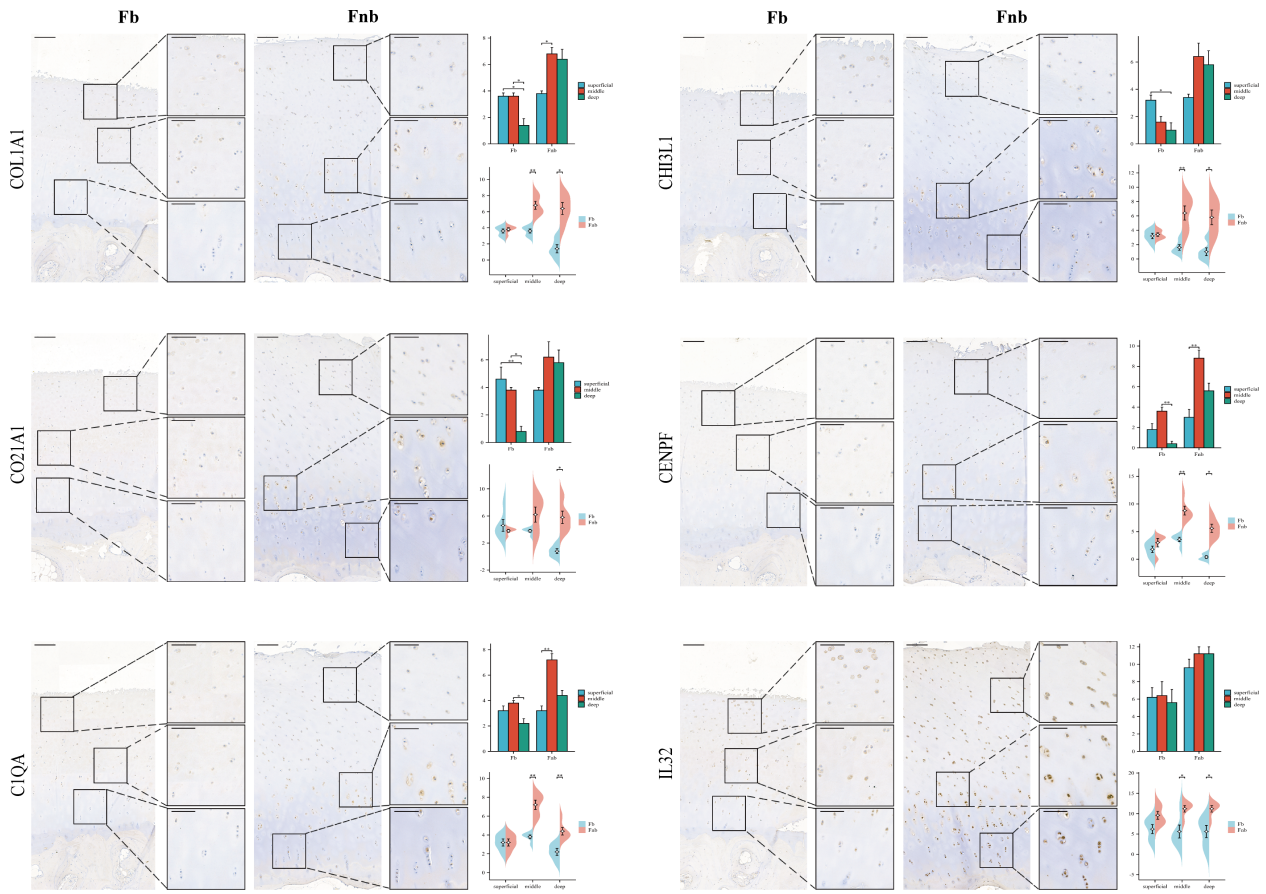

FIGURE 3
IHC results for specific markers for each cell type in different groups and layers. Scale bar, left, 200 μm; right, 100 μm. The scores of the indicated genes in the cartilage of both regions based on the immunohistochemistry assay are shown.*p<0.05, **p<0.01; otherwise, not significan Fb, femur weight-bearing region; Fnb, femur non-weight-bearing region.CPC, cartilage progenitor cells; EC, effector chondrocyte; FC, fibrocartilage chondrocyte; IrC, inflammatory related chondrocyte; MC, macrophage chondrocyte; RegC, regulatory chondrocyte.

clusters. The expression clusters of marker genes and the results of enrichment analysis of cluster1(SPP1) and cluster3(AREG) in repopulation were similar(Supplemental Data Figures 4, 5; Table 11), so cluster1 and cluster3 were combined to obtain three subpopulations of chondrocytes, SELENOP+, SPP1+, and IL32+ (Figure 6A). The Dot Plot of the genes suggested that the marker genes were selected with specificity (Figure 6B), with SELENOP+ and SPP1+ positive cells mainly originating from MC. IL32+ cells were mainly derived from IrC (Figure 6C). Then we validated it by matching cell IDs. We found that 95% (311/326) of the cells in the IL32+ were from IrC (Figure 6E; Supplemental Data Table 12). Expression clustering plots (Figure 6D) show the distribution of each cell type by a specific marker, validated using IHC (Figure 6F). The results suggest that SELENOP+(SELENOP) and SPP1+(SPP1) were distributed in the whole cartilage layer, mainly in the middle and deep layers, and less in the weight-bearing region.

The GO and KEGG enrichment analysis of the two cell subpopulation marker genes (Supplemental Data Table 13) suggested that SELENOP+ MCs were associated with immune response, complement activation, and monocyte chemotaxis; SPP1+ MCs were associated with ATP generation and focal adhesion (Figure 7A). The proportion of each subpopulation of MC in the Fb and Fnb groups was calculated and compared (Figure 7B). We used the independent samples t-test to compare the number of each cell subpopulation between the two groups (Figure 7C), and the characteristics of the data format were in Supplemental Data Tables 14, 15. The proportion of SPP1+ cells in the Fb group was relatively high, but the statistical significance was not significant. Figure 7D showed the top5 TF of the 3 cell subpopulations, showing that MAF mainly affected SELENOP+ cells, while TAGLN2 had some specificity in SPP1+ cells.

4 Discussion

Rheumatoid arthritis (RA) is an autoimmune disease characterized by synovitis, bone erosion, and cartilage damage (progressive joint destruction), and its pathogenesis is not yet fully understood. Our team found heavy cartilage erosion in the weight-bearing region during RA knee replacement surgery. In this study, we investigated chondrocytes in the weight-bearing and non-weight-bearing regions of femoral cartilage in RA patients using single-cell sequencing technology and performed analysis and experimental validation of chondrocyte subsets and marker genes.

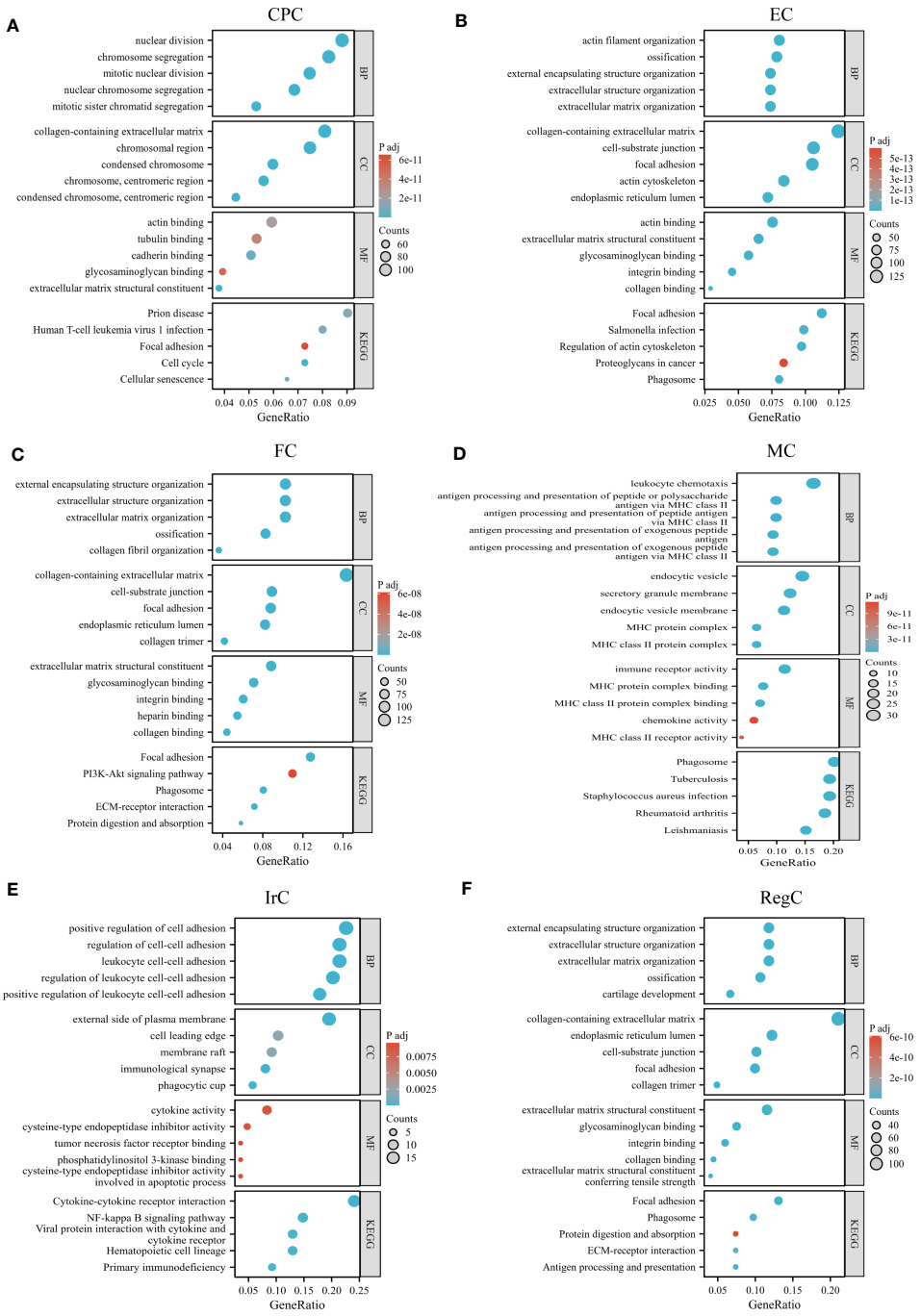

FIGURE 4
GO/KEGG enrichment analysis results of each cell type. **(A–F)** GO/KEGG enrichment results for different cell subpopulations, circle color indicates the p-value of each term, and circle size indicates the number of genes enriched in each term. CPC, cartilage progenitor cells; EC, effector chondrocyte; FC, fibrocartilage chondrocyte; IrC, inflammatory related chondrocyte; MC, macrophage chondrocyte; RegC, regulatory chondrocyte.

It is worth mentioning that we identified immune-related subtypes of chondrocytes, new markers, and signaling pathways that may be involved in the pathogenesis of RA based on scRNA-seq analysis, hoping to provide some reference and help in the diagnosis and treatment of human RA.

Our sequencing analysis of femoral cartilage from RA patients screened for a total of six cell subsets, including two of our newly defined immune-related chondrocyte subsets (MC and IrC). The finding by Tang et al. that some of the RegC cells with high expression of CD74, CD86, and HLA-DPA1 might have immune cell functions during OA progression corroborates with the findings of MC and IrC in this study (12). The psuedotime analysis resulted in a binary branching structure (Figure 1E), where the EC is located at the beginning of cellular evolution on the graph, which is also consistent with the study by Tang et al. (12). CPCs are less frequent at the start of differentiation, accumulating mainly at the ends of

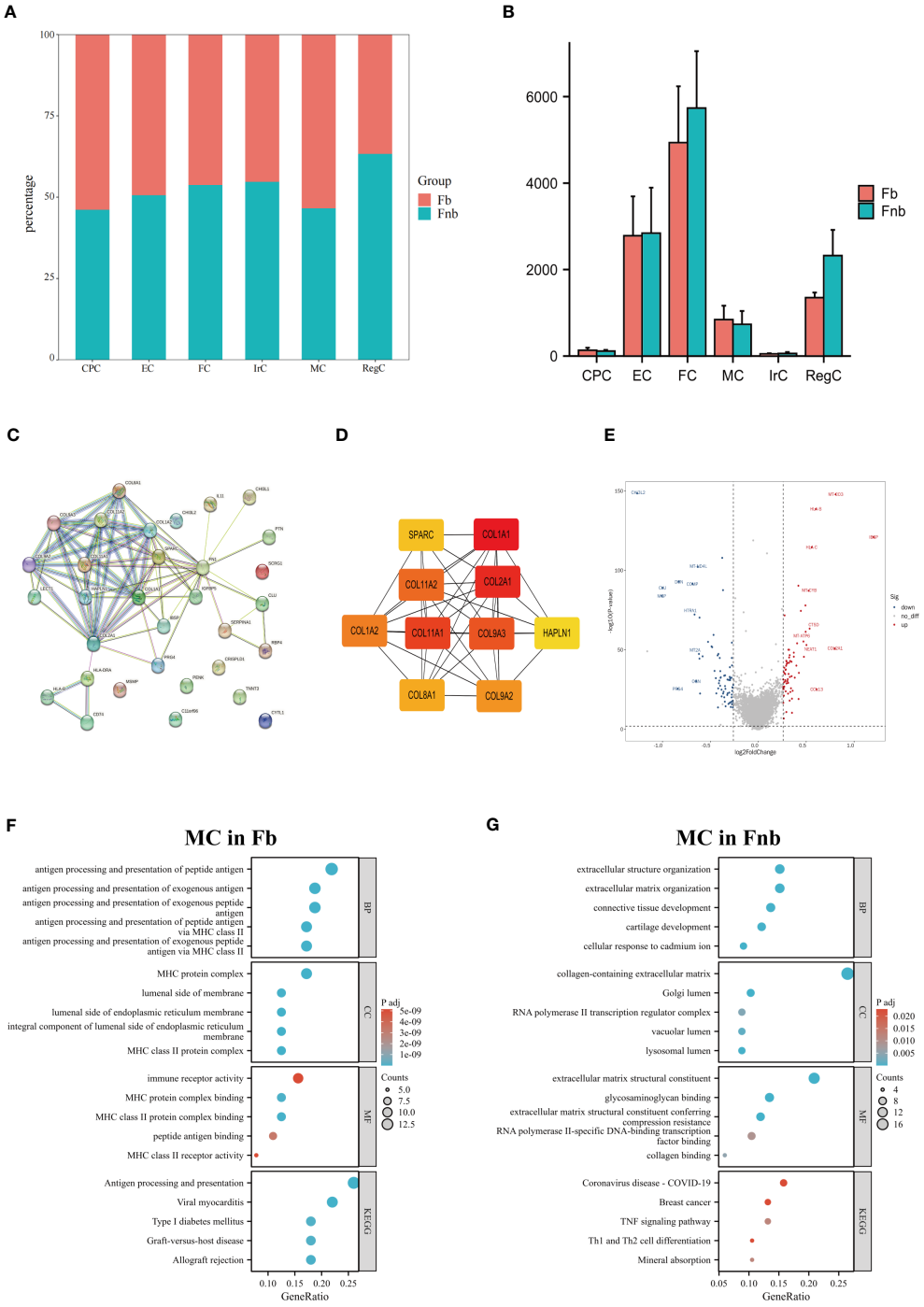

FIGURE 5
Results of differences analysis between Fb and Fnb. **(A)** Differences in the proportion of cell subpopulations. **(B)** Differences in the number of cell subpopulations. **(C)** The PPI network constructed by the String tool. Nodes represented proteins produced by protein-coding genes, and connections between nodes represented predicted protein interactions. **(D)** The top 10 Hub genes predicted by Cytoscape. **(E)** Volcano plot of MC DEGs between Fb and Fnb groups. The horizontal coordinate in the plot represented logFC and the vertical coordinate represented p-values. **(F–G)** Results of GO and KEGG enrichment analysis of MC between Fb and Fnb groups. The size of the circle indicated the number of enriched DEGs and the color represented the p-value. Fb, femur weight-bearing region; Fnb, femur non-weight-bearing region; GO, gene ontology; CPC, cartilage progenitor cells; EC, effector chondrocyte; FC, fibrocartilage chondrocyte; IrC, inflammatory related chondrocyte; MC, macrophage chondrocyte; RegC, regulatory chondrocyte.

branches and at the ends of trajectories. Notably, FC and RegC subpopulations are present throughout the developmental trajectory, with FC accumulating mainly at the end of branches and RegC significantly less at the end of the trajectory. In contrast, MC and IrC accumulate mainly at the end of the differentiation trajectory. We also performed an in-depth analysis of cellular interactions (Supplemental Data Table 1), with CPC interacting relatively closely with cellular subpopulations such as FC/RegC/MC

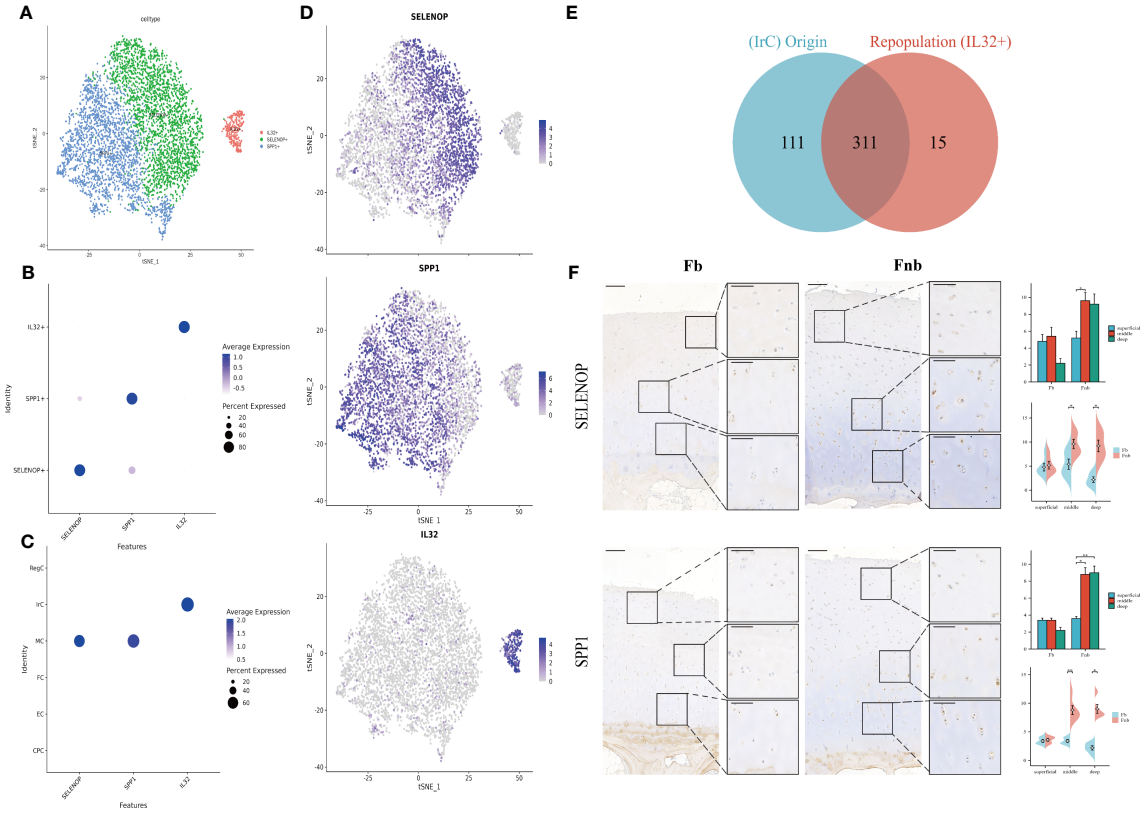

FIGURE 6
Marker genes for Immune-related chondrocytes. **(A)** Clustering plot of three cell subpopulations. **(B, C)** DotPlot of the cell marker genes. **(D)** A scatter plot of the cell marker genes, with the color of the dots representing expression levels. **(E)** Venn diagram for cell ID comparison of IrC and IL32+. The overlap represented the number of repetitive cells in the subpopulation. **(F)** IHC results for marker genes in different groups and layers. Scale bar, left, 200 μm; right, 100 μm. The scores of the indicated genes in the cartilage of both regions based on the immunohistochemistry assay are shown. *p<0.05, **p<0.01; otherwise, not significant. CPC, cartilage progenitor cells; EC, effector chondrocyte; FC, fibrocartilage chondrocyte; IrC, inflammatory-related chondrocyte; MC, macrophage chondrocyte; RegC, regulatory chondrocyte.

(Figure 1F). CD74, a receptor-related molecule associated with the antigen presentation process, has a high degree of activation between MC and six cell types, including itself, where CD74-MIF may play a role in regulating macrophage migration. It has been suggested that sufficient ferritin can be loaded with large amounts of iron ions and can lead to further oxygen radical damage (16). Our study also found that the molecules SCARA5 and FTL/FTH1, which are associated with iron ion transport, have a greater impact on the interaction species between MC/IrC and various other cell subpopulations, and perhaps the iron ion and RA relationship deserves further exploration. Molecular pairs of osteogenesis-related genes such as FN1 and integrin (α4β1) activate communication between RegC/EC/CPC, suggesting that these cell subpopulations may have a role in chondrocyte differentiation and collagen synthesis (17).

During RA progression, autoantigens would activate a specific immune response, with increased secretion of inflammatory cytokines and infiltration of synovial joints, resulting in arthritic symptoms (18). It was shown that joint disease with cartilage damage was closely related to immunological elements and it was recognized that the immune response was a key factor influencing cartilage repair (19, 20). During cartilage repair, immune cells such as macrophages could secrete anti-inflammatory factors which in turn promoted cartilage repair (21). However, the persistence of pro-inflammatory factors could also lead to chondrocyte death and accelerate the degradation of the cartilage (22). Therefore, understanding the relationship between chondrocytes and the immune response at the single-cell level could help to unravel the mechanisms underlying RA disease progression.

In this study, we identified two new subpopulations of immune chondrocytes. The MC subpopulation, located in the whole cartilage layer and more in the middle layer, showed high immunological activity and was mainly involved in immunological processes such as antigen processing and presentation, MHC class II protein complex, and immune receptor activity. KEGG suggested a close relationship with Rheumatoid arthritis. Our sequencing results revealed that HLA family genes such as HLA-DRA and HLA-DRB1 are highly expressed in MC, and the enrichment results of these genes showed an association with RA disease (Supplemental Data Tables 3, 4). Human leukocyte antigens (HLA) have gained some attention as antigen-presenting receptors, and many researchers suggested that HLA-DRB1 might be strongly associated with RA and influence the severity of the disease (23, 24). The interaction between macrophages and chondrocytes was also found in OA to increase the secretion of inflammatory cytokines and growth

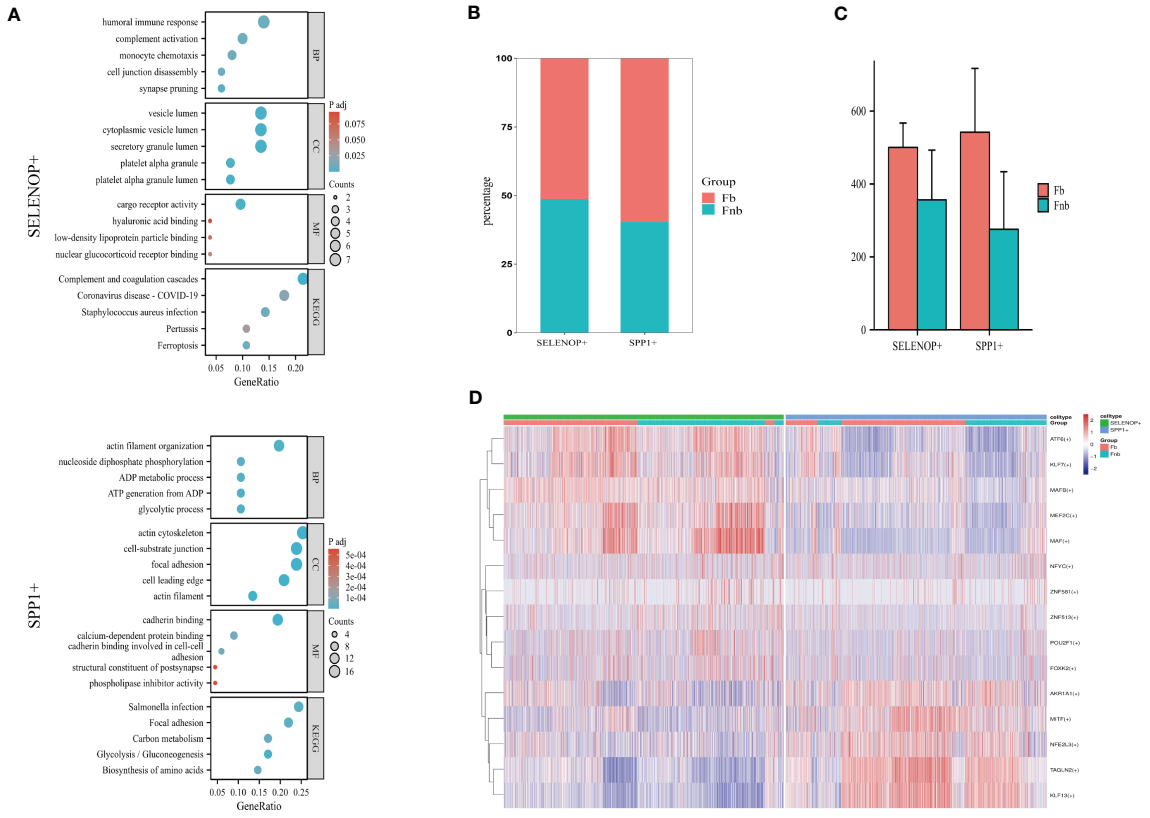

FIGURE 7
Characteristics of 3 clusters in Immune-related chondrocytes. **(A)** Results of GO and KEGG enrichment analysis for the three clusters. The size of the circles indicated the number of enriched DEGs, and colors represented p-values. **(B)** Differences in the proportion of cell subpopulations. **(C)** Differences in the number of cell subpopulations. **(D)** Differences in transcription factor expression between different groups and cell types. Colors indicate transcription factor AUC values in different cells. Fb, femur weight-bearing region; Fnb, femur non-weight-bearing region.

factors, leading to cartilage degeneration and destruction (25). This also suggests that the discovery of the MC subpopulation might provide new direction and value to the exploration of arthritic disease mechanisms (26). The IrC subpopulation was distributed in the whole cartilage layer, considered to be chondrocytes with inflammatory characteristics like immune cell adhesion, cytokine activity, and receptor. Leukocyte chemotactic genes were highly expressed in this subpopulation and these genes were enriched for the regulation of leukocyte cell-cell adhesion, immunological synapse, cytokine activity, and cytokine-cytokine receptor interaction. The KEGG results suggested a relationship between the NF-Kappa B signaling pathway and RA disease. It has been proposed that NF-kB was associated with bone erosion and the progression of RA disease, exhibiting high levels of inflammatory cytokines such as IL-1, TNF-α, and IL-6, and was believed to be one of the major inflammatory pathways in RA (27). Nuclear factor kappa B ligand (RANKL) was associated with the activation of NF-kB, which could lead to bone erosion and bone destruction, and the use of RANKL inhibitors could inhibit bone loss in RA by interfering with osteoclasts (28).

Based on the properties and functions of MC and IrC in the immune response, the analysis comparing the two cell subpopulations might improve our understanding of the role of chondrocytes in the pathogenesis of RA from an immunological perspective and even provide clues for RA cartilage regeneration. We performed a repopulation study of the two chondrocyte subpopulations, MC and IrC, and classified them into a total of three cell subpopulations, SELENOP+, IL32+, and SPP1+, based on the Marker gene of each subpopulation. Our study found that SELENOP+ cells and SPP1+ cells were mainly derived from MC, and Wang et al. also identified two macrophage clusters in immune cells, named SELENOP-Mφ and SPP1-Mφ (15), which also corroborated our definition of MC here. SELENOP protein is a transport carrier for the essential trace element selenium, which is mainly expressed in the liver and secreted into the plasma and has been shown to be associated with autoimmune diseases (29). SELENOP is also associated with oxidative stress, and the protein acts as an extracellular antioxidant with anti-inflammatory effects (30, 31). In addition, Wang et al. found that the SELENOP-Mφ cluster was also highly expressed in genes such as IL32, which participated in peptide metabolism, protein transport, and cytokine secretion, closely related to lymphocyte-related functions (15). SPP1, also known as OPN, has been shown to be involved in Mφ polarization and osteoclast attachment to the mineralized bone matrix, and also to promote chondrocyte proliferation through HOTAIR overexpression (32, 33). Knockdown of OPN could upregulate the expression of OA-related genes, and enhance chondrocyte senescence and apoptosis, accelerating the

progression of OA (34). Increased expression of IL32-encoded cytokines in RA synovium induces pro-inflammatory cytokine expression, which was highly correlated with the severity of inflammation, suggesting it might be a potential therapeutic target for RA (35). In addition, unlike the induction of TNF-α, IL-1β and IL-6 via p38-MAPK, IL-32 was able to induce monocytes to differentiate into macrophage-like cells through a non-apoptotic, caspase-3-dependent mechanism, suggesting that IL-32 not only participated in the host response by inducing pro-inflammatory cytokines, but also directly affected specific immunity by differentiating monocytes into macrophage-like cells (36).

The presence of mechanical loading would affect the inflammatory state and growth factor expression of chondrocytes and interfere with chondrocyte proliferation and migration (37), but the effects of mechanical loading on chondrocyte types remain underresearched. This study revealed a significantly larger proportion of RegCs in the non-weight-bearing region, and that RegCs with high expression levels of chondroprotective genes might deserve further in-depth study. Notably, the MCs in the Fb group were mainly associated with antigen processing and presentation and MHC class II protein complex binding, which was consistent with more severe cartilage damage in the weight-bearing region of RA patients. The MCs in the Fnb group were mainly enriched for activities such as cartilage development and extracellular matrix organization, suggesting that cartilage in non-weight-bearing regions of RA patients might have more activated cartilage growth and development. Considering that the mechanical loading in OA could affect chondrocyte pyroptosis by influencing macrophage polarization (38), it is strongly reasonable to speculate that there is a process of macrophage polarization transition in MCs in response to mechanical loading, as in macrophages. MCs in the weight-bearing region are mainly involved in activities such as initiation and maintenance of immune response, and promotion of antigen processing and presentation, which are similar to the function of pro-inflammatory macrophages(M1) (39). In contrast, MCs in non-weight-bearing region are associated with activities such as connective tissue and cartilage development, which may have similar functions such as inflammation relieving and repairing like anti-inflammatory macrophages(M2) (39). Intervening in this regulation of immune homeostasis might be a good inspiration for decelerating the progression of RA, which could provide a reference for gene regulation or extraction of relatively high-quality cartilage from non-weight-bearing regions for targeted transplantation to reverse cartilage damage in weight-bearing regions of RA.

There are still some limitations to our study. First, single-cell sequencing is expensive, the number of samples taken in this study was limited, and there is still space for improvement in sampling technique and sample quality. Secondly, the samples were taken from both weight-bearing and non-weight-bearing areas of RA cartilage, and the lack of controls with healthy groups might result in less significant differences between the groups, and in-depth analysis and validation with multiple samples of healthy cartilage would make the results more reliable. Thirdly, we have not conducted in-depth *in vivo* and *in vitro* experiments to validate our findings and the practical clinical value of the results of this study needs to be further explored.

5 Conclusions

In conclusion, our study dissociated and characterized RA chondrocytes at single-cell resolution and identified two new immune activities related chondrocyte subpopulations, MC and IrC, revealing the different functions of MCs under mechanical loading and specific markers as well as the key transcription factors involved in each cell subpopulation, providing new possibilities for the development of diagnostic and therapeutic strategies for RA.

Data availability statement

The datasets presented in this study can be found in online repositories. The names of the repository/repositories and accession number(s) can be found below: PRJNA999858 (SRA).

Ethics statement

The studies involving humans were approved by the Institutional Ethics Review Committee of the Affiliated Hospital of Qingdao University. The studies were conducted in accordance with the local legislation and institutional requirements. The participants provided their written informed consent to participate in this study.

Author contributions

MY, ZS, and TW contributed to the conception and design of the study. MY wrote the manuscript. HZ collected cartilage samples. MY and JW performed data analysis. TW, TY, and YZ supervised the manuscript. All authors contributed to the manuscript revision, read, and approved the submitted version.

Conflict of interest

The authors declare that the research was conducted in the absence of any commercial or financial relationships that could be construed as a potential conflict of interest.

Publisher's note

All claims expressed in this article are solely those of the authors and do not necessarily represent those of their affiliated organizations, or those of the publisher, the editors and the reviewers. Any product that may be evaluated in this article, or claim that may be made by its manufacturer, is not guaranteed or endorsed by the publisher.

Supplementary material

The Supplementary Material for this article can be found online at: https://www.frontiersin.org/articles/10.3389/fimmu.2023.1247355/full#supplementary-material

References

1. Weyand CM, Goronzy JJ. The immunology of rheumatoid arthritis. *Nat Immunol* (2021) 22(1):10–8. doi: 10.1038/s41590-020-00816-x

2. Lin Y-J, Anzaghe M, Schülke S. Update on the pathomechanism, diagnosis, and treatment options for rhe umatoid arthritis. *Cells* (2020) 9(4):880. doi: 10.3390/cells9040880

3. Feng F-B, Qiu H-Y. Effects of Artesunate on chondrocyte proliferation, apoptosis and auto phagy through the PI3K/AKT/mTOR signaling pathway in rat models with r heumatoid arthritis. *Biomed Pharmacother* (2018) 102:1209–20. doi: 10.1016/j.biopha.2018.03.142

4. Gilbert SJ, Bonnet CS, Blain EJ. Mechanical cues: bidirectional reciprocity in the extracellular matrix drives mechano-signalling in articular cartilage. *Int J Mol Sci* (2021) 22(24):13595. doi: 10.3390/ijms222413595

5. Xu B, Xing R, Huang Z, Yin S, Li X, Zhang L, et al. Excessive mechanical stress induces chondrocyte apoptosis through TRPV4 in an anterior cruciate ligament-transected rat osteoarthritis model. *Life Sci* (2019) 228:158–66. doi: 10.1016/j.lfs.2019.05.003

6. Chen L, Liu G, Li W, Wu X. Chondrogenic differentiation of bone marrow-derived mesenchymal stem cells following transfection with Indian hedgehog and sonic hedgehog using a rotary cell culture system. *Cell Mol Biol Lett* (2019) 24:16. doi: 10.1186/s11658-019-0144-2

7. Chen Z, Yan F, Lu Y. The function of mechanical loading on chondrogenesis. *Front Biosci (Landmark Ed)* (2016) 21(6):1222–32. doi: 10.2741/4452

8. Zeng L, Yang K, Zhang T, Zhu X, Hao W, Chen H, et al. Research progress of single-cell transcriptome sequencing in autoimmun e diseases and autoinflammatory disease: A review. *J Autoimmun* (2022) 133:102919. doi: 10.1016/j.jaut.2022.102919

9. Zhang F, Wei K, Slowikowski K, Fonseka CY, Rao DA, Kelly S, et al. Defining inflammatory cell states in rheumatoid arthritis joint synovial tissues by integrating single-cell transcriptomics and mass cytometry. *Nat Immunol* (2019) 20(7):928–42. doi: 10.1038/s41590-019-0378-1

10. Wu X, Liu Y, Jin S, Wang M, Jiao Y, Yang B, et al. Single-cell sequencing of immune cells from anticitrullinated peptide antibody positive and negative rheumatoid arthritis. *Nat Commun* (2021) 12(1):4977. doi: 10.1038/s41467-021-25246-7

11. Cheng L, Wang Y, Wu R, Ding T, Xue H, Gao C, et al. New insights from single-cell sequencing data: synovial fibroblasts an d synovial macrophages in rheumatoid arthritis. *Front Immunol* (2021) 12:709178. doi: 10.3389/fimmu.2021.709178

12. Ji Q, Zheng Y, Zhang G, Hu Y, Fan X, Hou Y, et al. Single-cell RNA-seq analysis reveals the progression of human osteoarthritis. *Ann Rheum Dis* (2019) 78(1):100–10. doi: 10.1136/annrheumdis-2017-212863

13. Wang T, Wang J, Sun Z, Zhang L, Yu C, Zhao H, et al. Single-cell RNA sequence presents atlas analysis for chondrocytes in t he talus and reveals the potential mechanism in coping with mechanical stress. *Front Cell Dev Biol* (2022) 10:1047119. doi: 10.3389/fcell.2022.1047119

14. Aşık MD, Gürsoy S, Akkaya M, Kozacı LD, Doğan M, Bozkurt M, et al. Microarray analysis of cartilage: comparison between damaged and non-weight-bearing healthy cartilage. *Connect Tissue Res* (2020) 61(5):456–64. doi: 10.1080/03008207.2019.1611797

15. Wang C, et al. The heterogeneous immune landscape between lung adenocarcinoma and squ amous carcinoma revealed by single-cell RNA sequencing. *Signal transduction targeted Ther* (2022) 7(1):289. doi: 10.1038/s41392-022-01130-8

16. Biemond P, Swaak AJ, van Eijk HG, Koster JF. Intraarticular ferritin-bound iron in rheumatoid arthritis. A factor t hat increases oxygen free radical-induced tissue destruction. *Arthritis Rheum* (1986) 29(10):1187–93. doi: 10.1002/art.1780291002

17. Zhang H, Chen X, Xue P, Ma X, Li J, Zhang J. FN1 promotes chondrocyte differentiation and collagen production via T. *Gene* (2021) 769:145253. doi: 10.1016/j.gene.2020.145253

18. Scherer HU, Häupl T, Burmester GR. The etiology of rheumatoid arthritis. *J Autoimmun* (2020) 110:102400. doi: 10.1016/j.jaut.2019.102400

19. Li M, Yin H, Yan Z, Li H, Wu J, Wang Y, et al. The immune microenvironment in cartilage injury and repair. *Acta Biomater* (2022) 140:23–42. doi: 10.1016/j.actbio.2021.12.006

20. Yan M, Zhao H, Sun Z, Chen J, Zhang Y, Gao J, et al. Identification of key diagnostic markers and immune infiltration in os teoarthritis. *Comb Chem High Throughput Screen* (2023) 26(2):410–23. doi: 10.2174/1386207325666220426083526

21. Fernandes TL, Gomoll AH, Lattermann C, Hernandez AJ, Bueno DF, Amano MT, et al. Macrophage: A potential target on cartilage regeneration. *Front Immunol* (2020) 11:111. doi: 10.3389/fimmu.2020.00111

22. Lin XC, Liu X, Li K, Zhao C, Xu S, Zhang Y, et al. B-cell-specific mamMalian target of rapamycin complex 1 activation res ults in severe osteoarthritis in mice. *Int Immunopharmacol* (2018) 65:522–30. doi: 10.1016/j.intimp.2018.09.038

23. Weyand CM, Hicok KC, Conn DL, Goronzy JJ. The influence of HLA-DRB1 genes on disease severity in rheumatoid arth ritis. *Ann Internal Med* (1992) 117 (10):801–6. doi: 10.7326/0003-4819-117-10-801

24. Padyukov L. Genetics of rheumatoid arthritis. *Semin immunopathol* (2022) 44 (1):47–62. doi: 10.1007/s00281-022-00912-0

25. Zhang H, Cai D, Bai X. Macrophages regulate the progression of osteoarthritis. *Osteoarthritis Cartilage* (2020) 28(5):555–61. doi: 10.1016/j.joca.2020.01.007

26. Kim K-W, Kim BM, Won JY, Min HK, Lee KA, Lee SH, et al. Regulation of osteoclastogenesis by mast cell in rheumatoid arthritis. *Arthritis Res Ther* (2021) 23 (1):124. doi: 10.1186/s13075-021-02491-1

27. Ilchovska DD, Barrow DM. An Overview of the NF-kB mechanism of pathophysiology in rheumatoid ar thritis, investigation of the NF-kB ligand RANKL and related nutrition al interventions. *Autoimmun Rev* (2021) 20(2):102741. doi: 10.1016/j.autrev.2020.102741

28. Chiu YG, Ritchlin CT. Denosumab: targeting the RANKL pathway to treat rheumatoid arthritis. *Expert Opin Biol Ther* (2017) 17(1):119–28. doi: 10.1080/14712598.2017.1263614

29. Sun Q, Mehl S, Renko K, Seemann P, Görlich CL, Hackler J, et al. Natural autoimmunity to selenoprotein P impairs selenium transport in hashimoto's thyroiditis. *Int J Mol Sci* (2021) 22(23):13088. doi: 10.3390/ijms222313088

30. Campo-Sabariz J, García-Vara A, Moral-Anter D, Briens M, Hachemi MA, Pinloche E, et al. Hydroxy-selenomethionine, an organic selenium source, increases seleno protein expression and positively modulates the inflammatory response of LPS-stimulated macrophages. *Antioxidants (Basel Switzerland)* (2022) 11(10):1876. doi: 10.3390/antiox11101876

31. Caviglia GP, Rosso C, Armandi A, Gaggini M, Carli F, Abate ML, et al. Interplay between oxidative stress and metabolic derangements in non-alcoholic fatty liver disease: the role of selenoprotein P. *Int J Mol Sci* (2020) 21(22):8838. doi: 10.3390/ijms21228838

32. Zhang Y, Du W, Chen Z, Xiang C. Upregulation of PD-L1 by SPP1 mediates macrophage polarization and fac ilitates immune escape in lung adenocarcinoma. *Exp Cell Res* (2017) 359(2):449–57. doi: 10.1016/j.yexcr.2017.08.028

33. Liang Q, Asila A, Deng Y, Liao J, Liu Z, Fang R, et al. Osteopontin-induced lncRNA HOTAIR expression is involved in osteoarthritis by regulating cell proliferation. *BMC Geriatr* (2021) 21(1):57. doi: 10.1186/s12877-020-01993-y

34. Tian J, Cheng C, Kuang SD, Su C, Zhao X, Xiong YL, et al. OPN deficiency increases the severity of osteoarthritis associated with aberrant chondrocyte senescence and apoptosis and upregulates the expression of osteoarthritis-associated genes. *Pain Res Manag* (2020) 2020:3428587. doi: 10.1155/2020/3428587

35. Alsaleh G, Sparsa L, Chatelus E, Ehlinger M, Gottenberg JE, Wachsmann D, et al. Innate immunity triggers IL-32 expression by fibroblast-like synoviocytes in rheumatoid arthritis. *Arthritis Res Ther* (2010) 12(4):R135. doi: 10.1186/ar3073

36. Netea MG, Lewis EC, Azam T, Joosten LA, Jaekal J, Bae SY, et al. Interleukin-32 induces the differentiation of monocytes into macrophage-like cells. *Proc Natl Acad Sci U.S.A.* (2008) 105(9):3515–20. doi: 10.1073/pnas.0712381105

37. Steinecker-Frohnwieser B, Kaltenegger H, Weigl L, Mann A, Kullich W, Leithner A, et al. Pharmacological treatment with diacerein combined with mechanical stimulation affects the expression of growth factors in human chondrocytes. *Biochem Biophys Rep* (2017) 11:154–60. doi: 10.1016/j.bbrep.2017.06.006

38. Shen P, Jia S, Wang Y, Zhou X, Zhang D, Jin Z, et al. Mechanical stress protects against chondrocyte pyroptosis through lipoxin A_4 via synovial macrophage M2 subtype polarization in a n osteoarthritis model. *Biomed Pharmacother* (2022) 153:113361. doi: 10.1016/j.biopha.2022.113361

39. Shapouri-Moghaddam A, Mohammadian S, Vazini H, Taghadosi M, Esmaeili SA, Mardani F, et al. Macrophage plasticity, polarization, and function in health and disease. *J Cell Physiol* (2018) 233(9):6425–40. doi: 10.1002/jcp.26429

frontiers | Frontiers in Immunology

TYPE Original Research
PUBLISHED 18 September 2023
DOI 10.3389/fimmu.2023.1251517

Check for updates

OPEN ACCESS

EDITED BY
Chuan-ju Liu,
New York University, United States

REVIEWED BY
Hongfei Xiang,
The Affiliated Hospital of Qingdao University, China
Yunhan Zhao,
Karolinska Institutet (KI), Sweden
Bin Li,
Soochow University, China

*CORRESPONDENCE
Jianlu Wei
Drjianluwei@163.com
Lei Cheng
Chenglei@email.sdu.edu.cn

RECEIVED 01 July 2023
ACCEPTED 28 August 2023
PUBLISHED 18 September 2023

CITATION
Meng Q, Liu K, Liu Z, Liu J, Tian Z, Qin S, Wei J and Cheng L (2023) Digoxin protects against intervertebral disc degeneration via TNF/NF-κB and LRP4 signaling. *Front. Immunol.* 14:1251517. doi: 10.3389/fimmu.2023.1251517

COPYRIGHT
© 2023 Meng, Liu, Liu, Liu, Tian, Qin, Wei and Cheng. This is an open-access article distributed under the terms of the Creative Commons Attribution License (CC BY). The use, distribution or reproduction in other forums is permitted, provided the original author(s) and the copyright owner(s) are credited and that the original publication in this journal is cited, in accordance with accepted academic practice. No use, distribution or reproduction is permitted which does not comply with these terms.

Digoxin protects against intervertebral disc degeneration via TNF/NF-κB and LRP4 signaling

Qunbo Meng[1,2], Kaiwen Liu[1,2], Zhenchuan Liu[1,2], Jinbo Liu[1,2], Ziyu Tian[2,3], Shanshan Qin[3], Jianlu Wei[1,4]* and Lei Cheng[1,4]*

[1]Department of Orthopaedic Surgery, Qilu Hospital, Cheeloo College of Medicine, Shandong University, Jinan, Shandong, China, [2]Qilu Hospital of Shandong University, Shandong University, Jinan, Shandong, China, [3]Department of Radiology, Qilu Hospital of Shandong University, Jinan, Shandong, China, [4]Qilu Hospital of Shandong University Spine and Spinal Cord Disease Research Center-International Chinese Musculoskeletal Research Society (ICMRS) Collaborating Center for Orthopaedic Translational Research, Shandong University, Jinan, Shandong, China

Background: Intervertebral disc degeneration (IVDD) is a leading cause of low back pain (LBP). The pathological process of IVDD is associated with inflammatory reactions and extracellular matrix (ECM) disorders. Digoxin is widely used for treating heart failure, and it has been reported to have anti-inflammatory effects.

Objective: This study is to investigate the role of digoxin in the pathogenesis of intervertebral disc degeneration as well as the involved molecular mechanism, particularly the potential target protein.

Methods: We exploited a rat needle model to investigate digoxin's role in intervertebral disc degeneration *in vivo*. Safranin O staining was used to measure cartilaginous tissue in the intervertebral disc. The morphological changes of intervertebral discs in animal models were determined by Hematoxylin-Eosin (H&E) staining and the pathological score. Primary nucleus pulposus cells (NP cells) from intervertebral discs of patients and murine were used in the present study. Western-Blotting assay, Real-time PCR assay, immunofluorescence staining, and immunochemistry were used to detect the role of digoxin in anti-TNF-α-induced inflammatory effects *in vitro*. Transfection of siRNA was used to regulate low-density lipoprotein receptor-related protein 4 (LRP4) expression in NP cells to investigate the potential protein target of digoxin.

Results: Digoxin protected against intervertebral disc degeneration in rat needle models. Digoxin was found to exert its disc-protective effects through at least three different pathways by a) suppressing TNF-α-induced inflammation, b) attenuating ECM destruction, c) significantly promoting ECM anabolism. Additionally, LRP4 was found to be the downstream molecule of digoxin in NP cells for anti-inflammation and regulation of ECM metabolism. The knockdown of LRP4 downregulated the protective effect of digoxin in NP cells.

Conclusion: These findings suggest that digoxin may be a potential therapeutic agent for intervertebral disc degeneration through anti-catabolism and pro-anabolism. Digoxin might also work as an alternative for other inflammation-related diseases.

KEYWORDS

digoxin, intervertebral disc degeneration, TNF, LRP4, inflammation

1 Introduction

Low back pain (LBP) is a widespread global health problem, a cause of long-term health problems for people across different incomes levels and countries (1, 2). According to the Global Burden of Disease Study of 2019 (GBD 2019), LBP was the leading cause of years lived with disability (YLDs) worldwide, accounting for about 7.4% (range: 6.2%–8.7%) of the total global YLDs. This translates to a staggering figure of approximately 63.7 million YLDs attributable to LBP. In Europe, the aggregate costs associated with LBP equate to about 0.1%–2% of the gross domestic product. Intriguingly, more than 80% of the total expenditure related to LBP is constituted by indirect costs, including productivity losses and disability-related disbursements (3, 4).

Intervertebral disc degeneration (IVDD) is a complication of LBP (2, 5). A healthy intervertebral disc is composed of a centrally located nucleus pulposus (NP) surrounded by an annulus fibrosus (AF) (6). As the degenerative process advances, particularly with the degeneration of the NP, the intervertebral disc may exhibit a marked reduction in height, decreased water content, rupture of the AF, and herniation of the NP, leading to nerve impingement at the corresponding spinal segment (7). The mechanism underlying intervertebral disc degeneration has not yet been fully elucidated (8). Nevertheless, inflammation is widely accepted as the main cause of disc degeneration (2).

Among the inflammatory molecules, tumor necrosis factor-alpha (TNF-α) is thought to be the key factor associated with IVDD. The pathogenesis of IVDD involves an increase in TNF-α levels (9), and a high TNF-α level is associated with low back pain (10). The nuclear factor kappa B (NF-κB) pathway is activated when TNF-α reaches its peak during inflammation, resulting in the activation of genes related to inflammation, such as chemokines and proinflammatory cytokines like IL-1β and IL-6 (11). Besides participating in the inception and advancement of the inflammatory response, TNF-α is involved in cellular processes such as apoptosis (12). Consequently, it is possible to treat inflammatory diseases by regulating TNF expression levels. Furthermore, managing IVDD can be treated by targeting the TNF signaling pathway, which has become a feasible therapeutic choice (13).

Digoxin, a cardiac glycoside derived from foxglove, is a potent inhibitor of Na^+/K^+-ATPase and one of the oldest medications used for treating heart disease (14–16). Generally, digoxin is widely used in managing various cardiac diseases, including congestive heart failure and atrial fibrillation (17, 18). Several studies have shown the beneficial effects of digoxin in various inflammatory diseases, such as rheumatoid arthritis, inflammatory bowel disease, and autoimmune arthritis (19, 20). Researchers also found that digoxin treatment in mice with acute liver injury resulted in a significant decrease in proinflammatory cytokine levels, including IL-17A, IL-1β, TNF-α, and inhibited NF-κB activation (21). These studies suggest that digoxin possesses anti-inflammatory effects. Despite the anti-inflammatory effect, digoxin also demonstrated anabolic promotion in recent studies (22). However, whether digoxin suppresses TNF-α-mediated inflammation and whether digoxin has a protective effect in IVDD is still unknown.

Inflammation plays an important role in IVDD (23). The anti-inflammatory properties of digoxin have been demonstrated in different diseases (24). However, it is unclear how digoxin affects IVDD. This study explored the role of digoxin in IVDD and the associated molecular mechanisms, including the downstream proteins influenced by digoxin.

2 Materials and methods

2.1 Isolation and culture of nucleus pulposus cells

Human intervertebral disc tissue samples were obtained from spinal surgical procedures with written informed consent from the donors in accordance with ethical guidelines. The intervertebral discs were dissected, and under aseptic conditions, the NP tissue from the central part of the disc was isolated to the best possible extent. The isolated NP tissue was then minced into tissue fragments smaller than 1 mm^3 in size. The collected NP tissue fragments were digested with 0.25% trypsin (Gibco, America) for 20 minutes, and the excess trypsin was discarded. Subsequently, the tissue fragments were enzymatically digested using type II collagenase (Solarbio, China) at a concentration of 0.2%. The tissue fragments were incubated at 37°C with 5% CO_2 for 2–4 hours. After incubation, the digested tissue was filtered using a cell filter with a pore size of 70 μm to separate the released cells from the undigested tissue fragments. The resulting cell pellet was obtained by low-speed centrifugation (800 rpm) for five minutes. DMEM/F12 medium (Gibco, America) was used to resuspend the pellet of

cells, supplemented with 10% fetal bovine serum (Gibco, America) and 1% penicillin-streptomycin (Solarbio, China). The isolated NP cells were seeded in culture flasks or dishes and maintained in a humidified incubator at 37°C with 5% CO_2. The culture medium was replaced every two days, and subculturing was performed when the cells reached 80%–90% confluence.

Following euthanasia, mice used in the experiment were surface disinfected with 75% ethanol. Under aseptic conditions, the skin and subcutaneous tissue of the dorsal region were incised, and the paraspinal muscles were dissected to isolate the entire spine. Intervertebral disc tissue was collected, and the AF was separated under a microscope. The NP tissue was gently washed with Phosphate Buffered Saline (PBS) for five minutes. The remaining procedures for processing were similar to the previously described method for human NP cell isolation.

2.2 Isolation and culture of intervertebral disc tissue

Endoscopic surgical methodologies in spinal orthopedics were used to surgically extract human NP tissues from intervertebral discs. These samples were subsequently processed in a sterilized environment, which included the removal of extraneous AF and ligamentum flavum. The isolated human NP tissues were then bathed in PBS for five minutes and then transferred into a culture dish containing complete medium (DMEM/F12 medium supplemented with 10% fetal bovine serum and 1% penicillin-streptomycin), where they were cultivated for further experimentation.

Following euthanasia, the spines of mice used in the experiment were procured via previously outlined procedures. Subsequent intervertebral disc tissue isolation encompassed portions of the adjoining superior and inferior vertebral bodies, intact cartilaginous endplates, and the intervertebral disc itself. The separated murine intervertebral disc tissues were rinsed in PBS five-minute and relocated to a culture dish with complete medium, where they were cultivated for subsequent experimental use.

2.3 Rat needle puncture model establishment

For this experiment, eight weeks old male rats were selected and anesthetized using isoflurane inhalation. After achieving complete sedation, the rats were positioned prone on the surgical table, with their tails immobilized. The caudal vertebrae were designated as the puncture site, and a 21-gauge needle was used to penetrate the AF of the intervertebral disc. The needle was inserted parallel to the vertebral body, maintaining a depth of 5 mm. Following insertion, the needle was rotated 360° and held *in situ* for 30 seconds prior to a gradual withdrawal along the initial insertion trajectory. Subsequent to model establishment, intraperitoneal injections were administered twice weekly, containing either a low concentration of DMSO (<0.1%) or digoxin at a 50 nM concentration. Four weeks post-surgery, magnetic resonance imaging (MRI) assessments were performed under anesthesia. Upon the anticipated conclusion of the treatment regimen, rats were euthanized, and their caudal vertebrae were procured for subsequent histological examinations to assess the degree of IVDD.

2.4 Histological staining and analysis

The harvested intervertebral disc tissue was immersed in a 4% paraformaldehyde (Solarbio, China) fixative solution for 48 hours to preserve tissue morphology. The tissue was decalcified using a 10% EDTA solution (pH 7.2–7.4) for two weeks, with daily solution changes. Subsequently, the tissue was dehydrated through a series of graded ethanol baths, cleared with an environmentally friendly clearing agent (Solarbio, China), and embedded in paraffin wax. The paraffin-embedded tissue was then sectioned into 5 μm-thick slices using a microtome. Appropriate histological stains were then applied based on the instructions provided in the respective staining kits. Hematoxylin and eosin (H&E) staining (Solarbio, China) was used to observe the histological morphology of the intervertebral disc, while Safranin O staining (Solarbio, China) was used for visualizing cartilaginous components within the disc. Histological scoring of the H&E and Safranin O-stained samples was performed using the methodologies outlined in prior literature. The stained results were evaluated from five perspectives. Each category was assigned a score ranging from 1–3, yielding a cumulative score between 5 and 15. Higher scoring levels indicated greater degrees of degeneration (25, 26).

2.5 Immunohistochemical staining and analysis

Paraffin-embedded tissue sections were subjected to a thermal regimen at 65°C for an hour to facilitate the subsequent deparaffinization with an environmentally friendly clearing agent. The sections were then hydrated via a graded series of ethanol solutions. Then, sections were heated in a citrate buffer with a pH of 6.0 to retrieve antigens, after which they were allowed to cool slowly. An opaque incubation with 3% hydrogen peroxide was then conducted, followed by a 30-minute blockade with 5% Bovine Serum Albumin (BSA). Primary antibodies were diluted according to the manufacturer's instructions, and the sections were incubated with these antibodies: COX-2 (1:100, Proteintech, China), IL-1β (1:100, Cell Signaling Technology, America), MMP-13 (1:100, Affinity, China), ADAMTS-4 (1:100, Abcam, America), Col-2 (1:100, Proteintech, China), Aggrecan (1:100, Proteintech, China), and LRP4 (1:50, Abcam, America). The sections were incubated overnight at 4°C. The following day, the sections were washed and incubated with a secondary goat anti-rabbit/mouse immunoglobulin G (IgG) antibody (ZSGB, China) at 37°C for an hour. Visualization of the antibodies was facilitated by applying 3,3'-Diaminobenzidine (DAB), followed by a counterstain with 1% hematoxylin. The images were captured and analyzed for the percentage of positive cells using the ImageJ software. For details, we measured the average gray value (staining intensity) and the percentage of positive area (stained area) of positive cells. Thus, the

mean gray value is computed to evaluate the staining intensity. The procedure was taken by imageJ. The consistency of parameters is ensured when analyzing the staining intensity of each group.

2.6 Total RNA extraction and reverse transcription polymerase chain reaction

Total RNA from the cells was extracted using either the TRIzol reagent (Takara Bio, Japan) or a general RNA extraction kit (Fastagen, China), adhering to the manufacturer's respective protocol, and RNA concentration was recorded. The extracted RNA was retro-transcribed into complementary DNA (cDNA) using a reverse transcription kit (Toyobo, Japan), following the specific instructions provided in the kit's manual. This newly synthesized cDNA was then used as the template for the Polymerase Chain Reaction (PCR) to amplify specific gene sequences. A PCR system is set up with the SYBR Green-PCR Master Mix (Toyobo, Japan) serving as the dye, and the Real-time PCR reaction is executed following the instructions provided by the manufacturer. Glyceraldehyde 3-phosphate dehydrogenase (GAPDH) was used as an internal reference gene to normalize the target genes. The specificity of the PCR product was ascertained through melt curve analysis. We computed the relative levels of relative mRNA expression using the ΔΔCT method. As shown in Table 1, the primer sequences to the Real-time PCR experiments are listed in Table 1. Each experiment was replicated more than three times to ensure data reliability.

2.7 Western blot

Human NP cells were cultivated *ex vivo* in six-well plates, with protein extraction performed at the appropriate time points. During

TABLE 1 Real-time PCR primers.

Target	Forward Primers,5′-3′	Reverse Primers,5′-3′
Human		
COX-2	TCCTTGGGTGTCAAAGGTAAA	TGGCCCTCGTTATGATCTG
iNOS	CGTGGAGACGGGAAAGAAGT	GACCCCAGGCAAGATTTGGA
IL-1β	CAACAAGTGGTGTTCTCCATGTC	ACACGCAGGACAGGTACAGA
IL-6	AGACAGCCACTCACCTCTTCA	GGCTTGTTCCTCACTACTCTC
MMP-13	ATTAAGGAGCATGGCGACTTCT	GCCCAGGAGGAAAAGCATGA
ADAMTS-4	ATGGCTATGGGCACTGTCTC	CTGGCGGTCAGCATCATAGT
Col-2	GATGGCTGCACGAAACATACC	GCCCTATGTCCACACCGAAT
Aggrecan	AAACCTGGCGTGAGAACTGT	CCACTGACACACCTCGGAAG
Bax	GAGGTCTTTTTCCGAGTGGCA	GGCAAAGTAGAAAAGGGCGAC
Bcl-2	GGGTGAACTGGGGGAGGATT	ATCTCCCGGTTGACGCTCTC
Casp3	GAGCACTGGAATGTCATCTCGCTCTG	AGACCGAGATGTCATTCCAGTGCTT
GAPDH	GCACCGTCAAGGCTGAGAAC	TGGTGAAGACGCCAGTGGA
LRP4	ACCTACCTGTTCCCCTCTTGA	GTCCTGCTCATCCGAGTCATC
Mouse		
COX-2	TGCTGGTGGAAAAACCTCGT	AAAACCCACTTCGCCTCCAA
iNOS	CCTGCTTTGTCGAAGTGTC	GCCAAACACCAAGCTCATGC
IL-1β	GTGTCTTTCCCGTGGACCTT	AATGGGAACGTCACACACCA
IL-6	GCCTTCTTGGGACTGATGCT	GCCATTGCACAACTCTTTTCTCA
MMP-13	TGATGATGAAACCTGGACAAGCA	GGTCCTTGGAGTGATCCAGACCTA
Col-2	CCAGATTGAGAGCATCCGCA	ACTTTCATGGCGTCCAAGGT
Aggrecan	AAACCTGGCGTGAGAACTGT	CCACTGACACACCTCGGAAG
Bax	CTGAGCTGACCTTGGAGC	GACTCCAGCCACAAAGATG
Bcl-2	TGTGGTCCATCTGACCCTCC	ACATCTCCCTGTTGACGCTCT
Casp3	AGGAGGGACGAACACGTCT	CAAAGAAGGTTGCCCCAATCT
GAPDH	CTTCACCACCATGGAGAAGGC	GACGGACACATTGGGGGTAG

the extraction of total cellular proteins, the culture medium was discarded from the six-well plates, followed by a gentle washing of the cells thrice using PBS. Subsequently, the cells were lysed for 30 minutes using the RIPA buffer (Solarbio, China) containing Protease Inhibitor Cocktail (NCM, China) and protein phosphatase inhibitors (NCM, China) on ice. The entire lysate was then drawn into Eppendorf tubes and further processed with a non-contact ultrasonic disintegrator (New Bioruptor Pro, Belgium). The EP tubes containing lysate were placed in a high-speed centrifuge and spun at 12,000 rpm at 4°C for 15 minutes. The supernatant was carefully aspirated into new Eppendorf tubes for storage. The nuclear protein extraction kit (Solarbio, China) instructions were followed to extract nuclear protein, allowing for the separation of nuclear and cytoplasmic proteins. The extracted proteins were initially quantified using a BCA assay kit (Solarbio, China), followed by mixing with loading buffer (EpiZyme, China) and heat denaturation before gel electrophoresis. SDS-PAGE gels were prepared based on the kDa of the proteins to be analyzed. The concentrations used in this experiment were 7.5%,10% and 12.5%. Proteins were separated in SDS-PAGE gels and transferred to PVDF membranes in equal amounts, and PVDF membranes were blocked using 5% BSA for an hour after transfer. The blocked PVDF membranes were incubated at 4°C for 12–16 hours with primary antibodies diluted according to the instructions, including COX-2 (1:1000, Proteintech, China), iNOS (1:1000, Abclonal, China), MMP-13 (1:1000, Proteintech, China), ADATMS-5 (1:1000, Abcam, America), Col-2 (1:1000, Proteintech, China), Aggrecan (1:1000, Proteintech, China), Bax (1:1000, Affinity, China), Bcl-2 (1:1000, Affinity, China), Cleaved-Caspase3 (1:1000, Affinity, China), LRP4 (1:500, Abcam, America), P-P65 (1:500, Cell Signaling Technology, America), P65 (1:1000, Affinity, China), P-AKT (1:500, Cell Signaling Technology, America), AKT (1:1000, Cell Signaling Technology, America), P-ERK1/2 (1:500, Zenbio, China), ERK1/2 (1:1000, Zenbio, China), P-IκBα (1:500, Cell Signaling Technology, America), Lamin-B1 (1:1000, Abways, China), and GAPDH (1:3000, Abways, China). The blocked PVDF membranes were washed with TBST to remove excess primary antibodies and incubated with secondary antibodies (Proteintech, China) for one hour, followed by image acquisition using a chemiluminescence imaging analyzer (Tanon5200, China). Image analysis was conducted using ImageJ software.

2.8 Immunofluorescence staining

Cultures of human NP cells were performed in 24-well plates to achieve the desired density and fixed with 4% paraformaldehyde. After fixation, the cells were permeabilized for 10 minutes with 0.2% Triton X-100 and then blocked for 30 minutes with 1% BSA to impede nonspecific antibody binding. Thereafter, the cells were incubated overnight at 4°C with specifically diluted primary antibodies as per the instructions provided. The primary antibodies involved in this experiment included COX-2(1:200, Proteintech, China), MMP-13 (1:200, Affinity, China), and C-Caspase3(1:200, Affinity, China). On the following day, the cells were rinsed three times for five minutes each with PBS containing Tween-20 to remove excess primary antibodies. Then, the cells were incubated for an hour at room temperature with a fluorescently labeled goat anti-rabbit secondary antibody (1:200 ZSGB-BIO, China). The cells are then washed three times with PBS and treated with an appropriate amount of DAPI-containing anti-quenching agent (Solarbio, China) to ensure complete and uniform coverage of the cell surface. Finally, fluorescence images were captured using an inverted fluorescence microscope and measured using the software. In order to compare the fluorescence intensity, we measured the fluorescent area ImageJ and integrated the density of each image. The mean fluorescence intensity of each image was then analyzed while ensuring consistent parameters.

2.9 TUNEL staining

Human NP cells were inoculated into 24-well plates and stimulated with TNF-α for 48 hours to induce apoptosis. The treatment group was pre-treated with 50 nM of digoxin. Following the manufacturer's instructions, cells were stained using the TUNEL assay kit (ELabScience Biotech, China), and images were captured using an inverted fluorescence microscope.

2.10 3-(4,5-dimethylthiazol-2-yl)-2,5-diphenyltetrazolium bromide assay (MTT assay)

Human NP cells are cultivated *in vitro* in a 96-well plate, with each well incubated with 100 μL of complete culture medium. After 24 hours, the cells were treated with digoxin at varying concentrations of 10, 20, 30, 50, and 100 nM and concurrently incubated for an additional 24 hours. Subsequently, MTT assays were performed according to the instructions provided with the MTT kit (Solarbio, China), culminating in the measurement of absorbance at a wavelength of 570 nm. The cell viability was represented as the percentage of the average cell survival rate in the treatment groups relative to that in the control group.

2.11 Alcian Blue staining

Human NP cells, isolated from original tissue, were uniformly distributed into a six-well plate, with each well containing 2 mL of complete medium for optimal growth conditions. The experimental group of cells was treated with 50 nM digoxin. Subsequently, on the 3rd, 7th, and 14th days post-inoculation, these cells were stained with the Alcian Blue Stain Kit For Cell (Solarbio, China) according to the manufacturer's detailed instructions. To compare the relative staining level of Alcian Blue, we measured the fluorescent area and integrated the density of each image using the ImageJ software. The relative staining level of each image was analyzed while ensuring consistent parameters.

2.12 Transfection

The NP cells derived from humans were cultured in complete media until they attained an approximate confluence of 40%–50%,

after which the media was promptly discarded, and the cells were rinsed with PBS. Subsequently, siRNA (Ribo, China) and transfection reagent (Ribo, China) were meticulously combined in accordance with the manufacturer's guidelines. This synergistic mixture was then incorporated into an antibiotic-free complete media environment to facilitate cell cultivation. A series of downstream experiments were performed after 48 hours. The effectiveness of the gene knockdown was subsequently verified using Western blot analysis. The protocol for transfection with overexpression plasmids was similar to the previously detailed process.

2.13 Ethics statement

This research was approved by the Medical Ethics Committee at Qilu Hospital of Shandong University. During the study, 31 patients—17 women and 14 men, aged 18–65 years—voluntarily participated and gave their informed consent. All participants underwent lumbar disc excision surgery at Qilu Hospital of Shandong University, and the collection of intervertebral disc tissue adhered to medical standards. Prior to surgery, MRI scans of the patients were obtained, and the collected human NP tissue samples were graded according to the Pfirrmann classification system based on the intensity of T2-weighted (T2WI) signals in the intervertebral discs. These samples were then used for further experimental study. The details of the patients of the sample provided in Table 2. All animal experiments involved in this study were conducted following the International Guiding Principles for Animal research, were approved by the Animal Experimentation Center of Shandong University and met the welfare requirements for experimental animals.

2.14 Statistical analysis

The present investigation used a blind method to gather all experimental data. Statistical analysis was performed in GraphPad Prism 9. T-tests were used to compare the means of two groups, while the analysis of variance (ANOVA) was used for comparisons involving more than two groups. Depending on the specific research context, ANOVA could be either one-way (one independent variable) or two-way (two independent variables), with Tukey's HSD *post hoc* test conducted using SPSS 22.0 software following the variance analysis. A p-value of less than 0.05 was considered statistically significant. Each value was expressed as the mean ± Standard Error of the Mean (SEM).

TABLE 2 Summary of clinical and demographic features of patients.

Subject Number	Gender	Age	Level	Pfirrmann Grade
1	Female	29	L4/5	II
2	Male	18	L4/5	II
3	Female	31	L5/S1	II
4	Female	27	L4/5	II
5	Male	22	L5/S1	II
6	Female	28	L5/S1	II
7	Male	34	L4/5	II
8	Female	37	L5/S1	II
9	Female	25	L5/S1	II
10	Male	51	L4/5	III
11	Female	47	L4/5	III
12	Male	43	L5/S1	III
13	Female	36	L5/S1	III
14	Male	41	L5/S1	III
15	Female	40	L4/5	III
16	Male	53	L5/S1	III
17	Female	55	L4/5	IV
18	Female	58	L5/S1	IV
19	Female	49	L4/5	IV
20	Male	57	L5/S1	IV
21	Male	63	L4/5	IV
22	Male	60	L4/5	IV
23	Female	55	L5/S1	IV
24	Male	58	L5/S1	IV
25	Female	49	L5/S1	V
26	Male	65	L4/5	V
27	Male	62	L5/S1	V
28	Female	57	L4/5	V
29	Male	60	L4/5	V
30	Female	62	L5/S1	V
31	Female	59	L4/5	V

3 Results

3.1 Digoxin inhibited TNF-α-induced inflammation in the disc

To determine whether digoxin has an anti-TNF-α-induced inflammatory effect in IVDD, we isolated mouse intervertebral disc tissue for *ex-vivo* culture and performed immunohistochemical staining for cyclooxygenase-2 (COX-2). We found that digoxin downregulated TNF-α-induced COX-2 expression compared to the control group (Figures 1A, B). Furthermore, immunohistochemical staining of cultured human NP tissue indicated that digoxin inhibited IL-1β expression *in vitro* (Figures 1C, D). Additionally, the immunofluorescence staining of COX-2 demonstrated that digoxin significantly suppressed the TNF-α-induced inflammatory response in primary human NP cells

10.3389/fimmu.2023.1251517

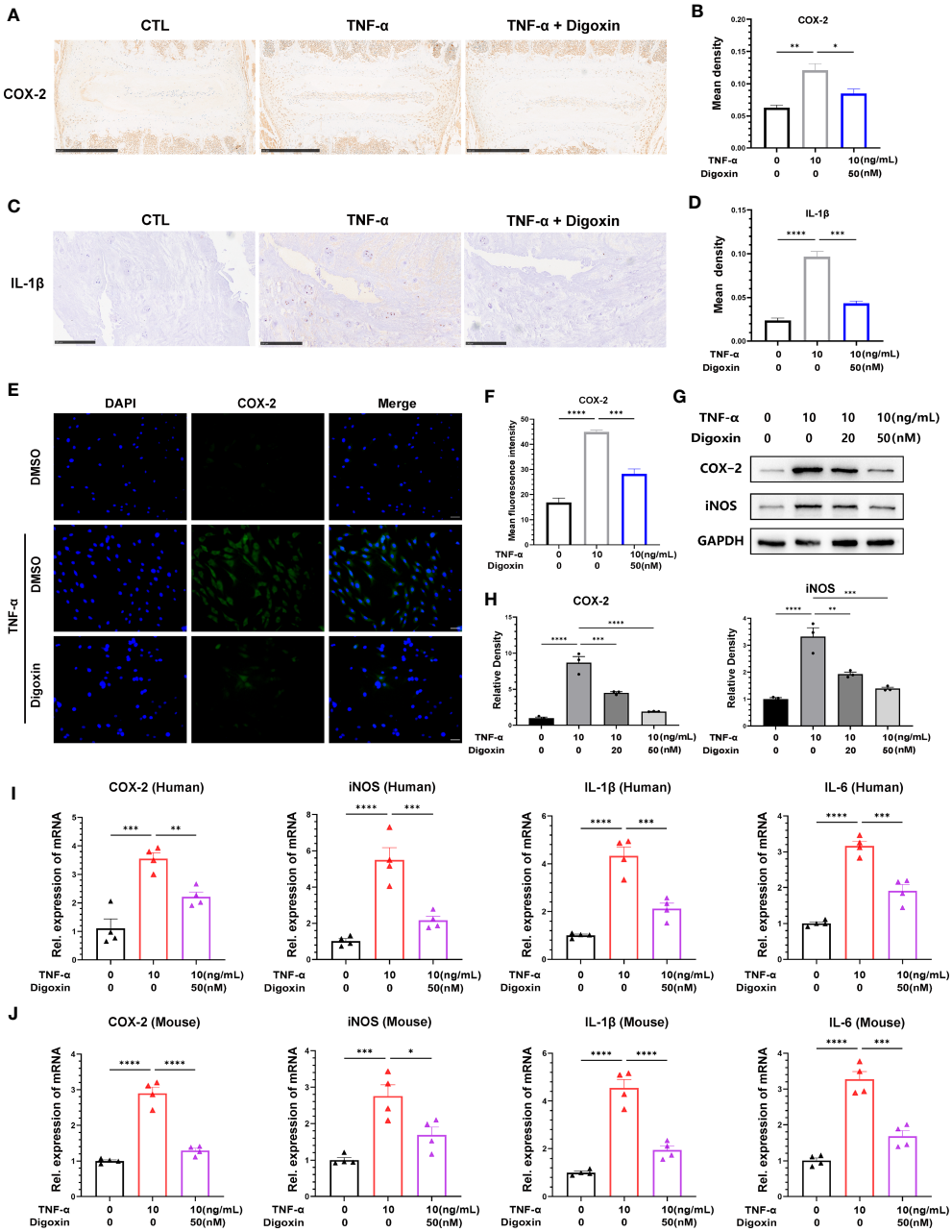

FIGURE 1
Digoxin inhibited TNF-α-induced inflammation in intervertebral disc. **(A)** Immunohistochemical staining of COX-2 in mouse disc tissues. The brown signal indicates positive. Scale bar = 500 μm. **(B)** The mean density of brown signal based on panel A; six groups of mice intervertebral disc tissues were used for observation. **(C)** Immunohistochemical staining of IL-1β in human disc tissues. The brown signal indicates positive. Scale bar = 250 μm. **(D)** The mean density of the brown signal based on panel **(C)**, six groups of human nucleus pulposus tissues were used for observation. **(E)** Immunofluorescence staining of COX-2 in human nucleus pulposus cells. Scale bar = 100 μm. **(F)** The mean density of green signal based on panel **(E)**. **(G)** The impact of different concentrations of digoxin on the protein expression of COX-2 and iNOS was assessed in human nucleus pulposus cells treated with 10 ng/mL TNF-α for 48 hours using Western blot analysis. **(H)** Relative density of bands based on Western blot. **(I, J)** The effect of digoxin on the transcriptional levels of COX-2, iNOS, IL-1β, and IL-6 was evaluated in human/mouse nucleus pulposus cells treated with 10 ng/mL TNF-α for 24 hours using Real-time PCR assay. The statistical analysis used ordinary one-way analysis of variance (ANOVA) to assess the differences between groups, followed by Tukey's multiple comparisons test as a *post hoc* analysis. The values shown above represent the mean ± standard error of the mean (SEM) * $P \leq 0.05$, ** $P \leq 0.01$, *** $P \leq 0.001$, **** $P \leq 0.0001$ versus the comparison group.

(Figures 1E, F). To further confirm this finding at the protein level, we isolated human nucleus NP for *in vitro* culture. As shown in Figures 1G, H, Western blot results showed upregulation in the protein expression of COX-2 and inducible nitric oxide synthase (iNOS) in the presence of TNF-α, while additional use of digoxin decreased their expression. Real-time PCR analysis on both human and mouse NP cells was conducted to determine transcriptional levels of proinflammatory cytokines. As Figures 1I, J indicate, digoxin significantly reduced TNF-α-induced cytokines mRNA expression, including COX-2, iNOS, IL-1β, and IL-6.

3.2 Digoxin protects against intervertebral disc from matrix destruction

We developed a rat puncture model to further investigate the protective effects of digoxin on IVDD. T2-weighted Magnetic Resonance Imaging (T2WI MRI) showed that the disc signal intensity and intervertebral space height of the digoxin-treated group rats were higher than those of the puncture group rats (Figure 2A). Subsequently, tissue samples were collected for histological staining and scoring. As shown in Figures 2B–E, intervertebral discs treated with digoxin displayed better histological morphology in H&E staining. Additionally, Safranin O/Fast Green staining demonstrated a reduction in loss of cartilaginous components in the intervertebral disc tissue after treatment with digoxin compared to the puncture group, which is considered a morphological manifestation of IVDD. Additionally, we also performed histological staining and scoring on mouse intervertebral discs cultured *ex vivo*. The results of H&E staining analysis indicated a significant reduction in histological scores for intervertebral discs treated with digoxin compared to the TNF-α stimulated group (Figures 2F, G). Furthermore, Safranin O/Fast Green staining showed that digoxin reduced the decrease in cartilage content induced by TNF-α in mouse intervertebral discs (Figures 2H, I).

The extracellular matrix (ECM) of the NP is mainly maintained by type II collagen (Col-2) and Aggrecan in a healthy state, and ECM degradation is crucial for disc degeneration. To explore the effect of digoxin on the regulation of ECM degradation in intervertebral discs, we performed *ex vitro*-cultured mouse intervertebral discs and human NP tissues. As shown in Figures 3A, B, digoxin downregulated the TNF-α-induced increase of A Disintegrin And Metalloproteinase with ThromboSpondin motif 5 (ADAMTS-5) in the mouse intervertebral disc. Figures 3C, D demonstrated that digoxin inhibited the TNF-α-mediated expression of matrix metallopeptidase 13 (MMP-13) in human disc tissue. The cell immunofluorescence staining for MMP-13 in primary HNPCs also showed that digoxin suppressed TNF-α-mediated acceleration of ECM degradation metalloproteinase MMP-13 (Figures 3E, F). A Western blot assay was performed to investigate the involved molecular mechanism further. As shown in Figures 3G, H, TNF-α increased MMP-13 and ADAMTS-5 levels, and additional use of digoxin showed decreased expression of metalloproteinases. Figure 3I demonstrated that digoxin significantly reduced TNF-α-induced the expression of ECM degradation metalloproteinases, including MMP-13 and ADAMTS-4, in both mouse and human NP cells. These findings suggest digoxin reduced TNF-α-mediated matrix metalloproteinase expression, leading to decreased matrix destruction.

To confirm the defensive impact of digoxin on ECM degradation mediated by TNF-α, we directly measured the expression levels of Col-2 and Aggrecan. As illustrated in Figures 4A, B, *ex-vivo* culture of murine discs revealed significant inhibition of Col-2 loss by digoxin. Additionally, in human disc tissue, TNF-α dramatically caused Aggrecan loss, but the process was effectively reversed by digoxin (Figures 4C, D). To address the involved pathway, primary human NP cells were cultured. Figures 4E, F revealed that digoxin significantly reversed TNF-α-mediated Col-2 and Aggrecan loss *in vitro* by Western blot assay. Accordingly, Real-time PCR was performed in human and mouse NP cells to determine the transcriptional level change. As revealed in Figures 4G, H, digoxin effectively reversed the decreased expression of Col-2 and Aggrecan after TNF-α stimulation.

Collectively, digoxin exerted its matrix protective effect by inhibiting destructive metalloproteinase and rescuing TNF-α-mediated matrix loss.

3.3 Digoxin inhibits TNF-α-induced nucleus pulposus cell apoptosis

It is thought that NP cells apoptosis plays a key role in disc degeneration. We hypothesized whether digoxin could counteract TNF-α-induced apoptosis of NP cells. To address this issue, we examined the apoptosis-related proteins in HNPCs with or without digoxin in the presence or absence of TNF-α. As shown in Figures 5A, B, digoxin rescued the TNF-α-mediated increased Bcl-2-associated X protein (Bax) and Cleaved-Caspase3 (C-Caspase3) levels and restored the expression of B-cell lymphoma 2 (Bcl-2) in the presence of TNF-α. Real-time PCR results for human and mouse NP cells showed that Bcl-2 mRNA levels increased with the additional use of digoxin compared to the TNF-α-stimulated group. However, Bax and Caspase3 transcriptional levels decreased with digoxin treatment (Figures 5C, D). Immunofluorescence staining for C-Caspase3 showed that HNPCs treated with digoxin had lower fluorescence intensity compared to those stimulated with TNF-α (Figures 5E, F). TUNEL (terminal deoxynucleotidyl transferase nick end labeling) is a frequently used method to detect DNA fragments, a hallmark of apoptotic cell death. As shown in Figures 5G, H, TUNEL staining of HNPCs demonstrated that digoxin reduced TNF-α-induced DNA fragmentation and inhibited HNPCs apoptosis.

3.4 Digoxin suppressed TNF-α-mediated inflammation via NF-κB signaling

NF-κB signaling plays a critical role in the pathogenesis of IVDD by triggering inflammation, ECM degradation, and cell death. Owing to the ability of digoxin to counteract TNF-α-induced disc degeneration, we then sort to determine the underlying mechanism. As shown in Figure 6A, TNF-α strongly activated the phosphorylation of p65 and effectively reduced TNF-α-induced p65 phosphorylation. Furthermore, cytoplasmic and nuclear proteins were extracted from HNPCs for Western blotting. The results showed that TNF-α stimulation caused a time-dependent decrease in cytoplasmic p65 expression and an increase in nuclear p65 expression, while digoxin treatment significantly attenuated this trend (Figure 6B). Immunofluorescence staining showed that digoxin significantly inhibited TNF-α-induced nuclear translocation of p65 in HNPCs, further confirming the effect of digoxin on TNF-α-mediated activation of the NF-κB pathway (Figure 6C).

10.3389/fimmu.2023.1251517

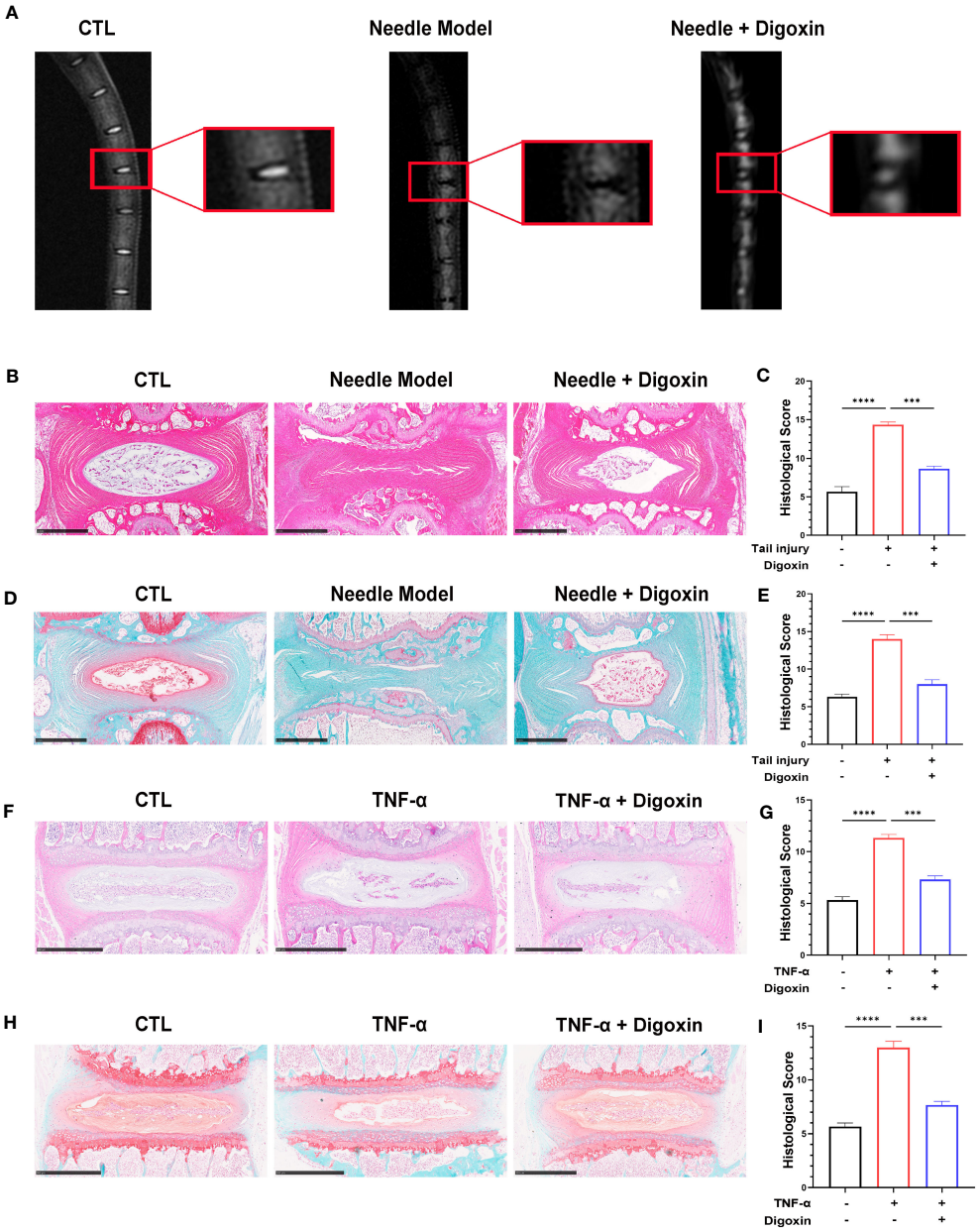

FIGURE 2
Digoxin alleviated intervertebral disc degeneration in the murine model. **(A)** T2WI MRI images of rat intervertebral discs after establishing the puncture model—each group comprised six adult rats aged eight weeks old. **(B)** Hematoxylin and Eosin (H&E) staining of rat intervertebral discs puncture model. Scale bar = 1 mm. **(C)** Histological score assessment based on H&E staining. **(D)** Safranin O and Fast Green staining of rat intervertebral discs puncture model. Scale bar = 1 mm. **(E)** Histological score assessment based on Safranin O and Fast Green staining. **(F, G)** H&E staining was conducted on mouse intervertebral disc tissue with or without TNF-α *ex vitro*, and histological scoring was performed to assess the tissue changes. Scale bar = 500 μm. **(H, I)** Safranin O and Fast Green staining was performed on mouse intervertebral disc tissue with or without TNF-α *ex vitro*, and histological scoring was conducted to evaluate the tissue changes. Scale bar = 500 μm. The intervertebral disc tissues of six groups of rats were used for observation. The statistical analysis employed ordinary one-way ANOVA to assess the differences between groups, followed by Tukey's multiple comparisons test as a *post hoc* analysis. The values shown above represent the mean ± SEM ***p < 0.001 and ****p < 0.001 versus the comparison group.

3.5 Digoxin promotes anabolism via AKT and ERK1/2 pathways

To determine whether digoxin can directly promote the anabolism in discs, we used culture media containing different concentrations of digoxin to culture primary HNPCs. As shown in Figure 7A, treatment with 20 nM and 50 nM digoxin significantly upregulated the transcriptional levels of Col-2 and Aggrecan. The MTT assay results demonstrated that the use of digoxin did not affect the viability of NP cells. Subsequently, HNPCs were cultured in a medium supplemented with 50 nM digoxin, and Alcian Blue staining was performed on days 3, 7, and 14. Following the addition of 50 nM digoxin, the expression levels of proteoglycans in NPCs were significantly upregulated on the 3rd, 7th, and 14th days.

10.3389/fimmu.2023.1251517

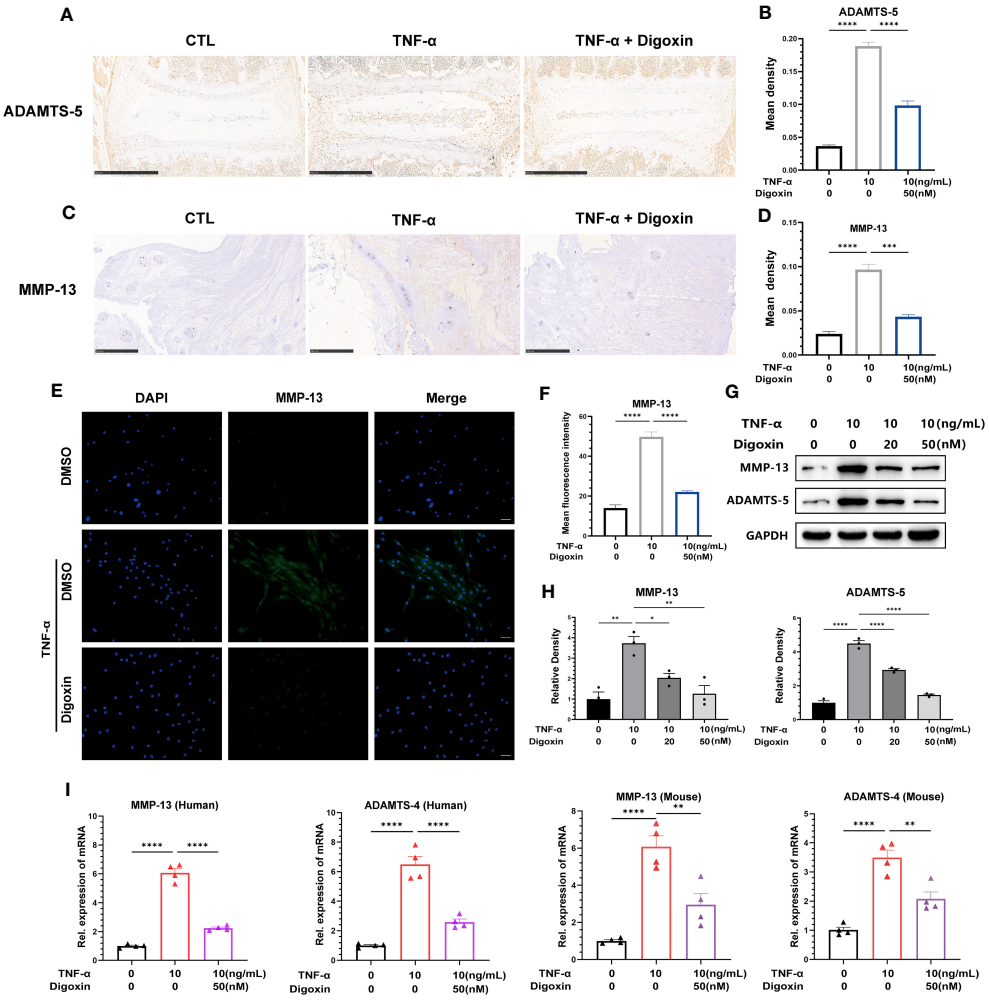

FIGURE 3
Digoxin inhibits TNF-α-mediated metalloproteinase expression in intervertebral discs. **(A)** Immunohistochemical staining analysis of ADAMTS-5 was conducted on *ex-vitro* mouse intervertebral disc tissues treated with 10 ng/mL TNF-α, with or without 50 nM digoxin. The brown signal indicates positive. Scale bar = 500 μm. **(B)** The mean density of brown signal based on panel A; six groups of mice intervertebral disc tissues were utilized for observation. **(C)** Immunohistochemical staining analysis of MMP-13 in human nucleus pulposus tissues cultured *ex vitro* under conditions of TNF-α treatment, with or without 50 nM Digoxin. The brown signal indicates positive. Scale bar = 250 μm. **(D)** The mean density of the brown signal based on panel C, six groups of human nucleus pulposus tissues were used for observation. **(E)** Immunofluorescence staining of MMP-13 in human nucleus pulposus cells in the presence or absence of 50 nM digoxin with or without TNF-α treatment. The green signal indicates positive. Scale bar = 100 μm. **(F)** The mean fluorescence intensity of green signal based on **(E)**. **(G)** Western blot analysis was performed to examine the expression of MMP-13 and ADAMTS-5 proteins in human nucleus pulposus cells treated with different concentrations of digoxin in the presence or absence of 10 ng/mL TNF-α. **(H)** Relative density of bands based on Western blot. **(I)** Real-time PCR assay was employed to assess the changes in transcriptional levels of MMP-13 and ADAMTS-4 in human and mouse nucleus pulposus cells, with or without 10 ng/mL TNF-α, and in the presence or absence of 50 nM digoxin. Ordinary one-way ANOVA was used to assess the differences between groups, followed by Tukey's multiple comparisons test as a *post hoc* analysis. The values shown above represent the mean ± SEM * $P \leq 0.05$, ** $P \leq 0.01$, *** $P \leq 0.001$, **** $P \leq 0.0001$ versus the comparison group.

Furthermore, these expression levels were higher compared to the control group, indicating a significant increase in proteoglycan expression induced by digoxin treatment (Figures 7B, C). The ERK1/2 and AKT pathways play crucial roles in regulating ECM synthesis (27, 28). To investigate whether the activation of the ERK1/2 and AKT pathways is involved in digoxin-mediated anabolism, we stimulated HNPCs with 50 nM digoxin and extracted total proteins at different time points, followed by Western blot analysis. The results depicted in Figure 7D demonstrated that AKT and ERK1/2 were phosphorylated by the addition of digoxin. To further confirm this finding, specific pathway inhibitors (U0126, Wortmannin) were added. As illustrated in Figure 7E, the phosphorylation of ERK1/2 and AKT decreased. Moreover, to confirm whether the pro-anabolism of digoxin depends on the activation of the ERK1/2 and AKT pathways, we pre-treated HNPCs with U0126 or Wortmannin for one hour, followed by treatment with 50 nM digoxin for 24 hours. The Real-time PCR results showed a decreased expression of Col-2 and Aggrecan at transcriptional levels, indicating that digoxin promotes ECM anabolism in HNPCs through the ERK1/2 and AKT pathways (Figure 7F).

10.3389/fimmu.2023.1251517

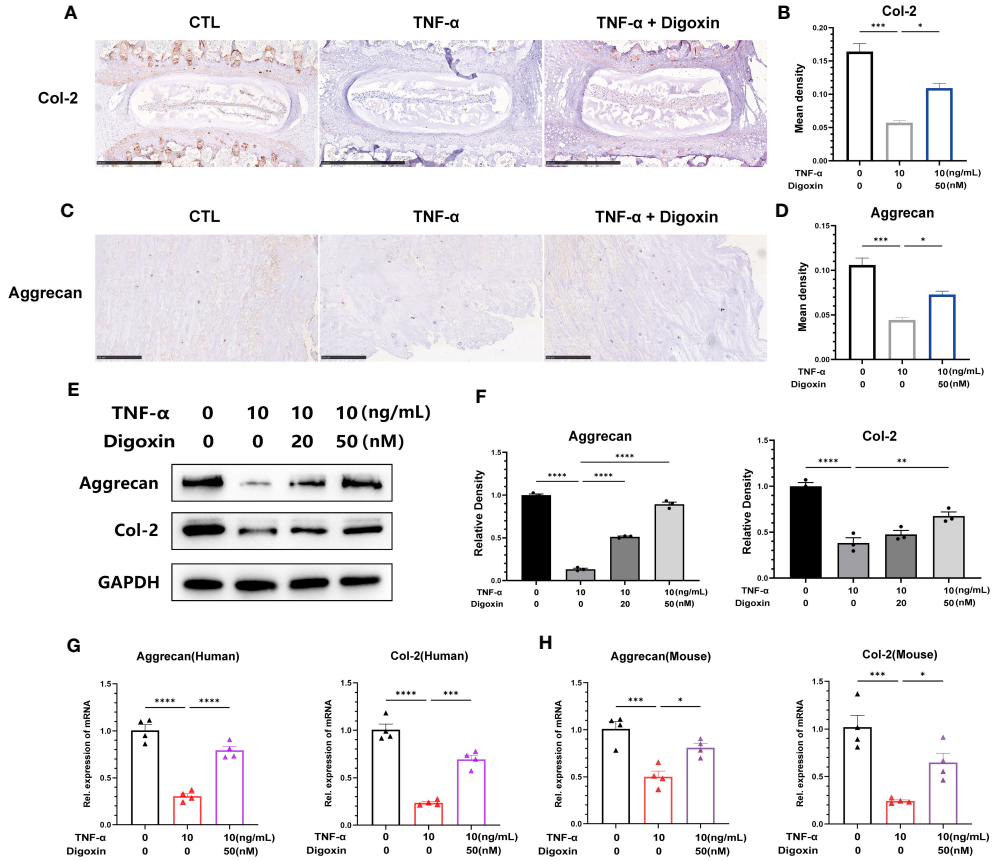

FIGURE 4
Digoxin attenuates TNF-α-mediated extracellular matrix loss in discs. **(A)** Immunohistochemical analysis of Col-2 in mouse disc tissue in the presence or absence of 10 ng/mL TNF-α, with or without 50 nM digoxin. The brown signal indicates positive. Scale bar = 500 μm. **(B)** The mean density of brown signal based on panel A; six groups of mice intervertebral disc tissues were used for observation. **(C)** Immunohistochemical analysis of Aggrecan in human disc tissue cultured in the presence or absence of 10 ng/mL TNF-α, with or without 50 nM digoxin. The brown signal indicates positive. Scale bar = 250 μm. **(D)** The mean density of the brown signal based on panel C, six groups of human nucleus pulposus tissues were used for observation. **(E)** Human nucleus pulposus cells were cultured *in vitro* and treated with or without 10 ng/mL TNF-α, along with 20 nM or 50 nM digoxin or without digoxin. Western blot analysis was employed to assess the protein levels of Col-2 and Aggrecan. **(F)** Relative density of bands based on Western blot. **(G, H)** Human or mouse nucleus pulposus cells were cultured *in vitro* in the presence or absence of 10 ng/mL TNF-α, with or without 50 nM digoxin. Real-time PCR analysis was performed to analyze the relative transcriptional levels of Col-2 and Aggrecan. Ordinary one-way ANOVA was used to assess the differences between groups, followed by Tukey's multiple comparisons test as a *post hoc* analysis. The values shown above represent the mean ± SEM * $P \leq 0.05$, ** $P \leq 0.01$, *** $P \leq 0.001$, **** $P \leq 0.0001$ versus the comparison group.

3.6 Digoxin protects against intervertebral disc degeneration target LRP4

Digoxin is a Na^+/K^+-ATPase inhibitor widely used in clinical practice, and its inhibitory effect on Na^+/K^+-ATPase is well-recognized. However, surprisingly, we have found that the protective effect exerted by digoxin seems to be unrelated to the inhibition of Na^+/K^+-ATPase (Supplementary Figure 1A). Low-density lipoprotein receptor-related protein 4 (LRP4) is a transmembrane protein involved in various cellular processes, including cell adhesion, migration, and signal transduction (29, 30). Recent studies have indicated that LRP4 is a novel target involved in digoxin-mediated regulation of cartilage metabolism (22). The results from Figure 8A and Supplementary Figure 1B also demonstrate a decrease in LRP4 expression disc with increasing grades of IVDD. However, The results of the Western blot analysis showed that digoxin attenuated the degradation of LRP4 in the rat needle model (Supplementary Figure 1C). To investigate whether the protective effect of digoxin against disc degeneration depended on LRP4 protein, we cultured primary human NP and transfected siRNA to knock down LRP4. As shown in Figure 8B, HNPCs exhibited a significant LRP4 expression reduction. Then, the transfected cells were stimulated with TNF-α in the absence or presence of 50 nM digoxin. After 48 hours, total proteins were extracted for Western blot analysis. Figure 8C demonstrates that in the presence of digoxin, the siLRP4 group showed elevated expression of COX-2, iNOS, MMP-13, ADAMTS-5, and C-Caspase3, while the protein expression of Bcl-2 decreased. However, after restoring LRP4, this trend was reversed. Next, to determine whether the anti-inflammatory and ECM synthesis-promoting effects of digoxin depended on LRP4 protein, we used Western blotting for the signaling test. The Western blot results showed that LRP4 knockdown increased the phosphorylation of IκBa, while restoration of LRP4 expression rescued this process (Figure 8D). Meanwhile, inhibition of digoxin-mediated activation of ERK1/2 and AKT signaling was observed in LRP4-knockdown HNPCs. However, this inhibitory effect was attenuated when LRP4 was restored (Figure 8D). Next, we

10.3389/fimmu.2023.1251517

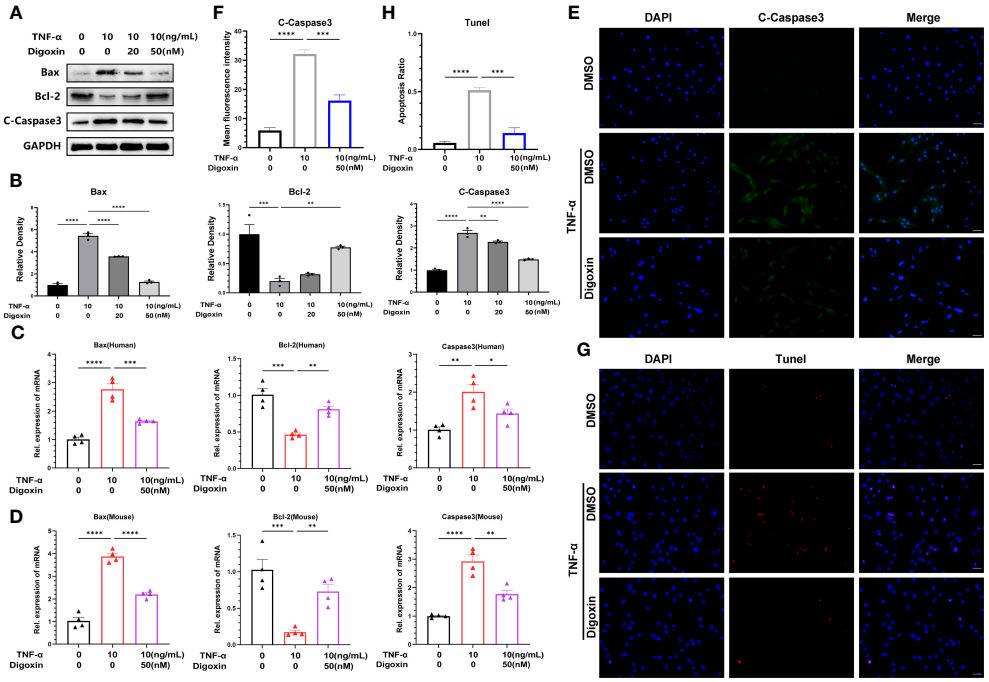

FIGURE 5
Digoxin inhibits TNF-α-induced apoptosis of nucleus pulposus cells. **(A, B)** The changes in Bax, Bcl-2, and Cleaved-Caspase3 proteins were assessed by Western blot analysis in human nucleus pulposus cells cultured *in vitro* and treated with 10 ng/mL TNF-α, with various concentrations of Digoxin. **(C, D)** Real-time PCR was performed to evaluate the relative mRNA levels of Bax, Bcl-2, and Caspase3 in human or mouse nucleus pulposus cells in the presence or absence of 10 ng/mL TNF-α, with or without 50 nM Digoxin. **(E, F)** Immunofluorescence analysis was conducted to examine the protein expression of Cleaved-Caspase3 in human nucleus pulposus cells stimulated with TNF-α, with or without 50 nM Digoxin. Scale bar = 100 μm. **(G, H)** TUNEL staining was used to analyze the nuclear DNA fragmentation in human nucleus pulposus cells treated with 50 nM digoxin following stimulation with 10 ng/mL TNF-α. Scale bar = 100 μm. Ordinary one-way ANOVA was used to assess the differences between groups, followed by Tukey's multiple comparisons test as a *post hoc* analysis. The values shown above represent the mean ± SEM * $P \leq 0.05$, ** $P \leq 0.01$, *** $P \leq 0.001$, **** $P \leq 0.0001$ versus the comparison group.

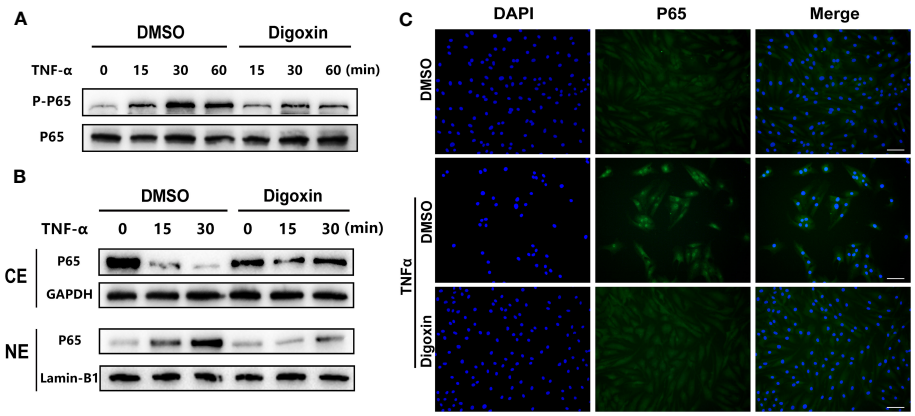

FIGURE 6
Digoxin suppressed TNF-α/NF-κB signaling pathway. **(A)** Human nucleus pulposus cells were treated with TNF-α in the presence or absence of 50 nM Digoxin. The total expression of p65 and phosphorylated p65 at various time points were analyzed by Western blot analysis. **(B)** Human nucleus pulposus cells were treated with TNF-α in the presence or absence of 50 nM digoxin. Nuclear and cytoplasmic protein was collected separately and followed by Western blot analysis for p65 expression. **(C)** Immunofluorescence staining of p65 protein in human nucleus pulposus cells after 30 minutes of TNF-α stimulation, in the presence or absence of 50 nM Digoxin. Scale bar = 100 μm.

10.3389/fimmu.2023.1251517

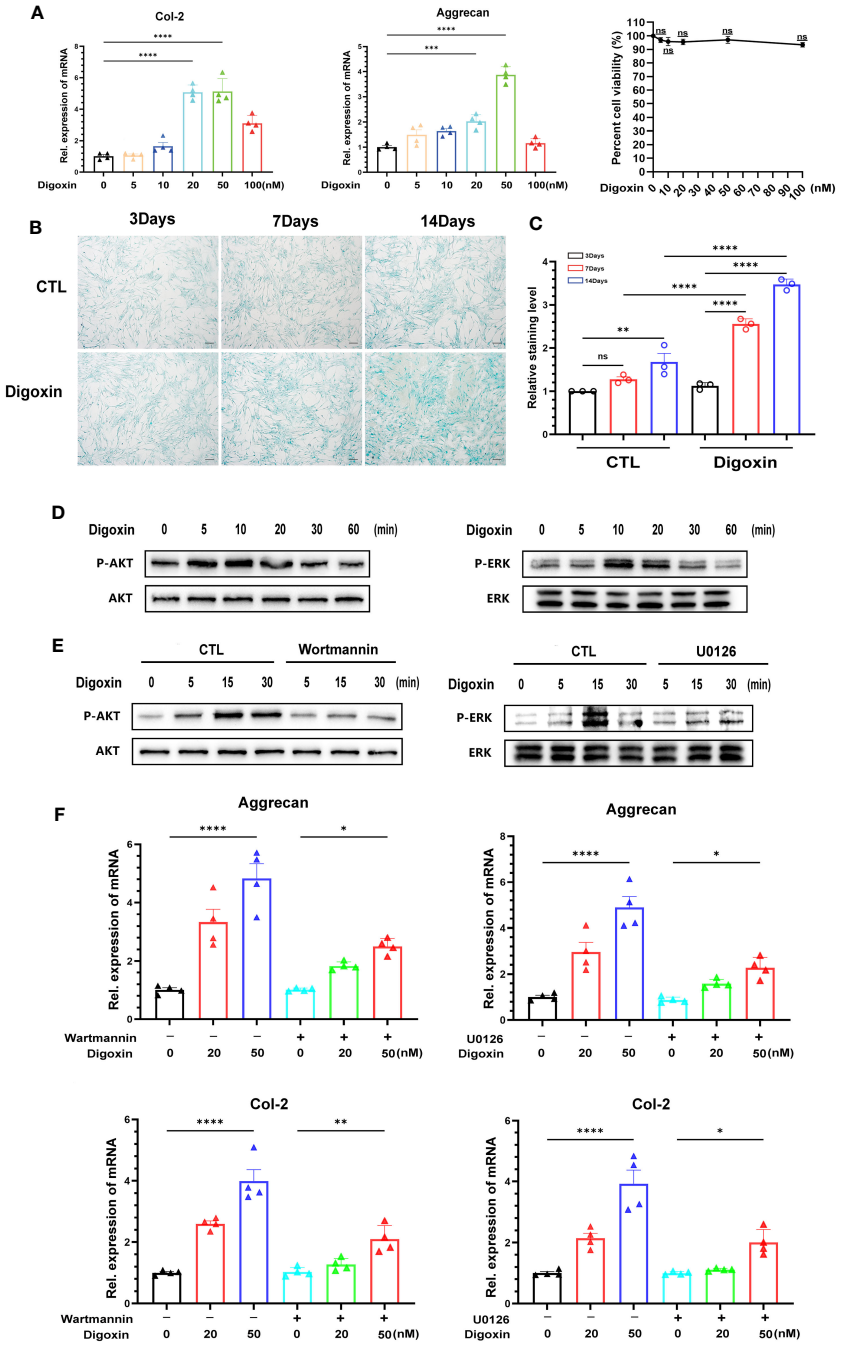

FIGURE 7
Digoxin promotes anabolism through AKT and ERK1/2 pathways. **(A)** Transcriptional levels of Col-2 and Aggrecan were assessed by Real-time PCR assay after 24 hours of treatment with different concentrations of digoxin in human nucleus pulposus cells. The impact of different digoxin concentrations on cell viability was analyzed using the MTT assay. **(B)** Alcian Blue staining was performed to analyze proteoglycan expression in human discs after treatment with 50 nM digoxin at days 3, 7, and 14. Scale bar = 200 μm. **(C)** The mean density of the blue signal is based on Alcian Blue staining. **(D)** Western blot analysis was conducted to evaluate the phosphorylation and total levels of AKT and ERK1/2 in human nucleus pulposus cells in the presence of 50 nM digoxin at various time points. **(E)** Phosphorylation and total levels of AKT and ERK1/2 in human nucleus pulposus cells at various time points in the presence of 50 nM digoxin with or without Wortmannin or U0126. **(F)** Transcriptional levels of Aggrecan and Col-2 in human nucleus pulposus cells treated with 50 nM digoxin, with or without Wortmannin or U0126. Ordinary one-way ANOVA was used to assess the differences between groups, followed by Tukey's multiple comparisons test as a *post hoc* analysis. The values shown above represent the mean ± SEM * $P \leq 0.05$, ** $P \leq 0.01$, *** $P \leq 0.001$, **** $P \leq 0.0001$ versus the comparison group. ns, no significance.

assessed the mRNA levels of inflammation and ECM metabolism-related genes in transfected HNPCs. Consistent with the protein level analysis, the Real-time PCR results revealed that LRP4 knockdown increased the mRNA levels of COX-2, iNOS, MMP-13, and ADAMTS-4, and a decrease in mRNA levels of Col-2 and Aggrecan in TNF-α-stimulated HNPCs. This trend was not reversed by prior treatment with digoxin. However, upon restoration of LRP4 expression, the digoxin-treated group exhibited a decrease in mRNA levels of COX-

10.3389/fimmu.2023.1251517

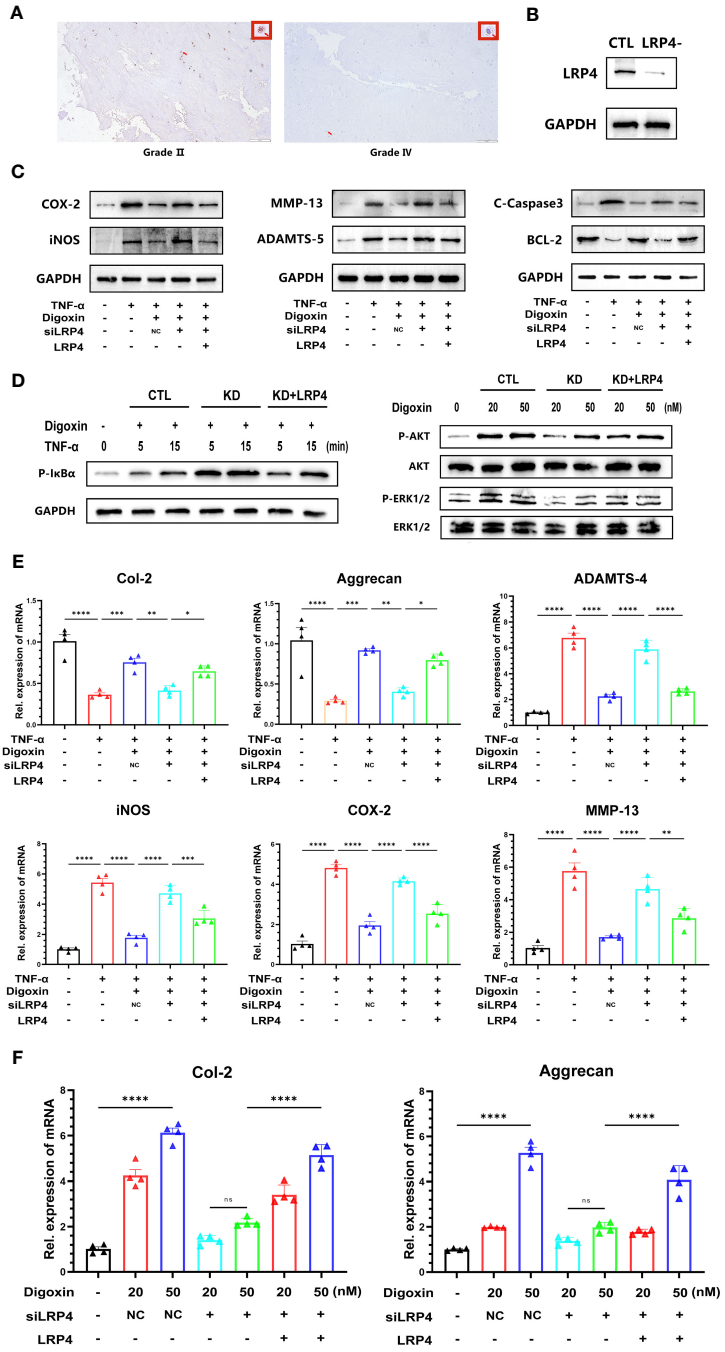

FIGURE 8
Digoxin protects against intervertebral disc degeneration via targeting LRP4. **(A)** Immunohistochemistry staining of LRP4 in human disc tissue. The first lane was from a Pfirrmann grade II disc, while the second lane was from a Pfirrmann grade IV disc. Scale bar = 200 μm. **(B)** Western blot analysis was conducted to examine the expression of LRP4 protein in primary human nucleus pulposus cells following siRNA transfection. **(C)** Western blot analysis was performed to evaluate the protein levels of COX-2, iNOS, MMP-13, ADAMTS-5, Bcl-2, and Cleaved Caspase-3 in human nucleus pulposus cells. LRP4 knockdown, KD, Negative control, NC. **(D)** Western blot for phosphorylated and total IκBα, phosphorylated and total AKT, and phosphorylated and total ERK1/2 after LRP4 knockdown and backup. GAPDH was examined as an internal control. **(E)** Real-time PCR assay was used to detect transcriptional levels of Col-2, Aggrecan, ADAMTS-4, iNOS, COX-2, and MMP-13 in primary human nucleus pulposus cells with LRP4 knockdown or LRP4 expression recovery, with or without treatment of 10 ng/mL TNF-α and with or without 50 nM digoxin. **(F)** Real-time PCR assay was used to analyze transcriptional levels of Col-2 and Aggrecan in human nucleus pulposus cells with LRP4 knockdown or LRP4 backup after treatment with different concentrations of digoxin. Ordinary one-way ANOVA was used to assess the differences between groups, followed by Tukey's multiple comparisons test as a *post hoc* analysis. The values shown above represent the mean ± SEM * $P \leq 0.05$, ** $P \leq 0.01$, *** $P \leq 0.001$, **** $P \leq 0.0001$ versus the comparison group. ns, no significance.

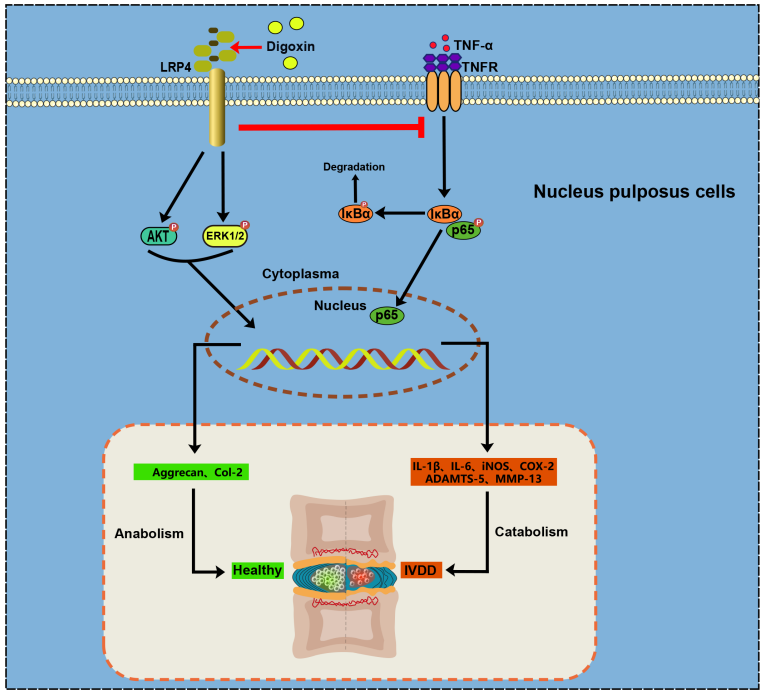

FIGURE 9
Proposal for Digoxin in intervertebral disc degeneration.

2, iNOS, MMP-13, and ADAMTS-4 compared to the siLRP4 group, while the mRNA levels of Col-2 and Aggrecan increased (Figure 8E). Finally, we treated transfected HNPCs with different concentrations of digoxin for 24 hours and measured the mRNA levels of Col-2 and Aggrecan. As depicted in Figure 8F, after LRP4 knockdown, the stimulatory effect of digoxin on the upregulation of Col-2 and Aggrecan mRNA expression was significantly inhibited, but this effect was reversed after restoring LRP4.

4 Discussion

IVDD is a significant contributor to back pain and disability worldwide (2, 31). It involves an imbalance between anabolic and catabolic processes (32). Progressive degradation of the ECM ensues in the course of IVDD, accompanied by an augmentation of cellular apoptosis and a concomitant exacerbation of inflammatory responses (32, 33). This multifaceted pathological process underscores the necessity of comprehensive therapeutic strategies that address these pivotal aspects of IVDD (33).

Pharmacological approaches for IVDD have been extensively investigated, but the development of effective therapeutics remains challenging (7, 34) chiefly due to the complexity of the mechanisms involved in IVDD. Moreover, most current pharmacological treatments for disc degeneration mainly focus on managing symptoms and reducing inflammation (35, 36). Consequently, the discovery of drugs that can modify the disease course is of paramount importance. Our study sheds light on the potential of digoxin in addressing this unmet need.

The pathophysiology of IVDD is significantly influenced by the TNF-α and NF-κB signaling pathways (36, 37). TNF-α, a potent proinflammatory cytokine, is responsible for the initiation and progression of disc degeneration by stimulating the NF-κB pathway, which promotes inflammation, ECM degradation, and apoptosis. TNF-α upregulates key mediators of inflammation and catabolic activities, such as COX-2, iNOS, and IL-1β (8, 13). The results of our study indicate that digoxin may have anti-inflammatory properties, as evidenced by its ability to inhibit the upregulation of COX-2 and iNOS induced by TNF-α, as well as its ability to reduce the expression of IL-1β in the intervertebral disc. These findings suggest that digoxin has the potential to mitigate the inflammatory response associated with IVDD.

Aggrecan and Col-2 are crucial components of the ECM in the intervertebral disc, responsible for maintaining hydration, compressive resistance, and structural integrity (38, 39). Dysregulation of Aggrecan and Col-2 contributes to the breakdown of the disc (40). The loss of these constituents is a major feature of IVDD. The degradation of Col-2 and Aggrecan is attributed to the upregulation of MMPs, specifically MMP-13, and A Disintegrin and Metalloproteinase with Thrombospondin Motifs (ADAMTS), specifically ADAMTS-4/5. Our findings revealed that digoxin treatment inhibited the upregulation of MMP-13 and ADAMTS4/5 induced by TNF-α, leading to restoration of the expression of Col-2 and Aggrecan, indicating its potential role in inhibiting ECM degradation in disc degeneration. Besides matrix degradation metalloproteinase, it is reported digoxin alone exerts strong anabolic promotive effects in the cartilage repair process. Given this importance, the present study found digoxin has a dual

effect on IVDD by inhibiting catabolic destruction and promoting anabolism.

Apoptosis, or programmed cell death, is a prominent feature of disc degeneration. Increased apoptotic activity in NP cells contributes to the loss of cellularity and ECM components in the disc (41). When TNF-α is present in excessive amounts, as is often the case in pathological conditions like disc degeneration, it can lead to an increase in Bax and a decrease in Bcl-2, tipping the balance toward apoptosis. Caspase-3 operates as a pivotal executioner in the apoptosis pathway, becoming activated in the aftermath of apoptotic initiation (13). Our findings revealed that digoxin treatment downregulated TNF-α-induced apoptosis in NP cells, as evidenced by the reduced expression of the pro-apoptotic protein Bax and decreased cleaved caspase-3 levels. This suggests a potential role of digoxin in inhibiting apoptosis and preserving the viability of NP cells in disc degeneration.

Throughout the course of IVDD, TNF-α plays a crucial role in regulating the inflammatory response and ECM metabolism by activating the NF-κB pathway. As a transcription factor, NF-κB modulates the expression of a wide range of genes associated with inflammation, such as COX-2, iNOS, and MMPs. Upon TNF-α stimulation, NF-κB is triggered and migrates into the cell nucleus, where it associates with specific DNA sequences, consequently promoting the synthesis and release of inflammatory mediators, provoking ECM degradation, and ultimately accelerating IVDD. Our investigation indicates that digoxin diminishes the phosphorylation of p65 protein post TNF-α treatment and significantly impedes the nuclear translocation of p65, highlighting the suppression of TNF-α induced activation of the NF-κB pathway by digoxin.

The ERK1/2 and AKT signaling pathways play crucial roles in regulating ECM synthesis and anabolism in NP cells (42). Activation of these pathways promotes the expression of anabolic factors, including Aggrecan and Col-2, and enhances ECM deposition. Interestingly, our study demonstrated that digoxin treatment activated the ERK1/2 and AKT pathways, leading to increased mRNA expression of Aggrecan and Col-2, suggesting its potential role in promoting ECM anabolism and counteracting the catabolic processes in disc degeneration. Furthermore, the ERK1/2 and AKT signaling pathways can modulate apoptosis in NPCs through diverse mechanisms. Digoxin, through its ability to activate the ERK1/2 and AKT pathways, potentially counteracts cellular apoptosis. Nevertheless, additional experiments are necessary to explore the reciprocal relationship between digoxin's demonstrated anti-apoptotic capabilities and these two pathways.

LRP4 acts as a transmembrane protein implicated in myriad cellular processes, demonstrated to engage in the Agrin-mediated homeostasis of chondrocytes. Antecedent reports have depicted LRP4 as a therapeutic target for digoxin in osteoarthritis treatment (22), while our research reveals a correlation between its dysregulation and IVDD. As the severity of IVDD intensifies, a parallel decline in the expression of LRP4 in the NP tissues is observed. When LRP4 is knockdown, the capacity of digoxin to counteract the inflammation and ECM degradation mediated by the TNF-α/NF-κB pathway weakens, and its ability to stimulate ECM anabolism via the ERK1/2 and AKT pathways is obstructed. However, these effects were reversed after restoring LRP4 expression, suggesting that LRP4 could potentially serve as a latent target for digoxin in protecting against IVDD.

In conclusion, our findings underscore the potential of digoxin as a multifaceted therapeutic agent for IVDD (Figure 9). It appears capable of modulating inflammation, promoting ECM anabolism, and decreasing apoptosis. The suggested involvement of LRP4 in these processes provides a new direction for further research into the molecular mechanisms underlying IVDD and its treatment.

Data availability statement

The original contributions presented in the study are included in the article/Supplementary Material. Further inquiries can be directed to the corresponding authors.

Ethics statement

The studies involving humans were approved by Medical Ethics Committee at Qilu Hospital of Shandong University. The studies were conducted in accordance with the local legislation and institutional requirements. The participants provided their written informed consent to participate in this study. The animal study was approved by Animal Experimentation Center of Shandong University. The study was conducted in accordance with the local legislation and institutional requirements.

Author contributions

QM: Performed the experiments, analyzed data, and draft manuscript. KL: draft manuscript, established animal models. ZL: Analyzed and interpreted the data. JL: Maintained the mice and primary cells. ZT and SQ: collected tissues and achieved MRI scans. JW and LC: Conceived and designed the experiments, draft the manuscript. We confirm that the order of authors listed in the manuscript has been approved by all of us. We further confirm that all authors have read and approved the final version of the manuscript, have agreed to its submission for publication, and accept accountability for all aspects of the work in ensuring that questions related to the accuracy or integrity of any part of the work are appropriately investigated and resolved.

Funding

This study received funding from the National Natural Science Foundation of China (82272548). Funds supporting this research also include the Natural Science Foundation of Shandong Pvince, China (ZR2023MH194, ZR2022MH019).

Acknowledgments

Our study demonstrated that Digoxin may have a positive effect on the cells within intervertebral discs, encouraging their natural

repair mechanisms while simultaneously slowing down the process that contributes to their breakdown. This two-pronged approach might offer a new, non-invasive treatment option for those affected by this degenerative condition.

Conflict of interest

The authors declare that the research was conducted in the absence of any commercial or financial relationships that could be construed as a potential conflict of interest.

Publisher's note

All claims expressed in this article are solely those of the authors and do not necessarily represent those of their affiliated organizations, or those of the publisher, the editors and the reviewers. Any product that may be evaluated in this article, or claim that may be made by its manufacturer, is not guaranteed or endorsed by the publisher.

Supplementary material

The Supplementary Material for this article can be found online at: https://www.frontiersin.org/articles/10.3389/fimmu.2023.1251517/full#supplementary-material

SUPPLEMENTARY FIGURE 1

(A) Human nucleus pulposus cells were subjected to treatment with or without 0.1 μM Istaroxime hydrochloride in the presence of 50 nM Digoxin for a duration of 24 hours, following which, the mRNA levels related to COX-2, iNOS, MMP-13, ADAMTS-4, Aggrecan, and Col-2 were evaluated using Real-time PCR. **(B)** Western blot and Real-time PCR analyses were employed to investigate the expression levels of LRP4 in human nucleus pulposus cells of varying Pfirrmann grades (n=6). **(C)** Following euthanasia, rat nucleus pulposus cells were isolated for ex vivo cultivation in the control group, needle surgery group, and the group receiving 50 nM Digoxin treatment post-needle surgery. Subsequently, Western blot analyses were conducted to ascertain the changes in LRP4 expression within rat nucleus pulposus cells (n=6). The statistical analysis employed ordinary one-way ANOVA to assess the differences between groups, followed by Tukey's multiple comparisons test as a *post hoc* analysis. The values shown above represent the mean ± SEM **p < 0.01, *** P ≤ 0.001, **** P ≤ 0.0001 versus the comparison group. ns, no significance.

References

1. Brown RB. Non-specific low back pain, dietary salt intake, and posterior lumbar subcutaneous edema. *Int J Environ Res Public Health* (2022) 19(15):9158. doi: 10.3390/ijerph19159158

2. Knezevic NN, Candido KD, Vlaeyen JWS, Van Zundert J, Cohen SP. Low back pain. *Lancet* (2021) 398(10294):78–92. doi: 10.1016/S0140-6736(21)00733-9

3. Ferreira ML, De Luca K, Haile LM, Steinmetz JD, Culbreth GT, Cross M, et al. Global, regional, and national burden of low back pain, 1990–2020, its attributable risk factors, and projections to 2050: a systematic analysis of the Global Burden of Disease Study 2021. *Lancet Rheumatol* (2023) 5(6):e316–e29. doi: 10.1016/S2665-9913(23)00098-X

4. James SL, Abate D, Abate KH, Abay SM, Abbafati C, Abbasi N, et al. Global, regional, and national incidence, prevalence, and years lived with disability for 354 diseases and injuries for 195 countries and territories, 1990–2017: a systematic analysis for the Global Burden of Disease Study 2017. *Lancet* (2018) 392(10159):1789–858. doi: 10.1016/S0140-6736(18)32279-7

5. Zehra U, Tryfonidou M, Iatridis JC, Illien-Jünger S, Mwale F, Samartzis D. Mechanisms and clinical implications of intervertebral disc calcificat ion. *Nat Rev Rheumatol* (2022) 18(6):352–62. doi: 10.1038/s41584-022-00783-7

6. Ashinsky B, Smith HE, Mauck RL, Gullbrand SE. Intervertebral disc degeneration and regeneration: a motion segment pe rspective. *Eur Cells Materials* (2021) 41:370–80. doi: 10.22203/eCM.v041a24

7. Liu K, Wei J, Li G, Liu R, Zhao D, Zhang Y, et al. Fexofenadine protects against intervertebral disc degeneration through TNF signaling. *Front Cell Dev Biol* (2021) 9:687024. doi: 10.3389/fcell.2021.687024

8. Yu H, Zhang Z, Wei F, Hou G, You Y, Wang X, et al. Hydroxytyrosol ameliorates intervertebral disc degeneration and neurop athic pain by reducing oxidative stress and inflammation. *Oxid Med Cell Longevity* (2022), 2240894. doi: 10.1155/2022/1835900

9. Francisco V, Pino J, González-Gay MÁ, Lago F, Karppinen J, Tervonen O, et al. A new immunometabolic perspective of intervertebral disc degeneration. *Nat Rev Rheumatol* (2022) 18(1):47–60. doi: 10.1038/s41584-021-00713-z

10. Pinto EM, Neves JR, Laranjeira M, Reis J. The importance of inflammatory biomarkers in non-specific acute and chronic low back pain: a systematic review. *Eur Spine J* (2023). doi: 10.1007/s00586-023-07717-1

11. Zhang C, Tong T, Miao D-C, Wang L-F. Vitamin D inhibits TNF-α induced apoptosis of human nucleus pulposus cells through regulation of NF-kB signaling pathway. *J Orthopaedic Surg Res* (2021) 16(1):411. doi: 10.1186/s13018-021-02545-9

12. Dong X, Yang C, Luo Y, Dong W, Xu X, Wu Y, et al. USP7 Attenuates Endoplasmic Reticulum Stress and NF-κB Signalin g to Modulate Chondrocyte Proliferation, Apoptosis, and Inflammatory R esponse under Inflammation. *Oxid Med Cell Longevity* (2022), 1835900. doi: 10.1155/2022/1835900

13. Chen S, Lei L, Li Z, Chen F, Huang Y, Jiang G, et al. Grem1 accelerates nucleus pulposus cell apoptosis and intervertebral disc degeneration by inhibiting TGF-β-mediated Smad2/3 phosphorylation. *Exp Mol Med* (2022) 54(4):518–30. doi: 10.1038/s12276-022-00753-9

14. Gerakaris A, Mulita F, Koniari I, Artopoulou E, Mplani V, Tsigkas G, et al. Digoxin impact on heart failure patients with atrial fibrillation. *Med Arch* (2022) 76(1):23–8. doi: 10.5455/medarh.2022.76.23-28

15. Ambrosy AP, Butler J, Ahmed A, Vaduganathan M, van Veldhuisen DJ, Colucci WS, et al. The use of digoxin in patients with worsening chronic heart failure: r econsidering an old drug to reduce hospital admissions. *J Am Coll Cardiol* (2014) 63(18):1823–32. doi: 10.1016/j.jacc.2014.01.051

16. Ke Y-S, Wang H-G, Wang D-G, Zhang G-B. Endoxin-mediated myocardial ischemia reperfusion injury in rats in vit ro. *Can J Physiol Pharmacol* (2004) 82(6):402–8. doi: 10.1139/y04-041

17. Ziff OJ, Kotecha D. Digoxin: The good and the bad. *Trends Cardiovasc Med* (2016) 26(7):585–95. doi: 10.1016/j.tcm.2016.03.011

18. Vamos M, Erath JW, Hohnloser SH. Digoxin-associated mortality: a systematic review and meta-analysis of the literature. *Eur Heart J* (2015) 36(28):1831–8. doi: 10.1093/eurheartj/ehv143

19. Saeed H, Mateen S, Moin S, Khan AQ, Owais M. Cardiac glycoside digoxin ameliorates pro-inflammatory cytokines in PB MCs of rheumatoid arthritis patients in *vitro*. *Int Immunopharmacol* (2020) 82:106331. doi: 10.1016/j.intimp.2020.106331

20. Tani S, Takano R, Tamura S, Oishi S, Iwaizumi M, Hamaya Y, et al. Digoxin attenuates murine experimental colitis by downregulating th17- related cytokines. *Inflammation Bowel Dis* (2017) 23(5):728–38. doi: 10.1097/MIB.0000000000001096

21. Shaker ME, Hamed MF, Shaaban AA. Digoxin mitigates diethylnitrosamine-induced acute liver injury in mice via limiting production of inflammatory mediators. *Saudi Pharm J* (2022) 30(3):291–9. doi: 10.1016/j.jsps.2022.01.007

22. Wang KD, Ding X, Jiang N, Zeng C, Wu J, Cai XY, et al. Digoxin targets low density lipoprotein receptor-related protein 4 and protects against osteoarthritis. *Ann Rheum Dis* (2022) 81(4):544–55. doi: 10.1136/annrheumdis-2021-221380

23. Zheng J, Wang J, Liu H, Chen F, Wang H, Chen S, et al. Alarmins S100A8/A9 promote intervertebral disc degeneration and inflam mation-related pain in a rat model through toll-like receptor-4 and ac tivation of the NF-κB signaling pathway. *Osteoarthritis Cartilage* (2022) 30(7):998–1011. doi: 10.1016/j.joca.2022.03.011

24. Patel S, Gururani R, Jain S, Tripathi N, Paliwal S, Paliwal S, et al. Repurposing of digoxin in pain and inflammation: An evidence-based stu dy. *Drug Dev Res* (2022) 83(5):1097–110. doi: 10.1002/ddr.21935

25. Keorochana G, Johnson JS, Taghavi CE, Liao JC, Lee KB, Yoo JH, et al. The effect of needle size inducing degeneration in the rat caudal disc: evaluation using radiograph, magnetic resonance imaging, histology, and immunohistochemistry. *Spine J* (2010) 10(11):1014–23. doi: 10.1016/j.spinee.2010.08.013

26. Han B, Zhu K, Li F-C, Xiao Y-X, Feng J, Shi Z-L, et al. A simple disc degeneration model induced by percutaneous needle punctu re in the rat tail. *Spine* (2008) 33(18):1925–34. doi: 10.1097/BRS.0b013e31817c64a9

27. Duan L, Ma B, Liang Y, Chen J, Zhu W, Li M, et al. Cytokine networking of chondrocyte dedifferentiation in *vitro* and its implications for cell-based cartilage therapy. *Am J Transl Res* (2015) 7(2):194–208.

28. Sun K, Luo J, Guo J, Yao X, Jing X, Guo F. The PI3K/AKT/mTOR signaling pathway in osteoarthritis: a narrative review. *Osteoarthritis Cartilage* (2020) 28(4):400–9. doi: 10.1016/j.joca.2020.02.027

29. Yan M, Xiong M, Wu Y, Lin D, Chen P, Chen J, et al. LRP4 is required for the olfactory association task in the piriform co rtex. *Cell Biosci* (2022) 12(1):54. doi: 10.1186/s13578-022-00792-9

30. Jing H, Chen P, Hui T, Yu Z, Zhou J, Fei E, et al. Synapse-specific Lrp4 mRNA enrichment requires Lrp4/MuSK signaling, mu scle activity and Wnt non-canonical pathway. *Cell Biosci* (2021) 11(1):105. doi: 10.1186/s13578-021-00619-z

31. Hoy D, Bain C, Williams G, March L, Brooks P, Blyth F, et al. A systematic review of the global prevalence of low back pain. *Arthritis Rheum* (2012) 64(6):2028–37. doi: 10.1002/art.34347

32. Risbud M, Shapiro I. Role of cytokines in intervertebral disc degeneration: pain and disc content. *Nat Rev Rheumatol* (2014) 10(1):44–56. doi: 10.1038/nrrheum.2013.160

33. Khan AN, Jacobsen HE, Khan J, Filippi CG, Levine M, Lehman RA Jr., et al. Inflammatory biomarkers of low back pain and disc degeneration: a revi ew. *Ann NY Acad Sci* (2017) 1410(1):68–84. doi: 10.1111/nyas.13551

34. Lim S, An SB, Jung M, Joshi HP, Kumar H, Kim C, et al. Local delivery of senolytic drug inhibits intervertebral disc degenera tion and restores intervertebral disc structure. *Adv Healthc Mater* (2021) 11(2):e2101483. doi: 10.1002/adhm.202101483

35. Ohnishi T, Iwasaki N, Sudo H. Causes of and molecular targets for the treatment of intervertebral di sc degeneration: A review. *Cells* (2022) 11(3):394. doi: 10.3390/cells11030394

36. Chao-Yang G, Peng C, Hai-Hong Z. Roles of NLRP3 inflammasome in intervertebral disc degeneration. *Osteoarthritis Cartilage* (2021) 29(6):793–801. doi: 10.1016/j.joca.2021.02.204

37. Sun K, Zhu J, Yan C, Li F, Kong F, Sun J, et al. CGRP Regulates Nucleus Pulposus Cell Apoptosis and Inflammation via th e MAPK/NF-κB Signaling Pathways during Intervertebral Disc Dege neration. *Oxid Med Cell Longevity* (2021), 2958584. doi: 10.1155/2021/2958584

38. Liang H, Luo R, Li G, Zhang W, Song Y, Yang C. The proteolysis of ECM in intervertebral disc degeneration. *Int J Mol Sci* (2022) 23(3):1715. doi: 10.3390/ijms23031715

39. Xing H, Zhang Z, Mao Q, Wang C, Zhou Y, Zhou X, et al. Injectable exosome-functionalized extracellular matrix hydrogel for me tabolism balance and pyroptosis regulation in intervertebral disc dege neration. *J Nanobiotechnol* (2021) 19(1):264. doi: 10.1186/s12951-021-00991-5

40. Zhang G-Z, Liu M-Q, Chen H-W, Wu Z-L, Gao Y-C, Ma Z-J, et al. NF-κB signalling pathways in nucleus pulposus cell function and interv ertebral disc degeneration. *Cell Prolif* (2021) 54(7):e13057. doi: 10.1111/cpr.13057

41. Shi S, Kang XJ, Zhou Z, He ZM, Zheng S, He SS. Excessive mechanical stress-induced intervertebral disc degeneration is related to Piezo1 overexpression triggering the imbalance of autophagy/apoptosis in human nucleus pulpous. *Arthritis Res Ther* (2022) 24(1):119. doi: 10.1186/s13075-022-02804-y

42. Xu D, Jin H, Wen J, Chen J, Chen D, Cai N, et al. Hydrogen sulfide protects against endoplasmic reticulum stress and mitochondrial injury in nucleus pulposus cells and ameliorates intervertebral disc degeneration. *Pharmacol Res* (2017) 117:357–69. doi: 10.1016/j.phrs.2017.01.005

frontiers | Frontiers in Immunology

TYPE Original Research
PUBLISHED 21 November 2023
DOI 10.3389/fimmu.2023.1228122

Check for updates

OPEN ACCESS

EDITED BY
Chuan-ju Liu,
New York University, United States

REVIEWED BY
Anna Lisa Giuliani,
University of Ferrara, Italy
Krzysztof Guzik,
Jagiellonian University, Poland

*CORRESPONDENCE
Gilles Kaplanski
gilles.kaplanski@ap-hm.fr

†These authors have contributed equally to this work

RECEIVED 24 May 2023
ACCEPTED 27 October 2023
PUBLISHED 21 November 2023

CITATION
Cambon A, Rebelle C, Bachelier R, Arnaud L, Robert S, Lagarde M, Muller R, Tellier E, Kara Y, Leroyer A, Farnarier C, Vallier L, Chareyre C, Retornaz K, Jurquet A-L, Tran T-A, Lacroix R, Dignat-George F and Kaplanski G (2023) Macrophage IL-1β-positive microvesicles exhibit thrombo-inflammatory properties and are detectable in patients with active juvenile idiopathic arthritis. *Front. Immunol.* 14:1228122. doi: 10.3389/fimmu.2023.1228122

COPYRIGHT
© 2023 Cambon, Rebelle, Bachelier, Arnaud, Robert, Lagarde, Muller, Tellier, Kara, Leroyer, Farnarier, Vallier, Chareyre, Retornaz, Jurquet, Tran, Lacroix, Dignat-George and Kaplanski. This is an open-access article distributed under the terms of the Creative Commons Attribution License (CC BY). The use, distribution or reproduction in other forums is permitted, provided the original author(s) and the copyright owner(s) are credited and that the original publication in this journal is cited, in accordance with accepted academic practice. No use, distribution or reproduction is permitted which does not comply with these terms.

Macrophage IL-1β-positive microvesicles exhibit thrombo-inflammatory properties and are detectable in patients with active juvenile idiopathic arthritis

Audrey Cambon[1,2†], Charlotte Rebelle[1,3†], Richard Bachelier[1], Laurent Arnaud[4], Stéphane Robert[1], Marie Lagarde[1], Romain Muller[1,5], Edwige Tellier[1], Yéter Kara[1], Aurélie Leroyer[1], Catherine Farnarier[6], Loris Vallier[1], Corinne Chareyre[1], Karine Retornaz[3], Anne-Laure Jurquet[3], Tu-Anh Tran[7], Romaric Lacroix[1,4], Françoise Dignat-George[1,4] and Gilles Kaplanski[1,5*]

[1]Aix-Marseille University, Institut National de la Santé Et de la Recherche Médicale (INSERM), Institut National de la Recherche pour l'Agriculture et l'Environnement (INRAE), Centre de Recherche en CardioVasculaire et Nutrition (C2VN), Marseille, France, [2]Service de Médecine interne et d'Infectiologie, Hôpital d'Instruction des Armées (HIA) Sainte-Anne, Service de Santé des Armées (SSA), Toulon, France, [3]Service de Pédiatrie, Assistance Publique des Hôpitaux de Marseille (AP-HM), Hôpital Nord, Marseille, France, [4]Laboratoire d'Hématologie, Assistance Publique des Hôpitaux de Marseille (AP-HM), La Timone, Marseille, France, [5]Service de Médecine interne et d'Immunologie clinique, Assistance Publique des Hôpitaux de Marseille (AP-HM), La Conception, Marseille, France, [6]Laboratoire d'Immunologie, Assistance Publique des Hôpitaux de Marseille (AP-HM), La Conception, Marseille, France, [7]Service de Pédiatrie, Centre Hospitalo-Universitaire (CHU) Nîmes, Hôpital Carémeau, Nîmes, France

Objective: IL-1β is a leaderless cytokine with poorly known secretory mechanisms that is barely detectable in serum of patients, including those with an IL-1β-mediated disease such as systemic juvenile idiopathic arthritis (sJIA). Leukocyte microvesicles (MVs) may be a mechanism of IL-1β secretion. The first objective of our study was to characterize IL-1β-positive MVs obtained from macrophage cell culture supernatants and to investigate their biological functions *in vitro* and *in vivo*. The second objective was to detect circulating IL-1β-positive MVs in JIA patients.

Methods: MVs were purified by serial centrifugations from PBMCs, or THP-1 differentiated into macrophages, then stimulated with LPS ± ATP. MV content was analyzed for the presence of IL-1β, NLRP3 inflammasome, caspase-1, P2X7 receptor, and tissue factor (TF) using ELISA, Western blot, or flow cytometry. MV biological properties were studied *in vitro* by measuring VCAM-1, ICAM-1, and E-selectin expression after HUVEC co-culture and factor-Xa generation test was realized. *In vivo*, MVs' ability to recruit leukocytes in a murine model of peritonitis was evaluated. Plasmatic IL-1β-positive MVs were studied *ex vivo* in 10 active JIA patients using flow cytometry.

Results: THP-1-derived macrophages stimulated with LPS and ATP released MVs, which contained NLRP3, caspase-1, and the 33-kDa precursor and 17-kDa mature forms of IL-1β and bioactive TF. IL-1β-positive MVs expressed P2X7

receptor and released soluble IL-1β in response to ATP stimulation *in vitro*. In mice, MVs induced a leukocyte peritoneal infiltrate, which was reduced by treatment with the IL-1 receptor antagonist. Finally, IL-1β-positive MVs were detectable in plasma from 10 active JIA patients.

Conclusion: MVs shed from activated macrophages contain IL-1β, NLRP3 inflammasome components, and TF, and constitute thrombo-inflammatory vectors that can be detected in the plasma from active JIA patients.

KEYWORDS

microvesicles, IL-1β, NLRP3-inflammasome, tissue factor, juvenile idiopathic arthritis

1 Introduction

IL-1β is a major cytokine in innate immunity, involved in the pathogenesis of various rheumatic diseases, notably systemic juvenile idiopathic arthritis (sJIA). Juvenile idiopathic arthritis (JIA) is a generic term to define pediatric inflammatory arthritis of unknown cause, which may occur with different clinical presentations. JIA could present as oligoarthritis, polyarthritis with or without circulating rheumatoid factor, psoriatic arthritis, enthesitis-related arthritis, and sJIA. sJIA is a rare form of the disease (10% of JIA) with systemic symptoms such as arthralgia, fever, evanescent rash, and a major biological inflammatory syndrome with neutrophilic polynuclear leukocytosis, elevated C-reactive protein (CRP), and hyperferritinemia, reflecting hypercytokinemia IL-1; notably, it has been shown to play an important role in the pathogenesis of sJIA and at a lower degree in other forms of JIA, since blocking IL-1 using the recombinant form of the IL-1 receptor antagonist or anti-IL-1β monoclonal antibody is an efficient strategy (1, 2). However, circulating IL-1β is usually not detectable, in patients, using immunoassays.

IL-1β belongs to the IL-1 family of cytokines, which, except for the IL-1 receptor antagonist, lack a leader sequence and do not follow the classical Golgi apparatus secretory pathway. This may in part, explain the low detectable circulating concentrations in the serum from patients (3). After priming through TLR activation and gene transcription, IL-1β is synthesized as a 33-kDa precursor. After a second activation cell signal, such as P2X7 purinergic receptor activation by ATP, an intra-cytoplasmic protein complex called inflammasome is assembled by the association of a NOD-like-receptor (NLR), mainly NLRP3, an adaptor-protein (ASC) and pro-caspase-1 (4). NLRP3 assembly and activation lead to pro-caspase-1 auto-cleavage in active caspase-1, followed by the processing of the IL-1β precursor in its 17-kDa mature form. The same mechanism is involved in the processing of IL-18, another important IL-1 family member (5). Following or concomitantly with this step, several mechanisms of IL-1β secretion have been proposed (6, 7). One may involve secretory lysosomes, which may be similar to autophagosomes and are released by cells when cytoplasmic autophagy is inhibited (8–11). Another mechanism may involve secretion of HLA class II-positive exosomes (12). When cells are more strongly activated or for a longer period of time, caspase-1 may induce IL-1β processing and the cleavage of gasdermin-D, which, in turn, induces a new type of cell death called pyroptosis (13–16). In this case, the 17-kDa mature IL-1β is released out of the cells through membrane pores (17). In addition, IL-1β may be released via another kind cell death independent of caspase-1, called necroptosis (18).

A different way of IL-1β release, barely detectable by usual assays, may be due to the shedding of membrane microvesicles (MVs) (19–21). MVs are small membrane extracellular vesicles (0.1–1 μm) shed by various cells during activation or cell death (22). Their role as a vector of bioactive molecules has been suggested, since MVs bear cell-surface receptors, contain various cytosolic proteins including cytokines, signaling molecules, or RNA, depending on cell origin and the kind of stimulus that induces their formation (23). Exposure of phosphatidylserine (PS) resulting from loss of plasma membrane symmetry is essential for the formation of MVs and enables their detection by flow cytometry, using annexin-V labeling (24). MVs are thought to be involved in many processes such as coagulation, inflammation, and angiogenesis and have been identified as potential biomarkers of diseases with high vascular risk (25). Many cellular types can release MVs, among them myeloid cells (26). MVs issued from activated monocytes or macrophages have been shown to contain bioactive IL-1β *in vitro*; however, their pro-inflammatory functions *in vivo* as well as their detection in human diseases have not been reported to date. Here, we sought to evaluate IL-1β-positive MV pro-inflammatory functions, using *in vitro* and *in vivo* models and tried to detect them in patients with JIA, in a pilot study.

2 Materials and methods

2.1 Cell culture

The cells used were macrophages differentiated from THP-1 cells treated with phorbol myristate acetate (PMA, Sigma-Aldrich, USA) for 24 h or from peripheral blood mononuclear cells (PBMCs) treated with GM-CSF (Sargramostim, 50 ng/mL) for 7 days and human umbilical vein endothelial cells (HUVECs). All culture conditions are described in Supplementary Methods.

2.2 Generation, numeration, and characterization of MV population

Cell culture media issued from the different conditions of stimulation were collected and centrifuged at 300*g* for 10 min, to eliminate cellular debris. Supernatants were centrifuged at 4,500*g* for 10 min at 4°C to remove apoptotic bodies, then at 70,000*g* for 90 min to pellet MVs. MVs were washed with phosphate buffered saline (PBS), resuspended in PBS, and stored at −80°C until being used. MVs were analyzed using a Gallios flow cytometer (Beckman Coulter, USA). Protocol settings and gates as forward scatter by side scatter were adjusted by using 0.5-, 0.9-, and 3-µm Megamix beads (Biocytex, France), as previously described (27). Isolated MVs were stained with 250 µg/mL FITC-labeled annexin A5 Kit (Tau Technologies, the Netherlands) for 30 min at room temperature in the dark, before adding 500 µL of annexin-V-binding buffer and flow-counting beads (Biocytex, France) (28).

To detect the presence of IL-1β, MVs were permeabilized in PBS containing 0.2% saponin, which, at this low concentration, guaranteed preservation of the integrity of the MV phospholipid bilayer, and then incubated at 4°C for 1 h with 25 µg/mL Alexa Fluor 647 anti-human IL-1β antibody (BioLegend, clone JK-1B-1, Cat# 508207, RRID: AB_604133, USA) or 25 µg/mL Alexa Fluor 647 mouse IgG1 control isotype (BioLegend Cat# 400155, RRID: AB_2832978). After washing, permeabilized MVs were stained with annexin-V-FITC to separate MVs from background in flow cytometry analysis. The same permeabilization procedure was used for double labeling of IL-1β and P2X7R, with the further use of an anti-P2X7R rabbit monoclonal antibody (Cell Signaling Technology Cat# 13809, RRID: AB_2798319) or a control rabbit IgG (Cell Signaling Technology Cat# 2729, RRID: AB_1031062), followed by addition of Alexa 488-conjugated goat anti-rabbit IgG (Thermo Fisher Scientific Cat# A78953, RRID: AB_2925776).

2.3 Western blot experiments

Cells and MVs were lysed in buffer containing 20 mM tris, pH 7.5,150 µM NaCl, 2 mM EDTA pH 8, 0.1% NP40, and a cocktail of protease inhibitors (Thermo Fisher Scientific, USA). Protein concentrations were measured using the BCA protein assay kit (Thermo Fisher Scientific, USA). For Western blot analysis, equal amounts of proteins (15 to 30 µg) were separated on a 4%–12% gradient Novex gel (Thermo Fisher Scientific, Waltham, United States), and then transferred on nitrocellulose membranes (GE Healthcare, USA). Blots were blocked with TBST (150 mM NaCl, 50 mM Tris-HCl at pH 7.5, and 0.1% Tween 20) containing 5% BSA for 1 h, then probed with the following primary antibodies: mouse anti-human IL-1β 1:1,000 (3A6, Cell Signaling Technology Cat# 12242, RRID : AB_2715503), rabbit anti-caspase-1 p10 1:200 (Santa Cruz Biotechnology Cat# sc-515, RRID : AB_630975), rabbit anti-human caspase-1 1:200 (Santa Cruz Biotechnology Cat# sc-622, RRID : AB_2069053), mouse anti-human NLRP3 1:1,000 (Enzo Life Sciences Cat# ALX-804-819-C100, RRID : AB_2051972), rabbit anti-human P2X7 1:200 (Sigma-Aldrich Cat# P9122, RRID : AB_477418), rabbit anti-human tissue factor (TF) 1:1,000 (Abcam Cat# ab151748, RRID : AB_2814773), rabbit anti-human ICAM-1 1:1,000 (Cell Signaling Technology Cat# 4915, RRID : AB_2280018), rabbit anti-E-selectin 1:200 (Santa Cruz Biotechnology Cat# sc-14011, RRID : AB_2186684), and rabbit anti-human VCAM-1 1:200 (Santa Cruz Biotechnology Cat# sc-8304, RRID : AB_2214058). Membranes were then incubated with horseradish peroxidase-conjugated secondary antibodies (Thermo Fisher Scientific, USA), using ECL or ECL Plus substrates (Thermo Fisher Scientific, USA) and chemiluminescence detection system (G:Box, Synoptics, UK).

2.4 Cytokine assays

After the lysis of MVs by three freeze–thawing cycles, IL-1β concentrations were measured using a highly sensitive ELISA assay (IL-1 beta Human ELISA Kit, High Sensitivity, Life Technologies, Cat # BMS224HS USA). The same ELISA kit was used for measuring IL-1β concentration in blood samples.

2.5 Tissue factor activity

TF activity was measured using a Factor Xa generation assay, as previously described (29). MVs were resuspended in HEPES (Sigma, St Louis, United States), and then incubated in a 96-well plate with anti-TF monoclonal antibody (clone 183 SBTF-1, BioCytex, Marseille, France) or control isotype (clone a-DNP 2H11–2H12, BioCytex, Marseille, France) antibodies for 30 min. A reaction mix containing FVII, Factor X, and $CaCl_2$ (Sigma, St Louis, United States) was then added to each well to trigger the coagulation cascade and generate FXa. After 2 h of incubation, FXa activity was monitored by the addition of a fluorogenic substrate (factor Xa substrate, Stago 390/450nm, Biocytex, Marseille) (30) and fluorescence was measured, using a fluorimeter (Fluoroskan, Thermo Scientific, United States).

2.6 Transmission electronic microscopy

After thawing, MVs were centrifuged at 70,000*g* for 90 min at 4°C, then fixed in a PBS solution containing 2% paraformaldehyde and 0.2% glutaraldehyde. A 3-µL aliquot was applied on 100-mesh nickel formvar-coated grids (Euromedex, France). After 15 min, MVs were permeabilized with 3 µL of PBS–5% BSA–0.1% saponin for 1 h, then incubated for 1 h with anti-TF rabbit monoclonal antibody (Sigma-Aldrich clone 2L10 ZooMAb®, Cat# ZRB1811, RRID : AB_2938655) and anti-IL-1β mouse antibody (Cell Signaling Technology Cat# 12242, RRID : AB_2715503) diluted 1:25 in PBS–0.3% BSA. After three washes in PBS, MVs were labeled for 1 h with goat anti-rabbit IgG coupled with 10-nm gold beads (Thermo Fisher Scientific Cat# N-24916, RRID : AB_2539796) and goat anti-mouse IgG coupled with 5-nm gold beads (Tebu-Bio, Cat# 220GA1003, RRID : AB_2938656). Immunogold-labeled MVs were fixed for 5 min in cacodylate buffer containing 2.5% glutaraldehyde, then grids were negatively

stained with 0.3% phosphotungstic acid for 1 min, before observation with a transmission electron microscope (JEM 1400 JEOL, United States).

2.7 Endothelial cell activation by MVs

MVs isolated from macrophages were incubated with HUVECs for 4 h at 37°C. Cell pellets were labeled for 1 h with specific anti-ICAM-1/CD54-PE (Beckman Coulter Cat# IM1239U, RRID : AB_131186), anti-VCAM-1/CD106-PE (Beckman, A66085, RRID : AB_2938658), anti-E-selectin/CD62E-PE (BioLegend, HCD62E RRID : AB_2938659), or control isotype antibodies IgG1-PE (Beckman Coulter Cat# A07796, RRID : AB_2832963) and IgG2aκ-PE (BioLegend Cat# 400213, RRID : AB_2800438) (5 µL/reaction) for flow cytometry analysis. For Western blot experiments, cells were washed and scraped in PBS, centrifuged, and lysed in RIPA buffer.

2.8 Animal studies

Mice experiments were conducted according to the institutional ethical committees for animal care from the local animal ethics committee of Marseille. C57BL/6J mice received intraperitoneal injections of PBS or IL-1 receptor antagonist IL-1Ra (30 mg/kg), with or without subsequent one peritoneal injection of 25×10^6 MVs in PBS. Peripheral blood and peritoneal fluids were collected. The details of experimental conditions are described in Supplementary Methods.

2.9 Patient cohort

Ten patients with JIA according to the International League of Associations for Rheumatology (ILAR) definition were recruited from the Department of Paediatrics at Marseille and Nimes hospitals, during 2015–2016. Parents (or patient's legal guardians) and patients received information and consent of parents (or patient's legal guardians) was obtained for all individual participants included in the study. Clinical presentations consisted mainly in refractory polyarticular and systemic forms of the disease, but all patients presented active disease defined as AJI flare according to Juvenile Arthritis Disease Activity Score 10 (JADAS10). The main demographic, clinical, and biological characteristics are shown in Table 1. Ten healthy adult donors were also included.

2.10 Patient blood sampling and platelet-poor plasma preparation

Sampling was justified by the flare of the disease. A fasting blood sample was obtained by venipuncture in citrate-containing tubes, which were centrifuged twice at 2,500*g* for 15 min at room temperature in order to obtain platelet-poor plasma (PPP), within a maximum of 2 h after blood collection, as previously described (31). The resulting plasma was divided into aliquots and stored at −80°C until analysis.

2.11 Determination of patients' MV profile by flow cytometry

PPP aliquots were thawed at room temperature and centrifuged at 20,000*g* for 90 min to pellet MVs. Resuspended MVs (30 µL) were transferred into different tubes for MV labeling. Annexin V-FITC (Tau Technologies, the Netherlands) and conjugated antibodies (Ab) were added to identify specific MV subsets: CD31-Phycoerythrin (PE) Ab (Beckman Coulter Cat# IM2409, RRID : AB_131205), CD41-PC7 Ab (Beckman Coulter Cat# 6607115, RRID : AB_2800448), CD11b-APC Ab (Beckman Coulter Cat#A87782, RRID : AB_2938661), CD235a-Alexa 750 Ab (Beckman Coulter Cat# A89314, RRID : AB_2938662), CD14-APC Ab (Beckman Coulter Cat# IM2580, RRID : AB_2800451), CD66b-APC Ab (Beckman Coulter Cat# B08756, RRID : AB_2893284), and CD11b-PE Ab (Beckman Coulter Cat# IM2581U, RRID : AB_131334). The numeration of total MVs and MVs derived from specific cell subsets (absolute number/mL plasma) were calculated according to the acquired counts of MVs and microbeads and the dilution performed during sample preparation.

2.12 Statistical analysis

Data represent the cumulative results of all experiments and are expressed as median with interquartile range for the indicated number (n) of experiments. Statistical analysis was performed with Prism version 9 software. Significant differences were determined by using nonparametric Mann–Whitney and Wilcoxon test; p-values < 0.05 were considered statistically significant.

3 Results

3.1 MVs from stimulated macrophages contain NLRP3 inflammasome components necessary for caspase-1-dependent IL-1β processing

According to the Minimal Information for Studies of Extracellular Vesicles (MISEV) 2018 guidelines (32), MVs issued from THP-1 differentiated into macrophages by PMA treatment were then purified by successive centrifugations and ultracentrifugations (Figure 1A). MVs from unstimulated and stimulated macrophages were characterized using several methods. First, using flow cytometry, the classical gating strategy was determined (Supplementary Figure S1). Then, the presence of typical membranous and cytosolic MV-associated molecules was confirmed by detecting CD18 (integrin subunit β2) and Annexin-V

TABLE 1 Characteristics of patients with active juvenile idiopathic arthritis (JIA).

Patients	Age	Sex	Form	Time of Evolution	ANA	HLAB27	Clinical A.	Arthritis	Ocular Manifestation	Systemic A.	Biological A.	Current Treatment	Previous Treatment
1	16	F	polyA	16	–	neg	yes	hips knees	uveitis	no	CRP = 3 mg/L ESR = 13 mm HG normal	Abatacept + MTX	CS DMARDS Etanercept Adalimumab
2	9	F	polyA	3	–	neg	yes	hips knees ankles	no	no	CRP = 2 mg/L ESR = 3 mm HG normal	Tocilizumab	CS DMARDS Etanercept Adalimumab Abatacept Tocilizumab
3	13	M	oligoA	11	–	neg	yes	hips	no	fever rash	CRP = 3 mg/L ESR = 20 mm HG normal	Tocilizumab	CS DMARDS Etanercept Anakinra
4	10	M	polyA	2	–	neg	yes	cuffs hips	no	fever rash	CRP = 74 mg/L ESR = 30 mm PNN: 12,000/mm^3	CS	CS
5	16	F	polyA	5	RF + ANA + CCP +	neg	yes	ankles cuffs fingers	no	no	CRP = 2 mg/L ESR = 5 mm HG normal	Abatacept + MTX	CS DMARDS Adalimumab Etanercept Adalimumab + MTX Abatacept + MTX Tocilizumab
6	7	F	polyA	6	–	neg	yes	knees cuffs hips	uveitis	no	CRP = 3 mg/L ESR = 8 mm HG normal	Tocilizumab + MTX	CS DMARDS Etanercept Adalimumab Abatacept
7	16	F	polyA	14	–	neg	yes	elbows cuffs knees ankles fingers	no	fever rash	CRP = 3 mg/L ESR = 30 mm HG normal	Abatacept + MTX	CS DMARDS Etanercept + MTX Adalimumab + MTX Abatacept
8	5	M	polyA	3	–	neg	yes	knees cuffs hips	no	fever rash	CRP = 9 mg/L ESR = 2 mm HG normal	Tocilizumab	CS Anakinra Tocilizumab

(Continued)

10.3389/fimmu.2023.1228122

10.3389/fimmu.2023.1228122

TABLE 1 Continued

Patients	Age	Sex	Form	Time of Evolution	ANA	HLAB27	Clinical A.	Arthritis	Ocular Manifestation	Systemic A.	Biological A.	Current Treatment	Previous Treatment
9	8	M	polyA	1	-	neg	yes	fingers elbows knees cuffs	no	fever	CRP = 230 mg/L ESR = 50 mm Ferritin = 883 µg/L PNN: 23,000/mm^3	MTX	CS Anakinra MTX
10	11	M	polyA	5	-	neg	yes	hips shoulders	no	fever	CRP = 122mg/L ESR = 45 mm Ferritin = 309 µg/L PNN: 17,400/mm^3	-	CS MTX Tocilizumab

Demographic characteristics, clinical and biological disease activities, and treatments for 10 patients with active JIA are described.
Age, years; F, female; M, male; PolyA, polyarticular; OligoA, oligoarticular; ANA, anti-nuclear antibodies; RF, rheumatoid factor; CCP, anti cyclic-citrullinated peptide antibody; neg, negative; Clinical A, clinical activity; Systemic A, systemic activity; Biological A, biological activity; CRP, C-reactive protein; ESR, erythrocyte sedimentation rate; HG, hemogram; PNN, polynuclear neutrophils; CS, corticosteroids; DMARDS, disease-modifying antirheumatic drugs; MTX, methotrexate.

binding on purified MVs (Figure 1B). In addition, the presence of integrin subunit β3 and CD81 was confirmed by Western blotting (Figure 1C, upper panel), with no major contamination by soluble proteins such as albumin (Figure 1C, lower panel). Then, tunable resistive pulse sensing assays showed that vesicles had similar average sizes (respectively 299, 215, and 205 nm for conditions CTRL, LPS, and LPS+ATP), which correspond to the range of large MVs (Figure 1D). Taken together, molecular and size features of MV preparations were consistent with the definition of MV according to the MISEV 2018.

To determine the biological activity of IL-1β conveyed by MVs, we used MVs purified from supernatants of THP-1 cells differentiated into macrophages by PMA treatment and stimulated with LPS or LPS+ATP. MV numeration showed that the same number of MVs were issued from LPS-stimulated or non-stimulated macrophages (ns, Figure 1E). Further addition of ATP tended to increase the total number of MVs compared to non-stimulated macrophages, despite heterogeneous results (58% increase, $p < 0.05$, Figure 1E). Similar results were obtained using MVs from PBMC differentiated into macrophages ($p < 0.005$, Supplementary Figure S2).

We then studied NLRP3 inflammasome components carried by MVs from THP-1 treated with PMA and differentiated in macrophages. Using ELISA, we observed that IL-1β concentration was significantly higher in MV lysates issued from LPS- and LPS +ATP-stimulated macrophages compared to MV lysates from non-stimulated macrophages ($p < 0.05$, Figure 2A). We used flow cytometry to detect IL-1β in MVs after membrane permeabilization by saponin, as previously reported (33) (Figure 2B) and observed a significant increase of IL-1β-positive MV population shed from macrophages stimulated with LPS+ATP as compared to non-stimulated ones [8.1 (2–13.9) vs. 0.115 (0.03–0.475)%, $p < 0.01$, Figure 2C].

Western blot experiments were performed only with MVs purified from the supernatant of PMA-treated THP-1 cells, as large amounts of MVs were required for protein expression analysis. MVs from non-stimulated macrophages contained small concentrations of the IL-1β precursor (33 kDa), likely resulting from THP-1 cell activation by PMA. After LPS stimulation, increased levels of IL-1β precursor (pro-IL-1β) and very low amounts of mature IL-1β (17 kDa) as well as intermediary IL-1β (28 kDa) form were observed, suggesting that priming with LPS induced pro-IL-1β synthesis by macrophages. With the addition of exogenous ATP, IL-1β mature form increased in MVs, consistent with ATP-induced pro-IL-1β maturation (Figure 2D).

We then investigated the presence of NLRP3 and caspase-1 in MVs from THP-1 treated with PMA, differentiated in macrophages. Using Western blot, NLRP3 (Figure 2E) and the 40-kDa procaspase-1 and the 10-kDa mature and 20-kDa mature caspase-1 forms (Figure 2F) were clearly detected in MVs secreted by stimulated macrophages, indicating that MVs issued from activated macrophages contained all the machinery necessary for the processing of IL-1β. In addition, when PMA-treated THP-1 cells were pre-treated by caspase-1-inhibitor YVAD then stimulated with LPS+ATP, MV content was modified showing less IL-1β mature form and increased concentrations of pro-IL-1β

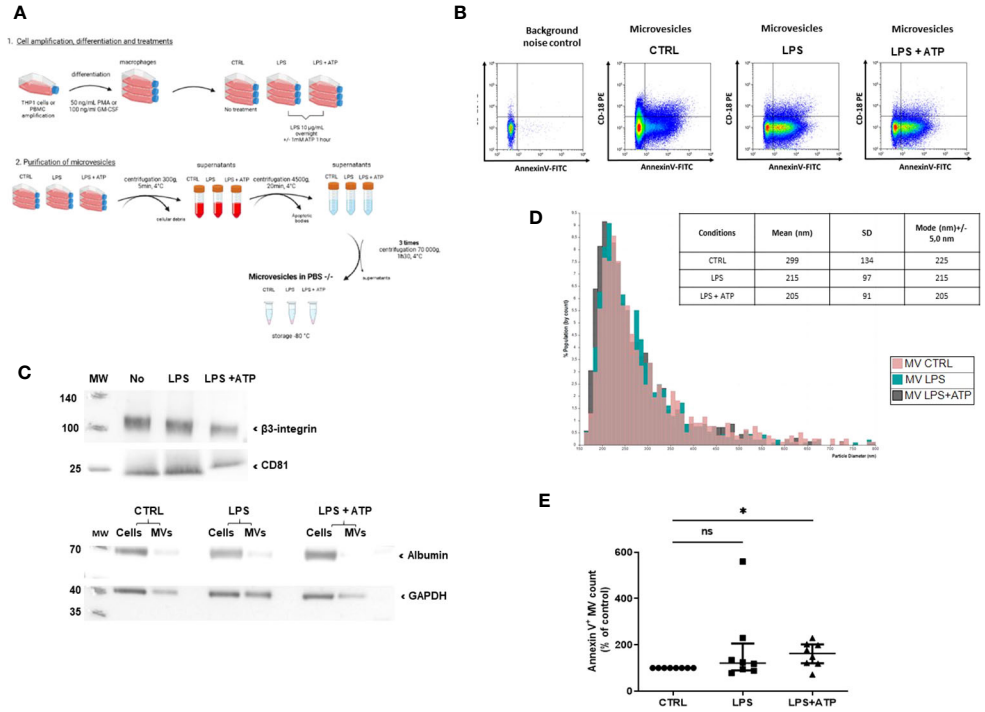

FIGURE 1
Macrophage MV purification and characterization process. **(A)** Schematization of the preparation and the purification of MVs. MVs were collected from macrophage supernatants (purified THP-1 treated with PMA), either non-stimulated (CTRL) or stimulated with LPS or LPS+ATP. Then, they were purified by serial centrifugations to remove dead cells and apoptotic bodies and ultracentrifugation. **(B)** Flow-cytometry-based quantification of MVs collected from non-stimulated or LPS- or LPS+ATP-stimulated macrophage supernatants. MVs were characterized by annexin-V and CD18 expression. **(C)** After lysis, 17, 150, or 236 millions of MVs (CTRL, LPS, and LPS+ATP) were analyzed by Western blot to detect the presence of β3-integrin and CD81 (upper panel). The same number of MVs and 10 µg of their corresponding cells were lysed and a Western blot of albumin was realized to attest purification. GAPDH was used as charge control (lower panel). **(D)** Size distribution by tunable resistive pulse sensing (qNANO) with p150 nanopores. **(E)** MVs isolated from THP-1 treated with PMA and differentiated into macrophages and non-stimulated (CTRL) or stimulated by LPS or LPS+ATP were stained with annexin-V-FITC, and then quantified by flow cytometry, using counting beads. Results are expressed as mean percentage of increase compared to control expressed in each experiment at 100% (ns, $p > 0.05$; *$p < 0.05$, $n = 8$).

(Figure 2G), demonstrating that IL-1β maturation in MVs was caspase-1-dependent.

3.2 MVs from stimulated macrophages are thrombo-inflammatory vectors

Next, we studied the pro-inflammatory and pro-coagulant properties of IL-1β-positive MVs. Since MVs contain all the molecules necessary to generate the 17-kDa mature IL-1β, we asked whether they could process and release IL-1β *in vitro*. First, using flow cytometry analysis and gating on large permeabilized Annexin-V-positive MVs, in order to reduce exosome contamination, we observed co-expression of IL-1β and P2X7 receptor in and on the same MV. More than 80% of MVs issued from non-stimulated macrophages expressed only P2X7R, whereas permeabilized MVs issued from LPS+ATP-stimulated macrophages expressed both P2X7R and IL-1β (Figure 3A). Western blot analysis confirmed the presence of P2X7R in MV lysates (Figure 3B). MVs were purified from LPS-stimulated macrophages before being incubated with PBS or ATP. After ultracentrifugation to eliminate MVs, IL-1β concentration was measured in MV-free supernatant and a threefold increase of IL-1β concentrations was observed in the supernatant of MVs stimulated with ATP, compared to the supernatant of MVs stimulated with PBS alone ($p < 0.05$, Figure 3C).

MVs issued from macrophages have been reported to carry TF (34); we thus asked whether MVs contained both IL-1β and TF. MVs were isolated from supernatants of macrophages derived from THP-1 and MV lysates were subjected to Western blot analysis. Both IL-1β and TF could be detected in the same MV issued from LPS+ATP-stimulated macrophages (Figure 3D left and right panels, respectively). Moreover, using transmission electronic microscopy (TEM) on MV double-labeled for both IL-1β and TF, we observed that some MVs contained both IL-1β and TF (Figure 3E). To confirm TF procoagulant activity on MVs, an *in vitro* Factor-Xa-generation-assay was performed. TF activity was significantly increased with MVs issued from LPS+ATP-stimulated macrophages, when compared with MVs issued from LPS-stimulated macrophages and non-stimulated macrophages ($p < 0.05$ respectively, Figure 3F).

3.3 MVs from stimulated macrophages have pro-inflammatory effects *in vitro* and *in vivo*

To determine whether IL-1β-positive MVs were biologically active, we first studied the ability of MVs issued from LPS+ATP-

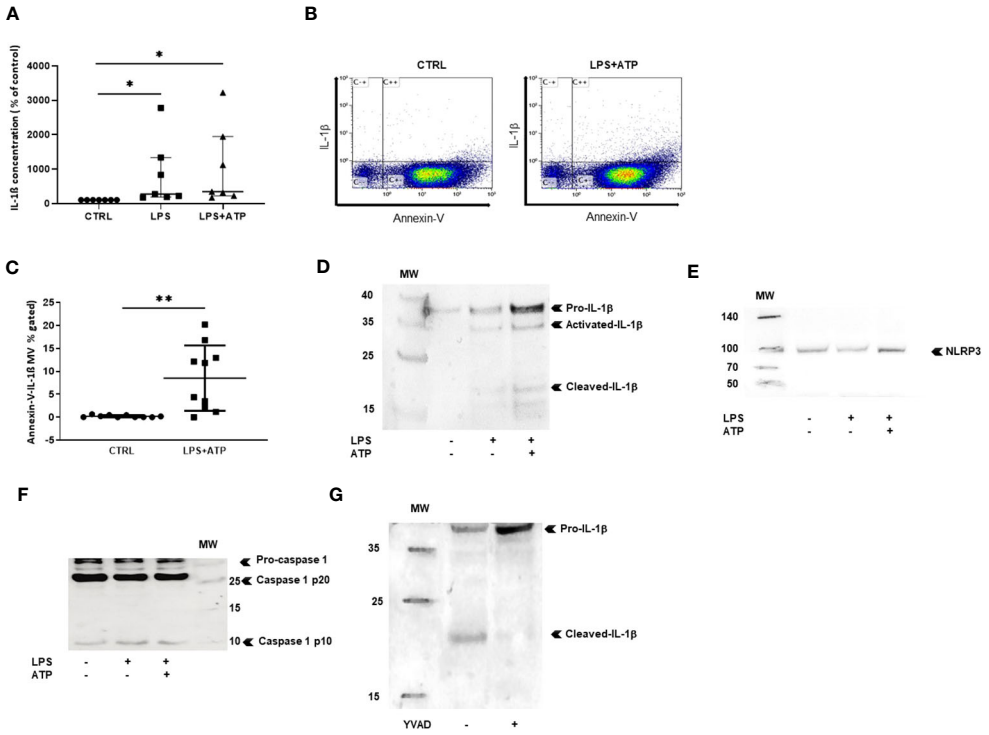

FIGURE 2
MVs shed from stimulated macrophages convey IL-1b and NLRP3 inflammasome components. **(A)** IL-1b was measured by ELISA in MV lysates isolatedfrom PBMC differentiated into macrophages stimulated with either LPS or LPS+ATP or non-stimulated (CTRL). Results are expressed as percentageof increase compared to control (*p < 0.05, n = 7). **(B)** Scatter dot plot after MV purification, permeabilization, and co-labeling with annexin-V andIL-1b. **(C)** MVs were isolated from THP-1 differentiated into macrophages. Quantification of annexin-V and IL-1b-positive MVs (**p < 0.01, n = 10).Detection of **(D)** IL-1b, **(E)** NLRP3, and **(F)** pro-caspase-1 and mature caspase-1 (p10) and (p20) in MV lysates from THP-1 differentiated intomacrophages, by Western blotting, **(G)** detection of IL-1b by Western blotting in MV lysates from THP-1 differentiated into macrophages aftertreatment with the caspase-1 inhibitor YVAD. All Western blots were realized at least three times.

stimulated macrophages to activate endothelial cells *in vitro*. Using Western blotting, we observed that MVs significantly increased ICAM-1 and VCAM-1 expression ($p < 0.01$ and $p < 0.001$, respectively, Figure 4A, upper panel a and middle panel b) but not E-selectin expression on HUVECs (ns, Figure 4A, lower panel c). Interestingly, MV pre-incubation with IL-1Ra did not reduce either ICAM-1 or VCAM-1 expression on endothelial cells (ns, Figure 4A). Endothelial cell activation was also confirmed by cytometry analysis on HUVECs using the same conditions (Supplementary Figure S3; Supplementary Table 1).

Then, we studied the ability of MVs issued from LPS+ATP-stimulated macrophages to induce leukocyte recruitment in mice. Fifteen hours after intra-peritoneal injection of MVs, leukocyte recruitment (CD45+ cells) into peritoneal cavity was significantly increased ($p < 0.01$, Figure 4B), a process that was significantly reduced in the presence of IL-1 receptor antagonist ($p < 0.05$, Figure 4B).

3.4 Detection of IL-1β-positive MVs in patients with juvenile idiopathic arthritis

To support the existence of these MVs in human disease, we studied the presence of circulating MVs in the plasma of patients with JIA or from healthy donors. Ten patients (sex ratio = 1) with a mean age of 11.1 years [5–16 years], were studied (Table 1). All patients had active disease according to JADAS10, which motivate a therapeutic increment. Among them, nine patients presented a polyarticular form including three with systemic clinical and biological symptoms consistent with a systemic form (sJIA: patients #4, #9, and #10). No patient was treated with anakinra at the time of the flare. The absolute number of total MVs and of leukocyte-derived MVs were not significantly different in plasma of JIA patients compared to healthy controls, possibly due to the relatively low number of patients (data not shown). However, if the concentration of $CD11b^+$MVs derived from myeloid cells was not significantly higher in JIA patients compared to healthy controls (ns, Figure 5A), $CD45^+CD66^-$MVs issued from myeloid cells after exclusion of neutrophils were significantly increased in JIA patients ($p < 0.05$, Figure 5B). Importantly, using flow cytometry analysis, we could detect higher concentrations of circulating IL-1β+Annexin-V-positive MVs in JIA patients compared to healthy controls ($p < 0.05$, Figure 5C). Circulating IL-1β+Annexin-V-positive MVs represented a small proportion of total MVs (Figure 5D) but were detectable in all patients, especially in those with an active polyarticular disease (patient#1: 0.47%, patient#2: 0.31%) and with biological systemic inflammation (patient#9: 0.27%, and patient #10: 1.06% respectively).

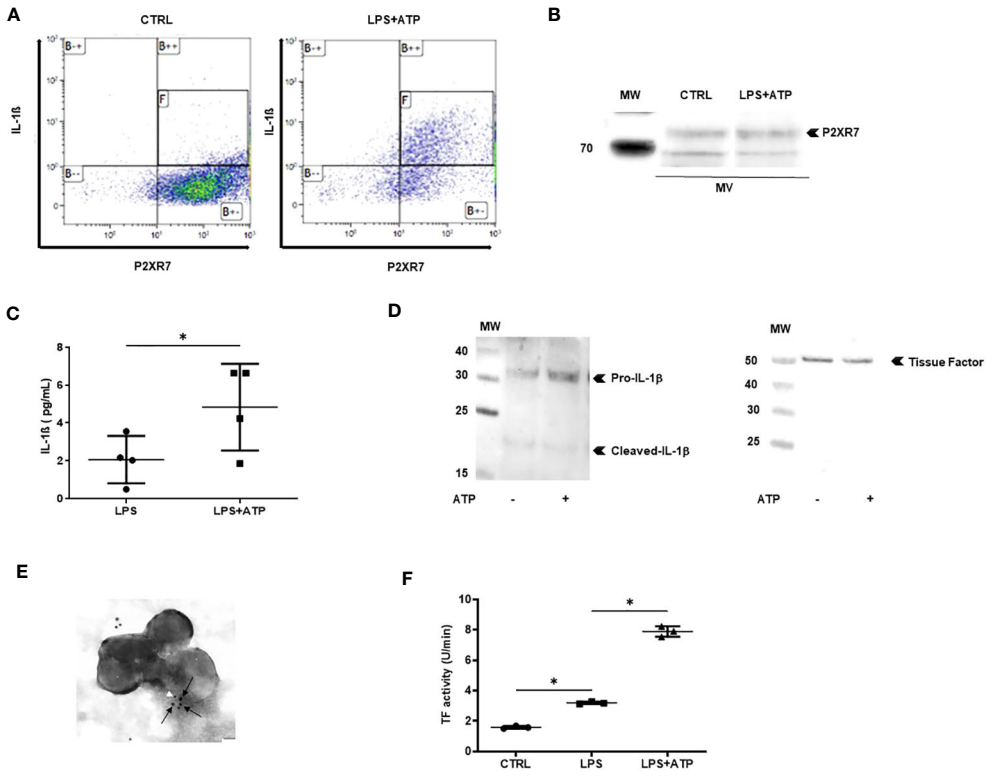

FIGURE 3
MVs from stimulated macrophages are thrombo-inflammatory vectors. **(A)** Detection by flow cytometry of IL-1β and P2X7R in permeabilized annexin-V-positive MVs isolated from PBMC differentiated into macrophages then stimulated with LPS+ATP or not stimulated (CTRL). Quadrant [F] shows MVs positive for IL-1β and P2X7R among annexin-V-positive MVs. **(B)** P2X7 was detected by Western blot in MVs or cell lysates from PBMC differentiated into macrophages then stimulated with LPS+ATP or not stimulated. **(C)** MVs purified from LPS-stimulated THP-1 differentiated into macrophages were incubated with PBS or ATP (1 mM) for 1 h at 37°C. IL-1β concentration was determined in MV supernatant using ELISA (*$p < 0.05$, $n = 4$). **(D)** Detection of IL-1β (left) and tissue factor (right) by Western blot in 10 µg of MV lysate purified from THP-1 treated with PMA and differentiated into macrophages, then stimulated with LPS+ATP. **(E)** Immunogold labeling of IL-1β (white arrowhead, 5 nm beads) and tissue factor (black arrows, 10 nm beads) captured by transmission electronic microscopy in MVs from THP-1-derived macrophages stimulated with LPS+ATP. **(F)** Tissue factor activity (U/min) measured using a Factor Xa generation assay in MVs from THP-1-derived macrophages incubated with PBS (CTRL) or stimulated with either LPS or LPS+ATP (*$p < 0.05$, $n = 3$).

4 Discussion

In this study, we observed that macrophages issued from either PBMCs or the THP-1 cell line release pro-inflammatory and pro-thrombotic MVs upon priming with LPS and activation with ATP. MVs contained the precursor and mature forms of IL-1β, NLRP3 inflammasome, pro-caspase-1, and activated capsase-1 and expressed P2X7R on their membranes. Upon ATP stimulation, MVs were able to release IL-1β in its mature form *in vitro* and increased ICAM-1 and VCAM-1 expression on HUVECs. In addition, MVs induced a peritoneal leukocyte infiltrate in mice that was reduced by IL-1Ra pre-treatment. After ATP stimulation, MVs also contained TF and exhibited an increased TF-dependent pro-coagulant activity *in vitro*. As a proof of concept of their existence and potential pathogenic roles in human pathogenesis, using flow cytometry analysis, we could detect IL-1β-positive MVs in the plasma of patients with active JIA, a well-known IL-1β-mediated disease.

As a leaderless protein, IL-1β secretion does not follow the classical secretory pathway (3). Several alternative releasing pathways have however been proposed, notably linked to inhibition of autophagy and secretory lysosome exocytosis (8–11). Secretory lysosomes have been shown to contain pro- and mature IL-1β, NLRP3, ASC, and caspase-1 (8). Other secretion mechanisms may occur after more prolonged macrophage activation through caspase-1-dependent pyroptosis or cathepsin B-dependent necroptosis. In these cases, free mature IL-1β is secreted (16, 18). Our results argue for the release of mature IL-1β by MVs issued from activated macrophages in a process associated with NLRP3 inflammasome and caspase-1 activation. Extracellular vesicles contain several different subpopulations such as, first, apoptotic bodies labeled by annexin-V, containing DNA, and histones with a size range between 1 and 3 µm; second, annexin-V-positive membrane MVs containing RNA and proteins, whose size is between 0.1 and 1 µm; and third, exosomes, which are annexin-V-negative but contain HLA class II with a small size between 50 and 80 nm (35). Apoptotic bodies have been reported to contain bioactive IL-1α (33) and some exosomes may contain IL-1β (12). In 2001, McKenzie et al. first reported the evidence of pro- and mature IL-1β-positive vesicles issued from LPS +ATP-stimulated THP-1; however, no centrifugation procedure or size criteria were clearly reported in this previous study (20). In 2007, Pizzirani et al. showed the presence of both forms of IL-1β, as well as caspase-1 in 0.1–1 µm cathepsin B-positive microvesicles issued from

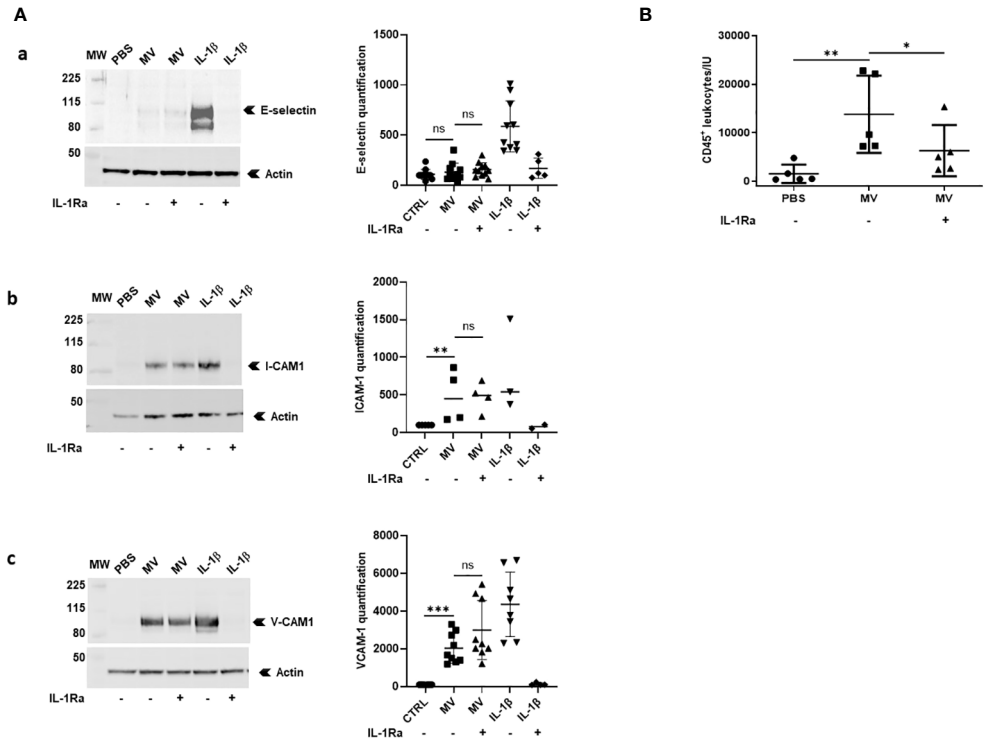

FIGURE 4
MVs from stimulated macrophages demonstrate IL-1β-dependent pro-inflammatory properties *in vitro* and *in vivo*. **(A)** HUVECs were pre-incubated or not with IL-1Ra (10 µg/mL) for 10 min and were then incubated with PBS or with 20 × 10^6 MVs from THP-1-derived macrophages stimulated with LPS+ATP or with IL-1β (500 pg/mL). Cell lysates (30 µg) were then subjected to Western blot for ICAM-1, VCAM-1, E-selectin detection, and actin for each point (for MV stimulations: ICAM-1: $n = 4$, VCAM-1: $n = 9$, and E-selectin: $n = 11$; ns, $p > 0.05$, $^{**}p < 0.01$, $^{***}p < 0.001$). **(B)** Peritoneal leukocyte counts after peritoneal injection in mice ($n = 5$) of 25x10^6 MVs from THP-1-derived macrophages treated with LPS+ATP. Four mice received intraperitoneal injections of PBS or IL-1Ra (30 mg/kg) 30 min before the MV injections ($^{*}p < 0.05$, $^{**}p < 0.01$).

ATP-stimulated dendritic cells, but in this work, no specific labeling was used for purification; thus, this extracellular preparation was likely to contain both MV and secretory lysosomes (21). In 2011, Wang et al. reported the presence of IL-1β in annexin-V-positive MVs issued from LPS-activated THP-1, without the addition of ATP (19). MVs contained both forms of IL-1β, NLRP3, ASC, and caspase-1 and were shown to stimulate HUVECs *in vitro*, in an IL-1β-dependent manner. Our data confirm the pro-inflammatory nature of IL-1β-positive MVs and extend the study of Wang et al. in several ways. First, we could detect and characterize MV population and, among them, IL-1β-positive MVs by flow cytometry analysis, according to MISEV 2018 guidelines. Second, in agreement with another report (21), we observed that these MVs co-express IL-1β and P2X7R and are sensitive to ATP stimulation for the release of soluble 17 kDa mature IL-1β. Third, since IL-1β-positive MV-induced endothelial activation appeared partially IL-1-dependent *in vitro*, we showed for the first time that IL-1β-positive MVs exert an IL-1-mediated pro-inflammatory effect *in vivo* in a murine model of sterile peritonitis.

Therefore, these MVs may be considered as complete pro-inflammatory circulating entities protecting both IL-1β and NLRP3 inflammasome components from rapid degradation. The presence of MVs containing various pro-inflammatory molecules has now been well-established in various pathogenic models, notably ischemic (36). However, MVs as well as apoptotic bodies expose phosphatidyl-serine on their membranes, which is an important "eat-me signal" for macrophages leading to M2 anti-inflammatory phenotype differentiation (37), raising the question of the real pro-inflammatory properties of MVs *in vivo*. In fact, the role of MVs may well depend on the balance between the MVs produced during tissue injury and the phagocytosis capacities of macrophages. In physiological, macrophages may phagocytose MVs, preventing inflammation. During acute ischemic stress, necrotic cells have been shown to liberate very large concentrations of MVs (38), which may temporarily exceed macrophage phagocytosis. Alternatively, in patients prone to develop auto-immune diseases, such as systemic lupus erythematosus, the intrinsic phagocytic abilities of macrophages have been shown to be altered and circulating MVs have been reported (39, 40). Both situations may lead to increased circulating MVs and localized or systemic inflammation. MVs may deliver an IL-1β-mediated pro-inflammatory signal in several ways. First, as shown in other models, MVs may be endocytosed by target cells through phosphatidyl serine/phosphatidyl serine receptor interactions (41). Noteworthy is the fact that in this setting, NLRP3 may remain active into the cell cytoplasm (42). Through their P2X7 receptor, MVs may also interact with ATP liberated by necrotic cells, thus activating NLRP3 into the MV cytoplasm and MV IL-1β release, as suggested by our *in vitro* data. Third, MVs may experience secondary necrosis and the release of IL-1β precursor,

10.3389/fimmu.2023.1228122

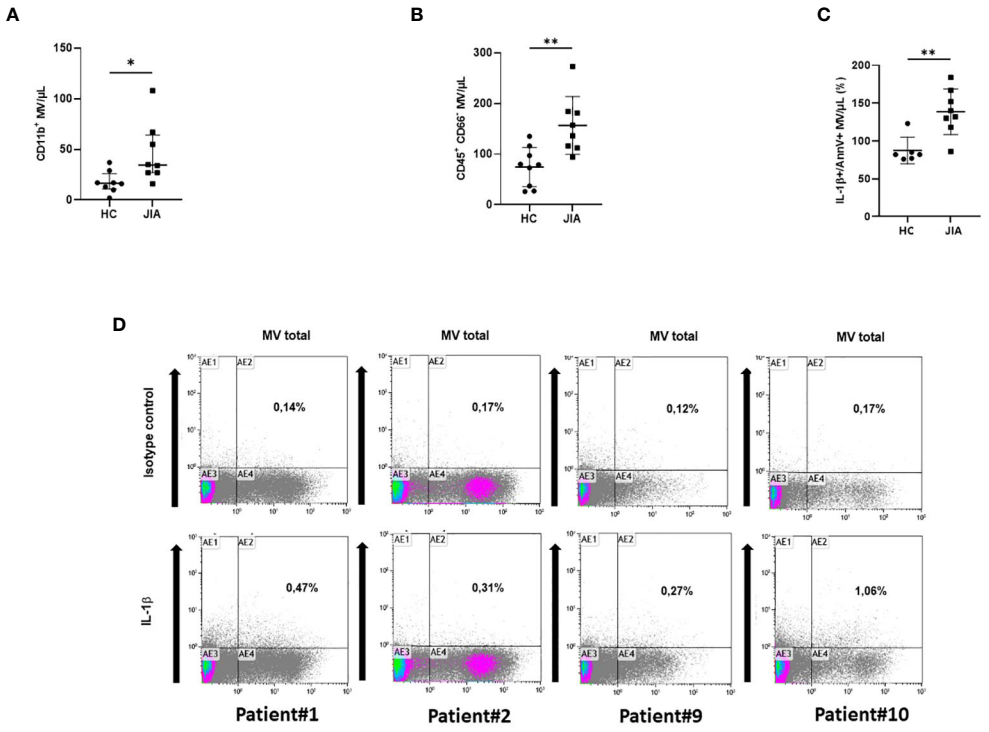

FIGURE 5
Detection of circulating IL-1β-positive MVs in plasma from JIA patients. **(A)** Determination by flow cytometry of myeloid MVs (CD11b+MV) isolated from the plasma of 10 JIA patients and 8 healthy controls (HC) and **(B)** of myeloid MVs after exclusion of neutrophils (CD45+CD66-MV). (*$p< 0.05$, **$p< 0.01$). **(C)** Detection by flow cytometry of circulating IL-1β-positive MVs among total MVs in 10 JIA patients versus six healthy controls (HC), expressed as percentage of the total annexin-V-positive MV population. **(D)** Illustration of dot plot from selected patients with active disease: #1, #2, #9, and #10. Percentage of IL-1β and annexin-V-positive MVs is expressed on each graph.

NLRP3, caspase-1, and other enzymes, leading to some IL-1β processing in the target cell microenvironment and interaction with the IL-1R1 on target cells (43).

MVs may be able to deliver bioactive IL-1β in inflammatory sites (synovium, skin, bone marrow, and liver) distant from the original cell source. Interestingly, IL-1β-positive MVs may also be inflammatory through phagocytosis or membrane fusion by targeting fibroblast-like-synoviocytes or macrophages and direct intra-cytoplasmic delivery of both NLRP3 inflammasome components and pro-IL-1β, as previously suggested (42). In addition, Rothmeier et al. have shown that LPS+ATP-stimulated murine macrophages release MVs over 500 nm, which carry a bioactive form of TF, but do not contain IL-1β (34). Unlike data from these authors, we were able to detect both IL-1β and bioactive TF in MVs issued from LPS+ATP-stimulated macrophages using Western blot and *in vitro* bioassay. However, we could not show co-expression of IL-1β and TF on the same MV, using flow cytometry analysis, since TF was not detectable on MVs using this method, despite the use of different anti-TF antibodies. Therefore, we performed TEM on IL-1β and TF-double-labeled MVs and observed that a sub-population of MVs issued from LPS+ATP-stimulated macrophages indeed contained both IL-1β and TF. The relative differences with the previous report from Rothmeier et al. may possibly be due to the different experimental conditions, since we used lower concentrations of ATP (1 mM vs. 4 mM), possibly protecting macrophage MVs from pyroptosis and 17-kDa IL-1β release.

By stimulating HUVECs with IL-1β-positive MVs, we observed that endothelial activation was not inhibited by IL-1Ra, indicating that MVs may contain other pro-angiogenic and pro-inflammatory components, such as mitochondria for example (44), or other IL-1 family cytokines such as IL-18 or IL-33, which could induce endothelial activation in an IL-1β-independent manner (45). Membrane interaction of MVs could also be involved in endothelial activation. MVs expose phosphatidyl-serine on their membrane, resulting in an interaction with their endothelial phosphatidyl-serine receptor linked to ICAM-1 and VCAM-1 expression (46). *In vivo*, the pro-inflammatory properties induced by IL-1β-positive MVs injected into the peritoneal cavity could involve endothelial–leukocyte adhesion molecules (ICAM-1, VCAM-1) but also other mechanisms induced by IL-1β, such as regulation of chemokines, cytokine-induced neutrophil chemoattractant-1 (CINC-1), or integrin-β6 expression by epithelial cells (45). Thus, the permeability of the vasculature could be increased by regulating the expression of cell–cell junction components in an IL-1β-independent manner, and IL-1β can also induce the activation of leukocytes, fibroblast-like-synoviocytes, and endothelial cells, which could modify the vasculature permeability (47). Thus, MVs from stimulated macrophages are thrombo-inflammatory vectors and induce

endothelial activation *in vitro* and leukocyte recruitment *in vivo*, in an IL-1β-dependant manner.

Finally, to determine whether our *in vitro* and murine data had some relevance in human diseases and as a proof of concept, we tried to detect IL-β-positive MVs in active JIA, a well-known IL-1β-mediated disease. In JIA patients, serum concentrations of IL-1β remain poorly detectable despite the demonstration of an IL-1β transcriptional signature in PBMCs and the well-established therapeutic efficiency of IL-1β-blocking antibody canakinumab or recombinant IL-1 receptor antagonist, anakinra (1, 48). We succeeded in detecting circulating IL-1β-positive MVs in patient plasma and observed a significantly higher count of myeloid IL-1β-positive MVs in 10 active JIA patients, compared to healthy controls. To our knowledge, this is the first time that IL-1β-positive MVs are detected in plasma from JIA patients.

5 Conclusion

In this study, we characterized a population of LPS-primed macrophage-derived MVs containing pro-IL-β, NLRP3, caspase-1, and TF and releasing IL-1β upon P2X7R activation by ATP. We showed their pro-inflammatory and pro-coagulant biological functions *in vitro* and *in vivo*. Furthermore, IL-1β-positive MVs were detectable in plasma from patients with active JIA; thus MVs may represent a pathway of IL-1β release in IL-1β-dependent diseases.

Data availability statement

The original contributions presented in the study are included in the article/Supplementary Material. Further inquiries can be directed to the corresponding author.

Ethics statement

Ethical approval was not required for the studies on humans in accordance with the local legislation and institutional requirements because only commercially available established cell lines were used. The animal studies were approved by APAFIS#4228-2016022410055380 v5. The studies were conducted in accordance with the local legislation and institutional requirements. Written informed consent was obtained from the minor(s)' legal guardian/next of kin for the publication of any potentially identifiable images or data included in this article.

Author contributions

AC, CR, and RB conducted the experiments and interpreted the data; AC, RB, SR, AL, and LV contributed to MV analysis by flow cytometry; AC, CR, RB, LA, ML, RM, YK, and ET contributed to MV production and ELISA experiment realization; CF, KR, A-LJ, T-AT, RL, FD-G, and GK contributed to sample collection and analysis of clinical data; FD-G handled funding of the manuscript; RL made a critical revision of the manuscript; GK took care of patients and handled funding and supervision of the project, helped with the interpretation of the experiments, and wrote the manuscript with AC. All authors contributed to the article and approved the submitted version.

Acknowledgments

We thank Alexandre ALTIE (PMET Electronic Microscopy Platform, C2VN) for technical assistance with transmission electronic microscopy.

Conflict of interest

The authors declare that the research was conducted in the absence of any commercial or financial relationships that could be construed as a potential conflict of interest.

Publisher's note

All claims expressed in this article are solely those of the authors and do not necessarily represent those of their affiliated organizations, or those of the publisher, the editors and the reviewers. Any product that may be evaluated in this article, or claim that may be made by its manufacturer, is not guaranteed or endorsed by the publisher.

Supplementary material

The Supplementary Material for this article can be found online at: https://www.frontiersin.org/articles/10.3389/fimmu.2023.1228122/full#supplementary-material

References

1. Pascual V, Allantaz F, Arce E, Punaro M, Banchereau J. Role of interleukin-1 (IL-1) in the pathogenesis of systemic onset juvenile idiopathic arthritis and clinical response to IL-1 blockade. *J Exp Med* (2005) 201(9):1479–86. doi: 10.1084/jem.20050473

2. Allantaz F, Chaussabel D, Stichweh D, Bennett L, Allman W, Mejias A, et al. Blood leukocyte microarrays to diagnose systemic onset juvenile idiopathic arthritis and follow the response to IL-1 blockade. *J Exp Med* (2007) 204(9):2131–44. doi: 10.1084/jem.20070070

3. Rubartelli A, Cozzolino F, Talio M, Sitia R. A novel secretory pathway for interleukin-1 beta, a protein lacking a signal sequence. *EMBO J* (1990) 9(5):1503–10. doi: 10.1002/j.1460-2075.1990.tb08268.x

4. Ferrari D, Chiozzi P, Falzoni S, Dal Susino M, Melchiorri L, Baricordi OR, et al. Extracellular ATP triggers IL-1 beta release by activating the purinergic P2Z receptor of human macrophages. *J Immunol* (1997) 159(3):1451–8. doi: 10.4049/jimmunol.159.3.1451

5. Kaplanski G. Interleukin-18: Biological properties and role in disease pathogenesis. *Immunol Rev* (2018) 281(1):138–53. doi: 10.1111/imr.12616

6. Carta S, Lavieri R, Rubartelli A. Different members of the IL-1 family come out in different ways: DAMPs vs. Cytokines? *Front Immunol* (2013) 4:123. doi: 10.3389/fimmu.2013.00123

7. Sitia R, Rubartelli A. The unconventional secretion of IL-1β: Handling a dangerous weapon to optimize inflammatory responses. *Semin Cell Dev Biol* (2018) 83:12–21. doi: 10.1016/j.semcdb.2018.03.011

8. Andrei C, Dazzi C, Lotti L, Torrisi MR, Chimini G, Rubartelli A. The secretory route of the leaderless protein interleukin 1beta involves exocytosis of endolysosome-related vesicles. *Mol Biol Cell* (1999) 10(5):1463–75. doi: 10.1091/mbc.10.5.1463

9. Andrei C, Margiocco P, Poggi A, Lotti LV, Torrisi MR, Rubartelli A. Phospholipases C and A2 control lysosome-mediated IL-1 beta secretion: Implications for inflammatory processes. *Proc Natl Acad Sci USA* (2004) 101 (26):9745–50. doi: 10.1073/pnas.0308558101

10. Shi CS, Shenderov K, Huang NN, Kabat J, Abu-Asab M, Fitzgerald KA, et al. Activation of autophagy by inflammatory signals limits IL-1β production by targeting ubiquitinated inflammasomes for destruction. *Nat Immunol* (2012) 13(3):255–63. doi: 10.1038/ni.2215

11. Blott EJ, Griffiths GM. Secretory lysosomes. *Nat Rev Mol Cell Biol* (2002) 3 (2):122–31. doi: 10.1038/nrm732

12. Qu Y, Franchi L, Nunez G, Dubyak GR. Nonclassical IL-1 beta secretion stimulated by P2X7 receptors is dependent on inflammasome activation and correlated with exosome release in murine macrophages. *J Immunol* (2007) 179 (3):1913–25. doi: 10.4049/jimmunol.179.3.1913

13. Broz P. Immunology: Caspase target drives pyroptosis. *Nature* (2015) 526 (7575):642–3. doi: 10.1038/nature15632

14. Kayagaki N, Stowe IB, Lee BL, O'Rourke K, Anderson K, Warming S, et al. Caspase-11 cleaves gasdermin D for non-canonical inflammasome signalling. *Nature* (2015) 526(7575):666–71. doi: 10.1038/nature15541

15. Shi J, Zhao Y, Wang K, Shi X, Wang Y, Huang H, et al. Cleavage of GSDMD by inflammatory caspases determines pyroptotic cell death. *Nature* (2015) 526(7575):660–5. doi: 10.1038/nature15514

16. Liu X, Zhang Z, Ruan J, Pan Y, Magupalli VG, Wu H, et al. Inflammasome-activated gasdermin D causes pyroptosis by forming membrane pores. *Nature* (2016) 535(7610):153–8. doi: 10.1038/nature18629

17. He Wt, Wan H, Hu L, Chen P, Wang X, Huang Z, et al. Gasdermin D is an executor of pyroptosis and required for interleukin-1β secretion. *Cell Res* (2015) 25 (12):1285–98. doi: 10.1038/cr.2015.139

18. Edwan JH, Goldbach-Mansky R, Colbert RA. Identification of interleukin-1β-producing monocytes that are susceptible to pyronecrotic cell death in patients with neonatal-onset multisystem inflammatory disease. *Arthritis Rheumatol* (2015) 67 (12):3286–97. doi: 10.1002/art.39307

19. Wang JG, Williams JC, Davis BK, Jacobson K, Doerschuk CM, Ting JPY, et al. Monocytic microparticles activate endothelial cells in an IL-1β-dependent manner. *Blood* (2011) 118(8):2366–74. doi: 10.1182/blood-2011-01-330878

20. MacKenzie A, Wilson HL, Kiss-Toth E, Dower SK, North RA, Surprenant A. Rapid secretion of interleukin-1beta by microvesicle shedding. *Immunity* (2001) 15 (5):825–35. doi: 10.1016/s1074-7613(01)00229-1

21. Pizzirani C, Ferrari D, Chiozzi P, Adinolfi E, Sandonà D, Savaglio E, et al. Stimulation of P2 receptors causes release of IL-1beta-loaded microvesicles from human dendritic cells. *Blood* (2007) 109(9):3856–64. doi: 10.1182/blood-2005-06-031377

22. Akers JC, Gonda D, Kim R, Carter BS, Chen CC. Biogenesis of extracellular vesicles (EV): exosomes, microvesicles, retrovirus-like vesicles, and apoptotic bodies. *J Neurooncol* (2013) 113(1):1–11. doi: 10.1007/s11060-013-1084-8

23. Dignat-George F, Boulanger CM. The many faces of endothelial microparticles. *Arterioscler Thromb Vasc Biol* (2011) 31(1):27–33. doi: 10.1161/ATVBAHA.110.218123

24. Distler JHW, Huber LC, Gay S, Distler O, Pisetsky DS. Microparticles as mediators of cellular cross-talk in inflammatory disease. *Autoimmunity* (2006) 39 (8):683–90. doi: 10.1080/08916930601061538

25. Morel O, Toti F, Hugel B, Bakouboula B, Camoin-Jau L, Dignat-George F, et al. Procoagulant microparticles: disrupting the vascular homeostasis equation? *Arterioscler Thromb Vasc Biol* (2006) 26(12):2594–604. doi: 10.1161/01.ATV.0000246775.14471.26

26. Piccin A, Murphy WG, Smith OP. Circulating microparticles: pathophysiology and clinical implications. *Blood Rev* (2007) 21(3):157–71. doi: 10.1016/j.blre.2006.09.001

27. Lacroix R, Robert S, Poncelet P, Kasthuri RS, Key NS, Dignat-George F, et al. Standardization of platelet-derived microparticle enumeration by flow cytometry with calibrated beads: results of the International Society on Thrombosis and Haemostasis SSC Collaborative workshop. *J Thromb Haemost* (2010) 8(11):2571–4. doi: 10.1111/j.1538-7836.2010.04047.x

28. Cointe S, Judicone C, Robert S, Mooberry MJ, Poncelet P, Wauben M, et al. Standardization of microparticle enumeration across different flow cytometry platforms: results of a multicenter collaborative workshop. *J Thromb Haemost* (2017) 15(1):187–93. doi: 10.1111/jth.13514

29. Agouti I, Cointe S, Robert S, Judicone C, Loundou A, Driss F, et al. Platelet and not erythrocyte microparticles are procoagulant in transfused thalassaemia major patients. *Br J Haematol* (2015) 171(4):615–24. doi: 10.1111/bjh.13609

30. Vallier L, Bouriche T, Bonifay A, Judicone C, Bez J, Franco C, et al. Increasing the sensitivity of the human microvesicle tissue factor activity assay. *Thromb Res* (2019) 182:64–74. doi: 10.1016/j.thromres.2019.07.011

31. Lacroix R, Judicone C, Mooberry M, Boucekine M, Key NS, Dignat-George F, et al. Standardization of pre-analytical variables in plasma microparticle determination: results of the International Society on Thrombosis and Haemostasis SSC Collaborative workshop. *J Thromb Haemost* (2013) 15(6):1236. doi: 10.1111/jth.12207

32. Théry C, Witwer KW, Aikawa E, Alcaraz MJ, Anderson JD, Andriantsitohaina R, et al. Minimal information for studies of extracellular vesicles 2018 (MISEV2018): a position statement of the International Society for Extracellular Vesicles and update of the MISEV2014 guidelines. *J Extracell Vesicles* (2018) 7(1):1535750. doi: 10.1080/20013078.2018.1535750

33. Berda-Haddad Y, Robert S, Salers P, Zekraoui L, Farnarier C, Dinarello CA, et al. Sterile inflammation of endothelial cell-derived apoptotic bodies is mediated by interleukin-1α. *Proc Natl Acad Sci USA* (2011) 108(51):20684–9. doi: 10.1073/pnas.1116848108

34. Rothmeier AS, Marchese P, Petrich BG, Furlan-Freguia C, Ginsberg MH, Ruggeri ZM, et al. Caspase-1-mediated pathway promotes generation of thromboinflammatory microparticles. *J Clin Invest* (2015) 125(4):1471–84. doi: 10.1172/JCI79329

35. Théry C, Ostrowski M, Segura E. Membrane vesicles as conveyors of immune responses. *Nat Rev Immunol* (2009) 9(8):581–93. doi: 10.1038/nri2567

36. Cypryk W, Nyman TA, Matikainen S. From inflammasome to exosome-does extracellular vesicle secretion constitute an inflammasome-dependent immune response? *Front Immunol* (2018) 9:2188. doi: 10.3389/fimmu.2018.02188

37. Mohning MP, Thomas SM, Barthel L, Mould KJ, McCubbrey AL, Frasch SC, et al. Phagocytosis of microparticles by alveolar macrophages during acute lung injury requires MerTK. *Am J Physiol Lung Cell Mol Physiol* (2018) 314(1):L69–82. doi: 10.1152/ajplung.00058.2017

38. Hu Q, Lyon CJ, Fletcher JK, Tang W, Wan M, Hu TY. Extracellular vesicle activities regulating macrophage- and tissue-mediated injury and repair responses. *Acta Pharm Sin B* (2021) 11(6):1493–512. doi: 10.1016/j.apsb.2020.12.014

39. Biemmi V, Milano G, Ciullo A, Cervio E, Burrello J, Dei Cas M, et al. Inflammatory extracellular vesicles prompt heart dysfunction via TRL4-dependent NF-κB activation. *Theranostics* (2020) 10(6):2773–90. doi: 10.7150/thno.39072

40. Dalvi P, Sun B, Tang N, Pulliam L. Immune activated monocyte exosomes alter microRNAs in brain endothelial cells and initiate an inflammatory response through the TLR4/MyD88 pathway. *Sci Rep* (2017) 7(1):9954. doi: 10.1038/s41598-017-10449-0

41. Wei X, Liu C, Wang H, Wang L, Xiao F, Guo Z, et al. Surface phosphatidylserine is responsible for the internalization on microvesicles derived from hypoxia-induced human bone marrow mesenchymal stem cells into human endothelial cells. *PloS One* (2016) 11(1):e0147360. doi: 10.1371/journal.pone.0147360

42. Baroja-Mazo A, Martín-Sánchez F, Gomez AI, Martínez CM, Amores-Iniesta J, Compan V, et al. The NLRP3 inflammasome is released as a particulate danger signal that amplifies the inflammatory response. *Nat Immunol* (2014) 15(8):738–48. doi: 10.1038/ni.2919

43. Baxter AA. Stoking the fire: how dying cells propagate inflammatory signalling through extracellular vesicle trafficking. *Int J Mol Sci* (2020) 21(19):7256. doi: 10.3390/ijms21197256

44. Puhm F, Afonyushkin T, Resch U, Obermayer G, Rohde M, Penz T, et al. Mitochondria are a subset of extracellular vesicles released by activated monocytes and induce type I IFN and TNF responses in endothelial cells. *Circ Res* (2019) 125(1):43–52. doi: 10.1161/CIRCRESAHA.118.314601

45. Fahey E, Doyle SL. IL-1 family cytokine regulation of vascular permeability and angiogenesis. *Front Immunol* (2019) 10:1426. doi: 10.3389/fimmu.2019.01426

46. Wautier JL, Wautier MP. Molecular basis of erythrocyte adhesion to endothelial cells in diseases. *Clin Hemorheology Microcirculation* (2013) 53(1–2):11–21. doi: 10.3233/CH-2012-1572

47. Ruperto N, Martini A. Current and future perspectives in the management of juvenile idiopathic arthritis. *Lancet Child Adolesc Health* (2018) 2(5):360–70. doi: 10.1016/S2352-4642(18)30034-8

48. Quartier P, Allantaz F, Cimaz R, Pillet P, Messiaen C, Bardin C, et al. A multicentre, randomised, double-blind, placebo-controlled trial with the interleukin-1 receptor antagonist anakinra in patients with systemic-onset juvenile idiopathic arthritis (ANAJIS trial). *Ann Rheum Dis* (2011) 70(5):747–54. doi: 10.1136/ard.2010.134254

Glossary

IL	interleukin
JIA	juvenile idiopathic arthritis
sJIA	systemic juvenile idiopathic arthritis
MVs	microvesicles
PBMCs	peripheral blood mononuclear cells
THP-1	Tohoku Hospital Pediatrics-1
PMA	phorbol 12-myristate 13-acetate
NLRP3	nucleotide-binding domain
P2X7R	P2X purinoceptor 7
TF	tissue factor
ELISA	enzyme-linked immunoassay
HUVECs	human umbilical vein endothelial cells
LPS	lipopolysaccharide
ATP	adenosine triphosphate
kDa	kilodaltons
TLR	toll-like receptors
NLR	nucleotide-binding oligomerization domain (NOD)-like receptors ASC, apoptosis-associated speck-like protein containing a CARDS
CARD	caspase recruitment domain
HLA	human leukocyte antigen
RNA	ribonucleic acid
ILAR	International League of Associations for Rheumatology
JADAS10	Juvenile Arthritis Disease Activity Score 10
PPP	platelet-poor plasma
FITC	fluorescein isothiocyanate
CD	cluster of differentiation
PC7	phycoerythrin cyanine 7
APC	allophycocyanin
Ab	antibody
PBS	phosphate-buffered saline
IgG	immunoglobulin G
ICAM-1	intercellular adhesion molecule 1/CD54
VCAM-1	vascular cell adhesion protein 1/CD106
HEPES	hydroxyethylpiperazine ethane sulfonic acid
BSA	bovine serum albumin
IL-1Ra	IL-1 receptor antagonist
ANA	antinuclear antibody
CRP	C-reactive protein
ESR	erythrocyte sedimentation rate
MISEV	Minimal Information for the Study of Extracellular Vesicles
CTRL	control
YVAD	acetyl-tyrosyl-valyl-alanyl-aspartyl
DNA	deoxyribonucleic acid
Ca^{2+}	calcium
TEM	transmission electron microscopy
CINC-1	cytokine-induced neutrophil chemoattractant-1
HC	healthy control
GADPH	glyceraldehyde-3-phosphate dehydrogenase
polyA	polyarticular
oligoA	oligoarticular
F	feminine
M	male
HG	hemogram
CS	corticosteroids
DMARDS	disease-modifying antirheumatic drugs
RIPA	radio-immunoprecipitation assay buffer

frontiers | Frontiers in Immunology

TYPE Mini Review
PUBLISHED 24 November 2023
DOI 10.3389/fimmu.2023.1285554

Check for updates

OPEN ACCESS

EDITED BY
Yuehong Chen,
Sichuan University, China

REVIEWED BY
Samuel García Pérez,
Fundación Biomédica Galicia Sur, Spain

*CORRESPONDENCE
Mihir D. Wechalekar
Mihir.Wechalekar@sa.gov.au

RECEIVED 30 August 2023
ACCEPTED 07 November 2023
PUBLISHED 24 November 2023

CITATION
Small A, Lowe K and Wechalekar MD (2023) Immune checkpoints in rheumatoid arthritis: progress and promise. *Front. Immunol.* 14:1285554. doi: 10.3389/fimmu.2023.1285554

COPYRIGHT
© 2023 Small, Lowe and Wechalekar. This is an open-access article distributed under the terms of the Creative Commons Attribution License (CC BY). The use, distribution or reproduction in other forums is permitted, provided the original author(s) and the copyright owner(s) are credited and that the original publication in this journal is cited, in accordance with accepted academic practice. No use, distribution or reproduction is permitted which does not comply with these terms.

Immune checkpoints in rheumatoid arthritis: progress and promise

Annabelle Small[1], Katie Lowe[1] and Mihir D. Wechalekar[1,2]*

[1]Department of Rheumatology, College of Medicine and Public Health, Flinders University, Adelaide, SA, Australia, [2]Department of Rheumatology, Flinders Medical Centre, Adelaide, SA, Australia

Rheumatoid arthritis (RA) is one of the most prevalent autoimmune inflammatory conditions, and while the mechanisms driving pathogenesis are yet to be completely elucidated, self-reactive T cells and immune checkpoint pathways have a clear role. In this review, we provide an overview of the importance of checkpoint pathways in the T cell response and describe the involvement of these in RA development and progression. We discuss the relationship between immune checkpoint therapy in cancer and autoimmune adverse events, draw parallels with the involvement of immune checkpoints in RA pathobiology, summarise emerging research into some of the lesser-known pathways, and the potential of targeting checkpoint-related pathways in future treatment approaches to RA management.

KEYWORDS

rheumatoid arthritis, T cells, immune checkpoints, co-stimulatory pathways, CTLA-4, PD-1

1 Introduction

Rheumatoid arthritis (RA) is a chronic, systemic, inflammatory autoimmune disease that affects up to 1% of the population (1). Inflammation predominantly targets the synovial tissue (ST; the joint lining), leading to pain, swelling and irreversible joint deformities. Disease complications are not confined to joints, and include systemic involvement (pulmonary, cardiac, haematological, amongst others). Despite treatment advances, a majority of patients do not attain remission, and sustained remission occurs in as few as 15% of patients (2). Although the eventual inflammatory milieu in the RA ST is diverse, checkpoint, or co-stimulatory pathways controlling immune cell activation are critical in engendering, maintaining, and perpetuating the inflammatory response, driven by chronic autoimmune antigenic drive. In parallel with the rise of immune checkpoint inhibitors (ICIs) that have transformed oncologic therapeutics, has been the greater recognition of checkpoint pathways in RA pathogenesis.

In this review, we provide an overview of immune checkpoints at various stages of immune cell development and describe the involvement of these in the development and progression of RA. We discuss the involvement of immune checkpoints in RA pathobiology, the relationship between immune checkpoint therapy in cancer and

autoimmune adverse events, and the potential to manipulate these pathways as a future treatment strategy.

2 Immune checkpoints: dictators of the T cell response

T cell activation is a tightly regulated, intricate, and specific process requiring multiple initiating signals. The first is provided through the interaction between a peptide antigen presented by an antigen presenting cell (APC), and a T cell expressing a cognate T cell receptor (TCR). The T cell then requires a secondary signal, referred to as co-stimulation, and the proteins that provide this are called co-stimulatory, or checkpoint molecules. In helper T cells, this is provided through the B7/CD28 co-stimulation axis (3). CD28 expressed on the T cell binds to either CD80 (B7.1) or CD86 (B7.2) on the APC, and together with TCR signalling, provides survival and activation signalling to initiate T cell proliferation (Figure 1). The extent of co-stimulation controls the extent of the initial T cell proliferative response (4), and further signalling provided through specific cytokines dictates cell lineage (5).

Checkpoint molecule expression is largely controlled by the tissue microenvironment, and is influenced by alterations in homeostasis (6). These molecules can exert stimulatory or inhibitory signals in either direction of the interaction (i.e., in the APC and in the T cell) and cumulatively dictate the threshold of T cell activation, allowing for finetuning of the immune response (7, 8). Inhibitory checkpoints, including cytotoxic T-lymphocyte-associated protein 4 (CTLA-4) and programmed death protein 1 (PD-1) are upregulated during cell activation, and are important for limiting the response duration, aiding resolution, and maintaining self-tolerance (7). The importance of immune checkpoints in restricting the immune response is exemplified by disturbances in these pathways. Patients with inherited CTLA-4 deficiencies present with a range of clinical features including recurrent respiratory tract infections and increased risk of autoimmunity (9), while inherited PD-1 deficiency has been linked with early-onset autoimmunity and severe tuberculosis (10). Mice deficient in CTLA-4 experience lethal lymphoproliferative disorders (11), and those deficient in PD-1 develop accelerated autoimmunity and lethal pathology in response to acute infection (12–14).

3 The T cell response in RA

The importance of the T cell response in RA has long been appreciated (15–18) and evidence suggests T cell-driven autoimmunity may occur years prior to clinical onset (19, 20). Distinct changes have been observed in the proportions of T follicular helper (Tfh) and $CD19^+$ B cells in the lymph nodes of patients at risk of developing RA (individuals with rheumatoid factor (RF) and anti-citrullinated protein antibodies (ACPA) but asymptomatic for arthritis) (21), and altered proportions of naïve T cells and T regulatory cells (Treg) have been observed in the peripheral blood (22). In lymph nodes, stromal cells from at-risk patients had distinct hypomethylated sites in genes associated with antigen processing and presentation compared to healthy controls, suggesting altered antigen presentation pathways prior to clinically identifiable disease (23), implicating stromal-lymphoid cell interactions in early RA. Finally, it is well established that RF and ACPA can often be detected in the serum for years in individuals who progress to develop inflammatory arthritis (20, 24).

In clinically identifiable early and established RA, T cells accumulate in the ST sublining layer, where they're found in association with activated macrophages and B cells (16), and often cluster in aggregates consisting of T cells, B cells, and

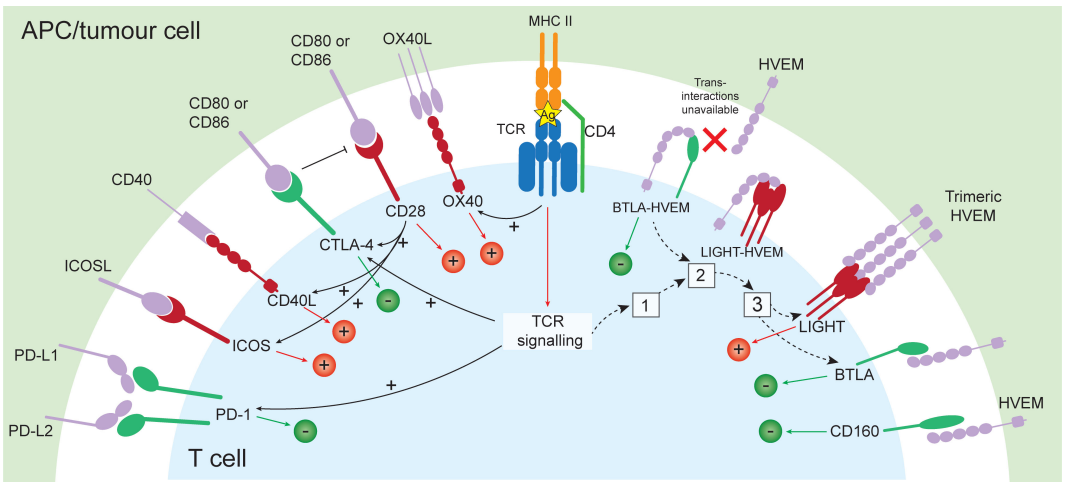

FIGURE 1
Co-signalling pathways with either stimulatory (+) or inhibitory function (-), and the relationship between their expression. Following presentation of antigen by APC or tumour cell and recognition by a T cell expressing a cognate TCR and co-stimulation provided through CD28 binding CD80/CD86, stimulatory (OX40, CD40L, ICOS, LIGHT) and inhibitory checkpoints are induced (CTLA-4, PD-1). In the resting state, BTLA and HVEM form a *cis*- complex which exerts constitutive inhibitory signalling to the T cell. Following T cell activation, LIGHT is rapidly and transiently induced (1), and LIGHT disrupts BTLA-HVEM complexes, sequestering HVEM from BTLA. This results in internalisation of HVEM (2), and leaves surface LIGHT and BTLA available for *trans*- interactions with HVEM (3), capable of inducing stimulatory or inhibitory signals, respectively. Ag, antigen.

dendritic cells (DC) (17). While there is enormous variability in synovitis in RA (17, 25), evidence suggests a T helper 1 (Th1) bias in the ST (17), and the demonstration of T cell involvement across all stages of disease suggests that T cell targeting may be efficacious therapeutically broadly throughout disease progression.

Aligning with the importance of the T cell response in RA progression, CTLA-4 fusion protein (CTLA-4-Ig; Abatacept), a soluble protein that binds CD80/CD86 expressed by activated APCs and outcompetes CD28 expressed by T cells at the beginning of the immune response, was approved for use in RA in 2005. Abatacept therefore inhibits circulating and synovial T cell activation by inhibiting CTLA-4:CD28 interactions, and has shown remarkable efficacy in disease management (26), reducing progression of undifferentiated arthritis to RA, and reduction of radiological progression and levels of anti-CCP antibodies (27). Early outcomes from two ongoing trials further suggest Abatacept may also prevent RA development in at-risk healthy individuals (28–30).

4 Inflammatory arthritis as an adverse event of checkpoint therapy in cancer

In cancer, tumour cells can exploit checkpoint pathways controlling the adaptive immune response to neoantigens, inducing tolerance and immune evasion (31, 32). ICIs targeting co-inhibitory receptors in the tumour microenvironment have had remarkable success by unleashing the anti-tumour function of T cells. However, ICI usage is complicated by the occurrence of immune-related adverse events (irAEs) which can present with broad manifestations varying by ICI type (33). Additionally, while combinations of ICIs have shown improved oncologic therapeutic response compared to monotherapies (34), the proportion of patients who developed treatment-related severe irAEs were markedly higher with combination therapy (55%) compared with those in the nivolumab- (16.3%) or ipilimumab-only groups (27.3%), demonstrating that combination therapy may dramatically increase irAE risk (34).

Rheumatological complications occur in ~5-10% of patients treated with ICIs (35), and can manifest in the form of joint inflammation indistinguishable from RA (36), which can persist after therapy cessation (37) and exacerbate existing RA symptoms (38). Additionally, inflammatory arthritis is the most common irAE reported in trials of ICIs (39), an occurrence that has offered a serendipitous window into RA pathogenesis.

5 The role of co-stimulatory pathways in RA

5.1 CTLA-4/CD28/CD80/CD86 pathway

The most well-studied checkpoint pathway in RA is the CTLA-4/CD28/CD80/CD86 pathway. CTLA-4 is the first co-inhibitory molecule to be upregulated following lymphocyte activation (Figure 1) and is critical for controlling initial naïve T cell activation in lymph nodes (40, 41). CTLA-4 is important for Treg function, and binds CD80 with approximately 20 times the affinity of CD28 (42), enabling it to potently inhibit T cell activation. Following binding to CD80/CD86, CTLA-4 can transendocytose its ligands from the APC which are then degraded by the T cell, further impairing co-stimulation through CD28 (43–45).

The most compelling evidence of the role of the CTLA-4/CD28 pathway in the pathogenesis of RA is demonstrated by the efficacy of Abatacept in treating RA. Accordingly, polymorphisms in *CTLA4* have been associated with both the development and a decreased risk of RA (46, 47). In RA, serum concentrations of soluble CTLA-4 and CD28 were higher than in healthy controls and serum CTLA-4 correlated positively with disease activity (DAS28) (48), while CTLA-4 expression on RA Tregs was lower compared with healthy controls (49). However, despite the clear role of the CTLA-4/CD28 pathway in the RA immune response, many patients do not respond adequately to Abatacept, indicating disease biology driven by alternative inflammatory pathways (possibly including other checkpoint mechanisms) and highlight the critical unmet need for the development of individualised targeted therapy in RA. Further research into the potential of targeting other co-stimulatory pathways may provide these new approaches, and our knowledge of the role of these pathways in RA is summarised below.

5.2 The PD-1 pathway

Inhibitory signalling through PD-1 regulates activated T cells in later stages of activation (Figure 1) primarily in peripheral tissues, and is associated with chronic antigen exposure (12, 40). PD-1 signalling results in immunoreceptor tyrosine-based switch motif phosphorylation and recruits the tyrosine phosphatase SHP-2, inhibiting cell proliferation and cytokine production (50). In the chronically inflamed RA synovium, in line with the relationship between PD-1/PD-L1 inhibitors and the development of irAEs, expression of PD-1 correlated with synovial inflammation (51), and PD-1 expressing T cells were enriched in the early and established RA ST and periphery (52, 53). These were T peripheral helper (Tph) cells, which contribute to pathogenesis by high production of CXCL13 and interleukin (IL)-21, enabling them to provide B cell help outside of germinal centres (53, 54). Tph cells express high levels of MAF and BATF, and unlike Tfh cells, low levels of *BCL6* (53). Additionally, accumulation of PD-1$^+$ activated B cells characterised by increased CD80, CD86, IL-1β and GM-CSF have been demonstrated in the RA ST and SF (55).

Elevated soluble PD-1 (sPD-1) produced by alternative splicing has been demonstrated in the RA periphery (56), and sPD-1 levels positively correlated with RF titres (57) and levels of TNF in the synovial fluid (58). Meanwhile, the PD-1 ligand PD-L1 was conspicuously absent from the ST (56), and sPD-1 has been demonstrated to bind PD-L1 and PD-L2 (59). Therefore, the findings of elevated PD-1$^+$ T cells in the synovium along with elevated sPD-1 and undetectable PD-L1 suggest that the PD-1 pathway is dysregulated in RA, and this lack of PD-1-mediated

inhibitory signalling may result in chronic T cell activation, thus contributing to pathogenesis (58, 60).

The evidence suggesting PD-1 pathway dysregulation in RA and the identification of pathogenic PD-1-expressing cells, particularly in early RA, suggests the therapeutic potential of targeting this pathway. In a phase IIa trial, Peresolimab, an anti-PD-1 agonistic antibody, induced a significant reduction in DAS28-CRP by week 12 (61), while another PD-1 agonist Rosnilimab, is awaiting entry into phase II trials in the near future (62). However, given the success of PD-1 inhibition in cancer, longer phase III trials will be required to fully assess the safety profiles of these therapies with regards to oncologic risk.

Finally, recent studies have highlighted the interplay between the PD-1 and CTLA-4/CD28 pathways. On APCs, PD-L1 can form a complex in *cis* with CD80 (63). This duplex prevents PD-1:PD-L1 binding, inhibiting PD-1 function. Approaches to disrupt this complex using anti-CD80 antibody alleviated autoimmune symptoms (including experimental arthritis) in mice (64), and therefore further study into how the interplay between these pathways contributes to RA pathogenesis is warranted to determine whether similar approaches may be of therapeutic benefit.

5.3 CD40-CD40L pathway

CD40 ligand (CD40L) is a stimulatory checkpoint upregulated on T cells following activation. CD40-CD40L signalling promotes antibody production and class-switching in B cells (65), induces proinflammatory cytokines, chemokines, and adhesion molecules, and can regulate other immune checkpoints (66). Disruption of CD40-CD40L caused by inherited loss-of-function mutations in *CD40* or *CD40L* lead to the X-linked hyper-IgM syndrome, severely compromising humoral immunity (67). Conversely, gain-of-function mutations in *CD40* are associated with RA risk and patients homozygous for these alleles express increased B cell CD40 (68). Additionally, in undifferentiated arthritis, and early and established RA, expression of *CD40* and *CD40LG* were increased compared to osteoarthritis and healthy controls, while expanded $CD8^+CD40L^+$ ST T cells clones from RA patients expressed CD40L (69), further suggesting a role for increased local CD40- CD40L signalling in the RA ST (70). Finally, supporting the association between increased CD40-CD40L signalling and RA, a recent genome-wide protein quantitative trait locus (pQTL) study demonstrated association with elevated serum CD40 and RA risk (71).

While disruption of CD40-CD40L in patients with homozygous mutations is associated with immunodeficiency, heterozygous carriers are unaffected, indicating that therapeutic inhibition of CD40-CD40L may be well-tolerated (68). Indeed, in a phase 1b clinical trial assessing the therapeutic benefit of systemic CD40L blockade in RA, a CD40L-binding protein VIB4920 significantly decreased disease activity and demonstrated an acceptable safety profile (72). At week 12, 41.7% of patients in the VIB4920 1500 mg group achieved a DAS28-CRP score of <2.6, compared to 6.7% in the placebo group (72). Subsequently, VIB4920 has entered phase II trials alongside anti-TNF.

5.4 ICOS

The inducible T cell co-stimulator (ICOS) is expressed by T cells following CD28-co-stimulation (Figure 1) and is structurally similar to CD28, yet differs functionally by its ability to induce IL-10 following ligation, and inability to induce IL-2 (73). Interaction with its ligand ICOSL induces phosphoinositide 3-kinase (PIK3)-dependent signalling, promoting T cell differentiation and germinal centre formation (74). ICOS signalling was shown to be required for collagen induced arthritis (75, 76), and ICOS-ICOSL blockade targeting ICOSL significantly ameliorated joint inflammation, disease progression and severity (77). In RA, patients had increased proportions of $ICOS^+$ synovial fluid T cells compared to RA peripheral blood T cells (78).

Acaziocolcept, a dual ICOS/CD28 inhibitor trialed for therapeutic efficacy in a murine model of systemic sclerosis (79), inhibited collagen-induced arthritis more potently than Abatacept, and inhibited human T cell function more effectively than inhibition of either ICOS or CD28 alone, suggesting its potential therapeutic use in human disease (80).

5.5 OX40L

OX40 (CD134), similarly to CTLA-4, PD-1 and ICOS, is predominantly expressed by T cells after activation (81). Its ligand OX40L can be induced on APC, Langerhans cells, endothelial cells, mast cells, and NK cells, suggesting a range of functions in lymphoid and non-lymphoid pathways (82). OX40 signalling on T cells provides synergistic signalling alongside CD80-CD28 that prolongs T cell proliferation and enhances IL-2 production (83), while bidirectional signalling through OX40L induces the production of proinflammatory mediators and increased antibody production (84).

In early RA, soluble OX40L was increased and positively correlated with ACPA and RF (85). In the joints, OX40L inhibited osteoclastogenesis (84), and mice lacking OX40L showed decreased bone integrity and enhanced osteoclastogenic capacity (84). Despite this, OX40L blockade in collagen induced arthritis reduced inflammation and inhibited inflammatory cytokine production by OX40L-expressing macrophages (84). Interestingly, patients with RA have been shown to have an abundance of $OX40^+$ Tfh cells capable of producing IL-17 (86), and OX40 was enhanced on Tfh cells within the lymph nodes and demonstrated that severity of arthritis was reduced by blockade using anti-OX40L in glucose-6-phosphate isomerase-induced arthritis.

5.6 BTLA/HVEM/CD160/LIGHT regulatory network

B- and T-lymphocyte attenuator (BTLA) is a member of the CD28 immunoglobulin super family, and is expressed broadly by T and B cells, NK cells, and DCs (87). BTLA forms an intricate regulatory network together with CD160, and LIGHT (TNFSF14), sharing the ligand HVEM (herpes virus entry mediator;

TNFRSF14) (88, 89). This network can elicit inhibitory or stimulatory signals depending on the cells expressing them and whether their interactions occur in *cis*- or *trans*- (Figure 1) (88). BTLA and HVEM were present in the established RA ST (90), while in the peripheral blood, BTLA was increased on circulating $CD3^+$ T cells while HVEM and LIGHT were decreased compared to healthy controls (91). *BTLA* polymorphisms have also been associated with RA risk (92). HVEM also binds glycoprotein D (gD) which competes for binding with BTLA and CD160 (88, 93); efforts into blocking the BTLA-HVEM interaction using gD fragments for future cancer therapy are ongoing (94). Reciprocal approaches to free HVEM for interaction with BTLA and CD160 may induce inhibitory signalling and provide a future therapeutic approach in RA.

6 Other pathways

Research into other inhibitory immune checkpoints including TIGIT, TIM-3, and LAG-3 is currently underway in cancer (32, 95), and are tantalising future targets in RA. Increased TIGIT expression on $CD4^+$ RA T cells correlated with autoantibody levels and DAS28 (96), and an agonistic anti-TIGIT antibody, capable of inhibiting Tfh and Tph cells and enhancing Treg function, has recently been described (97). Tregs expressing TIGIT supressed Th1 and Th17 cell responses (98) and signalling through TIGIT on functionally defective Tregs from patients with multiple sclerosis restored suppressive function (99), highlighting the potential of TIGIT-targeting. LAG-3 is constitutively expressed on Tregs; LAG-3 positive Tregs in peripheral blood were reduced in RA patients with higher disease activity, and increased following abatacept therapy (100). Additionally, soluble LAG-3 was increased in early and established RA, correlated with ACPA/RF status and erosive progression in early RA, and decreased inflammatory cytokine release in chronic RA (101). Finally, T cell expression of TIM-3, was increased in RA patients and correlated with decreased DAS28 (102).

Leukocyte-associated immunoglobulin receptors 1 and 2 (LAIR-1 and LAIR-2, respectively) are inhibitory immune receptors for collagens that are expressed broadly across the immune compartment (103, 104). LAIR-1 engagement by collagen or the complement component C1q induces inhibitory T cell signalling (105), and in collagen-induced arthritis, administration of anti-LAIR-1 antibodies significantly attenuated disease (106, 107). In RA, T cell expression of LAIR-1 is reduced compared to healthy and osteoarthritis controls and elevated on ST monocytes and macrophages (108). LAIR-2 is a secreted homolog capable of inhibiting LAIR-1-mediated inhibitory signalling, and is elevated in the RA synovial fluid (109), suggesting dysregulated LAIR-1 action in RA. Together, these suggest that manipulating inhibitory LAIR-1 signalling may offer a future therapeutic approach for RA.

VSIG4 (complement receptor immunoglobulin; CRIg) is a B7-family related protein capable of modulating T cells through interaction with a yet to be identified receptor and has additional roles in immunosuppression (110, 111). VSIG4 binds the complement fragment C3b, inhibiting the alternative complement pathway (112), and approaches utilising this function have shown efficacy in rodent models of RA (113, 114). Administration of soluble VSIG4 reduced disease severity and prevented bone erosion in murine arthritis models (114), and administration of the dual complement inhibitor CRIg-CD59 alleviated symptoms in an adjuvant-induced arthritis rat model (113). In humans, VSIG4 is expressed by tissue-resident regulatory macrophages in the healthy and RA ST from patients in remission (115), and importantly, polymorphisms in *VSIG4* have been associated with RA severity (116).

Finally, the signalling lymphocytic activation molecule (SLAM) family has gained recent attention in RA. SLAMF6 was increased in osteoarthritis and early RA ST (117), and in circulating early RA $PD\text{-}1^+CD4^+$ cells (54) and inhibition of SLAMF6 on $CD4^+PD\text{-}1^+$ peripheral cells from established RA patients decreased IgG production and plasmablast differentiation (53).

7 Future directions

With their undeniable role in the RA autoimmune milieu, the potential of targeting immune checkpoint pathways with novel approaches is an area of immense interest in RA research. These include modulation utilising small molecules including non-coding microRNAs, and their use in downregulating inhibitory checkpoint pathways are currently under investigation in cancer (118, 119). These are attractive because of their ability to target not only a single gene, but entire pathways (120). Similar strategies capable of inducing these pathways may therefore be efficacious in alleviating autoimmune inflammation. Indeed, MEG3, a long non-coding RNA can modulate TIGIT expression on $CD4^+$ T cells from aplastic anaemia patients (121).

The co-expression of checkpoint molecules on individual cells suggests the approach of targeting multiple checkpoints simultaneously, and there has been significant recent interest in targeting dual targets by bi-specific antibodies. CTLA-4/OX40 (ATOR-1015) (122), and PD-L1/CTLA-4 (KN046) bi-specifics are currently in trial for use in cancer (123). In RA, bi-specific approaches have the potential advantage of targeting checkpoint molecules specifically in the inflammatory niche. For instance, a bi-specific targeting TNF and synovial-specific domain scFv-A7, shows remarkable tissue and disease specificity for the microvascular compartment of the human arthritic ST (124). Interestingly, fewer irAEs appear to be observed following the use of bi-specific antibodies in cancer therapy compared to combination therapy, likely as a result of their site-specific nature (125).

Finally, while the adverse events associated with the use of ICIs in cancer therapy are reasonably well documented, the current lack of agonistic antibodies targeted to checkpoint pathways in human trials makes it difficult to remark on the potential risks associated with the use of checkpoint agonists for the treatment of chronic diseases such as RA. In initial trials, severe adverse events were documented while testing an anti-CD28 agonist in healthy control patients (126), while early trials of Peresolimab in RA do not suggest the development of severe adverse events (61), and in cancer, agonistic antibodies targeting OX40 showed acceptable safety

profiles (127). However longer, and larger trials are required to fully assess safety profiles and effect on oncologic risk (61).

8 Concluding remarks

The role of immune checkpoint molecules in RA is a growing area of research, and the elucidation of how these pathways influence the breaching of self-tolerance and drive RA pathogenesis will undoubtedly be critical for selecting the most appropriate therapy for individual patients. However, much remains to be explored, from deciphering the complex interactions between immune cells to fine-tuning the delicate equilibrium of immune activation and suppression. As this field progresses, agonistic immune checkpoint-based therapies may emerge as valuable therapeutic tools for treating RA and may offer new avenues for improved patient care and quality of life.

Author contributions

AS: Conceptualization, Writing – original draft, Writing – review & editing. KL: Writing – original draft, Writing – review & editing. MW: Conceptualization, Funding acquisition, Project administration, Resources, Supervision, Writing – review & editing.

Funding

The author(s) declare financial support was received for the research, authorship, and/or publication of this article. We acknowledge that AS was supported by funding from an Ideas Grant from the National Health and Medical Research Council (NHMRC) of Australia (Grant Number APP2004839).

Conflict of interest

The authors declare that the research was conducted in the absence of any commercial or financial relationships that could be construed as a potential conflict of interest.

Publisher's note

All claims expressed in this article are solely those of the authors and do not necessarily represent those of their affiliated organizations, or those of the publisher, the editors and the reviewers. Any product that may be evaluated in this article, or claim that may be made by its manufacturer, is not guaranteed or endorsed by the publisher.

References

1. Finckh A, Gilbert B, Hodkinson B, Bae S-C, Thomas R, Deane KD, et al. Global epidemiology of rheumatoid arthritis. *Nat Rev Rheumatol* (2022) 18(10):591–602. doi: 10.1038/s41584-022-00827-y

2. Prince FHM, Bykerk VP, Shadick NA, Lu B, Cui J, Frits M, et al. Sustained rheumatoid arthritis remission is uncommon in clinical practice. *Arthritis Res Ther* (2012) 14(2):R68. doi: 10.1186/ar3785

3. Sharpe AH, Freeman GJ. The B7–CD28 superfamily. *Nat Rev Immunol* (2002) 2 (2):116–26. doi: 10.1038/nri727

4. Heinzel S, Marchingo JM, Horton MB, Hodgkin PD. The regulation of lymphocyte activation and proliferation. *Curr Opin Immunol* (2018) 51:32–8. doi: 10.1016/j.coi.2018.01.002

5. Magee CN, Boenisch O, Najafian N. The role of costimulatory molecules in directing the functional differentiation of alloreactive T helper cells. *Am J Transplant* (2012) 12(10):2588–600. doi: 10.1111/j.1600-6143.2012.04180.x

6. Chen L, Flies DB. Molecular mechanisms of T cell co-stimulation and co-inhibition. *Nat Rev Immunol* (2013) 13(4):227–42. doi: 10.1038/nri3405

7. Sharpe AH. Introduction to checkpoint inhibitors and cancer immunotherapy. *Immunol Rev* (2017) 276(1):5–8. doi: 10.1111/imr.12531

8. Beier KC, Kallinich T, Hamelmann E. Master switches of T-cell activation and differentiation. *Eur Respir J* (2007) 29(4):804. doi: 10.1183/09031936.00094506

9. Verma N, Burns SO, Walker LSK, Sansom DM. Immune deficiency and autoimmunity in patients with CTLA-4 (CD152) mutations. *Clin Exp Immunol* (2017) 190(1):1–7. doi: 10.1111/cei.12997

10. Ogishi M, Yang R, Aytekin C, Langlais D, Bourgey M, Khan T, et al. Inherited PD-1 deficiency underlies tuberculosis and autoimmunity in a child. *Nat Med* (2021) 27 (9):1646–54. doi: 10.1038/s41591-021-01388-5

11. Khattri R, Auger JA, Griffin MD, Sharpe AH, Bluestone JA. Lymphoproliferative disorder in CTLA-4 knockout mice is characterized by CD28-regulated activation of Th2 responses. *J Immunol* (1999) 162(10):5784–91. doi: 10.4049/jimmunol.162.10.5784

12. Sharpe AH, Pauken KE. The diverse functions of the PD1 inhibitory pathway. *Nat Rev Immunol* (2018) 18(3):153–67. doi: 10.1038/nri.2017.108

13. Nishimura H, Nose M, Hiai H, Minato N, Honjo T. Development of lupus-like autoimmune diseases by disruption of the PD-1 gene encoding an ITIM motif-carrying immunoreceptor. *Immunity* (1999) 11(2):141–51. doi: 10.1016/S1074-7613(00)80089-8

14. Frebel H, Nindl V, Schuepbach RA, Braunschweiler T, Richter K, Vogel J, et al. Programmed death 1 protects from fatal circulatory failure during systemic virus infection of mice. *J Exp Med* (2012) 209(13):2485–99. doi: 10.1084/jem.20121015

15. Weyand CM, Bryl E, Goronzy JJ. The role of T cells in rheumatoid arthritis. *Arch Immunol Ther Exp (Warsz)* (2000) 48(5):429–35.

16. Smith MD, J, Highton J, Palmer DG, Rozenbilds M, Roberts-Thomson PJ. Immunohistochemical analysis of synovial membranes from inflammatory and non-inflammatory arthritides: scarcity of CD5 positive B cells and IL2 receptor bearing T cells. *Pathology* (1992) 24(1):19–26. doi: 10.3109/00313029209063615

17. Cope AP. T cells in rheumatoid arthritis. *Arthritis Res Ther* (2008) 10(1):S1. doi: 10.1186/ar2412

18. Fournier C. Where do T cells stand in rheumatoid arthritis? *Joint Bone Spine* (2005) 72(6):527–32. doi: 10.1016/j.jbspin.2004.12.012

19. Hähnlein JS, Nadafi R, Jong T, Ramwadhdoebe TH, Semmelink JF, Maijer KI, et al. Impaired lymph node stromal cell function during the earliest phases of rheumatoid arthritis. *Arthritis Res Ther* (2018) 20(1):35. doi: 10.1186/s13075-018-1529-8

20. Tracy A, Buckley CD, Raza K. Pre-symptomatic autoimmunity in rheumatoid arthritis: when does the disease start? *Semin Immunopathol* (2017) 39(4):423–35. doi: 10.1007/s00281-017-0620-6

21. Anang DC, Ramwadhdoebe TH, Hähnlein JS, van Kuijk B, Smits N, van Lienden KP, et al. Increased frequency of CD4+ Follicular helper T and CD8+ Follicular T cells in human lymph node biopsies during the earliest stages of rheumatoid arthritis. *Cells* (2022) 11(7):1104. doi: 10.3390/cells11071104

22. Hunt L, Hensor EM, Nam J, Burska AN, Parmar R, Emery P, et al. T cell subsets: an immunological biomarker to predict progression to clinical arthritis in ACPA-positive individuals. *Ann Rheum Dis* (2016) 75(10):1884–9. doi: 10.1136/annrheumdis-2015-207991

23. Karouzakis E, Hähnlein J, Grasso C, Semmelink JF, Tak PP, Gerlag DM, et al. Molecular characterization of human lymph node stromal cells during the earliest phases of rheumatoid arthritis. *Front Immunol* (2019) 10. doi: 10.3389/fimmu.2019.01863

24. Nielen MM, van Schaardenburg D, Reesink HW, van de Stadt RJ, van der Horst-Bruinsma IE, Koning MH, et al. Specific autoantibodies precede the symptoms of rheumatoid arthritis: a study of serial measurements in blood donors. *Arthritis Rheum* (2004) 50(2):380–6. doi: 10.1002/art.20018

25. Dennis G Jr., Holweg CTJ, Kummerfeld SK, Choy DF, Setiadi AF, Hackney JA, et al. Synovial phenotypes in rheumatoid arthritis correlate with response to biologic therapeutics. *Arthritis Res Ther* (2014) 16(2):R90–0. doi: 10.1186/ar4555

26. Maxwell L, Singh JA. Abatacept for rheumatoid arthritis. *Cochrane Database Syst Rev* (2009) 2009(4):Cd007277. doi: 10.1002/14651858.CD007277.pub2

27. Emery P, Durez P, Dougados M, Legerton CW, Becker JC, Vratsanos G, et al. Impact of T-cell costimulation modulation in patients with undifferentiated inflammatory arthritis or very early rheumatoid arthritis: a clinical and imaging study of abatacept (the ADJUST trial). *Ann Rheum Dis* (2010) 69(3):510–6. doi: 10.1136/ard.2009.119016

28. Al-Laith M, Jasenecova M, Abraham S, Bosworth A, Bruce IN, Buckley CD, et al. Arthritis prevention in the pre-clinical phase of RA with abatacept (the APIPPRA study): a multi-centre, randomised, double-blind, parallel-group, placebo-controlled clinical trial protocol. *Trials* (2019) 20(1):429. doi: 10.1186/s13063-019-3403-7

29. Rech J, Kleyer A, Østergaard M, Hagen M, Valor L, Tascilar K, et al. Abatacept delays the development of RA–clinical results after 18 months from the randomized, placebo-controlled ARIAA study in RA-at risk patients. *Ann Rheum Dis* (2022) 81:526. doi: 10.1136/annrheumdis-2022-eular.1693

30. Cope A, Jasenecova M, Vasconcelos J, Filer A, Raza K, Qureshi S, et al. Abatacept in individuals at risk of developing rheumatoid arthritis: results from the Arthritis Prevention in the Pre-Clinical Phase of RA with Abatacept (APIPPRA) trial. *Ann Rheum Dis* (2023) 82:86. doi: 10.1136/annrheumdis-2023-eular.1751

31. Sadeghi Rad H, Monkman J, Warkiani ME, Ladwa R, K, Rezaei N, et al. Understanding the tumor microenvironment for effective immunotherapy. *Med Res Rev* (2021) 41(3):1474–98. doi: 10.1002/med.21765

32. Shiravand Y, Khodadadi F, Kashani SMA, Hosseini-Fard SR, Hosseini S, Sadeghirad H, et al. Immune checkpoint inhibitors in cancer therapy. *Curr Oncol* (2022) 29(5):3044–60. doi: 10.3390/curroncol29050247

33. Conroy M, Naidoo J. Immune-related adverse events and the balancing act of immunotherapy. *Nat Commun* (2022) 13(1):392. doi: 10.1038/s41467-022-27960-2

34. Larkin J, Chiarion-Sileni V, Gonzalez R, Grob JJ, Cowey CL, Lao CD, et al. Combined nivolumab and ipilimumab or monotherapy in untreated melanoma. *New Engl J Med* (2015) 373(1):23–34. doi: 10.1056/NEJMoa1504030

35. Abdel-Wahab N, Suarez-Almazor ME. Frequency and distribution of various rheumatic disorders associated with checkpoint inhibitor therapy. *Rheumatol (Oxford)* (2019) 58(Suppl 7):vii40–8. doi: 10.1093/rheumatology/kez297

36. Murray-Brown W, Wilsdon TD, Weedon H, Proudman S, Sukumaran S, Klebe S, et al. Nivolumab-induced synovitis is characterized by florid T cell infiltration and rapid resolution with synovial biopsy-guided therapy. *J immunother Cancer* (2020) 8 (1):e000281. doi: 10.1136/jitc-2019-000281

37. Tawnie JB, Julie RB, Patrick MF, Dung L, Evan JL, Jarushka N, et al. Immune checkpoint inhibitor-induced inflammatory arthritis persists after immunotherapy cessation. *Ann Rheum Dis* (2020) 79(3):332. doi: 10.1136/annrheumdis-2019-216109

38. Jaberg-Bentele NF, Kunz M, Abuhammad S, Dummer R. Flare-up of rheumatoid arthritis by anti-CTLA-4 antibody but not by anti-PD1 therapy in a patient with metastatic melanoma. *Case Rep Dermatol* (2017) 9(1):65–8. doi: 10.1159/000454875

39. Cappelli LC, Shah AA, Bingham CO 3rd. Immune-related adverse effects of cancer immunotherapy- implications for rheumatology. *Rheum Dis Clin North Am* (2017) 43(1):65–78. doi: 10.1016/j.rdc.2016.09.007

40. Buchbinder EI, Desai A. CTLA-4 and PD-1 pathways: similarities, differences, and implications of their inhibition. *Am J Clin Oncol* (2016) 39(1):98–106. doi: 10.1097/COC.0000000000000239

41. Brunet JF, Denizot F, Luciani MF, Roux-Dosseto M, Suzan M, Mattei MG, et al. A new member of the immunoglobulin superfamily–CTLA-4. *Nature* (1987) 328 (6127):267–70. doi: 10.1038/328267a0

42. Linsley PS, Brady W, Urnes M, Grosmaire LS, Damle NK, Ledbetter JA. CTLA-4 is a second receptor for the B cell activation antigen B7. *J Exp Med* (1991) 174(3):561–9. doi: 10.1084/jem.174.3.561

43. Kennedy A, Waters E, Rowshanravan B, Hinze C, Williams C, Janman D, et al. Differences in CD80 and CD86 transendocytosis reveal CD86 as a key target for CTLA-4 immune regulation. *Nat Immunol* (2022) 23(9):1365–78. doi: 10.1038/s41590-022-01289-w

44. Rowshanravan B, Halliday N, Sansom DM. CTLA-4: a moving target in immunotherapy. *Blood* (2018) 131(1):58–67. doi: 10.1182/blood-2017-06-741033

45. Qureshi OS, Zheng Y, Nakamura K, Attridge K, Manzotti C, Schmidt EM, et al. Trans-endocytosis of CD80 and CD86: A molecular basis for the cell-extrinsic function of CTLA-4. *Science* (2011) 332(6029):600–3. doi: 10.1126/science.1202947

46. Zhou C, Gao S, Yuan X, Shu Z, Li S, Sun X, et al. Association between CTLA-4 gene polymorphism and risk of rheumatoid arthritis: a meta-analysis. *Aging (Albany NY)* (2021) 13(15):19397–414. doi: 10.18632/aging.203349

47. Liu W, Yang Z, Chen Y, Yang H, Wan X, Zhou X, et al. The association between CTLA-4, CD80/86, and CD28 gene polymorphisms and rheumatoid arthritis: an original study and meta-analysis. *Front Med (Lausanne)* (2021) 8:598076. doi: 10.3389/fmed.2021.598076

48. Cao J, Zou L, Luo P, Chen P, Zhang L. Increased production of circulating soluble co-stimulatory molecules CTLA-4, CD28 and CD80 in patients with rheumatoid arthritis. *Int Immunopharmacol* (2012) 14(4):585–92. doi: 10.1016/j.intimp.2012.08.004

49. Flores-Borja F, Jury EC, Mauri C, Ehrenstein MR. Defects in CTLA-4 are associated with abnormal regulatory T cell function in rheumatoid arthritis. *Proc Natl Acad Sci U.S.A.* (2008) 105(49):19396–401. doi: 10.1073/pnas.0806855105

50. Okazaki T, Chikuma S, Iwai Y, Fagarasan S, Honjo T. A rheostat for immune responses: the unique properties of PD-1 and their advantages for clinical application. *Nat Immunol* (2013) 14(12):1212–8. doi: 10.1038/ni.2762

51. Raptopoulou AP, Bertsias G, Makrygiannakis D, Verginis P, Kritikos I, Tzardi M, et al. The programmed death 1/programmed death ligand 1 inhibitory pathway is up-regulated in rheumatoid synovium and regulates peripheral T cell responses in human and murine arthritis. *Arthritis Rheum* (2010) 62(7):1870–80. doi: 10.1002/art.27500

52. Murray-Brown W, Guo Y, Small A, Lowe K, Weedon H, Smith MD, et al. Differential expansion of T peripheral helper cells in early rheumatoid arthritis and osteoarthritis synovium. *RMD Open* (2022) 8(2). doi: 10.1136/rmdopen-2022-002563

53. Rao DA, Gurish MF, Marshall JL, Slowikowski K, Fonseka CY, Liu Y, et al. Pathologically expanded peripheral T helper cell subset drives B cells in rheumatoid arthritis. *Nature* (2017) 542(7639):110–4. doi: 10.1038/nature20810

54. Lowe K, Small A, Song Q, Hao L-Y, Murray-Brown W, Proudman S, et al. Transcriptomic profiling of programmed cell death 1 (PD-1) expressing T cells in early rheumatoid arthritis identifies a decreased CD4 + PD-1 + signature post-treatment. *Sci Rep* (2023) 13(1):2847. doi: 10.1038/s41598-023-29971-5

55. Floudas A, Neto N, Marzaioli V, Murray K, Moran B, Monaghan MG, et al. Pathogenic, glycolytic PD-1+ B cells accumulate in the hypoxic RA joint. *JCI Insight* (2020) 5(21). doi: 10.1172/jci.insight.139032

56. Guo Y, Walsh AM, Canavan M, Wechalekar MD, Cole S, Yin X, et al. Immune checkpoint inhibitor PD-1 pathway is down-regulated in synovium at various stages of rheumatoid arthritis disease progression. *PloS One* (2018) 13(2):e0192704. doi: 10.1371/journal.pone.0192704

57. Liu C, Jiang J, Gao L, Wang X, Hu X, Wu M, et al. Soluble PD-1 aggravates progression of collagen-induced arthritis through Th1 and Th17 pathways. *Arthritis Res Ther* (2015) 17:340. doi: 10.1186/s13075-015-0859-z

58. Wan B, Nie H, Liu A, Feng G, He D, Xu R, et al. Aberrant regulation of synovial T cell activation by soluble costimulatory molecules in rheumatoid arthritis. *J Immunol* (2006) 177(12):8844–50. doi: 10.4049/jimmunol.177.12.8844

59. Khan M, Zhao Z, Arooj S, Fu Y, Liao G. Soluble PD-1: predictive, prognostic, and therapeutic value for cancer immunotherapy. *Front Immunol* (2020) 11. doi: 10.3389/fimmu.2020.587460

60. Canavan M, Floudas A, Veale DJ, Fearon U. The PD-1:PD-L1 axis in inflammatory arthritis. *BMC Rheumatol* (2021) 5(1):1–1. doi: 10.1186/s41927-020-00171-2

61. Tuttle J, Drescher E, Simón-Campos JA, Emery P, Greenwald M, Kivitz A, et al. A phase 2 trial of peresolimab for adults with rheumatoid arthritis. *N Engl J Med* (2023) 388(20):1853–62. doi: 10.1056/NEJMoa2209856

62. Mullard A. PD1 agonist antibody passes first phase II trial for autoimmune disease. *Nat Rev Drug Discovery* (2023) 22(7):526. doi: 10.1038/d41573-023-00087-9

63. Sugiura D, Maruhashi T, Okazaki IM, Shimizu K, Maeda TK, Takemoto T, et al. Restriction of PD-1 function by cis-PD-L1/CD80 interactions is required for optimal T cell responses. *Science* (2019) 364(6440):558–66. doi: 10.1126/science.aav7062

64. Sugiura D, Okazaki I-M, Maeda TK, Maruhashi T, Shimizu K, Arakaki R, et al. PD-1 agonism by anti-CD80 inhibits T cell activation and alleviates autoimmunity. *Nat Immunol* (2022) 23(3):399–410. doi: 10.1038/s41590-021-01125-7

65. Elgueta R, Benson MJ, de Vries VC, Wasiuk A, Guo Y, Noelle RJ. Molecular mechanism and function of CD40/CD40L engagement in the immune system. *Immunol Rev* (2009) 229(1):152–72. doi: 10.1111/j.1600-065X.2009.00782.x

66. Román-Fernández IV, García-Chagollán MA, Cerpa-Cruz S, Jave-Suárez LF, Palafox-Sánchez CA, García-Arellano S, et al. Assessment of CD40 and CD40L expression in rheumatoid arthritis patients, association with clinical features and DAS28. *Clin Exp Med* (2019) 19(4):427–37. doi: 10.1007/s10238-019-00568-5

67. Danese S, Sans M, Fiocchi C. The CD40/CD40L costimulatory pathway in inflammatory bowel disease. *Gut* (2004) 53(7):1035. doi: 10.1136/gut.2003.026278

68. Li G, Diogo D, Wu D, Spoonamore J, Dancik V, Franke L, et al. Human genetics in rheumatoid arthritis guides a high-throughput drug screen of the CD40 signaling pathway. *PloS Genet* (2013) 9(5):e1003487. doi: 10.1371/journal.pgen.1003487

69. Kang YM, Zhang X, Wagner UG, Yang H, Beckenbaugh RD, Kurtin PJ, et al. CD8 T cells are required for the formation of ectopic germinal centers in rheumatoid synovitis. *J Exp Med* (2002) 195(10):1325–36. doi: 10.1084/jem.20011565

70. Guo Y, Walsh AM, Fearon U, Smith MD, Wechalekar MD, Yin X, et al. CD40L-dependent pathway is active at various stages of rheumatoid arthritis disease progression. *J Immunol* (2017) 198(11):4490–501. doi: 10.4049/jimmunol.1601988

71. Zhao JH, Stacey D, Eriksson N, Macdonald-Dunlop E, Hedman ÅK, Kalnapenkis A, et al. Genetics of circulating inflammatory proteins identifies drivers of immune-mediated disease risk and therapeutic targets. *Nat Immunol* (2023) 24 (9):1540–51. doi: 10.1038/s41590-023-01588-w

72. Karnell JL, Albulescu M, Drabic S, Wang L, Moate R, Baca M, et al. A CD40L-targeting protein reduces autoantibodies and improves disease activity in patients with autoimmunity. *Sci Transl Med* (2019) 11(489). doi: 10.1126/scitranslmed.aar6584

73. Hutloff A, Dittrich AM, Beier KC, Eljaschewitsch B, Kraft R, Anagnostopoulos I, et al. ICOS is an inducible T-cell co-stimulator structurally and functionally related to CD28. *Nature* (1999) 397(6716):263–6. doi: 10.1038/16717

74. Gigoux M, Shang J, Pak Y, Xu M, Choe J, Mak TW, et al. Inducible costimulator promotes helper T-cell differentiation through phosphoinositide 3-kinase. *Proc Natl Acad Sci U.S.A.* (2009) 106(48):20371–6. doi: 10.1073/pnas.0911573106

75. Panneton V, Bagherzadeh Yazdchi S, Witalis M, Chang J, Suh WK. ICOS signaling controls induction and maintenance of collagen-induced arthritis. *J Immunol* (2018) 200(9):3067–76. doi: 10.4049/jimmunol.1701305

76. Hamel KM, Cao Y, Olalekan SA, Finnegan A. B cell-specific expression of inducible costimulator ligand is necessary for the induction of arthritis in mice. *Arthritis Rheumatol* (2014) 66(1):60–7. doi: 10.1002/art.38207

77. O'Dwyer R, Kovaleva M, Zhang J, Steven J, Cummins E, Luxenberg D, et al. Anti-ICOSL new antigen receptor domains inhibit T cell proliferation and reduce the development of inflammation in the collagen-induced mouse model of rheumatoid arthritis. *J Immunol Res 2018* (2018) p:4089459. doi: 10.1155/2018/4089459

78. Okamoto T, Saito S, Yamanaka H, Tomatsu T, Kamatani N, Ogiuchi H, et al. Expression and function of the co-stimulator H4/ICOS on activated T cells of patients with rheumatoid arthritis. *J Rheumatol* (2003) 30(6):1157–63.

79. Orvain C, Cauvet A, Prudent A, Guignabert C, Thuillet R, Ottaviani M, et al. Acazicolcept (ALPN-101), a dual ICOS/CD28 antagonist, demonstrates efficacy in systemic sclerosis preclinical mouse models. *Arthritis Res Ther* (2022) 24(1):13. doi: 10.1186/s13075-021-02709-2

80. Dillon SR, Evans LS, Lewis KE, Debrot S, Blair TC, Mudri S, et al. Non-redundant roles of T cell costimulation pathways in inflammatory arthritis revealed by dual blockade of ICOS and CD28 with acazicolcept (ALPN-101). *Arthritis Rheumatol* (2023) 75(8):1344–56. doi: 10.1002/art.42484

81. Alves Costa Silva C, Facchinetti F, Routy B, Derosa L. New pathways in immune stimulation: targeting OX40. *ESMO Open* (2020) 5(1):e000573. doi: 10.1136/esmoopen-2019-000573

82. Croft M, So T, Duan W, Soroosh P. The significance of OX40 and OX40L to T-cell biology and immune disease. *Immunol Rev* (2009) 229(1):173–91. doi: 10.1111/j.1600-065X.2009.00766.x

83. Gramaglia I, Weinberg AD, Lemon M, Croft M. Ox-40 ligand: a potent costimulatory molecule for sustaining primary CD4 T cell responses. *J Immunol* (1998) 161(12):6510–7. doi: 10.4049/jimmunol.161.12.6510

84. Gwyer Findlay E, Danks L, Madden J, Cavanagh MM, McNamee K, McCann F, et al. OX40L blockade is therapeutic in arthritis, despite promoting osteoclastogenesis. *Proc Natl Acad Sci U.S.A.* (2014) 111(6):2289–94. doi: 10.1073/pnas.1321071111

85. Laustsen JK, Rasmussen TK, Stengaard-Pedersen K, Hørslev-Petersen K, Hetland ML, Østergaard M, et al. Soluble OX40L is associated with presence of autoantibodies in early rheumatoid arthritis. *Arthritis Res Ther* (2014) 16(5):474. doi: 10.1186/s13075-014-0474-4

86. Kurata I, Matsumoto I, Ohyama A, Osada A, Ebe H, Kawaguchi H, et al. Potential involvement of OX40 in the regulation of autoantibody sialylation in arthritis. *Ann Rheum Dis* (2019) 78(11):1488–96. doi: 10.1136/annrheumdis-2019-215195

87. Ritthipichai K, Haymaker CL, Martinez M, Aschenbrenner A, Yi X, Zhang M, et al. Multifaceted role of BTLA in the control of CD8(+) T-cell fate after antigen encounter. *Clin Cancer Res* (2017) 23(20):6151–64. doi: 10.1158/1078-0432.CCR-16-1217

88. Rodriguez-Barbosa JI, Schneider P, Weigert A, Lee K-M, Kim T-J, Perez-Simon J-A, et al. HVEM, a cosignaling molecular switch, and its interactions with BTLA, CD160 and LIGHT. *Cell Mol Immunol* (2019) 16(7):679–82. doi: 10.1038/s41423-019-0241-1

89. Small A, Cole S, Wang JJ, Nagpal S, Hao LY, Wechalekar MD. Attenuation of the BTLA/HVEM regulatory network in the circulation in primary sjögren's syndrome. *J Clin Med* (2022) 11(3). doi: 10.3390/jcm11030535

90. Shang Y, Guo G, Cui Q, Li J, Ruan Z, Chen Y. The expression and anatomical distribution of BTLA and its ligand HVEM in rheumatoid synovium. *Inflammation* (2012) 35(3):1102–12. doi: 10.1007/s10753-011-9417-2

91. Yang B, Huang Z, Feng W, Wei W, Zhang J, Liao Y, et al. The expression of BTLA was increased and the expression of HVEM and LIGHT were decreased in the T cells of patients with rheumatoid arthritis [corrected]. *PloS One* (2016) 11 (5):e0155345. doi: 10.1371/journal.pone.0155345

92. Lin SC, Kuo CC, Chan CH. Association of a BTLA gene polymorphism with the risk of rheumatoid arthritis. *J BioMed Sci* (2006) 13(6):853–60. doi: 10.1007/s11373-006-9113-7

93. Whitbeck JC, Peng C, Lou H, Xu R, Willis SH, Ponce de Leon M, et al. Glycoprotein D of herpes simplex virus (HSV) binds directly to HVEM, a member of the tumor necrosis factor receptor superfamily and a mediator of HSV entry. *J Virol* (1997) 71(8):6083–93. doi: 10.1128/jvi.71.8.6083-6093.1997

94. Kuncewicz K, Battin C, Węgrzyn K, Sieradzan A, Wardowska A, Sikorska E, et al. Targeting the HVEM protein using a fragment of glycoprotein D to inhibit formation of the BTLA/HVEM complex. *Bioorg Chem* (2022) 122:105748. doi: 10.1016/j.bioorg.2022.105748

95. Qin S, Xu L, Yi M, Yu S, Wu K, Luo S. Novel immune checkpoint targets: moving beyond PD-1 and CTLA-4. *Mol Cancer* (2019) 18(1):155. doi: 10.1186/s12943-019-1091-2

96. Luo Q, Deng Z, Xu C, Zeng L, Ye J, Li X, et al. Elevated expression of immunoreceptor tyrosine-based inhibitory motif (TIGIT) on T lymphocytes is correlated with disease activity in rheumatoid arthritis. *Med Sci Monit* (2017) 23:1232–41. doi: 10.12659/MSM.902454

97. Kojima M, Suzuki K, Takeshita M, Ohyagi M, Iizuka M, Yamane H, et al. Anti-human-TIGIT agonistic antibody ameliorates autoimmune diseases by inhibiting Tfh and Tph cells and enhancing Treg cells. *Commun Biol* (2023) 6(1):500. doi: 10.1038/s42003-023-04874-3

98. Joller N, Lozano E, Burkett PR, Patel B, Xiao S, Zhu C, et al. Treg cells expressing the coinhibitory molecule TIGIT selectively inhibit proinflammatory Th1 and Th17 cell responses. *Immunity* (2014) 40(4):569–81. doi: 10.1016/j.immuni.2014.02.012

99. Lucca LE, Axisa PP, Singer ER, Nolan NM, Dominguez-Villar M, Hafler DA. TIGIT signaling restores suppressor function of Th1 Tregs. *JCI Insight* (2019) 4(3). doi: 10.1172/jci.insight.124427

100. Nakachi S, Sumitomo S, Tsuchida Y, Tsuchiya H, Kono M, Kato R, et al. Interleukin-10-producing LAG3(+) regulatory T cells are associated with disease activity and abatacept treatment in rheumatoid arthritis. *Arthritis Res Ther* (2017) 19 (1):97. doi: 10.1186/s13075-017-1309-x

101. Pedersen JM, Hansen AS, Skejo C, Juul-Madsen K, Junker P, Horslev-Petersen K, et al. Lymphocyte activation gene 3 is increased and affects cytokine production in rheumatoid arthritis. *Arthritis Res Ther* (2023) 25(1):97. doi: 10.1186/s13075-023-03073-z

102. Li S, Peng D, He Y, Zhang H, Sun H, Shan S, et al. Expression of TIM-3 on CD4 + and CD8+ T cells in the peripheral blood and synovial fluid of rheumatoid arthritis. *APMIS* (2014) 122(10):899–904. doi: 10.1111/apm.12228

103. Ramos MIP, Tian L, Ruiter EJ, Song C, Paucarmayta A, Singh A, et al. Cancer immunotherapy by NC410, a LAIR-2 Fc protein blocking human LAIR-collagen interaction. *eLife* (2021) 10:e62927. doi: 10.7554/eLife.62927.sa2

104. Olde Nordkamp MJ, van Roon JA, Douwes M, de Ruiter T, Urbanus RT, Meyaard L. Enhanced secretion of leukocyte-associated immunoglobulin-like receptor 2 (LAIR-2) and soluble LAIR-1 in rheumatoid arthritis: LAIR-2 is a more efficient antagonist of the LAIR-1-collagen inhibitory interaction than is soluble LAIR-1. *Arthritis Rheum* (2011) 63(12):3749–57. doi: 10.1002/art.30612

105. Park J-E, Brand DD, Rosloniec EF, Yi A-K, Stuart JM, Kang AH, et al. Leukocyte-associated immunoglobulin-like receptor 1 inhibits T-cell signaling by decreasing protein phosphorylation in the T-cell signaling pathway. *J Biol Chem* (2020) 295(8):2239–47. doi: 10.1074/jbc.RA119.011150

106. Myers LK, Winstead M, Kee JD, Park JJ, Zhang S, Li W, et al. 1,25-dihydroxyvitamin D3 and 20-hydroxyvitamin D3 upregulate LAIR-1 and attenuate collagen induced arthritis. *Int J Mol Sci* (2021) 22(24). doi: 10.3390/ijms222413342

107. Kim S, Easterling ER, Price LC, Smith SL, Coligan JE, Park J-E, et al. The role of leukocyte-associated ig-like receptor-1 in suppressing collagen-induced arthritis. *J Immunol* (2017) 199(8):2692–700. doi: 10.4049/jimmunol.1700271

108. Zhang Y, Lv K, Zhang CM, Jin BQ, Zhuang R, Ding Y. The role of LAIR-1 (CD305) in T cells and monocytes/macrophages in patients with rheumatoid arthritis. *Cell Immunol* (2014) 287(1):46–52. doi: 10.1016/j.cellimm.2013.12.005

109. Lebbink RJ, van den Berg MC, de Ruiter T, Raynal N, van Roon JA, Lenting PJ, et al. The soluble leukocyte-associated Ig-like receptor (LAIR)-2 antagonizes the collagen/LAIR-1 inhibitory immune interaction. *J Immunol* (2008) 180(3):1662–9. doi: 10.4049/jimmunol.180.3.1662

110. Widyagarini A, Nishii N, Kawano Y, Zhang C, Azuma M. VSIG4/CRIg directly regulates early CD8(+) T cell activation through its counter-receptor in a narrow window. *Biochem Biophys Res Commun* (2022) 614:100–6. doi: 10.1016/j.bbrc.2022.04.120

111. Yuan X, Yang BH, Dong Y, Yamamura A, Fu W. CRIg, a tissue-resident macrophage specific immune checkpoint molecule, promotes immunological tolerance in NOD mice, via a dual role in effector and regulatory T cells. *Elife* (2017) 6. doi: 10.7554/eLife.29540

112. Small AG, Al-Baghdadi M, Quach A, Hii C, Ferrante A. Complement receptor immunoglobulin: a control point in infection and immunity, inflammation and cancer. *Swiss Med Wkly* (2016) 146:w14301. doi: 10.4414/smw.2016.14301

113. Tao S, Yu H, You T, Kong X, Wei X, Zheng Z, et al. A dual-targeted metal–organic framework based nanoplatform for the treatment of rheumatoid arthritis by restoring the macrophage niche. *ACS Nano* (2023) 17(14):13917–37. doi: 10.1021/acsnano.3c03828

114. Katschke KJ Jr., Helmy KY, Steffek M, Xi H, Yin J, Lee WP, et al. A novel inhibitor of the alternative pathway of complement reverses inflammation and bone destruction in experimental arthritis. *J Exp Med* (2007) 204(6):1319–25. doi: 10.1084/jem.20070432

115. Alivernini S, MacDonald L, Elmesmari A, Finlay S, Tolusso B, Gigante MR, et al. Distinct synovial tissue macrophage subsets regulate inflammation and remission in rheumatoid arthritis. *Nat Med* (2020) 26(8):1295–306. doi: 10.1038/s41591-020-0939-8

116. Antunes Andrade F, Eibofner Goeldner I, Pieczarka C, Tong van H, Sena L, Skare T, et al. Impact of VSIG4 gene polymorphisms on susceptibility and functional status of rheumatoid arthritis. *Int J Immunogenet* (2021) 48(3):260–5. doi: 10.1111/iji.12533

117. Walsh AM, Wechalekar MD, Guo Y, Yin X, Weedon H, Proudman SM, et al. Triple DMARD treatment in early rheumatoid arthritis modulates synovial T cell activation and plasmablast/plasma cell differentiation pathways. *PloS One* (2017) 12(9): e0183928. doi: 10.1371/journal.pone.0183928

118. Alotaibi F. Exosomal microRNAs in cancer: Potential biomarkers and immunotherapeutic targets for immune checkpoint molecules. *Front Genet* (2023) 14:1052731. doi: 10.3389/fgene.2023.1052731

119. Kmiołek T, Paradowska-Gorycka A. miRNAs as biomarkers and possible therapeutic strategies in rheumatoid arthritis. *Cells* (2022) 11(3). doi: 10.3390/cells11030452

120. Baumann V, Winkler J. miRNA-based therapies: strategies and delivery platforms for oligonucleotide and non-oligonucleotide agents. *Future Med Chem* (2014) 6(17):1967–84. doi: 10.4155/fmc.14.116

121. Wang J, Liu X, Hao C, Lu Y, Duan X, Liang R, et al. MEG3 modulates TIGIT expression and CD4 + T cell activation through absorbing miR-23a. *Mol Cell Biochem* (2019) 454(1-2):67–76. doi: 10.1007/s11010-018-3453-2

122. Kvarnhammar AM, Veitonmäki N, Hägerbrand K, Dahlman A, Smith KE, Fritzell S, et al. The CTLA-4 x OX40 bispecific antibody ATOR-1015 induces anti-tumor effects through tumor-directed immune activation. *J ImmunoTher Cancer* (2019) 7(1):103. doi: 10.1186/s40425-019-0570-8

123. Yuxiang M, Jinhui X, Yuanyuan Z, Yang Z, Yan H, Yunpeng Y, et al. Phase I trial of KN046, a novel bispecific antibody targeting PD-L1 and CTLA-4 in patients with advanced solid tumors. *J ImmunoTher Cancer* (2023) 11(6):e006654. doi: 10.1136/jitc-2022-006654

124. Ferrari M, Onuoha SC, Fossati-Jimack L, Nerviani A, Alves PL, Pagani S, et al. Novel bispecific antibody for synovial-specific target delivery of anti-TNF therapy in rheumatoid arthritis. *Front Immunol* (2021) 12. doi: 10.3389/fimmu.2021.640070

125. Mortezaee K, Majidpoor J. Reinstating immunogenicity using bispecific anti-checkpoint/agent inhibitors. *BioMed Pharmacother* (2023) 162:114621. doi: 10.1016/j.biopha.2023.114621

126. Suntharalingam G, Perry MR, Ward S, Brett SJ, Castello-Cortes A, Brunner MD, et al. Cytokine storm in a phase 1 trial of the anti-CD28 monoclonal antibody TGN1412. *N Engl J Med* (2006) 355(10):1018–28. doi: 10.1056/NEJMoa063842

127. Curti BD, Kovacsovics-Bankowski M, Morris N, Walker E, Chisholm L, Floyd K, et al. OX40 is a potent immune-stimulating target in late-stage cancer patients. *Cancer Res* (2013) 73(24):7189–98. doi: 10.1158/0008-5472.CAN-12-4174

frontiers | Frontiers in Immunology

TYPE Brief Research Report
PUBLISHED 12 January 2024
DOI 10.3389/fimmu.2023.1268144

Check for updates

OPEN ACCESS

EDITED BY
Chuan-ju Liu,
New York University, United States

REVIEWED BY
Svetlana P. Chapoval,
University of Maryland, United States
Aranzazu Mediero,
Health Research Institute Foundation Jimenez Diaz (IIS-FJD), Spain

*CORRESPONDENCE
Samuel García
samuel.garcia@iisgaliciasur.es

RECEIVED 27 July 2023
ACCEPTED 26 December 2023
PUBLISHED 12 January 2024

CITATION
Martínez-Ramos S, Rafael-Vidal C, Malvar-Fernández B, Pérez N, Mouriño C, Pérez SG, Maceiras Pan FJ, Conde C, Pego-Reigosa JM and García S (2024) Semaphorin3B promotes an anti-inflammatory and pro-resolving phenotype in macrophages from rheumatoid arthritis patients in a MerTK-dependent manner. *Front. Immunol.* 14:1268144. doi: 10.3389/fimmu.2023.1268144

COPYRIGHT
© 2024 Martínez-Ramos, Rafael-Vidal, Malvar-Fernández, Pérez, Mouriño, Pérez, Maceiras Pan, Conde, Pego-Reigosa and García. This is an open-access article distributed under the terms of the Creative Commons Attribution License (CC BY). The use, distribution or reproduction in other forums is permitted, provided the original author(s) and the copyright owner(s) are credited and that the original publication in this journal is cited, in accordance with accepted academic practice. No use, distribution or reproduction is permitted which does not comply with these terms.

Semaphorin3B promotes an anti-inflammatory and pro-resolving phenotype in macrophages from rheumatoid arthritis patients in a MerTK-dependent manner

Sara Martínez-Ramos[1,2], Carlos Rafael-Vidal[1,2], Beatriz Malvar-Fernández[1,2], Nair Pérez[1,2], Coral Mouriño[1,2], Sara García Pérez[1,2], Francisco J. Maceiras Pan[1,2], Carmen Conde[3], Jose María Pego-Reigosa[1,2] and Samuel García[1,2]*

[1]Rheumatology and Immuno-mediated Diseases Research Group (IRIDIS), Galicia Sur Health Research Institute (IIS Galicia Sur), SERGAS-UVIGO, Vigo, Spain, [2]Rheumatology Department, University Hospital Complex of Vigo, Vigo, Spain, [3]Laboratorio de Reumatologia Experimental y Observacional y Servicio de Reumatologia, Instituto de Investigacion Sanitaria de Santiago (IDIS), Hospital Clinico Universitario de Santiago de Compostela (CHUS), Servizo Galego de Saude (SERGAS), Santiago de Compostela, Spain

Previous works from our group show that Semaphorin3B (Sema3B) is reduced in RA and plays a protective role in a mouse arthritis model. In turn, MerTK plays a protective function in murine arthritis models, is expressed by synovial tissue macrophages and is linked to remission in patients with RA. In this study, we examined the role of Sema3B in the phenotypic characteristics of RA macrophages and the implication of MerTK. Peripheral blood monocytes from RA patients were differentiated into IFN-γ (RA $MØ_{IFN-γ}$) or M-CSF (RA $MØ_{M-CSF}$) macrophages and stimulated with LPS, Sema3B or their combination. Alternatively, RA fibroblast like synoviocytes (FLS) were stimulated with RA $MØ_{IFN-γ}$ and RA $MØ_{M-CSF}$ supernatants. Gene expression was determined by qPCR and protein expression and activation by flow cytometry, ELISA and western blot. Sema3B down-regulated the expression of pro-inflammatory mediators, in both RA $MØ_{IFN-γ}$ and RA $MØ_{M-CSF}$. We observed a similar reduction in RA FLS stimulated with the supernatant of Sema3B-treated RA $MØ_{IFN-γ}$ and RA $MØ_{M-CSF}$. Sema3B also modulated cell surface markers in macrophages towards an anti-inflammatory phenotype. Besides, MerTK expression and activation was up-regulated by Sema3B, just as GAS6 expression, Resolvin D1 secretion and the phagocytic activity of macrophages. Importantly, the inhibition of MerTK and neuropilins 1 and 2 abrogated the anti-inflammatory effect of Sema3B. Our data demonstrate that Sema3B modulates the macrophage characteristics in RA, inducing a skewing towards an anti-inflammatory/pro-resolving phenotype in a MerTK-dependant manner. Therefore, here we identify a new mechanism supporting the protective role of Sema3B in RA pathogenesis.

KEYWORDS
rheumatoid arthritis, Semaphorin3B, macrophages, inflammation, MERTK

1 Introduction

Rheumatoid arthritis (RA) is a chronic autoimmune rheumatic and musculoskeletal disease (RMD) characterized by articular inflammation, bone erosion and cartilage destruction. Despite the advances in the last decades, current therapies only reach persistent responses in 30% of the patients (1).

Recent studies from our group have reported the relevance of Semaphorin3B (Sema3B) in the pathogenesis of RA. On one hand, Sema3B levels are reduced in the synovial tissue and serum of RA patients compared to arthralgia and undifferentiated arthritis patients, and these levels decrease during the progression of the disease. On the other hand, Sema3B reduces migration, invasion and the secretion of matrix metalloproteases (MMPs) in RA fibroblast-like synoviocytes (FLS). More importantly, Sema3B deficiency enhances the severity of serum-induced arthritis, while Sema3B administration abrogates this effect. This protective role is associated with a reduced mouse FLS migration and the expression of inflammatory mediators in the affected joints. We also found a reduced expression of the macrophage marker CD68, suggesting that Sema3B may modulate this cell population (2–4).

Macrophages are key mediators in RA and are involved in several pathogenic processes, including inflammation, angiogenesis and bone and cartilage destruction (5, 6) importantly, the number of synovial macrophages correlates with the clinical disease activity (7). Historically, macrophages have been classified as pro-inflammatory (M1) or wound healing/anti-inflammatory (M2) macrophages, although these are the extremes of a broad spectrum of intermediated states that depend on the environmental factors and the surrounding cells (5). Recent studies have reported the existence of several macrophage subsets in the synovium of RA patients with different functional roles. Notably, the frequency of these populations is also associated with the clinical status of the patients (8, 9).

Since the effect of Sema3B on RA macrophages is unknown, in the current study we examined the effect of Sema3B on the functional and phenotypic characteristics of this cell population.

2 Materials and methods

2.1 Patients

Peripheral blood mononuclear cells (PBMCs) (n = 33) and FLS (n = 4) were obtained from blood and inflamed joints of RA patients, respectively. All subjects provided written informed consent, and the protocols were approved by the Ethics Committee of Galicia prior to patient inclusion in this study (studies numbers 2020/159 and 2021/03). RA patients fulfilled the American College of Rheumatology/European Alliance of Associations for Rheumatology 2010 classification criteria for RA (10). Clinical characteristics of patients are detailed in Supplementary Table S1.

2.2 Monocyte purification, macrophage differentiation and stimulation

PBMCs were obtained by Ficoll gradient (STEMCELL Technologies) and $CD14^+$ monocytes were isolated by using the MagniSort Human pan-Monocyte isolation kit (Thermo Fisher Scientific). Monocytes were differentiated into RA macrophages (RA MØ) by culturing in Iscove's Modified Dulbecco's Medium (IMDM) supplemented with 10% of heat-inactivated fetal bovine serum (FBS, Corning™) and 10000 I.E penicillin-streptomycin (Lonza™ BioWhittaker™), in the presence of IFN-γ (10 ng/mL; R&D Systems; RA $MØ_{IFN-γ}$) or M-CSF (25 ng/mL; PeproTech; RA $MØ_{M-CSF}$) for 7 days. On one side, macrophages were differentiated in the presence or the absence of recombinant human (rh)Sema3B (200 ng/mL; R&D Systems) for 7 days. Conversely, RA $MØ_{IFN-γ}$ and RA $MØ_{M-CSF}$ were cultured for 7 days and stimulated for 24 h with LPS (10 ng/mL; InvivoGen) in the presence or absence of rhSema3B (200 ng/mL). RA $MØ_{IFN-γ}$ and RA $MØ_{M-CSF}$ were pre-incubated during 1 hour with neutralizing anti-Neuropilin-1 (α-NRP1) antibody (5μg/mL; R&D Systems), neutralizing anti-Neuropilin-2 (α-NRP2) antibody (5μg/mL; R&D Systems) or their respective isotype controls (sheep and goat IgG; 5μg/mL; R&D Systems), and stimulated with LPS (10 ng/mL) in the presence or absence of rhSema3B (200 ng/mL) for 24 h.

Alternatively, RA $MØ_{IFN-γ}$ and RA $MØ_{M-CSF}$ were also pre-incubated during 1 hour with DMSO or a specific MerTK inhibitor (100nM; UNC2881, Cayman Chemical) (11, 12) and stimulated with LPS in the presence or absence of rhSema3B for 24 h.

Cells were lysed for mRNA expression analysis or typsinized for Flow Cytometry. Cell-free supernatants were harvested for cytokine analysis.

2.3 RA FLS culture and stimulation

RA FLS were cultured in Dulbecco's Modified Eagle Medium (DMEM, Lonza™ BioWhittaker™) containing 10% FBS, 200 mM Glutamine (Lonza™) and 10,000 U/mL penicillin-streptomycin (Thermo Fisher Scientific) and used between passages 6 to 10.

Prior to stimulation, RA FLS were cultured overnight in DMEM containing 1% FBS. Afterwards, the cells were stimulated for 4 h with the supernatants (20%, v/v) from RA $MØ_{IFN-\gamma}$ and RA $MØ_{M-CSF}$.

2.4 RT-PCR and quantitative (q)PCR

RNA from RA MØ and RA FLS was isolated employing the NucleoSpin RNA/Protein Mini kit (Macherey-Nagel). Total RNA was reverse-transcribed using iScript (Biorad). cDNA was amplified by qPCRs in duplicates using SYBR green (Biorad) and specific primers (Integrated DNA Technologies (IDT); Supplementary Table S2) with a CFX96 Touch Real-Time PCR Detection System (Biorad). Relative levels of gene expression were normalized to the expression of 2 housekeeping genes (*GAPDH* and *B2M*). The relative quantity (RQ) of mRNA was calculated by using the formula $2^{-\Delta\Delta Ct}$.

2.5 ELISA

IL-12p70, IL-6, TNF (R&D Systems) and Resolvin D1 (Cayman Chemical) protein levels were measured by ELISA in cell-free supernatants, according to the manufacturing instructions.

2.6 Flow cytometry

Data were acquired on a CytoFLEX S analyser (Beckman Coulter). 10% of Anti-Hu Fc Receptor (Thermo Fisher Scientific) was used for avoiding non-specific binding. Macrophages were stained with Fixable Viability Dye eFluor for dead cell exclusion (e450; Thermo Fisher Scientific) and antibodies for CD14-PerCPCy5.5, CD64-FITC, CD80-BV510, CD86-PECy7, CD163-APC-Cy7, CD206-APC, HLA-DR-BV605 and MerTK-PE (all Biolegend). In the case of MerTK, Fluorescence Minus One (FMO) enabled the tagging of the positive population. After excluding debris, doublets and dead cells, cell populations were analyzed using CytExpert software and Cytobank platform (Beckman Coulter). Results were expressed as the Median Fluorescence Intensity (MFI).

2.7 Phagocytosis assay

Macrophage phagocytic activity was determined by the uptake of the fluorogenic substrate DQ Red BSA (FITC; Thermo Fisher Scientific). Stimulated RA $MØ_{IFN-\gamma}$ and RA $MØ_{M-CSF}$ were typsinized and plated in conical well plates. DQ Red BSA (20 ng/mL) was added for 0, 30 and 60 minutes. Uptake data were acquired on a CytoFLEX S analyser (Beckman Coulter) and results were expressed as percentage of DQ-BSA uptake versus 30 minutes basal uptake.

2.8 Immunoblotting

Protein from RA $MØ_{M-CSF}$ was isolated by Laemmli buffer. Equal quantities of total protein were submitted to electrophoresis on Polyacrylamide gels and transferred to PVDF Transfer membranes (Thermo Fisher Scientific). Membranes were incubated (4°C, overnight) with primary antibodies for (p)hosphoMerTK (FabGennix) and β-actin (R&D Systems) in 4% Milk-TBS/T, washed and incubated in 2% Milk-TBS/T containing HRP-conjugated secondary antibody (anti-mouse IgG, Thermo Fisher Scientific). Protein was developed with ECL Western Blotting Substrate (Thermo Fisher Scientific) employing a ChemiDocTM MP System (Biorad). Densitometry analysis was performed by ImageJ software and relative protein expression was normalized to the values for β-actin.

2.9 Gene expression from profiling data

The gene expression of Sema3B receptors in bone marrow-derived macrophages (BMDM) from wild type (WT) and MerTK deficient ($Mertk^{-/-}$) mice was retrieved from array profiling data available at the Gene Expression Omnibus (GEO–NCBI; GSE205070) (13).

2.10 Statistical analyses

Statistical analysis was performed by using Windows GraphPad Prism 8 (GraphPad Software, Inc.). Normality was analysed by Shapiro-Wilk and Kolmogorov-Smirnov tests. The potential differences between experimental groups following normal distribution were analysed by One-way ANOVA and Paired t tests, as applicable. Data non-following normal distribution were analysed by Friedman's test. P values < 0.05 were considered statistically significant.

3 Results

3.1 Sema3B modulates the inflammatory characteristics of RA MØ

We firstly analysed the effect of Sema3B in inflammatory macrophages (RA $MØ_{IFN-\gamma}$). Sema3B alone did not affect the expression of pro-inflammatory mediators, but significantly reduced the LPS-induced expression of *IL12B, IL23, CD86, TNF* and *CCL2*, while moderately *IL1B*, *IL6* and *CXCL10* (Figure 1A). In the case of anti-inflammatory mediators, Sema3B induced the expression of *STAB1*, but did not modulate the expression of *IL10*, *IL13* and *TGFB* (Supplementary Figure S1A).

The influence of Sema3B was also determined on RA MØ differentiated with M-CSF, which promotes an anti-inflammatory phenotype (14). Similarly to RA $MØ_{IFN-\gamma}$, Sema3B alone did not

10.3389/fimmu.2023.1268144

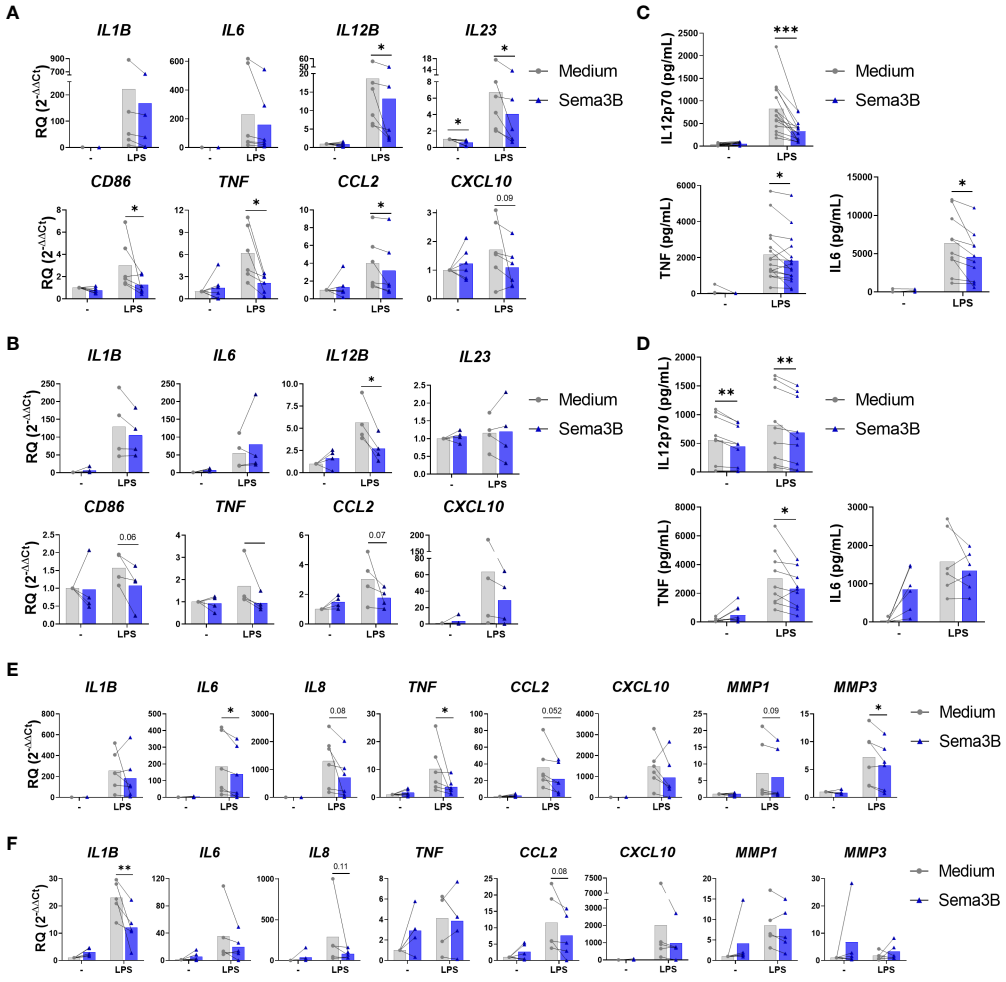

FIGURE 1
Sema3B reduces the inflammatory phenotype of RA MØ and RA FLS. **(A–D)** mRNA expression and protein secretion of inflammatory and anti-inflammatory mediators in RA $MØ_{IFN-γ}$ [n = 6 – 16] **(A, C)** and RA $MØ_{M-CSF}$ [n = 4 – 9] **(B, D)** stimulated with rhSema3B [200 ng/mL] in the presence or absence of LPS [10 ng/mL] for 24 h. **(E, F)** mRNA expression of inflammatory mediators in RA FLS stimulated with RA $MØ_{IFN-γ}$ [n = 6] **(E)** and RA $MØ_{M-CSF}$ [n = 5] **(F)** supernatants [20%, v/v] for 4 h. Data are shown as RQ (relative quantity) respect to unstimulated cells and serum concentration (pg/mL), and analysed by One-way ANOVA tests. Means and SEM are shown. *P < 0.05 and **P < 0.01 and ***P < 0.001.

affect the expression of pro-inflammatory mediators in RA $MØ_{M-CSF}$, but significantly down-regulated the LPS-induced expression of *IL12B*, besides reducing *CD86*, *TNF* and *CCL2* (Figure 1B). In contrast, the anti-inflammatory mediators *STAB1* and *TGFB* were up-regulated by Sema3B, alone and in combination with LPS (Supplementary Figure S1B).

We validated these findings at the protein level in both RA $MØ_{IFN}$ and RA $MØ_{M-CSF}$, in which Sema3B reduced the LPS-induced secretion of IL12p70, TNF-α and, in RA $MØ_{IFN-γ}$ specifically, IL-6 (Figures 1C, D).

With the aim of determining whether the anti-inflammatory effect of Sema3B could have functional consequences on effector cells, RA FLS were stimulated with cell-free supernatants from RA $MØ_{IFN-γ}$ and RA $MØ_{M-CSF}$. Interestingly, supernatants of those macrophages stimulated with LPS in combination with Sema3B reduced the expression of *IL1B, IL6, IL8, TNF, CCL2, CXCL10, MMP1 and MMP3* compared to supernatants of LPS-stimulated macrophages, although differences were not significant for all mediators (Figures 1E, F).

The effect of Sema3B on the modulation of M1 (CD80, CD86 and HLA-DR) and M2 (CD163 and CD206) surface markers expressed by RA synovial macrophages was also evaluated (6). In RA $MØ_{IFN-γ}$, Sema3B alone promoted CD64 and CD206 expression and, in LPS-stimulated macrophages, reduced the expression of CD64, HLA-DR and, significatively, CD86 (Figure 2A). In the case of RA $MØ_{M-CSF}$, we found that, in combination with LPS, Sema3B decreased the expression of CD64 and a trend for CD80 (Figure 2B). We also determined whether Sema3B was able to modulate the expression of specific markers during the macrophage differentiation process. Sema3B significantly down-regulated the expression of HLA-DR in IFN-γ-differentiated macrophages, but it did not modulate M2 markers. During the differentiation process with M-CSF, Sema3B reduced the expression of HLA-DR and CD64, while it significantly induced the expression of CD163 (Supplementary Figure S2).

10.3389/fimmu.2023.1268144

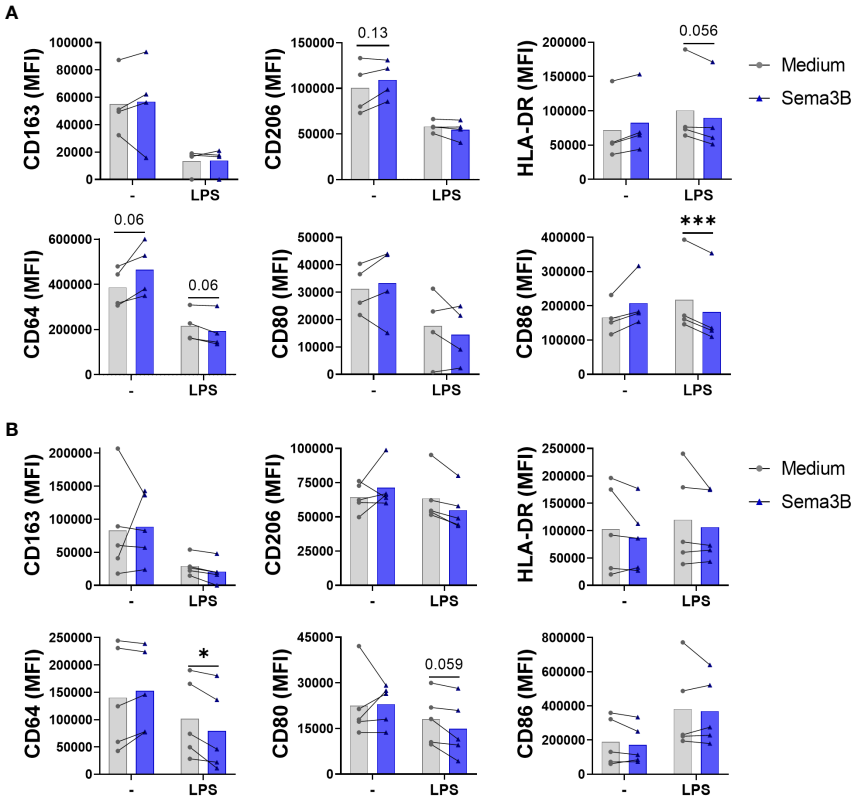

FIGURE 2
Sema3B promotes an anti-inflammatory phenotype in RA MØ. **(A, B)** CD163, CD206, HLA-DR, CD64, CD80 and CD86 cell surface marker expression in RA $MØ_{IFN-\gamma}$ [n = 4] **(A)** and RA $MØ_{M-CSF}$ [n = 5] **(B)** stimulated with rhSema3B [200 ng/mL] in the presence or absence of LPS [10 ng/mL] for 24 h. Data are shown as MFI (Median Fluorescence Intensity) of cells and analysed by Friedman **(A)** One-way ANOVA **(B)** tests. Means and SEM are shown. *P < 0.05, ***P < 0.001.

Altogether, these data demonstrate an anti-inflammatory effect of Sema3B in RA MØ, by reducing the expression of the inflammatory phenotype and modulating the phenotypic characteristics of RA MØ.

3.2 Sema3B promotes an anti-inflammatory and pro-resolving macrophage phenotype in a MerTK-dependant manner

We next sought the mechanisms involved in the anti-inflammatory effect of Sema3B. Sema3B did not modulate the expression of its known receptors, PlexinA1 and PlexinA2, and co-receptors, Neuropilin-1 (NRP-1) and Neurolipin-2 (NRP-2) in either RA $MØ_{IFN-\gamma}$ or RA $MØ_{M-CSF}$ (15, 16) (Figures 3A, B). However, the neutralization of both NRP-1 and NRP-2 abolished the Sema3B-mediated decrease of IL12p70 in RA $MØ_{IFN-\gamma}$, demonstrating that both Sema3B co-receptors are involved in the anti-inflammatory role of Sema3B (Figure 3C).

Due to the crucial role of MerTK in resolving inflammation in RA (9, 17, 18), the involvement of Sema3B on the expression of this tyrosine kinase receptor was also evaluated. Sema3B alone, but not in combination with LPS, up-regulated the mRNA and protein expression of MerTK, and the mRNA expression of the MerTK ligand GAS6 (19–21) in both RA $MØ_{IFN-\gamma}$ (Figure 4A) and RA $MØ_{M-CSF}$ (Figure 4B), although differences were more pronounced in the latter. Sema3B also increased MerTK expression during the differentiation process into RA $MØ_{M-CSF}$ (Supplementary Figure S2B). Importantly, Sema3B induced the activation of MerTK in RA $MØ_{M-CSF}$ at different time points, being this effect significant at 4 hours (Figure 4C).

Since $MerTK^+$ RA MØ are involved in the resolution of inflammation, we next analysed the effect of Sema3B in the phagocytic activity of macrophages and the synthesis of Resolvin D1, a lipid induced by macrophage MerTK signalling involved in resolving joint inflammation (22). In RA $MØ_{IFN-\gamma}$, Sema3B moderately increased Resolvin D1 secretion, although it did not modulate the macrophage phagocytic activity (Figure 4D). On their part, Sema3B-stimulated RA $MØ_{M-CSF}$ significantly raised the secretion of Resolvin D1, as well as their phagocytosis capacity, although it resulted insufficient counteracting the effect of LPS (Figure 4E).

Ultimately, we tested if these responses were mediated by MerTK, using a specific MerTK (i)nhibitor. Sema3B reduced the LPS-mediated secretion of IL12p70 in both RA $MØ_{IFN-\gamma}$ and RA

10.3389/fimmu.2023.1268144

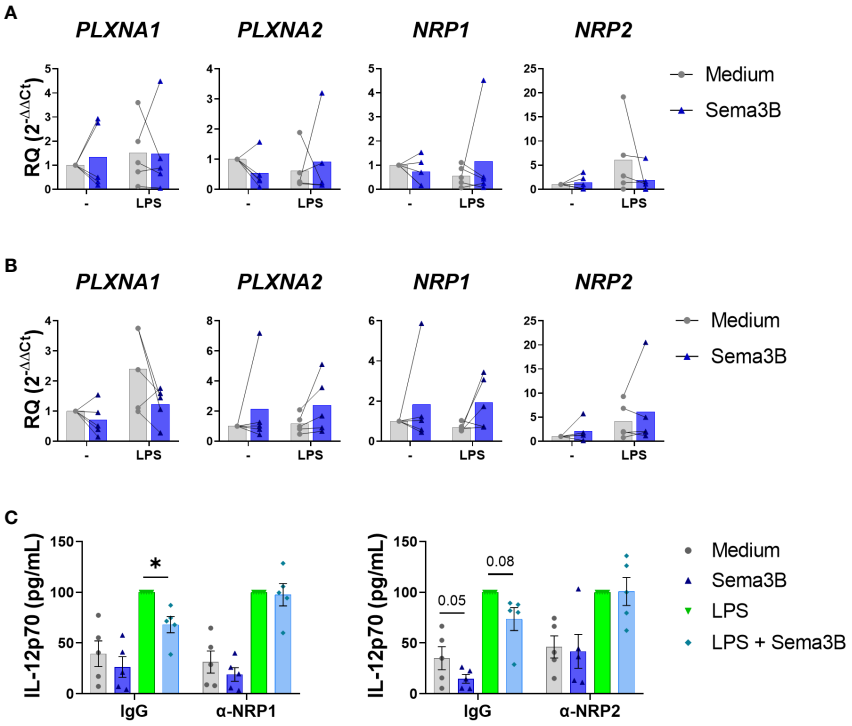

FIGURE 3
The protective effect of Sema3B in RA MØ is mediated by the co-receptors NRP1 and NRP2. **(A, B)** mRNA expression of Sema3B receptors in RA $MØ_{IFN-\gamma}$ [n = 5] **(A)** and RA $MØ_{M-CSF}$ [n = 5] **(B)** stimulated with rhSema3B [200 ng/mL] in the presence or absence of LPS [10 ng/mL] for 24 h. **(C)** IL12p70 secretion in RA $MØ_{IFN-\gamma}$ [n = 5] pre-incubated with neutralizing α-NRP1, α-NRP2 antibodies [5μg/mL] or their respective isotype controls, and stimulated with LPS [10 ng/mL] in the presence or absence of rhSema3B [200 ng/mL] for 24 h. Data are shown as RQ (relative quantity) respect to unstimulated cells and serum concentration (pg/mL) and analysed by One-way ANOVA tests. Means and SEM are shown. *P < 0.05.

$MØ_{M-CSF}$, and this effect was abrogated in the presence of the MerTKi (Figures 4F, G). Also, MerTK inhibition reversed the Sema3B-induced phagocytic activity of RA $MØ_{M-CSF}$ (Figure 4G).

Therefore, these results suggest that the anti-inflammatory and pro-resolving responses induced by Sema3B are, at least in part, mediated by MerTK.

4 Discussion

In this manuscript we demonstrate that Sema3B modulates the phenotypic characteristics of RA macrophages. More specifically, Sema3B induces a skewing towards an anti-inflammatory/pro-resolving phenotype in a MerTK-dependant manner. Through this work we have found a new protective effect of Sema3B in the pathogenesis of RA. This protective role is in line with previous results from our group, in which we described a reduced expression of inflammatory mediators in both joints and FLS of arthritic mice treated with Sema3B and an impaired invasive phenotype in Sema3B-stimulated RA FLS (2–4).

Firstly, Sema3B reduced the secretion of pro-inflammatory cytokines in monocytes-derived macrophages from RA patients. The expression of surface markers associated to M1 macrophages (CD86, HLA-DR and CD64) was also decreased by Sema3B, while the expression of M2 markers (Stabilin-1 and TGF-β) was raised. Neutralization experiments showed that co-receptors NRP-1 and NRP-2 are involved in the protective signalling induced by Sema3B. Since our previous findings identified NRP-2 and, in lower extent NRP-1, as Sema3B co-receptors essential for reducing the invasive ability of RA FLS (2), we demonstrate that Sema3B signals through these co-receptors in both cell types. Sema3B also increased the phagocytic activity in RA $MØ_{M-CSF}$, which is linked to the resolution of tissue inflammation (6). However, we did not observe this effect in RA $MØ_{IFN-\gamma}$. This might be due to the IFN-γ-induced M1-like phenotype, which could be modulated to a less inflammatory phenotype by Sema3B, but without reaching pro-resolving characteristics, as it would be the case for Sema3B-modulated RA $MØ_{M-CSF}$. In this regard, the higher phagocytic activity of RA $MØ_{M-CSF}$ compared to RA $MØ_{IFN-\gamma}$ (Supplementary Figure S3), and the lack of effect of Sema3B on LPS-stimulated macrophages, support this aim.

Secondly, we proved that the anti-inflammatory/resolving effect of Sema3B in RA MØ was mediated by MerTK. Sema3B has a dual role on MerTK activation. On one hand, Sema3B induced the expression and activation of MerTK. On the other hand, Sema3B up-regulated the macrophage expression of GAS6, which is a ligand that activates MerTK signalling (19–21). MerTK is a crucial tyrosine kinase for the macrophage differentiation towards an anti-inflammatory/resolving phenotype (23, 24) and its deficiency exacerbates the severity of collagen-induced arthritis, while MerTK signalling activation reduces it in this arthritis model (17, 18). Importantly, $MerTK^+$ synovial macrophages are associated with the disease status of RA patients. In

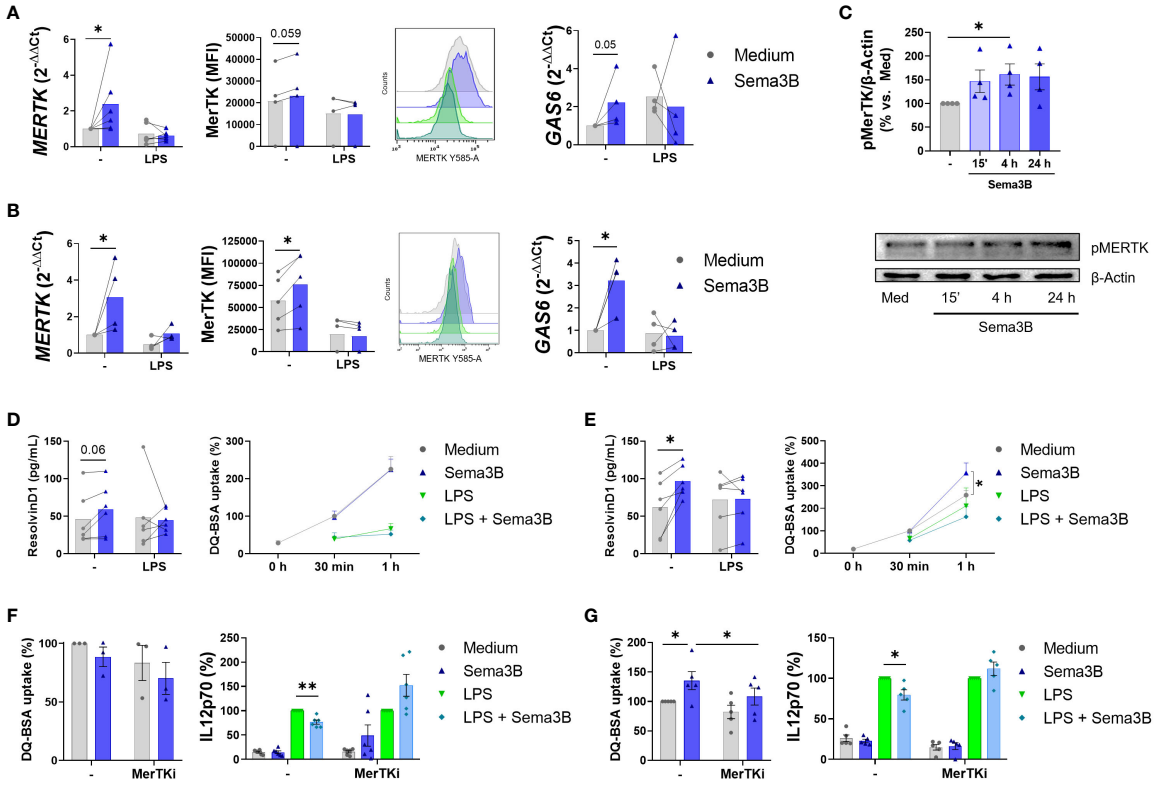

FIGURE 4
Sema3B induces an anti-inflammatory/pro-resolving phenotype in RA MØ via MerTK. **(A, B)** MerTK and GAS6 mRNA levels and MerTK cell surface expression in RA $MØ_{IFN-γ}$ [n = 4 – 6] **(A)** and RA $MØ_{M-CSF}$ [n = 4 – 5] **(B)** stimulated with Sema3B [200 ng/mL] in the presence or absence of LPS [10 ng/mL] for 24 h. **(C)** Densitometric analysis and representative immunoblot of MertK activation ((p)hosphoMerTK) in RA $MØ_{M-CSF}$ [n = 4] stimulated with rhSema3B [200 ng/mL] for 15 minutes, 4 and 24 hours. **(D, E)** Resolvin D1 secretion and phagocytic activity in RA $MØ_{IFN-γ}$ [n = 4 – 6] **(D)** and RA $MØ_{M-CSF}$ [n = 5 – 6] **(E)** after stimulation with rhSema3B [200 ng/mL] in the presence or absence of LPS [10 ng/mL] for 24 h. **(F, G)** Phagocytic activity and IL12p70 secretion in RA $MØ_{IFN-γ}$ [n = 3 – 6] **(F)** and RA $MØ_{M-CSF}$ [n = 5] **(G)** pre-incubated with the MerTKi (i)nhibitor UNC2881 [100 nM] and stimulated with rhSema3B [200 ng/mL] in the presence or absence of LPS [10 ng/mL] for 24 h. Data are shown as RQ (relative quantity) respect to unstimulated cells, MFI (Median Fluorescence Intensity) of cells, % of pMerTK compared to medium, serum concentration (pg/mL), % of DQ-BSA uptake compared to medium and % of IL12p70 secretion compared to LPS. Data are analysed by One-way ANOVA tests. Means and SEM are shown. *P < 0.05, **P < 0.01.

fact, the percentage of this macrophage population is reduced in patients with active RA compared to patients in remission and negatively correlates with the disease activity score-28 (DAS28). In contrast, $MerTK^-$ synovial MØ express inflammatory mediators, induce the production of inflammatory mediators by RA FLS and participate in both bone and cartilage destruction (9, 17). Therefore, the modulation of $MerTK^+$ macrophages by Sema3B may be a useful approach for the treatment of RA.

We cannot rule out the possibility that MertK modulates Sema3B signalling, since MerTK regulates the expression of the Sema3B receptor PlexinA1 (25). We analysed, using a public dataset (GSE205070), the expression of Sema3B receptors in bone marrow-derived macrophages (BMDM) from WT and *Mertk*$^{-/-}$ mice. Deficiency of MerTK significantly up-regulated the expression of *Plxna1* and *Nrp1* (Supplementary Figure 4), suggesting that MerTK signalling might modulate the Sema3B signalling. However, further studies are needed for elucidating this effect.

Sema3B is not the only class 3 semaphorin member able to modulate the macrophage phenotype characteristic. In fact, Sema3A and Sema3E also induce a skewing towards a resolving/anti-inflammatory phenotype in this cell type (26–29). In addition, Sema3A and Sema3F play protective roles in the pathogenesis of RA (2, 4, 29, 30). However, these semaphorins did not modulate the expression of MerTK (data non shown), suggesting that the MerTK regulation is specific for Sema3B.

Lastly, Sema3B also enhanced the secretion of Resolvin D1, a pro-resolving lipid triggered by the MerTK signalling activation, with a protective function in inflammatory arthritis (9, 22). Moreover, Resolvin D1 has been also involved in the modulation of macrophage polarization and in the skewing towards the anti-inflammatory/resolving phenotype (20, 31).

A limitation of this study is that we did not used liquid chromatography–mass spectrometry, the gold standard for the assessment of Resolvin D1 (32). Instead, we employed the well-validated ELISA technique. We neither utilized synovial macrophages from RA patients. We used instead *in vitro* M-CSF- and IFN-γ-differentiated macrophages from peripheral blood monocytes of RA patients, which possess anti-inflammatory/pro-resolving and pro-inflammatory characteristics, respectively (5, 14). Remarkably, MerTK expression was higher in RA $MØ_{M-CSF}$ than in RA $MØ_{IFN-}$

$_{\gamma}$, therefore these macrophage phenotypes partially mimic the phenotypes of MerTK^{+} and MerTK^{-} synovial macrophages.

Altogether, our work identifies a new anti-inflammatory mechanism of Sema3B, confirming the protective role of Sema3B in RA pathogenesis and pointing out this semaphorin as a promising therapeutic target.

Data availability statement

The raw data supporting the conclusions of this article will be made available by the authors, without undue reservation.

Ethics statement

The studies involving humans were approved by Ethics Committee of Galicia (studies numbers 2020/159 and 2021/03). The studies were conducted in accordance with the local legislation and institutional requirements. The participants provided their written informed consent to participate in this study.

Author contributions

SM-R: Conceptualization, Data curation, Formal analysis, Investigation, Methodology, Writing – original draft, Writing – review & editing. CR-V: Data curation, Formal analysis, Investigation, Methodology, Writing – review & editing. BM-F: Data curation, Formal analysis, Investigation, Methodology, Writing – review & editing. NP: Data curation, Investigation, Methodology, Writing – review & editing. CM: Data curation, Investigation, Methodology, Writing – review & editing. SGP: Data curation, Investigation, Methodology, Writing – review & editing. FJMP: Data curation, Investigation, Methodology, Writing – review & editing. CC: Conceptualization, Formal analysis, Writing – review & editing. JP-R: Formal analysis, Writing – review & editing. SG: Conceptualization, Data curation, Formal analysis, Funding acquisition, Investigation, Methodology, Project administration, Resources, Supervision, Writing – original draft, Writing – review & editing.

Funding

The author(s) declare financial support was received for the research, authorship, and/or publication of this article. This work was supported by Instituto de Salud Carlos III (ISCIII), #PI20/01472 (SG), #CP19/00005 (SG), #FI2100120 (SM-R) and #IFEQ21/00157, co-funded by the European Union; by Axencia Galega de Innovación, #IN607B-2022-18, #IN606A-2020/043 (CR-V), and by vouchers (#Q222RSV34 and #Q123PV87) from the European Alliance of Associations for Rheumatology (EULAR).

Acknowledgments

All patients are thanked for their selfless participation.

Conflict of interest

The authors declare that the research was conducted in the absence of any commercial or financial relationships that could be construed as a potential conflict of interest.

Publisher's note

All claims expressed in this article are solely those of the authors and do not necessarily represent those of their affiliated organizations, or those of the publisher, the editors and the reviewers. Any product that may be evaluated in this article, or claim that may be made by its manufacturer, is not guaranteed or endorsed by the publisher.

Supplementary material

The Supplementary Material for this article can be found online at: https://www.frontiersin.org/articles/10.3389/fimmu.2023.1268144/full#supplementary-material

References

1. Smolen JS, Aletaha D, Barton A, Burmester GR, Emery P, Firestein GS, et al. Rheumatoid arthritis. *Nat Rev Dis Primers* (2018) 4:1–23. doi: 10.1038/nrdp.2018.1

2. Tang MW, Malvar Fernández B, Newsom SP, van Buul JD, Radstake TRDJ, Baeten DL, et al. Class 3 semaphorins modulate the invasive capacity of rheumatoid arthritis fibroblast-like synoviocytes. *Rheumatol (Oxford)* (2018) 57:909–20. doi: 10.1093/rheumatology/kex511

3. Igea A, Carvalheiro T, Malvar-Fernández B, Martinez-Ramos S, Rafael-Vidal C, Niemantsverdriet E, et al. Central role of semaphorin 3B in a serum-induced arthritis model and reduced levels in patients with rheumatoid arthritis. *Arthritis Rheumatol* (2022) 74:972–83. doi: 10.1002/art.42065

4. Martínez-Ramos S, Rafael-Vidal C, Malvar-Fernández B, Rodriguez-Trillo A, Veale D, Fearon U, et al. HOXA5 is a key regulator of class 3 semaphorins expression in the synovium of rheumatoid arthritis patients. *Rheumatology* (2022) 62(7):2621–30. doi: 10.1093/rheumatology/keac654

5. Udalova IA, Mantovani A, Feldmann M. Macrophage heterogeneity in the context of rheumatoid arthritis. *Nat Rev Rheumatol* (2016) 12:472–85. doi: 10.1038/nrrheum.2016.91

6. Cutolo M, Campitiello R, Gotelli E, Soldano S. The role of M1/M2 macrophage polarization in rheumatoid arthritis synovitis. *Front Immunol* (2022) 13:867260. doi: 10.3389/fimmu.2022.867260

7. Haringman JJ, Gerlag DM, Zwinderman a. H, Smeets TJM, Kraan MC, Baeten D, et al. Synovial tissue macrophages: A sensitive biomarker for response to treatment in patients with rheumatoid arthritis. *Ann Rheum Dis* (2005) 64:834–8. doi: 10.1136/ard.2004.029751

8. Zhang F, Wei K, Slowikowski K, Fonseka CY, Rao DA, Kelly S, et al. Defining inflammatory cell states in rheumatoid arthritis joint synovial tissues by integrating single-cell transcriptomics and mass cytometry. *Nat Immunol* (2019) 20:928–42. doi: 10.1038/s41590-019-0378-1

9. Alivernini S, MacDonald L, Elmesmari A, Finlay S, Tolusso B, Gigante MR, et al. Distinct synovial tissue macrophage subsets regulate inflammation and remission in rheumatoid arthritis. *Nat Med* (2020) 26:1295–306. doi: 10.1038/s41591-020-0939-8

10. Aletaha D, Neogi T, Silman AJ, Funovits J, Felson DT, Bingham CO, et al. 2010 Rheumatoid arthritis classification criteria: An American College of Rheumatology/European League Against Rheumatism collaborative initiative. *Arthritis Rheum* (2010) 62:2569–81. doi: 10.1002/art.27584

11. Adomati T, Cham LB, Hamdan TA, Bhat H, Duhan V, Li F, et al. Dead Cells Induce Innate Anergy via Mertk after Acute Viral Infection. *Cell Rep* (2020) 30:3671–3681.e5. doi: 10.1016/j.celrep.2020.02.101

12. Zhang W, McIver AL, Stashko MA, Deryckere D, Branchford BR, Hunter D, et al. Discovery of Mer specific tyrosine kinase inhibitors for the treatment and prevention of thrombosis. *J Med Chem* (2013) 56:9693–700. doi: 10.1021/jm4013888

13. Akalu YT, Mercau ME, Ansems M, Hughes LD, Nevin J, Alberto EJ, et al. Tissue-specific modifier alleles determine Mertk loss- of- function traits. *Elife* (2022) 11: e80530. doi: 10.7554/eLife.80530

14. Hamilton TA, Zhao C, Pavicic PG, Datta S. Myeloid colony-stimulating factors as regulators of macrophage polarization. *Front Immunol* (2014) 5:554. doi: 10.3389/fimmu.2014.00554

15. Worzfeld T, Offermanns S. Semaphorins and plexins as therapeutic targets. *Nat Rev Drug Discovery* (2014) 13:603–21. doi: 10.1038/nrd4337

16. Garcia S. Role of semaphorins in immunopathologies and rheumatic diseases. *Int J Mol Sci* (2019) 20(2):374. doi: 10.3390/ijms20020374

17. Waterborg CEJ, Beermann S, Broeren MGA, Bennink MB, Koenders MI, van Lent PLEM, et al. Protective role of the MER tyrosine kinase via efferocytosis in rheumatoid arthritis models. *Front Immunol* (2018) 9:742. doi: 10.3389/fimmu.2018.00742

18. Van Den Brand BT, Abdollahi-Roodsaz S, Vermeij EA, Bennink MB, Arntz OJ, Rothlin CV, et al. Therapeutic efficacy of Tyro3, Axl, and Mer tyrosine kinase agonists in collagen-induced arthritis. *Arthritis Rheum* (2013) 65:671–80. doi: 10.1002/art.37786

19. Cai B, Dongiovanni P, Corey KE, Wang X, Shmarakov IO, Zheng Z, et al. Macrophage merTK promotes liver fibrosis in nonalcoholic steatohepatitis. *Cell Metab* (2020) 31:406–421.e7. doi: 10.1016/j.cmet.2019.11.013

20. Cai B, Kasikara C, Doran AC, Ramakrishnan R, Birge RB, Tabas I. MerTK signaling in macrophages promotes the synthesis of inflammation resolution mediators by suppressing CaMKII activity. *Sci Signal* (2018) 11(549):eaar3721. doi: 10.1126/scisignal.aar3721

21. Chen J, Carey K, Godowski PJ. Identification of Gas6 as a ligand for Mer, a neural cell adhesion molecule related receptor tyrosine kinase implicated in cellular transformation. *Oncogene* (1997) 14:2033–9. doi: 10.1038/sj.onc.1201039

22. Norling LV, Headland SE, Dalli J, Arnardottir HH, Haworth O, Jones HR, et al. Proresolving and cartilage-protective actions of resolvin D1 in inflammatory arthritis. *JCI Insight* (2016) 1(5):e85922. doi: 10.1172/jci.insight.85922

23. Triantafyllou E, Pop OT, Possamai LA, Wilhelm A, Liaskou E, Singanayagam A, et al. MerTK expressing hepatic macrophages promote the resolution of inflammation in acute liver failure. *Gut* (2018) 67:333–47. doi: 10.1136/gutjnl-2016-313615

24. Wu H, Zheng J, Xu S, Fang Y, Wu Y, Zeng J, et al. Mer regulates microglial/macrophage M1/M2 polarization and alleviates neuroinflammation following traumatic brain injury. *J Neuroinflamm* (2021) 18:1–20. doi: 10.1186/s12974-020-02041-7

25. Penberthy KK, Rival C, Shankman LS, Raymond MH, Zhang J, Perry JSA, et al. Context-dependent compensation among phosphatidylserine- recognition receptors. *Sci Rep* (2017) 7(1):14623. doi: 10.1038/s41598-017-15191-1

26. Rienks M, Carai P, Bitsch N, Schellings M, Vanhaverbeke M, Verjans J, et al. Sema3A promotes the resolution of cardiac inflammation after myocardial infarction. *Basic Res Cardiol* (2017) 112:1–13. doi: 10.1007/s00395-017-0630-5

27. Tian T, Chen L, Wang Z, Zhu M, Xu W, Wu B. Sema3A drives alternative macrophage activation in the resolution of periodontitis via PI3K/AKT/mTOR signaling. *Inflammation* (2023) 46:876–91. doi: 10.1007/s10753-022-01777-z

28. Mohammed A, Okwor I, Shan L, Onyilagha C, Uzonna JE, Gounni AS. Semaphorin 3E regulates the response of macrophages to lipopolysaccharide-induced systemic inflammation. *J Immunol* (2020) 204:128–36. doi: 10.4049/jimmunol.1801514

29. Teng Y, Yin Z, Li J, Li K, Li X, Zhang Y. Adenovirus-mediated delivery of Sema3A alleviates rheumatoid arthritis in a serum-transfer induced mouse model. *Oncotarget* (2017) 8:66270–80. doi: 10.18632/oncotarget.19915

30. Catalano A. The neuroimmune semaphorin-3A reduces inflammation and progression of experimental autoimmune arthritis. *J Immunol* (2010) 185:6373–83. doi: 10.4049/jimmunol.0903527

31. Schmid M, Gemperle C, Rimann N, Hersberger M. Resolvin D1 Polarizes Primary Human Macrophages toward a Proresolution Phenotype through GPR32. *J Immunol* (2016) 196:3429–37. doi: 10.4049/jimmunol.1501701

32. Dalli J, Gomez EA, Jouvene CC. Utility of the specialized pro-resolving mediators as diagnostic and prognostic biomarkers in disease. *Biomolecules* (2022) 12:353. doi: 10.3390/biom12030353

Frontiers in Immunology

Explores novel approaches and diagnoses to treat immune disorders.

The official journal of the International Union of Immunological Societies (IUIS) and the most cited in its field, leading the way for research across basic, translational and clinical immunology.

Discover the latest Research Topics

See more →

Frontiers

Avenue du Tribunal-Fédéral 34
1005 Lausanne, Switzerland
frontiersin.org

Contact us

+41 (0)21 510 17 00
frontiersin.org/about/contact